UNIVERSITÀ DEGLI STUDI DI PADOVA

Centro di Ricerca Interdipartimentale per le Biotecnologie Innovative

– CRIBI –

SCUOLA DI DOTTORATO DI RICERCA IN BIOCHIMICA E BIOTECNOLOGIE

INDIRIZZO DI BIOTECNOLOGIE

XXI CICLO

α-SYNUCLEIN AND POLYUNSATURATED FATTY ACIDS

MOLECULAR CHARACTERIZATION OF THE INTERACTION AND IMPLICATION IN PROTEIN AGGREGATION

Direttore della scuola: Chiar.mo Prof. Giuseppe ZANOTTI

Supervisore: Dr.ssa Patrizia POLVERINO DE LAURETO

Dottoranda: Giorgia DE FRANCESCHI

A. A. 2008/2009

Alla mia piccola,
grande famiglia

THESIS CONTENTS

Chapter 4

Appendix

ABBREVIATIONS

ApoMb	apomyoglobin
$ApoMb_{1-29}$	N-terminal region of apomyoglobin, spanning the first 29 residues
CD	circular dichroism
CAC	critical aggregates concentration
CMC	critical micelle concentration
DA	dopaminergic
Da	Dalton
DHA	4,7,10,13,16,19-docosahexaenoic acid [22:6(ω3)]
DLS	dynamic light scattering
TEM	transmission electron microscopy
ESI	electrospray ionization
E:S	enzyme to substrate ratio
FA	fatty acid
GdnHCl	guanidine hydrochloride
HPLC	high-performance liquid chromatography
LB	Lewy body
Mb	myoglobin
MM	molecular mass
MRW	mean residue weight
MS	mass spectrometry
MW	molecular weight
NAC	non-amyloid component
NMR	nuclear magnetic resonance
OA	oleic acid
OD	optical density
PA	palmitic acid
PBS	phosphate buffer saline
PD	Parkinson's disease
PUFA	polyunsaturated fatty acid
RP	reverse-phase
RT	retention time
SDS	sodium dodecyl sulphate
SDS-PAGE	polyacrylamide gel electrophoresis in presence of SDS
SUV	small unilamellar vesicles
α-Syn	α-synuclein
[θ]	mean residue ellipticity
TFA	trifluoroacetic acid
ThT	thioflavin T
Tris	tris(hydroxymethyl)aminomethane
UV	ultraviolet
w/w	weight/weight

AMINO ACID ABBREVIATIONS

Alanine	Ala	A
Arginine	Arg	R
Asparagine	Asn	N
Aspartic acid	Asp	D
Cysteine	Cys	C
Glutamic acid	Glu	E
Glutamine	Gln	Q
Glycine	Gly	G
Histidine	His	H
Isoleucine	Ile	I
Leucine	Leu	L
Lysine	Lys	K
Methionine	Met	M
Phenylalanine	Phe	F
Proline	Pro	P
Serine	Ser	S
Threonine	Thr	T
Tryptophan	Trp	W
Tyrosine	Tyr	Y
Valine	Val	V

RIASSUNTO

Il progetto della mia Tesi di dottorato riguarda il problema del folding di proteine ed il loro misfolding, in linea con la ricerca condotta nel laboratorio di Chimica delle Proteine dove è stato principalmente svolto lo studio. La ricerca svolta può essere divisa in due parti. Durante il primo anno di dottorato è stato studiato l'effetto del pH nella fibrillogenesi di proteine, mediante l'analisi delle caratteristiche di un peptide modello. Nel secondo e terzo anno di dottorato, è stata analizzato il complesso formato da α-sinucleina umana ed acidi grassi e le implicazioni di questa interazione nel processo di aggregazione della proteina. Di conseguenza, la Tesi è composta da una prima parte riguardante lo studio delle proprietà di aggregazione del peptide apoMb$_{1-29}$ (Capitolo 1, 2) e di una seconda parte dedicata alla caratterizzazione dell'interazione di α-sinucleina con acidi grassi (Capitolo 3, 4).

Molte malattie umane, definite anche *misfolding diseases*, derivano da una non corretta strutturazione delle proteine coinvolte. Un numero sempre maggiore di malattie, come il morbo di Alzheimer e di Parkinson, è correlato al fenomeno dell'aggregazione proteica e all'accumulo anomalo di depositi proteici in diversi tessuti e organi. Questi depositi patologici sono formati da aggregati proteici fibrillari, chiamati fibrille amiloidi. L'amiloide è un polimero proteico non-covalente, stabilizzato da struttura di tipo beta, in cui i diversi β-*strands* sono lateralmente associati e formano aggregati fibrillari. Poiché anche proteine e peptidi non direttamente coinvolti in patologie sono in grado di formare fibrille amiloidi in appropriate condizioni, si ritiene che la capacità di formare fibrille sia una proprietà generica delle *backbone* polipeptidico (Chiti and Dobson, 2006). Comunque, la tendenza ad aggregare e la stabilità delle fibrille dipende dalla sequenza aminoacidica, quindi determinanti intrinseci, come la carica netta, l'idrofobicità, la presenza di residui aromatici e la propensione a formare struttura beta, hanno un ruolo determinante nell'amiloidogenicità di una catena polipeptidica (Pawar et al., 2005).

Per comprendere l'importanza della carica netta di una proteina nel suo processo di aggregazione e per analizzare gli effetti dell'interazione elettrostatica nella stabilità delle risultanti fibrille, le proprietà di aggregazione di un peptide, corrispondente al frammento 1-29 di apomioglobina da cuore di cavallo (apoMb$_{1-29}$), sono state studiate in differenti condizioni di pH. Questo peptide forma velocemente fibrille amiloidi a pH acidi. Il processo a pH 2.0 segue un meccanismo di crescita nucleazione-dipendente, come determinato dall'analisi fluorimetrica mediante Tioflavina T (ThT). Osservazioni

mediante microscopia elettronica (TEM) confermano la presenza di fibrille e misure di dicroismo circolare (CD) indicano l'acquisizione di un alto contenuto di struttura secondaria di tipo beta. Mediante l'uso di peptidi derivanti dalla proteolisi di apoMb$_{1-29}$, è stata poi identificata la regione 7-16 come la più amiloidogenica, infatti, ha un alto grado di idrofobicità, propensione a formare β-sheet e bassa carica netta. In conclusione, la modulazione della carica netta dei peptidi analizzati, derivante da un cambiamento del pH, è il fattore che primariamente regola formazione di aggregati fibrillari. Inoltre, è stato dimostrato che interazioni di tipo elettrostatico hanno un ruolo determinante anche nel stabilizzare la struttura beta di fibrille mature. Infatti, ThT, TEM e CD hanno evidenziato una veloce e completa disaggregazione delle fibrille, se il pH della sospensione viene portato a valori più basici.

Nella seconda parte del mio progetto di dottorato, ho studiato i dettagli molecolari che regolano l'interazione tra α-sinucleina (α-syn) e acidi grassi, analizzando sia le caratteristiche conformazionali della proteina acquisite in presenza dell'acido grasso, sia lo stato fisico dello stesso lipide. Inoltre, è stato studiato il processo di aggregazione di α-syn mediato da acidi grassi, allo scopo di comprendere l'implicazione dei lipidi nella formazione amiloide *in vivo*.

α-Sinucleina è una proteina solubile di 140 aminoacidi, *natively unfolded* con funzione sconosciuta. Essa è altamente espressa nel sistema nervoso centrale ed è abbondante nei terminali presinaptici dei neuroni. Questa proteina è caratterizzata dalla presenza di sette ripetizioni imperfette di sequenza aminoacidica (KTKEGV) nella regione N-terminale, da una regione idrofobica centrale (NAC, non-amyloid component) e da una coda C-terminale che presenta numerosi residui acidi. La sovraespressione di α-syn e mutazioni nel suo gene sono associati a forme precoci della sindrome di Parkinson. Inoltre, α-syn è il componente principale dei corpi di Lewy, accumuli citoplasmatici caratteristici del morbo di Parkinson (Spillantini et al., 1998). Il meccanismo con cui un cambiamento nella struttura e nell'espressione della proteina possa portare allo sviluppo della malattia non è ancora stato chiarito. Nonostante l'evidenza di un ruolo chiave nella patogenesi, ci sono ancora poche informazioni sulla funzione fisiologica di α-syn a livello neuronale.

Tra le varie ipotesi, la funzione di α-syn è stata associata anche ad acidi grassi. α-Syn sembra essere in grado di interagire con acidi grassi insaturi e polinsaturi, ma non è ancora chiaro se l'interazione coinvolga molecole libere (Sharon et al., 2001), o stati

aggregati (micelle, vescicole, *oil droplets*) di acidi grassi (Broersen et al., 2006; Lücke et al., 2006). Questa interazione modula anche l'oligomerizzazione della proteina. Infatti, studi *in vitro* hanno evidenziato come α-Syn formi multimeri in seguito all'esposizione a vescicole formate da lipidi contenenti PUFA (Perrin et al., 2001). Inoltre, in linee cellulari neuronali trattate con PUFA è stato descritto un aumento della formazione di oligomeri di α-syn. Queste strutture potrebbero precedere la formazione di aggregati associati alla neurodegenerazione (Sharon et al., 2003).

In questo lavoro di tesi è stato effettuato in primo luogo uno studio sistematico sulle transizioni conformazionali di α-syn in presenza di diversi acidi grassi. Dato che il numero di insaturazioni e la lunghezza della catena acilica hanno un importante effetto sullo stato aggregativo dell'acido grasso (monomero, micella, vescicola o *oil droplet*) e di conseguenza anche nell'interazione con la proteina, l'analisi è stata condotta usando acidi grassi con diverse caratteristiche: acido palmitico (saturo), acido oleico (monoinsaturo) e acido docosaesaenoico (DHA, polinsaturo). Quest'ultimo è un acido grasso omega-3 abbondante a livello delle membrane neuronali. E' stato osservato che in aree del cervello di pazienti affetti da morbo di Parkinson contenenti inclusioni di α-syn, si registra un aumento nel livello di DHA. Gli effetti degli acidi grassi sulla struttura di α-syn sono stati analizzati mediante CD e *mapping* proteolitico. La proteina è *unfolded* in assenza degli acidi grassi e in presenza di acido palmitico, mentre in seguito al legame con acido oleico e DHA, acquisisce una conformazione α-elicoidale mediante una semplice transizione a due stadi. In presenza di DHA, α-syn è abbastanza resistente alla proteolisi con proteinasi K e tripsina e il segmento 70-90 contenuto nella regione NAC è maggiormente suscettibile all'attacco proteolitico rispetto alla regione N-terminale. Probabilmente, questo segmento è flessibile ed sufficientemente esposto all'azione proteolitica, nonostante l'analisi CD dimostri la presenza di struttura α-elica e gli esperimenti NMR indichino che solo 40 residui del C-terminale risultano essere destrutturati e mobili in presenza di DHA.

Successivamente, abbiamo osservato che α-syn altera il processo di auto-associazione di DHA. Lo stato fisico del lipide in presenza di α-syn è stato analizzato mediante misure di torbidità, *dynamic light scattering* (DLS), TEM e studi di fluorescenza utilizzando il pirene come sonda. DHA forma oil droplets polidisperse a pH neutro (Namani et al., 2007). α-Syn disgrega questi aggregati lipidici, favorendo una diversa forma di auto associazione di DHA. In presenza di α-syn sono necessarie

concentrazioni minori di acido grasso per ottenere questa specie, caratterizzata da forma più regolare, diametro inferiore e volume idrofobico ridotto.

Forme tronche di α-syn corrispondenti a diverse parti della catena polipeptidica (syn1-99, syn1-52, syn57-102, syn108-140) sono state utilizzate per ulteriori studi sul ruolo che ciascuna regione ha nell'interazione con il lipide. Analisi CD evidenziano come le sequenze ripetute svolgano un'importante funzione nella transizione ad α-elica e, di conseguenza, nell'interazione con DHA. Invece, la regione C-terminale sembra modulare la porzione di proteina che si colloca nel compartimento lipidico. Questi peptidi sono stati utilizzati anche nello studio delle proprietà aggregative di DHA. Ad eccezione di syn108-140, tutti gli altri peptidi alterano il processo di auto-associazione di DHA. Possiamo, quindi, ipotizzare che la regione N-terminale svolge un ruolo cruciale anche nel regolare il processo aggregativo di DHA.

Infine, in questo lavoro di tesi si discute l'abilità del DHA, e probabilmente di altri acidi grassi polinsaturi, di indurre la formazione di oligomeri e fibrille di α-syn (Perrin et al., 2001; Sharon et al., 2003; Broersen et al., 2006). Gli effetti molecolari di DHA sull'aggregazione di α-syn sono stati analizzati mediante CD, elettroforesi su gel nativo, ThT e TEM. La presenza di DHA in un rapporto molare [DHA]/[α-syn] di 10, promuove l'aggregazione e la formazione di fibrille della proteina. Al contrario, condizioni saturanti di DHA inducono la formazione di sole specie oligomeriche. DHA esercita un effetto diretto sulla struttura proteica, stabilizzandone una conformazione amiloidogenica, e crea un ambiente che promuove l'aggregazione proteica.

SUMMARY

The project of my PhD Thesis focuses on the general problem of the protein folding and misfolding in line with the research conducted in the laboratory of Protein Chemistry at CRIBI, where the work was mainly conducted.

My research activity can be divided in two parts. In the first year of the PhD course I studied the effect of pH in protein fibrillogenesis using a peptide model. During the second and the third years, my research was focused into the molecular interaction between α-synuclein and fatty acids and its implications in α-synuclein aggregation. Thus, this PhD Thesis is composed of a minor part concerning the analysis of the aggregative properties of the peptide model apoMb$_{1-29}$ (Chapter 1 and 2) and of a major part dealing with the characterization of the interaction of α-synuclein and fatty acids (Chapter 3 and 4).

Several human diseases, defined also misfolding disease, result from the failure of protein folding of the involved proteins. An increasing number of human diseases, such as Alzheimer's and Parkinson's diseases (PD), have been linked to protein aggregation and the aberrant accumulation of protein deposits in different tissues and organs. These pathological deposits are characterized by the presence of highly organized fibrillar aggregates called amyloid fibrils. Amyloid is a non-covalent polymer of extended, intermolecularly hydrogen bonded β-sheets that laterally self-assemble to yield twisted fibers. Since amyloid fibrils are formed from disease-associated as well as from disease unrelated proteins and peptides under appropriate conditions, there is the belief that the ability to form fibrils is a generic property of the polypeptide chain (Chiti and Dobson, 2006). However, the propensity to aggregate and the stability of the mature fibrils depends on the amino acid sequence, so intrinsic determinants, such as net charge, hydrophobicity, the presence of aromatic residues and β-sheet propensity, have important roles in amyloidogenicity of polypeptides (Pawar et al., 2005).

In order to investigate the role of the net charge in the aggregation process of unfolded proteins and to analyze the importance of electrostatic interaction in the stability of the resulting fibrils, the aggregation properties of a peptide model derived from the N-terminal region of apomyoglobin were analyzed under different pH conditions. The N-terminal fragment 1-29 of horse heart apomyoglobin (apoMb$_{1-29}$) is highly prone to form amyloid-like fibrils at low pH. Fibrillogenesis at pH 2.0 occurs following a nucleation-

dependent growth mechanism, as evidenced by the thioflavin T (ThT) assay. Transmission electron microscopy (TEM) confirms the presence of regular amyloid-like fibrils and far-UV circular dichroism (CD) spectra indicate the acquisition of a high content of β-sheet structure. Using peptides deriving from the proteolysis of apoMb$_{1–29}$, we identified the region 7-16 as the most amyloidogenic, indeed it contains in terms of hydrophobicity, β-sheet propensity and low net charge, all the determinants that favor the aggregation. In conclusion, the modulation of the net charge of apoMb1-29 and its sub-fragments by change of pH is of utmost importance for fibril formation. Moreover, we demonstrated that the electrostatic interaction, in apoMb$_{1-29}$ system, is the force that primarily stabilizes the β-sheet structure of the mature fibrils. Indeed, ThT assay, TEM and CD highlight fast and complete disaggregation of the fibrils, if the pH of a suspension of mature fibrils is increased to neutral values.

In the second part of my PhD project, I investigated the molecular details that regulate the interaction between α-synuclein (α-syn) and fatty acids (FAs), analyzing the conformational features of the protein bound to FAs and the physical state of the lipids. Moreover, the aggregation process FA-mediated was analyzed in order provides insights into the implication of lipids in amyloid formation *in vivo.*

Human α-syn is a 140 amino acid natively unfolded protein of still unknown function. It is highly expressed in the central nervous system and enriched in the presynaptic nerve terminals. α-Syn is characterized by 7 repetitive amino acid sequences (KTKEGV) in the N-terminal portion, by a central hydrophobic region (non-amyloid component, NAC) and by acidic stretches in the C-terminal tail. Mutations or overexpression of the human α-syn gene cause early-onset autosomal dominant Parkinson's disease (PD). α-Syn is the major component of Lewy bodies, the cytoplasmic proteinaceous aggregates pathognomonic for PD (Spillantini et al., 1998). The mechanism by which an abnormality in structure or expression of α-syn causes PD has not been elucidated. Despite the evidence for a key role of α-syn in the onset of PD, there is very little information about its physiological function in the brain.

Among several hypotheses, the role of α-syn is also associated to FAs. α-Syn seems to interact with unsatured and polyunsatured fatty acids (PUFAs), but it is not known if this interaction involves free FA molecules (Sharon et al., 2001), or aggregate states of FAs (micelles, vesicles, oil droplets) (Broersen et al., 2006; Lücke et al., 2006). Furthermore, this interaction promotes the oligomerization of α-syn. α-Syn forms

multimers *in vitro* upon exposure to vesicles containing certain PUFA acyl groups and this process occurs at physiological concentration (Perrin et al., 2001). Moreover, since exposure of neuronal cell lines to PUFA increases α-syn oligomer levels, the *in vivo* interaction of α-syn with PUFAs seems to promote the formation of soluble oligomers that precede the aggregates associated with neurodegeneration (Sharon et al., 2003).

First, a systematic study on the conformational transitions of α-syn in the presence of several fatty acids was conducted. Since the number of unsaturations and the length of the acyl chain have been shown to deeply affect the aggregate state of fatty acid (monomer, micelle, vesicle and oil droplet) and consequently, the interaction with the protein, the analysis was conducted using several fatty acids: palmitic acid (saturated), oleic acid (unsaturated), and docosahexaenoic acid (DHA, polyunsaturated). In particular, the last one is an essential omega-3 fatty acid, abundant in brain. DHA levels have been shown to be elevated in those brains areas containing α-syn inclusions in PD patients (Sharon et al., 2003). The FAs effects on α-syn structure were analyzed by far-UV circular dichroism and by proteolytic mapping. The protein is unfolded in the absence of FAs or in the presence of palmitic acid. Instead, upon binding to oleic acid (OA) and DHA, α-syn acquires α-helical conformation in a simple two-state transition. In the presence of DHA, α-syn is quite resistant to proteolysis by proteinase K and trypsin. We reported that the segment 70-90 in the NAC region is more susceptible to proteolytic attack than the N-terminal region. Probably, This region is flexible and sufficiently protruded to be protease-sensitive even if the analysis of CD spectra in the far-UV demonstrates that this region has an α-helix conformation and the NMR experiment indicates that only the C-terminal ~ 40 residues continue to be unfolded and mobile in the presence of DHA.

Furthermore, we observed that α-syn strongly affects the self-association process of DHA. The physical state of the lipid in the presence of the protein was analyzed by turbidity measurements, dynamic light scattering (DLS), pyrene fluorescence analysis and transmission electron microscopy (TEM). At pH 7.4, DHA assembles in oil droplets with a large size distribution (Namani et al., 2007). α-Syn disrupts these lipid aggregates, stabilizing a new product of DHA self-assembly. These species are formed at lower concentrations range and they have a regular shape, a smaller diameter and a reduced hydrophobic volume. Truncated forms of α-syn corresponding to different parts of its polypeptide chain (syn1-99, syn1-52, syn57-102, and syn108-140) were also used to

extend the knowledge on the role of different protein regions in the interaction with the lipid. CD data suggest that there is an important role of the repeats in the α-helix transition and thereby in the interaction with DHA. The C-terminal region, at variance, seems to modulate the portion of α-syn buried into the lipid compartment. Moreover, with the exception of syn 108-140, all the polypeptides affect the self-assembly process of DHA. We can hypothesize that the N-terminal region of α-syn has a crucial role even in the regulation of DHA aggregation process.

Finally, a general consideration concerns the ability of DHA and probably of other long chain PUFAs to induce oligomerization and fibrillation of α-syn (Perrin et al., 2001; Sharon et al., 2003; Broersen et al., 2006). The molecular effect of DHA on aggregation process of α-syn was analyzed by CD, native gel electrophoresis, Thioflavin T assay and TEM observation. The presence of DHA, in a molar ratio [DHA]/[α-syn] of 10, promotes aggregation and fibrils formation of α-syn. On the contrary, in the presence of saturating conditions of DHA, only oligomeric species are formed. DHA exerts a direct effect on protein structure, stabilizing an amyloidogenic conformation and generates an environment that can promote protein aggregation.

Sharon R., Goldberg M.S., Bar-Josef I., Betensky R.A., Shen J., Selkoe D.J. (2001). Alpha-Synuclein occurs in lipid-rich high molecular weight complexes, binds fatty acids, and shows homology to the fatty acid-binding proteins. *Proc. Natl. Acad. Sci. U S A.* **98**(16), 9110–9115.

Broersen K., van den Brink D., Fraser G., Goedert M., Davletov B. (2006). Alpha-synuclein adopts an alpha-helical conformation in the presence of polyunsaturated fatty acids to hinder micelle formation. *Biochem.* **45**(51), 15610–15616.

Chiti, F. and Dobson, C. M. (2006). Protein misfolding, functional amyloid, and human disease. *Annu. Rev. Biochem*., **75**, 333–366.

Lücke C., Gantz D. L., Klimtchuk E., Hamilton J. A. (2006). Interactions between fatty acids and alpha-synuclein. *J. Lipid Res.* **47**, 1714–1724.

Namani T., Ishikawa T., Morigaki K., Walde P. (2007). Vesicles from docosahexaenoic acid. *Colloids and Surfaces B: Biointerfaces.* **54**, 118–123.

Pawar, A. P., DuBay, K. F., Zurdo, J., Chiti, F., Vendruscolo, M. & Dobson, C. M. (2005). Prediction of “aggregation-prone” and “aggregation-susceptible” regions in proteins associated with neurodegenerative disease. *J. Mol. Biol.* **350**, 379–392.

Perrin R.J., Woods W.S., Clayton D.F., George J.M. (2001). Exposure to long chain polyunsaturated fatty acids triggers rapid multimerization of synucleins. *J. Biol. Chem*. **276**(45), 41958–41962.

Sharon R., Bar-Joseph I., Frosch M.P., Walsh D.M., Hamilton J.A., Selkoe D.J. (2003). The formation of highly soluble oligomers of alpha-synuclein is regulated by fatty acids and enhanced in Parkinson's disease. *Neuron*. **37**(4), 583–595.

Spillantini, M. G., Crowther, R. A., Jakes, R., Hasegawa, M. & Goedert, M. (1998). alpha-Synuclein in filamentous inclusions of Lewy bodies from Parkinson's disease and dementia with Lewy bodies. *Proc. Natl. Acad. Sci. U S A*, **95**, 6469–6473.

Chapter 1

Protein aggregation and amyloidosis

1.1 PROTEIN MISFOLDING DISEASES

A broad range of human diseases arises from the failure of a specific peptide or protein to adopt, or remain in, its native functional conformational state (Chiti and Dobson, 2006). These pathological conditions are generally referred to protein misfolding diseases. They include pathological states in which impairment in the folding efficiency of a given protein results in a reduction in the quantity of the protein that is available to play its normal role. This reduction can arise as the result of a posttranslational process, such as an increased probability of degradation via the quality control system of the endoplasmic reticulum, as occurs in cystic fibrosis (Amaral, 2004), or the improper trafficking of a protein, as seen in early-onset emphysema (Lomas & Carrel, 2002). The largest group of misfolding diseases, however, is associated with the conversion of specific peptides or proteins from their soluble functional states into highly organized fibrillar aggregates (Table 1.1). These structures are generally described as amyloid fibrils or plaques when they accumulate outside the cell. The term “intracellular inclusions” has been suggested as more appropriate when fibrils morphologically and structurally related to extracellular amyloid form inside the cell (Westermark et al., 2005).

Current interest in studying amyloid fibrils arises from their involvement in different fields. First, they play a crucial role in disorders such as Alzheimer’s and Parkinson’s diseases. Second, since it has been proved that all polypeptide chains form this kind of fibrils under appropriate conditions, the understanding of why and how this process happen has become central problem in protein knowledge. Last, the ordered ultrastructure characterizing amyloid fibrils may be thought as a basis for nanomaterials with possible technological applications (Cherny & Gazit, 2008). However, despite the ability of most proteins to form amyloid fibrils, very little is known about their structures and the factors that govern their formation.

Table 1.1 Human diseases associated with formation of extracellular amyloid deposits or intracellular inclusions with amyloid-like characteristics (Chiti & Dobson, 2006)

Disease	Aggregating protein or peptide	Native structure of protein or peptide
Neurodegenerative diseases		
Alzheimer's disease	Amyloid β peptide	Natively unfolded
Spongiform encephalopathies	Prion protein or fragments thereof	Natively unfolded (residues 1-120) and α-helical (residues 121-230)
Parkinson's disease	α-synuclein	Natively unfolded
Dementia with Lewy bodies	α-synuclein	Natively unfolded
Frontotemporal dementia with Parkinsonism	Tau	Natively unfolded
Amyotrophic lateral sclerosis	Superoxide dismutase I	All-β, Ig like
Huntington's disease	Huntingtin with polyQ expansion	Largely natively unfolded
Spinocerebellar ataxia	Ataxins with polyQ expansion	All-β, AXH domain (residues 562-694); the rest are unknown
Spinocerebellar ataxia 17	TATA box-binding protein with polyQ expansion	α+β, TBP like (residues 159-339); unknown (residues 1-158)
Spinal and bulbar muscular atrophy	Androgen receptor with polyQ expansion	All-α, (residues 669-919); the rest are unknown
Hereditary dentatorubral-pallidoluysian atrophy	Atrophin-1 with polyQ expansion	Unknown
Familial British dementia	ABri	Natively unfolded
Familial Danish dementia	ADan	Natively unfolded
Nonneuropathic systemic amyloidosis		
AL amyloidosis	Immunoglobulin light chains or fragments	All-β, Ig like
AA amyloidosis	Fragments of serum amyloid A protein	All-α, unknown fold
Familial Mediterranean fever	Fragments of serum amyloid A protein	All-α, unknown fold
Senile systemic amyloidosis	Wild-type transthyretin	All-β, prealbumin like
Familial amyloidotic polyneuropathy	Mutants of transthyretin	All-β, prealbumin like
Hemodialysis-related amyloidosis	β2-microglobulin	All-β, Ig like
ApoAI amyloidosis	N-terminal fragments of apolipoprotein AI	Natively unfolded
ApoAII amyloidosis	N-terminal fragments of apolipoprotein AII	Unknown
ApoAIV amyloidosis	N-terminal fragments of apolipoprotein AIV	Unknown
Finnish hereditary amyloidosis	Fragments of gelsolin mutants	Natively unfolded
Lysozyme amyloidosis	Mutants of lysozyme	α+β, lysozyme fold
Fibrinogen amyloidosis	Variants of fibrinogen α-chain	Unknown
Icelandic hereditary cerebral amyloid angiopathy	Mutant of cystatin C	α+β, cystatin like
Nonneuropathic localized diseases		
Type II diabetes	Amylin,also called islet amyloid poltpeptide (IAPP)	Natively unfolded
Medullary carcinoma of the tyroid	Calcitonin	Natively unfolded
Atrial amyloidosis	Atrial natriuretic factor	Natively unfolded
Hereditary cerebral haemorrhage with amyloidosis	Mutants of amyloid β peptide	Natively unfolded
Pituitary prolactinoma	Prolactin	All-α, 4-helical cytokines
Injection-localized amyloidosis	Insulin	All-α, insulin like
Aortic medial amyloidosis	Medin	Unknown
Hereditary lattice corneal dystrophy	Mainly C-terminal fragments of kerato-epithelin	Unknown
Corneal amyloidosis associated with trichiasis	Lactoferrin	α+β, periplasmic-binding protein like II
Cataract	γ-Crystallins	All-β, γ-crystallin like
Calcifying epithelial odontogenic tumors	Unknown	Unknown
Pulmonary alveolar proteinosis	Lung surfactant protein C	Unknown
Inclusion-body myositis	Amyloid β peptide	Natively unfolded
Cutaneous lichen amyloidosis	Keratins	Unknown

1.2 AMYLOID DISEASES AND AMYLOID FIBRIL STRUCRURE

A number of human diseases, including amyloidosis and many other neurodegenerative diseases, originate from the deposition of stable, ordered, filamentous protein aggregates, commonly referred to as amyloid fibrils. In each of these pathological states, a specific protein or protein fragment changes from its natural soluble form into insoluble fibrils, which accumulate in a variety of organs and tissues (Kelly, 1998; Dobson, 1999; Rochet & Lansbury, 2000). In Table 1.1 it is reported a list of diseases that are associated with the formation of extracellular amyloid fibrils or intracellular inclusions. The proteins primarily involved in these diseases are unrelated in terms of sequence or structure. Prior to fibrillation, amyloidogenic polypeptides may be rich in beta-sheet, alpha-helix, beta-helix, or contain both alpha-helix and beta-sheets (Fig.1.1 A). They may be globular proteins with rigid 3D-structure or belong to the class of natively unfolded (or intrinsically unstructured) proteins (Wright and Dyson, 1999; Uversky, 2002). Despite these differences, the fibrils from different pathologies display many common properties (Fig. 1.1 B, C). They have similar morphologies when observed with atomic force microscopy (AFM) or transmission electron microscopy (TEM). Typically mature fibrils consist of two to six unbranched protofilaments, 2-5 nm in diameter, associated laterally or twisted together to form fibrils with 7-13 nm diameter (Fändrich, 2007). Amyloid fibrils have a core cross-beta-sheet structure: within individual protofilaments a β-sheet structure is present, characterized by β-strand running parallel to each other and perpendicular to the axis of the fibrils. This repeated structure has a distinct X-ray diffraction pattern. The meridional reflection at 4.7-4.8 Å results from the interstrand repeats (the inter beta-strand distance), and the 10-11 Å equatorial reflection arises from intersheet packing (Fig. 1.1 C). Finally, the fibrils have the ability to bind specific dyes such as Thioflavin T (ThT) and Congo Red. However, it is difficult to obtain high-resolution structures of amyloid fibrils as these species are insoluble and non-crystalline. Recent advances in cryo-electron microscopy (cryoEM), solid state NMR (ssNMR), electron paramagnetic resonance (EPR) and X-ray crystallography are now provide detailed information on the fibril architecture both about the local structural order and about the overall fibril morphology, including the packing of protofilaments. Recently, for α-synuclein, the protein involved in Parkinson's disease, it was proposed a structural model for its mature amyloid fibrils by using the data obtained by ssNMR, hydrogen-deuterium exchange by NMR and high resolution cryoEM (Vilar et al., 2008).

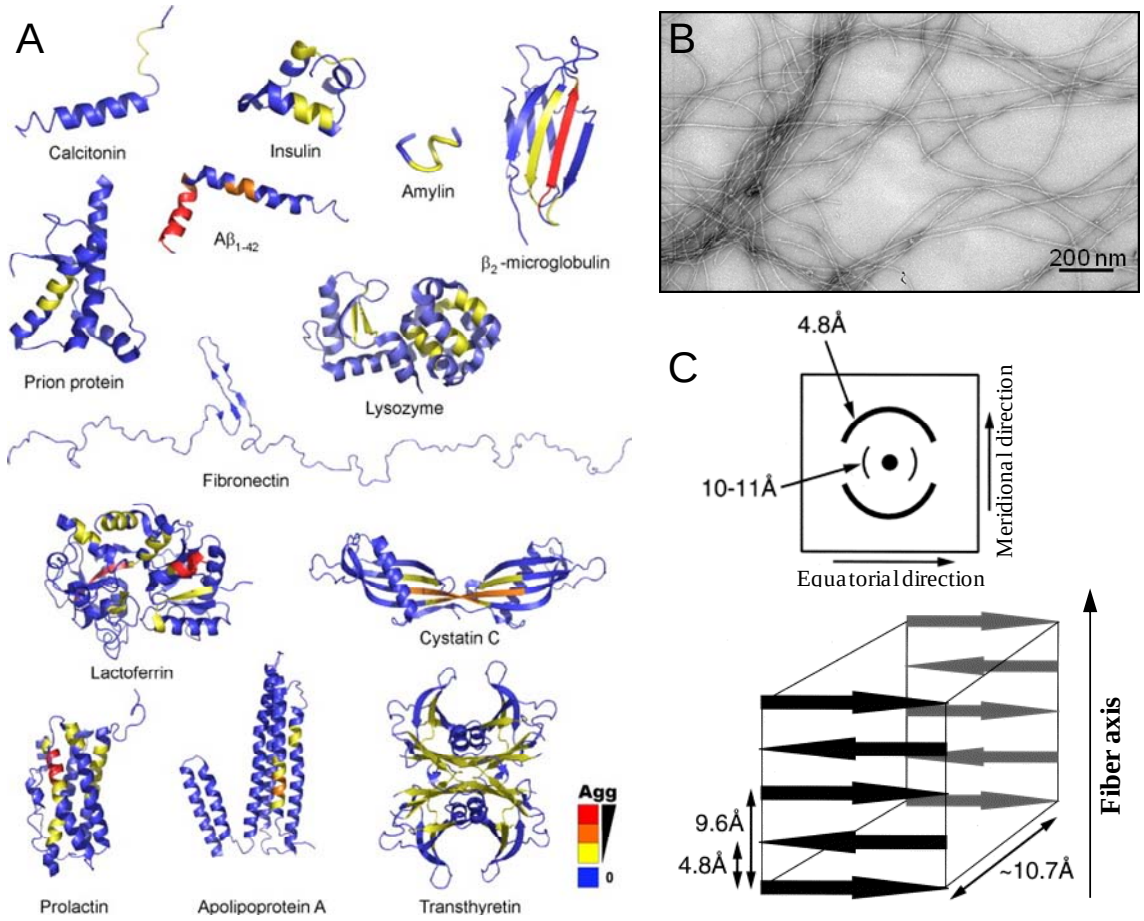

Fig. 1.1 (A) Representative structures of proteins involved in disease-related amyloid fibril formation (reprinted from Jahn & Radford, 2008). **(B)** Fibrils have a long and unbranched morphology. **(C)** Fibrils show a cross-β structure. This scheme represents the typical appearance of fibrils when analyzed by X-ray fibre diffraction (reprinted from Serpell, 2000)

The proposed fold (Fig.1.2) comprises a five-layered β1–loop– β2–loop–β3–loop– β4–loop– β5 β-sandwich, which, when incorporated into a protofilament of a fibril, generates five layers of parallel, in-register β-sheets. In the straight fibril type, two protofilaments align with each other to form a fibril, which can align again itself. In the twisted fibrils two protofilaments twist around each other, and such a twisted filament twists again with another one.

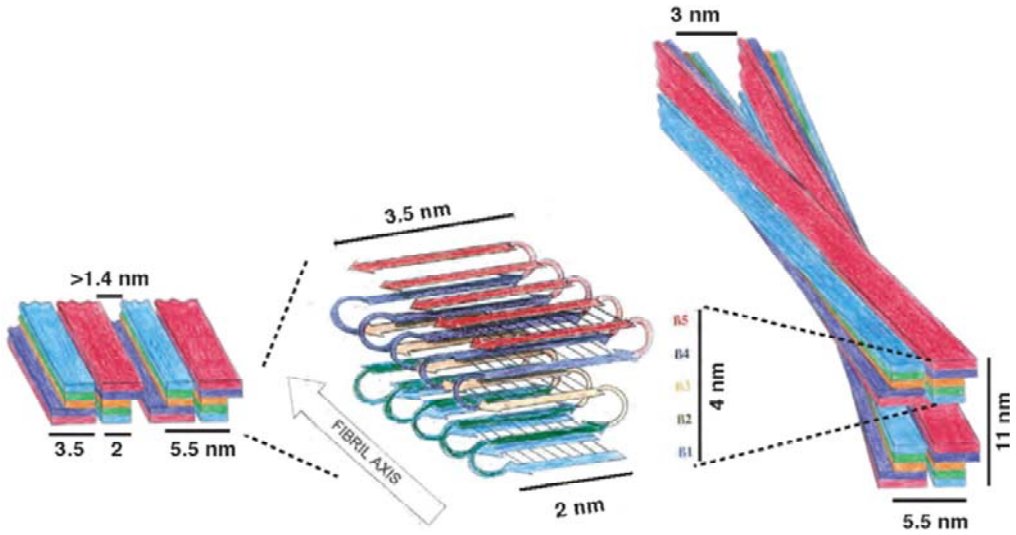

Fig. 1.2 α-Syn fibrils structure consistent with the experimental data obtained by ssNMR, hydrogen-deuterium exchange by NMR and high resolution cryoEM. The proposed fold of a monomeric α-syn within a protofilament is shown in *Center*. The incorporation of a protofilament into the straight (*Left*) and twisted (*Right*) fibril type is indicated by a schematic drawing (reprinted from Vilar et al., 2008).

Amyloid fibrils have been formed *in vitro* from disease-associated as well as from disease-unrelated proteins and peptides (Table 1.2). Moreover, there is an increasing belief that the ability to form fibrils is a generic property of the polypeptide chain, i.e. many proteins, perhaps all, are potentially able to form amyloid fibrils under appropriate conditions (Dobson, 1999, 2001; Fändrich et al., 2001).

Table 1.2 Non-disease-related amyloidogenic proteins and peptides

Protein (peptide)	Type of structure	Protein (peptide)	Type of structure
Betabellins 15D and 16D	β -Sandwich	Prothymosin a	Natively unfolded
Cytochrome c552	α-Helical	Myoglobin	α-Helical
Methionine aminopeptidase	α-Helical	Muscle acylphosphatase	α/β
Phosphoglycerate kinase	α/ β	Hen egg white lysozyme	α + β
Hen egg white lysozyme, β-domain	β-Sheet	Acidic fibriblast growth factor	β-Barrel
PI3-SH3 domain	β-Barrel	OspA protein, BH9–10 peptide	β-Turn
β-Lactoglobulin	β-Sheet (predominantly)	De novo ata peptide	α-Helix-turn-a-helix
Monellin	α/β	Lung surfactant protein C	α-Helix
Immunoglobulin light chain LEN	β-Sheet	α-Lactalbumin	α + β
HypF, N-terminal domain	α/ β	VL domain of mouse antibody F11	β-Sheet
Human complement receptor 1, 18– 34 fragment	Unfolded	Apolipoprotein C-II	Natively unfolded
Human stefin B	α/ β	Cold shock protein A	β-Barrel
GAGA factor	Natively unfolded	Protein G, B1 Ig-binding domain	Four-stranded β-sheet with a flanking α-helix
Yeast prion Ure2p	α- Helical/unfolded	Cold shock protein B, 1 –22 fragment	Unfolded
Herpes simplex virus glycoprotein B fragment	β-Structural	De novo proteins from combinatorial library	β-Structural
The fiber protein of adenovirus, 355–396 peptide from shaft	Fibrillar	Soluble homopolypeptides: poly-L-lysine poly-L-glutamic acid poly-L-threonine	Unordered

1.3 MECHANISMS OF AMYLOID FIBRIL FORMATION

Amyloid fibrils are formed in a nucleation-dependent manner, in which the protein monomer is converted into a fibrillar structure *via* a transiently populated aggregation nucleus (Harper & Lansbury, 1997). After the rate limiting step of nucleus formation, aggregates growth proceeds rapidly by addition of monomers or other assembly competent species. The first stage is thermodynamically unfavorable; on the contrary the elongation phase is highly favored. Indeed, in order to generate long-range interactions in such structures, a critical number of molecules must be present such that the favorably enthalpic terms, associated with their regular stacking, can mostly offset the accompanying loss of configurational entropy.

Recently, numerous studies have identified and characterized several intermediate structures populated during fibril formation, including soluble oligomers and protofibrils (spherical or annular particles and worm-like fibrils) (Lashuel et al., 2002). These prefibrillar species have been shown to be the most toxic for the cells (Bucciantini et al., 2002). However in some cases, oligomeric species have been suggested to be the direct precursors of mature fibrils, whilst in other cases, an off-pathway role has been proposed (Jahn & Radford, 2008; Necula et al., 2007).

To explain the molecular basis of amyloid fibril formation, it is important to elucidate which are the conformational states that can be the starting point for the aggregation. For globular proteins, it has been proposed that fibrillation can occur when the rigid native structure of a protein is destabilized, favoring partial unfolding and culminating in the formation of a partially unfolded conformation or intermediate (Rochet and Lansbury, 2000; Fink, 1998; Dobson, 2001). In fact, since all fibrils, independently of the original structure of the amyloidogenic protein, have a common cross-beta-structure, considerable protein conformation rearrangements have to occur to form fibrils. Such changes cannot take place in the typical tightly packed native protein conformation, due to the constraints of the tertiary structure. Thus, formation of non-native partially unfolded conformation is required. Presumably, such a partially unfolded conformation enables specific intermolecular interactions, including electrostatic attraction, hydrogen bonding and hydrophobic contacts, which are necessary for oligomerization and fibrillation (Fink, 1998). This model, however, cannot directly apply to intrinsically unstructured (natively unfolded) proteins, as they are devoid of secondary structure. Indeed, the primary step of their fibrillogenesis has been shown to be the stabilization of a partially folded conformation. Partial folding rather than unfolding occurs in natively

unfolded proteins (Uversky et al., 2001; Uversky et al., 2004). Although the "conformational change hypothesis" can account for the aggregation properties of many proteins, both globular and intrinsically disordered proteins, recent observations suggest that the aggregation of some globular proteins could occur *via* formation of native-like oligomers (Plakoutsi et al, 2005). For example, formation of amyloid-like fibrils of insulin at low pH is preceded by an oligomerization step in which a native-like α-helical content is retained, while β-sheet rich aggregates form only later on (Bouchard et al., 2000).

In conclusion, the different features of the aggregation processes, described in this section, reveal that polypeptide chains can adopt a multitude of conformational states and interconvert between them on a wide range of timescales. The network of equilibria, which link some of the most important of such states is schematically illustrated in Fig. 1.3 (Chiti and Dobson, 2006). Following biosynthesis on a ribosome, a polypeptide chain is initially unfolded. It can then populate a wide distribution of conformations, each of which contains little persistent structure, as in the case of natively unfolded proteins, or fold to a unique compact structure, often through one or more partly folded intermediates. In such a conformational state, the protein can remain as a monomer or associate to form oligomers or higher aggregates, some of which are functional with characteristics far from those of amyloid structures, such as in actin, myosin, and microtubules. Finally, the vast majority of proteins will be degraded, usually under very carefully controlled conditions as part of normal biochemical processes, with their amino acids often being recycled.

However, fully or partially unfolded ensembles on the pathways to their functional states (or generated as a result of stress, chemical modification, or genetic mutation) are particularly vulnerable to aggregation. Furthermore, peptides and proteins that are natively unfolded, as well as fragments of proteins generated by proteolysis and unable to fold in the absence of the remainder of the polypeptide chain, can also aggregate under some circumstances, for examples, if their concentrations become elevated. Some of the initial amorphous aggregates simply dissociate again, but others may reorganize to form oligomers and protofibrils that precede the amyloid fibril formation. The structured polypeptide aggregates can then sometimes grow into mature fibrils by further self-association or through the repetitive addition of monomers. Also proteins that adopt a folded structure under physiological conditions could aggregate. This latter type of

proteins can either unfold, fully or partially, and aggregate through the mechanism described above or they could oligomerize prior to such a substantial conformational change, forming native-like prefibrillar assembly.

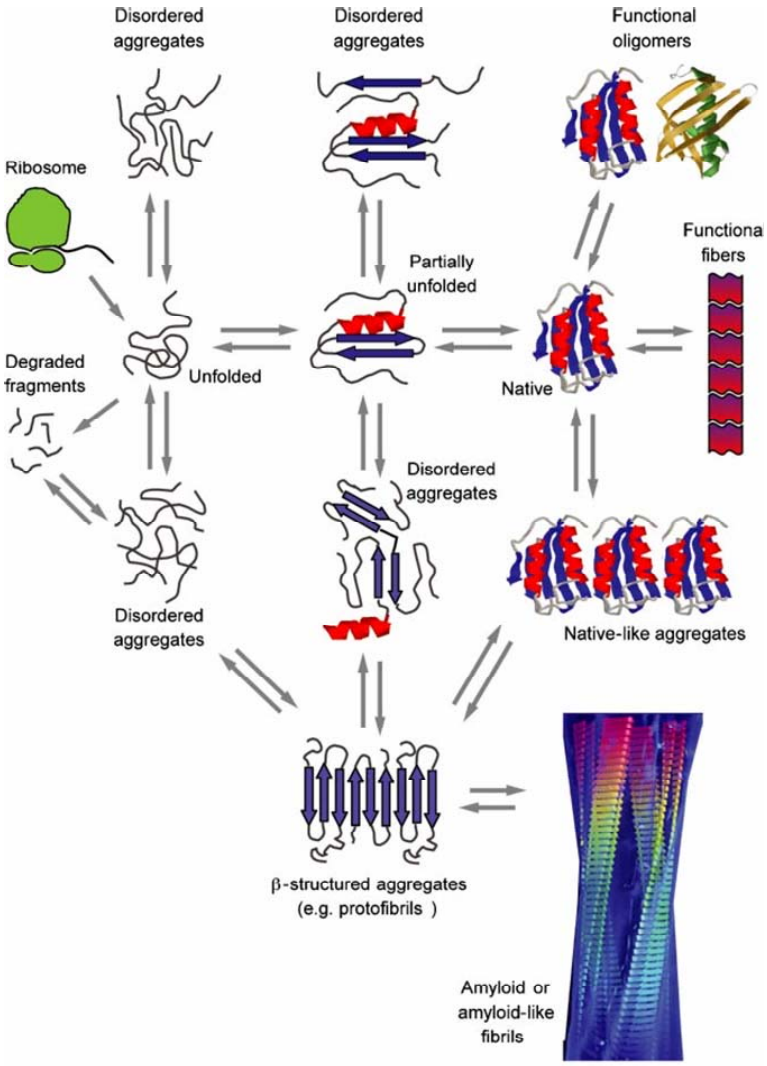

Fig. 1.3 Different conformational states can be populated by a polypeptide chain (reprinted from Chiti & Dobson, 2006). All of these different conformational states and their interconversions are carefully regulated in the biological environment, by using machinery such as molecular chaperones, degradatory systems, and quality control processes. Conformational diseases, in particular amyloid diseases, will occur when such regulatory systems fail. The several pathways that can result in amyloid fibrils formation are reported in the bottom of the figure.

1.4 REFERENCES

Amaral, M. D. (2004). CFTR and chaperones: processing and degradation. *J Mol Neurosci.*, **23**, 41–48.

Bouchard, M., Zurdo, J., Nettleton, E. J., Dobson, C. M., Robinson, C. V. (2000). Formation of insulin amyloid fibrils followed by FTIR simultaneously with CD and electron microscopy. *Protein Sci*., **9**, 1960–1967.

Bucciantini, M., Giannoni, E., Chiti, F., Baroni, F., Formigli, L., Zurdo, J., Taddei, N., Ramponi, G., Dobson, C. M., Stefani, M. (2002). Inherent toxicity of aggregates implies a common mechanism for protein misfolding diseases. *Nature*, **416**, 507–511.

Chiti, F. and Dobson, C. M. (2006). Protein misfolding, functional amyloid, and human disease. *Annu. Rev. Biochem.*, **75**, 333–366.

Cherny, I., Gazit, E. (2008). Amyloids: not only pathological agents but also ordered nanomaterials. *Angew. Chem. Int. Ed. Engl.*, **47**, 4062–4069.

Dobson, C. M. (1999). Protein misfolding, evolution and disease. *Trends Biochem. Sci.*, **24**, 329–332.

Dobson, C. M. (2001). Protein folding and its links with human disease. *Biochem. Soc. Symp.* 1–26.

Dobson, C. M. (2001). The structural basis of protein folding and its links with human disease. *Philos. Trans. R. Soc. Lond., B Biol. Sci.*, **356**, 133–145.

Fändrich, M. (2007). On the structural definition of amyloid fibrils and other polypeptude aggregates. *Cell. Mol. Life Sci.*, **64**, 2066–2078.

Fändrich, M., Fletcher, M. A., Dobson, C. M. (2001). Amyloid fibrils from muscle myoglobin. *Nature*, **410**, 165–166.

Fink, A. L. (1998). Protein aggregation: folding aggregates, inclusion bodies and amyloid. *Fold. Des.*, **3**, 9–15.

Harper, J. D., Lansbury, P. T. Jr. (1997). Models of amyloid seeding in Alzheimer's disease and scrapie: mechanistic truths and physiological consequences of the time-dependent solubility of amyloid proteins. *Annu. Rev. Biochem.*, **66**, 385–407.

Jahn, T. R., Radford, S. E. (2008). Folding versus aggregation: polypeptide conformations on competing pathways. *Arch. Biochem. Biophys.*, **469**, 100–117.

Kelly, J. W. (1998). The alternative conformations of amyloidogenic proteins and their multi-step assembly pathways. *Curr. Opin. Struct. Biol.*,**8**, 101–106.

Lashuel, H. A., Hartley, D., Petre, B. M., Walz, T., Lansbury, P. T. Jr. (2002). Neurodegenerative disease: amyloid pores from pathogenic mutations. *Nature*, **418**, 291.

Lomas, D. A. and Carrell, R. W. (2002). Serpinopathies and the conformational dementias. *Nat. Rev. Genet*., **3**, 759–768.

Necula, M., Kayed, R., Milton, S., Glabe, C. G. (2007). Small molecule inhibitors of aggregation indicate that amyloid beta oligomerization and fibrillization pathways are independent and distinct. *J. Biol. Chem*., **282**, 10311–10324.

Plakoutsi, G., Bemporad, F., Calamai, M., Taddei, N., Dobson, C. M., Chiti, F. (2005). Evidence for a mechanism of amyloid formation involving molecular reorganisation within native-like precursor aggregates. *J. Mol. Biol*., **351**, 910–922.

Rochet, J. C. and Lansbury, P. T. Jr. (2000). Amyloid fibrillogenesis: themes and variations. *Curr. Opin. Struck. Biol*., **10**, 60–68.

Serpell, L. C. (2000). Alzheimer's amyloid fibrils: structure and assembly. *Biochim Biophys Acta.*, **1502**, 16–30.

Uversky, V. N. (2002). Natively unfolded proteins: a point where biology waits for physics. *Protein Sci*., **11**, 739–756.

Uversky, V. N., Fink, A. L. (2004). Conformational constraints for amyloid fibrillation: the importance of being unfolded. *Biochim Biophys Acta*., **1698**, 131–153.

Uversky, V. N., Li, J., Fink, A. L. (2001). Evidence for a partially folded intermediate in alpha-synuclein fibril formation. *J. Biol. Chem*., **276**, 10737–10744.

Vilar, M., Chou, H. T., Lührs, T., Maji, S. K., Riek–Loher, D., Verel, R., Manning, G., Stahlberg, H., Riek, R. (2008) The fold of alpha-synuclein fibrils. *Proc. Natl. Acad. Sci. U S A*, **105**, 8637–8642.

Westermark, P., Benson, M. D., Buxbaum, J. N., Cohen, A. S., Frangione, B., Ikeda, S., Masters, C. L., Merlini, G., Saraiva, M. J., Sipe, J. D. (2005). Amyloid: toward terminology clarification. *Amyloid*., **12**, 1–4.

Wright, P. E. and Dyson, H. J. (1999). Intrinsically unstructured proteins: reassessing the protein structure-function paradigm. *J. Mol. Biol*., **293**, 321–331.

Chapter 2

Role of the electrostatic interactions in the formation and stabilization of fibrillar aggregates

2.1 INTRODUCTION

2.1.1 Net charge as a determinant in protein fibrillogenesis

A wide range of human diseases is associated with the conversion of specific peptides or proteins from their soluble state into highly organized aggregates known as amyloid fibrils (Stefani et al., 2003). It has been demonstrated that under appropriate conditions many, if not all, polypeptide chains can form amyloid-like fibrils (Guijarro et al., 1998), but it is clear that they show different propensities. Therefore, an understanding of the parameters that modulate the aggregation propensity of a polypeptide chain and the mechanism of fibrils formation is fundamental to gain insight into the pathogenesis of protein diseases and for a general knowledge of the process of amyloid formation.

A determinant factor in the aggregation process of an unfolded polypeptide chain is the hydrophobicity of its side chains. Amino acid substitutions within regions of the sequence, crucial for the aggregative behavior of the whole sequence, can reduce the aggregation propensity when they decrease the hydrophobicity at the site of mutation (Otzen et al., 2000; Calamai et al., 2003; Chiti et al., 2006). A low propensity to form α-helical structure and a high propensity to form β-sheet structure are also likely to be important factors for amyloid formation. Indeed, it has been shown that several proteins forming amyloid structures under physiological conditions present an α-helix in a segment that has a high propensity to form a β-strand according to secondary structure predictions (Kallberg et al., 2001; Villegas et al., 2000). It was also suggested that the presence of aromatic residues, particularly phenylalanine and tyrosine, promotes amyloid formation and stabilizes the resulting amyloid fibrils by a π-stacking interaction (Gazit, 2002; Porat et al., 2004).

Another property likely to be a key factor in protein aggregation is the charge, since a high net charge either globally or locally may hinder the protein self-association. Numerous observations indicate that the electrostatic interactions play an important role in the formation and stabilization of fibrillar aggregates. Ribonuclease Sa, for example, forms ThT-positive and β-sheet containing aggregates in the presence of denaturing concentrations of trifluoroethanol (Schmittschmitt and Scholtz, 2003). The minimum solubility of the trifluoroethanol-denatured protein was observed at a pH value corresponding to the isoionic point (pI) of ribonuclease Sa, when the protein has a net charge of zero. Two variants of ribonuclease Sa, having respectively 3 and 5 solvent-exposed acidic residues replaced by lysine (3K and 5K RNase Sa), displayed different profiles of protein solubility versus pH, but in both cases the pH of minimum solubility equaled the pI. This result indicates that amyloid aggregation of ribonuclease Sa is most favored under conditions in which the net charge of the protein molecules is equal to zero and the electrostatic repulsion is minimized. Along the same lines, the effects of single amino acid substitutions were investigated on the propensity of human muscle acylphosphatase, partially unfolded in trifluoroethanol, to aggregate. Mutations decreasing the positive net charge of the protein resulted in an accelerated formation of β-sheet containing aggregates able to bind CR and ThT, whereas mutations increasing the net charge resulted in the opposite effect (Chiti et al., 2002). Further indications of the importance of the charge in protein aggregation derive from observations on α-synuclein. At neutral pH α-synuclein has a high negative net charge due to the presence of several acidic residues in the C-terminal region. Deletions of the C-terminal segment cause fibril formation to be accelerated, with the acceleration being proportional to the extent of the truncation (Hoyer et al. 2004). Acceleration of fibril formation by full-length α-synuclein at neutral pH can also be achieved by polyamines having a high positive compensatory charge, such as spermine, or small cations such as Na^+ or Mg^{2+} (Hoyer et al., 2004). The relevance of electrostatic interactions in amyloid fibril formation is not limited to the chemistry of the process, as it clearly has implications for the pathogenesis of diseases arising from amyloid aggregation. It was shown that many mutations associated with familial forms of protein deposition diseases are pathogenic because they decrease the net charge of the protein forming the deposits in each specific case (Chiti et al., 2002).

The aim of this study is to investigate further the role of the net charge in the aggregation process of unfolded proteins and to analyze the importance of electrostatic

interaction in the stability of the resulting fibrils. For this purpose a peptide model derived from the N-terminal region of apomyoglobin, spanning the first 29 residues ($ApoMb_{1-29}$) was used (Fig. 2.1).

2.1.2 $ApoMb_{1-29}$, a peptide model

In this study, the peptide $apoMb_{1-29}$ is a suitable experimental model as it is unstructured and does not form a folded conformation in any condition investigated. Moreover it has a high ratio of acidic versus basic residues (Fig. 2.1), so it has a high negative net charge at neutral pH and a low net charge at acidic pH. This peptide was obtained by limited proteolysis of horse hearth apomyoglobin by pepsin. Previous studies on the independent propensity to aggregate of segments corresponding to different regions of the polypeptide chain of apoMb had demonstrated that the N-terminal region is highly prone to aggregate.

Myoglobin (Mb) is a full α-helical protein of 153 residues. The three-dimensional structure of sperm-whale myoglobin was solved in 1958 by Kendrew and co-workers and it was shown that this protein has a relatively simple and compact globular structure. The polypeptide chain of Mb is organized in 8 α-helical segments (designated helix A to H). Amino acid residues packed into the interior of the molecule have predominantly hydrophobic character, while those exposed on the surface are generally hydrophilic, thus making the molecule readily soluble in water, and making it a perfect model of globular proteins structure. The heme group is inserted in a hydrophobic cleft of the protein, in close contact with helices E and F (Kendrew et al., 1958; Jennings & Wright, 1993; Nishimura et al., 2002). Mb is an oxygen carrier protein, mainly found within striated and cardiac myocites. Mb was proposed to act as an oxygen storage protein, releasing the ligand to mitochondria upon periods of oxygen deprivation or intense metabolism, to support oxidative energy production. It was demonstrated that apoMb, even if it is not involved in any amyloid disorder, can aggregate and forms fibrillar structures under strong denaturant conditions (Fändrich et al., 2001). Moreover, the aggregation process can be selectively modulated changing the grade of unfolding of the polypeptide chain (Fändrich et al., 2003). In the same work, it was shown that the segment corresponding to G helix in the polypeptide chain of native Mb could be relevant in the α→β transition of the molecule during aggregation. Other studies demonstrated that the substitution of Trp residues in position 7 and 14 by Phe induces apoMb aggregation *in vitro* under

physiological conditions (Sirangelo et al., 2002). Moreover, early pre-fibrillar aggregates from mutated apoMb show cytotoxic activity on fibroblast cells (Sirangelo et al., 2004), in analogy with other amyloid-forming proteins (Bucciantini et al., 2002). W7FW14F apoMb fibrils elongation, but not their toxicity, can be inhibited by antibiotics such as tetracycline (Malmo et al., 2005). In conclusion, since Mb is a completely α-helix protein, it should be substantially destabilized in order to aggregate. However, Yoon & Welsh (2005) identified by an algorithm the regions 27-33 and 66-72 of the polypeptide chain of apoMb as "hidden regions" with the strongest propensity to form β-strand. These authors indicate also regions 10-19, 101-108 and 111-118, as potential amyloidogenic. More recently, prediction of aggregation profiles of globular proteins identified in Mb four region with a high intrinsic aggregation propensity (9-12, 31-33, 65-70 ad 108-118) (Tartaglia et al, 2008). However these regions that are the most amyloidogenic are not those with a low structural protection in the native state. This result provides an example of how native states of proteins have evolved to avoid aggregation.

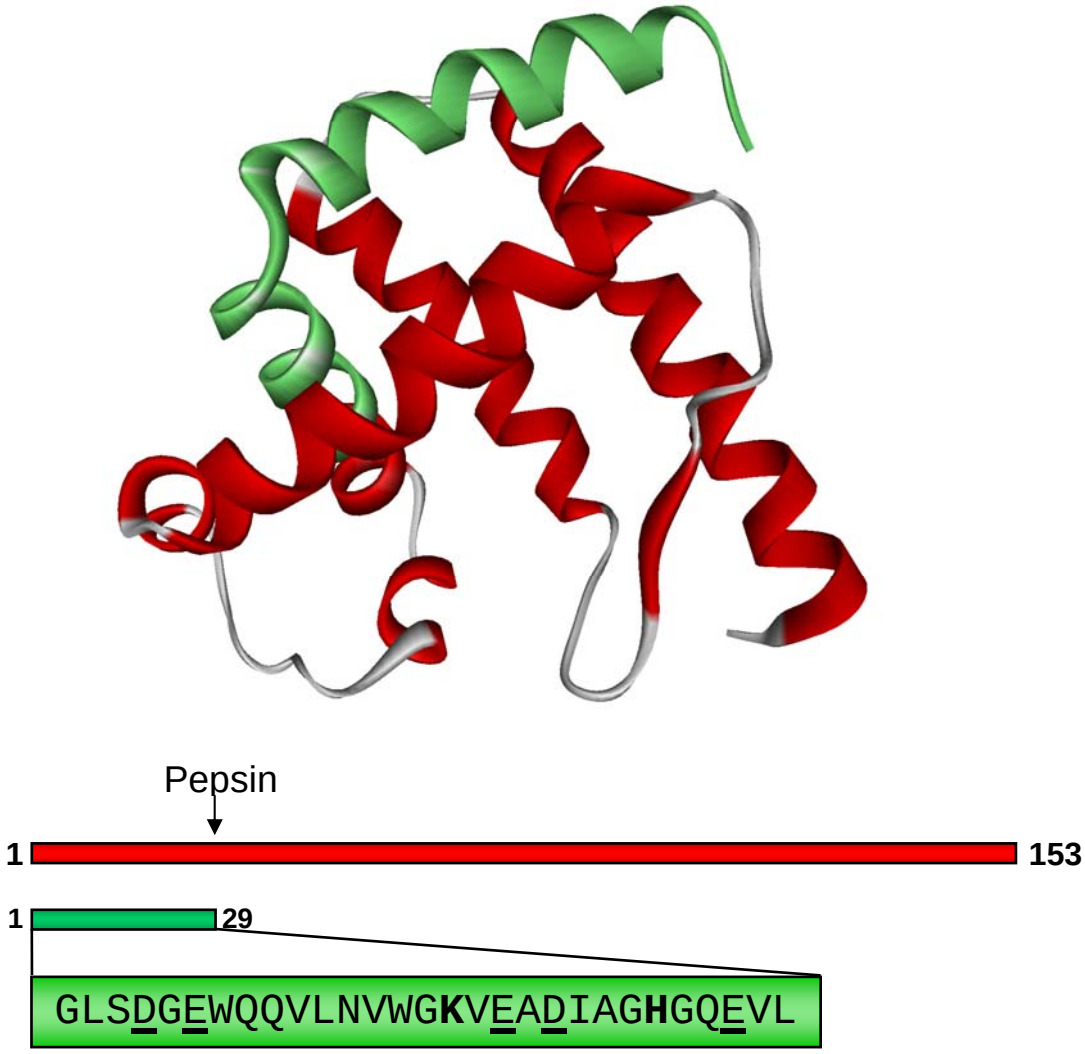

Fig. 2.1 (A) Three dimensional structure of horse heart apo-myoglobin taken from the Brookhaven Protein Data Bank (PDB file 1DWR), utilizing the program WebLab (Molecular Simulations Inc.). The model was obtained by Chu and coworkers from the X-ray diffraction analysis (Chu et al., 2000). Chain segment $apoMb_{1\text{-}29}$ is colored in green. **(B)** Schematic representation of the $apoMb_{1\text{-}29}$ fragment resulting from proteolysis of apomyoglobin (apoMb). In the sequence of $apoMb_{1\text{-}29}$ the acidic residues are underlined and the basic are bold.

2.2 EFFECT OF PH IN APOMB$_{1-29}$ FIBRIL FORMATION AND IDENTIFICATION OF THE MOST AMYLOIDOGENIC REGION

2.2.1 Materials and Methods

Materials

Horse heart myoglobin, porcine pepsin, trypsin from bovine pancreas, pepstatin A and thioflavin-T (ThT) were purchased from the Sigma Chemical Company (St. Luis, MO), whereas V8-protease (endoproteinase Glu-C) from *Staphylococcus aureus*, acetonitrile and triluoroacetic acid (TFA) from Fluka (Buchs, Switzerland). All other chemicals were of analytical reagent grade and were obtained from Sigma or Fluka. Apomyoglobin (apoMb) was obtained from holomyoglobin by removal of heme by the acetone extraction procedure (Ascoli et al., 1981). The possible contamination of apomyoglobin by heme was assessed checking the absorbance spectrum in the UV-vis region.

Preparation and purification of apomyoglobin fragments

Peptide apoMb$_{1-29}$ was produced by limited proteolysis of apoMb by pepsin (Fruton, 1970). Digestion was conducted at 25°C by incubating apoMb (2 mg/ml) in 0.01 M HCl, pH 2.0, at an E/S ratio of 1:100 (by weight). The reaction was stopped after 90 sec adding pepstatin A (1mg/ml) at an E/I ratio of 1:5 (by weight). The fragment was purified by hydrophobic interaction chromatography (HIC) using a Resource^{TM} Phe column (Amersham Bioscience, Uppsala, Sweden), eluted with a step gradient of 0.01 M HCl, 10 mM Tris-HCl and 6M Gnd·HCl at a flow rate of 1 ml/min. The effluent from the column was monitored at 280 nm. Further purification was obtained by RP-HPLC, using an Eclipse XDB-C$_8$ column (4.6 × 150 mm) (Zorbax Columns, USA) eluted with a linear gradient of acetonitrile, containing 0.1 % (v/v) TFA, from 5% to 40% in 5 min and from 40% and 60% in 25 min at a flow rate of 0.8 ml/min. Sub-fragments 1-16, 17-29, 7-18 and 7-16 were produced by proteolysis of peptide apoMb$_{1-29}$, in particular the complementary fragments 1-16 and 17-29 were prepared by trypsin digestion (Young, 1961) (E/S ratio of 1:100), whereas fragments 7-16 and 7-18 by proteolysis with trypsin and V8-protease (for both, E/S ratio of 1:50). Proteolysis were conducted at 37°C by incubating fragment 1-29 (0.2-0.3 mg/ml), in 10 mM Tris-HCl buffer, pH 8.0-8.5 for 24 hours with the proteases. Fragments were purified by RP-HPLC using an Eclipse XDB-

C_8 column (4.6 × 150 mm) (Zorbax Columns, USA) eluted with a linear gradient of acetonitrile, containing 0.1% (v/v) TFA from 5% to 60% in 30 min at a flow rate of 0.8 ml/min. The effluent was monitored by recording the absorbance at 226 nm. The identity of all fragments was assessed by mass-spectrometry. Electrospray ionization (ESI) mass spectrometry (MS) analysis of protein material was carried out on a Q-Tof Micro spectrometer (Micromass, Manchester, UK).

Aggregation and amyloid fibrils formation

Aggregation and fibrils formation were carried out incubating lyophilized fragments in 10 mM Tris-HCl at 37°C, adjusting the pH value with 1M HCl or 1M Tris, in order to follow the aggregation process under several pH conditions. The peptide solutions were clarified with 0.22 μm Millex®-GV filter (Millipore Corporation, Bedford, MA, USA) to eliminate soluble oligomers that could affect the aggregation process. For all fragments a peptide concentration of 0.2 mg/ml was used.

Spectroscopic measurements

CD spectra were recorded at 25°C with a Jasco J-710 spectropolarimeter (Tokyo, Japan) equipped with a thermostatically controlled cell holder. The instrument was calibrated with *d*-(+)10-camphorsulfonic acid. Quartz cells with a 1-mm and 10-mm path-length were used for measurements in the far-UV and near-UV region, respectively. The mean residue ellipticity [θ] (deg cm^2dmol^{-1}) was calculated using the formula $[\theta] = (\theta_{obs}/10)(MRW/lc)$, where θ_{obs} is the observed ellipticity in deg, *MWR* the mean residue molecular weight, *l* the path-length in cm and *c* the protein concentration in g/ml. Protein and fragment concentrations were evaluated from absorption measurements at 280 nm on a double-beam Lambda-25 spectrophotometer (Perkin Elmer, USA). Extinction coefficients at 280 nm were calculated according to Gill & von Hippel (1989). The concentration of fragment 17-29 was calculated by monitoring sample absorbance at 205 nm (Scopes, 1974). CD measurements were performed in 10 mM Tris-HCl buffer, pH 2.0, using a protein concentration of 0.2 mg/ml.

Thioflavin T fluorescence assays

Thioflavin-T (ThT) binding assay was performed according to LeVine (1993). A freshly prepared 25 μM ThT solution in 25 mM sodium phosphate (pH 6.0) was added to

protein samples from suspension containing aggregates (120 µl for a peptide concentration of 0.2 mg/ml) to reach a final volume of 500 µl. Fluorescence emission measurements were conducted at 25°C on a Perkin-Elmer model LS-50B spectrofluorimeter, utilizing a 10 mm path-length cuvette. The excitation wavelength was fixed at 440 nm and ThT fluorescence emission recorded at 485 nm. ThT fluorescence measurements of the fragments were plotted as a function of time and fitted to a sigmoid curve described by equation $y = a/(1+\exp(-(x-x_0)/b))$, where y is the fluorescence intensity and x_0 is the time to reach 50% of maximal fluorescence ($T_{Fmax/2}$). In some case, the ThT intensities have been normalized in percent data.

Transmission electron microscopy (TEM)

A drop of the peptide samples (0.2 mg/ml) was placed on a Butvar-coated copper grid (400-square mesh) (TAAB, Berks, UK) and dried. The samples were then negatively stained with a drop of 1% (w/v) uranyl acetate solution and observed with a Tecnai G^2 12 Twin transmission electron microscope (FEI Company, Hillsboro, OR), operating at an excitation voltage of 100 kV.

2.2.2 Results

Aggregation and fibrils formation of apoMb$_{1-29}$

Aggregation and fibrils formation of apoMb$_{1-29}$ were investigated under different pH conditions by ThT binding assay (LeVine et al., 1993), circular dichroism (CD) and transmission electron microscopy (TEM). In Fig. 2A the fluorescence emission values at 485 nm, after excitation at 440 nm, of a solution of ThT in the presence of apoMb$_{1-29}$, incubated at 37°C for 6 and 24 hours under different pH, are reported. A significant increase of ThT fluorescence intensity is observed at acidic pH. Indeed, as shown in Fig. 2.2 B, aggregation process of fragment apoMb$_{1-29}$ at pH 2.0 follows a nucleation-dependent growth mechanism, as described by a sigmoid curve. This process is characterized by a very short lag time, suggesting that the formation of the nuclei, on which fibrils growth proceeds, is very rapid. This phase is followed by a growth phase that reaches a plateau after 30 hours of incubation. The morphology of the aggregates, formed at different pH values, is shown in Fig. 2.2 C. Electron micrographs confirm that in acidic environment apoMb$_{1-29}$ forms fibrils. In particular, these fibrils are long and unbranched, with a diameter between 8-12 nm. Some fibrils show a twisted morphology, in which two filaments associate together to form a larger fibril. Amyloid-like fibrils were observed also at pH 5.0, but they are shorter and with a diameter between 5-7.5 nm. Samples incubated at pH 7.0 or at pH 9.0 do not form regular fibrils in 6 hours (Fig. 2.2 C, bottom), on the contrary TEM reveals the presence of amorphous aggregates.

The conformation analysis of apoMb$_{1-29}$ at different stages of aggregation under acidic conditions was carried out by using CD measurements (Fig. 2.3). In Fig. 2.3 A the far UV spectra acquired at pH 2.0 are reported. ApoMb$_{1-29}$ at pH 2.0 shows a spectrum typical of a random coil. During aggregation, the peptide undergoes a large conformational rearrangement and a band at 217 nm characteristic of β-structure appears after 6 hours of incubation. The negative band at 200 nm, indicative of a random structure, becomes less intense, while the band at 217 nm becomes gradually more pronounced upon more prolonged incubation. After 24 hours, the CD signal at 200 nm is absent and the spectrum is dominated by the band at 217 nm, evidencing a high content in β-structure. Fig. 2.3 B shows the evolution of the morphology of the fibrils of apoMb$_{1-29}$ at pH 2.0 monitored by TEM. A TEM image, taken after 3 hours of incubation at pH 2.0, shows the presence of small amount of ordered fibrils with a diameter of 8-12 nm. After 18 hours of incubation the diameter is always ranging from 8 to 12 nm, but the length

increases as well as the twisting between the fibrils (Fig. 2.3, middle). TEM pictures taken after 96 hours indicate that there is no further change in the morphology of the aggregates, but only the amount of ordered fibrils increases (Fig. 2.3 B, right). In conclusion, at pH 2.0 apoMb_{1-29} forms fibrillar aggregates those are morphologically, structurally and tinctorially indistinguishable from classical amyloid fibrils forming under pathological conditions.

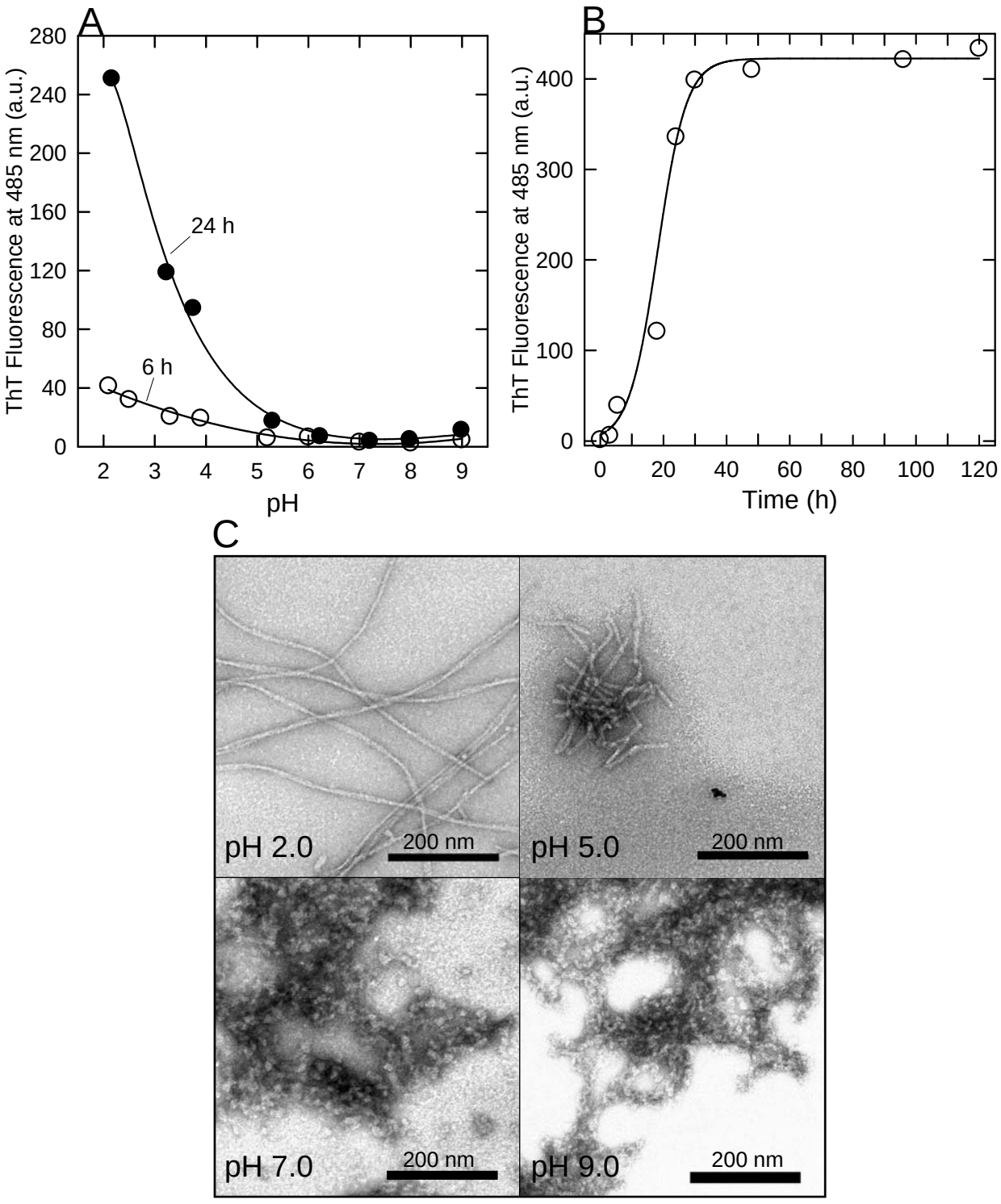

Fig. 2.2 (A) Fluorescence emission of ThT in the presence of fragment apoMb$_{1-29}$ (0.2 mg/ml) incubated for 6 or 24 h at 37°C at different pH values (2.0-9.0). **(B)** Time-course analysis of the aggregation process of apoMb$_{1-29}$ peptide at pH 2.0 and 37°C by ThT fluorescence. **(C)** Electron micrographs of apoMb$_{1-29}$ samples after 6 h of incubation at 37°C under different pH conditions. The scale bar represents 200 nm.

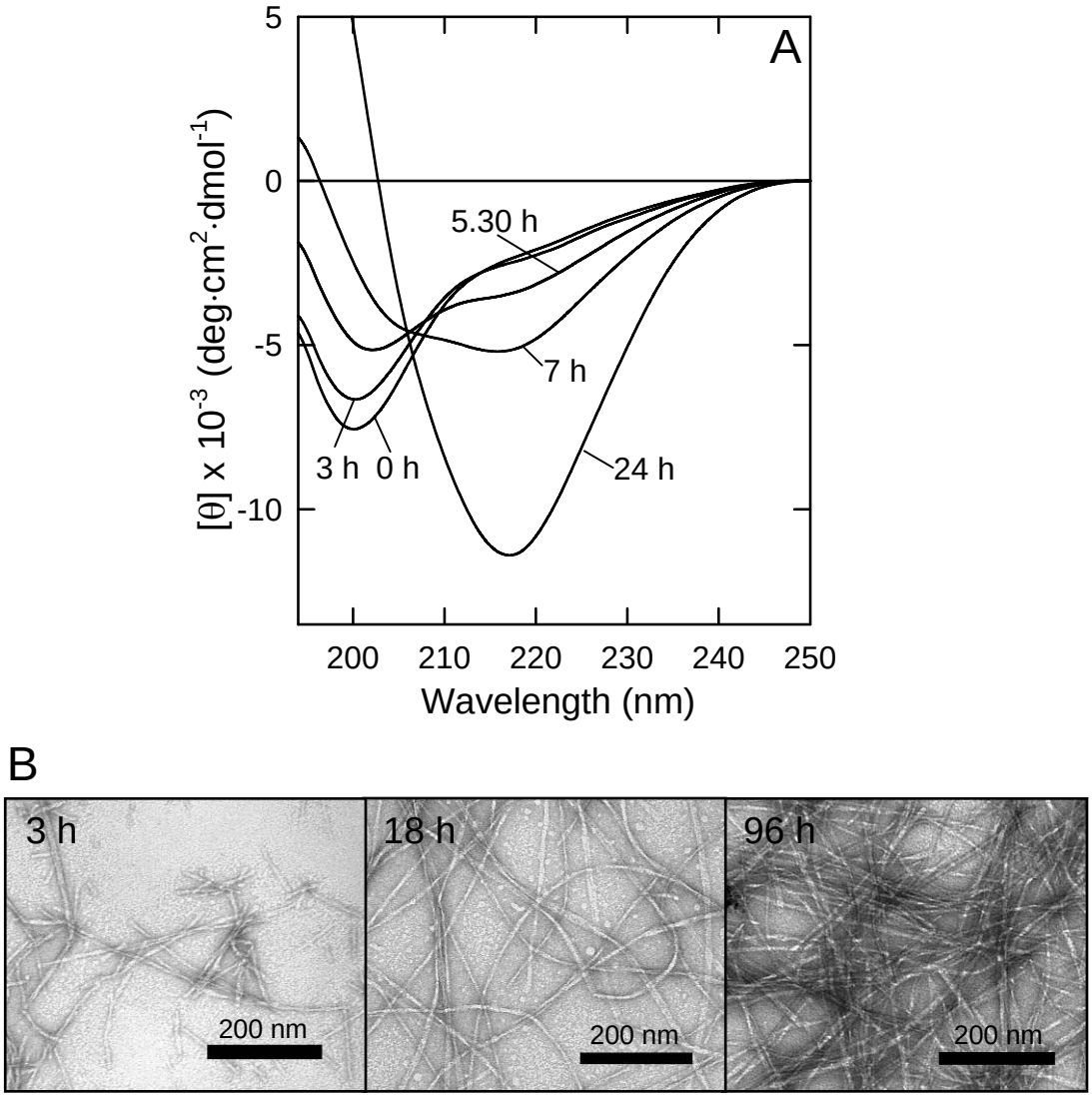

Fig. 2.3 (A) Evolution of the secondary structure of apoMb$_{1-29}$ fragment (0.2 mg/ml) monitored by far-UV during aggregation at pH 2.0 and 37°C. **(B)** Time evolution of apoMb$_{1-29}$ fibrils morphology at pH 2.0 and 37°C followed by TEM. The scale bar represents 200 nm

Dissection of apoMb$_{1-29}$ and identification of the most amyloidogenic region

ApoMb$_{1-29}$ peptide was subjected to proteolysis by using two proteases with different specificity and fragments of various lengths were obtained (Fig. 2.4). Taking advantage of the unique Lys residue in position 16 in the sequence, a proteolysis by trypsin was carried out, producing the complementary fragments 1-16 and 17-29. Furthermore, the presence of few Glu residues (position 6, 18 and 27) suggested the possibility to produce some peptides from apoMb$_{1-29}$ by using V8-protease, that in Tris-buffer, pH 7.5 selectively cleaves only Glu-X peptide bonds (Drapeau, 1977). In order to obtain also the decapeptide 7-16, a proteolysis, using both the proteases at the same time, was performed. However, the low solubility in aqueous buffer of this peptide makes very difficult its re-suspension after lyophilisation, even in acidic conditions. For this reason, the species 7-18, produced from the same reaction, was isolated and purified. All peptide species, purified by RP-HPLC, was characterized by mass spectrometry in order to assess their chemical composition (Table 2.1). The secondary structure of these peptides was analyzed by CD spectroscopy in the far UV range (data not shown); all the peptides show to be essentially random in solution at pH 2.0 and insoluble under neutral conditions, while, being the spectrum of 7-18 masked by the strong signal due to the two tryptophan residues, we can not evaluate if this peptide is unstructured or in β-conformation. The amyloidogenic properties and the kinetic of aggregation of fragments 1-29, 1-16, 17-29 and 7-18 were compared. As assessed by ThT assay (Fig. 2.5 A), fragments 1-16 and 7-18 aggregate very quickly, while the fluorescence emission in presence of fragment 17-29 does not change at all, also after long incubation time. In the case of fragments 1-16 and 7-18, there is a very short or nor lag time, indicating that their propensity to aggregate is very high, more than apoMb$_{1-29}$ and for both the peptides, the fluorescence emission of ThT reaches a plateau within 10 h of incubation. Electron micrographs taken from the solution of fragments apoMb$_{1-29}$, 1-16 and 7-18, after incubation for 18, 20 and 29 h respectively, are reported in Fig. 2.5 B. The TEM picture of 1-16 shows the presence of a large network of fibrils, with a diameter of 10-14 nm. The aggregates from peptide 7-18 exhibit the typical feature of amyloid fibrils but are straighter and shorter than those formed by apoMb$_{1-29}$ and 1-16. They are approximately 20-22 nm in width and appear to be composed of filaments laterally associated. They show a distribution of various lengths with some evidence of twisted ribbons morphology.

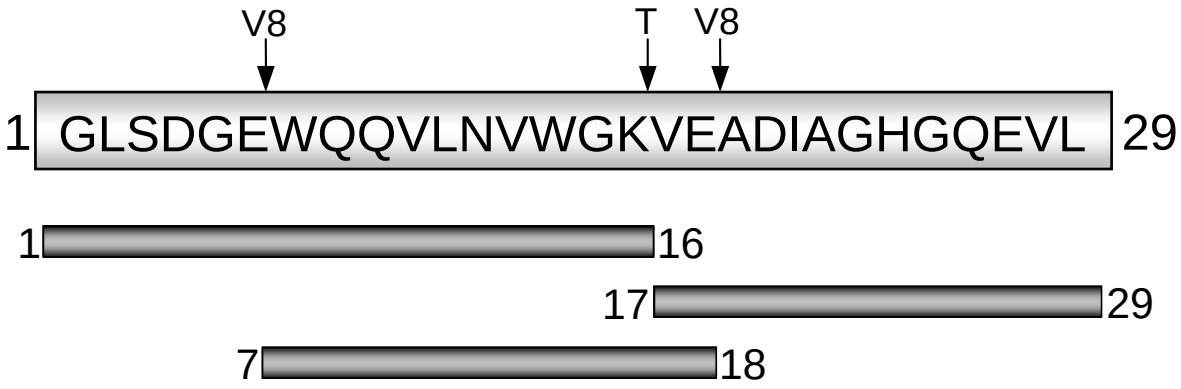

Fig. 2.4 Schematic representation of apoMb$_{1-29}$ peptide and its sub-fragments. The sites of cleavage by trypsin (T) and endoprotease Glu-C (V8) were indicated by arrows.

Table 2.1 Molecular masses of fragments obtained by proteolysis of apoMb$_{1-29}$ peptide

	Molecular Mass (Da)	
Fragment[a]	Found[b]	Calculated[c]
17-29	1336.6	1337.4
1-16	1816.9	1816.0
1-29	3138.3	3135.4
7-16	1256.7	1257.4
7-18	1484.8	1485.7
1-18	2043.8	2044.2

[a] Peptides obtained by proteolysis of apoMb$_{1-29}$.
[b] Experimental molecular masses determined by ESI-MS.
[c] Molecular masses calculated from the known amino acid sequence of horse heart apoMb.

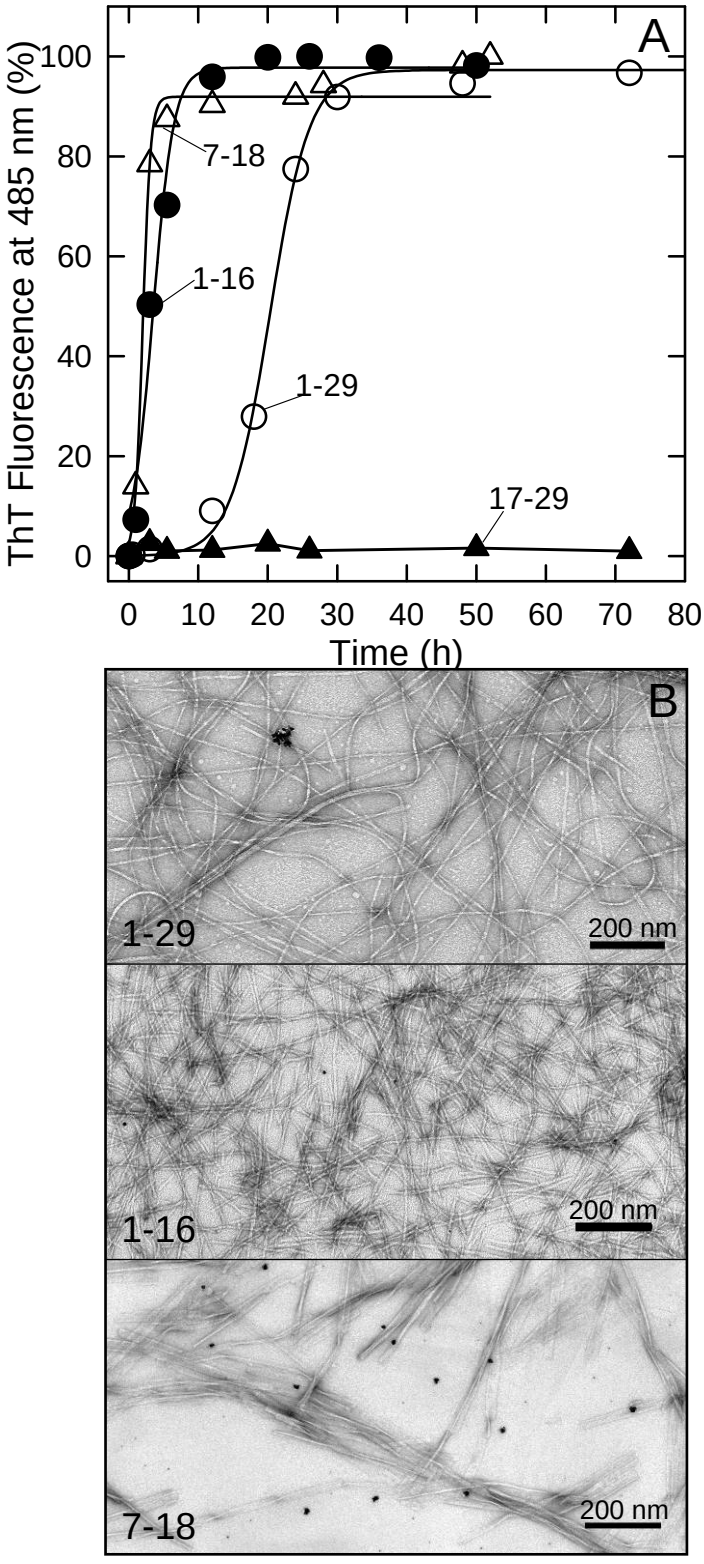

Fig. 2.5 (A) Time course analysis of aggregation of fragments apoMb$_{1\text{-}29}$, 1-16, 7-18 and 17-29 at pH 2.0, 37°C. **(B)** TEM pictures of peptide samples after 18 h (1-29), 20 h (1-16), and 29 h (7-18) of incubation at 37°C in 10 mM Tris-HCl pH 2.0. The scale bar represents 200 nm.

2.2.3 Discussion and Conclusions

ApoMb is able to form amyloid fibrils only under strong denaturing conditions (Fändrich et al., 2001; Fändrich et al., 2003) or under more physiological conditions substituting the Trp residues 7 and 14 with Phe (W7FW14F apoMb) (Sirangelo et al., 2002). Here, we demonstrated that the N-terminal region of apoMb is highly prone to aggregate, indeed peptide $ApoMb_{1-29}$ and its sub-fragments 1-16 and 7-18 readily form amyloid-like fibrils at pH 2.0. In the folded protein, the region comprised between amino acid residues 3 and 18 is involved in the formation of helix A, which, together with helices G and H, constitutes the main structural core of the folding pathway of apoMb (Reymond et al., 1997; Loh et al., 1995). Of note, the W7FW14F amino acid substitution in apoMb promotes misfolding and fibril formation of the protein even at neutral pH, as the mutation destabilizes the folding core of the protein, despite maintaining the aromatic character of the N-terminal region of apoMb (Sirangelo et al., 2002). At pH 2.0, apoMb is unfolded and the N-terminal region of the protein is exposed to the solvent, but the protein does not form fibrillar aggregates. The high degree of protonation of apoMb at pH 2.0 hinders intermolecular aggregation, due to electrostatic repulsion between positively charged apoMb monomers. ApoMb, therefore, despite the presence in its polypeptide chain of a region highly prone to aggregate, is protected from misfolding and loss of function by a compact three-dimensional structure that masks potentially amyloidogenic stretches of amino acids. The peptides studied here are isolated from protein and are unfolded in solution, so their intrinsic propensity to form amyloid fibril can be emphasized. The aggregation tendency can be evaluated in terms of net charge, β-sheet propensity, hydrophobicity and presence of aromatic residues (Chiti et al., 2003; Pawar et al., 2005). In $apoMb_{1-29}$, the net charge of the peptide changes upon acidification. The theoretical value of net charge of $apoMb_{1-29}$, calculated on the base of the average pKa of its amino acid residues, is + 2.6 at pH 2.0 and -2.6 at pH 5.0. However at pH 2.0 the presence of Cl^- anions (derived from the HCl used for the acidification) attenuates the electrostatic repulsive forces, resulting in an increase of the hydrophobic character of the peptide (Aggeli et al., 2003; Hoyer et al., 2004). On the other hand, this shielding effect does not occur at pH 5.0, slowing down the aggregation process. Under neutral and alkaline conditions the net charge is ~-4, value considered not suitable for aggregation (Calamai et al., 2003). Regarding the β-sheet propensity, secondary structure prediction analysis reveals that the region 9-16 shows the highest β-sheet propensity and a α-helical structure is not favored (Chou & Fasman, 1978; Garnier et al., 1996). The segment 22-29

on the contrary shows a preferentiality for random conformation. Taking together, these results suggest that there is an intrinsic strong tendency to form β-sheet that can lead to the easy association of the peptides corresponding to the N-terminal part of apoMb. The process is fastened at pH 2.0, because the hydrophobic collapse, important for the first step of protein aggregation (Meersman and Dobson, 2006), is promoted by the charge shielding effect (Goers et al., 2002; Hoyer et al., 2004). The complementary peptides 1-16 and 17-29 have the same net charge of +2 at pH 2.0, but only the fragment 1-16 quickly aggregates, while 17-29 is stable in acid solution as monomer. Several algorithms (Pawar et al., 2005; DuBay et al., 2004; Tartaglia et al., 2008) agree that N-terminal region of apoMb, spanning approximately 8-16, is one of the regions with high intrinsic aggregation propensity. In conclusion, we have clarified that in this system the electrostatic interactions have the main role in the aggregation process. So peptides, as $apoMb_{1-29}$, are an important research tool for analyzed the intrinsic determinants that regulate the molecular self-assembly in fibrillogenesis.

2.3 ELECTROSTATIC INTERACTION AS DETERMINANT IN APOMB$_{1-29}$ FIBRIL DISAGGREGATION

Since the aggregation process of apoMb$_{1-29}$ is highly regulated by pH and therefore by net charge, the effect of a change of net charge on the stability to dissociation of mature fibrils was studied. Investigations into the stability of amyloid fibrils in terms of stabilizing interactions can help to rationalize hypothesized kinetic and structural models (Meersman and Dobson, 2006). Moreover, elucidation of the factors that determine disaggregation may represent an additional approach to develop therapeutic strategies for the treatment of amyloid disease based on the conversion of misfolded proteins to their native states or on the clearance of amyloid deposits (Calamai et al., 2005; Calamai et al., 2008).

The mature apoMb$_{1-29}$ fibrils formed at pH 2.0 go into a fast and complete disaggregation, if the pH of the suspension is increased at 8.3. The variation of pH causes a large morphological alteration of the fibrils, as observed by TEM, Moreover, ThT assay and CD show a significant reversion of ordered aggregates into more immature specie, including the unstructured monomer. The increase of net charge of apoMb$_{1-29}$ caused by the change of pH back to neutral values promotes disaggregation. However, the amyloid-like fibrils form again if the sample is acidified.

In conclusion, the electrostatic interaction, in apoMb$_{1-29}$ system, is the force that primarily stabilized the β-sheet structure of the mature fibrils. However, other factors, such as hydrophobicity and the presence of two aromatic residues have an important role in the intrinsic aggregation propensity of the polypeptide.

The work attached hereby shows all the results relative to these studies and contains a more complete discussion. In this publication are reported also proteolysis experiments of the isolated fibrils. In brief, apoMb$_{1-29}$ fibrils are resistant to the proteolytic degradation by pepsin at pH 2.0, while the disaggregate fibrils are easily proteolyzed by V8 protease and trypsin at pH 8.3. However, in the last case, in the proteolytic mixture fibrillar aggregates can be isolated. The pellet is mostly constituted by fragments 7-16 and 7-18. These peptides, as described in 2.2.1, have an high tendency to aggregate and this property is much more highlighted at pH 8.3, since they have a net charge value of +1 and 0, respectively.

Published paper (Picotti et al., 2007, J.M B., 367, 1237–1245)

2.4 REFERENCES

Aggeli, A., Bell, M., Carrick, L. M., Fishwick, C. W., Harding, R., Mawer, P. J., Radford, S. E., Strong, A. E , Boden, N. (2003). pH as a trigger of peptide beta-sheet self-assembly and reversible switching between nematic and isotropic phases. *J. Am. Chem. Soc*., **125**, 9619−9628.

Ascoli, F., Fanelli, M. R., Antonini, E. (1981). Preparation and properties of apohemoglobin and reconstituted hemoglobins. *Methods Enzymol.,* **76**, 72−87.

Calamai, M., Canale, C., Relini, A., Stefani, M., Chiti, F., Dobson, C. M. (2005). Reversal of protein aggregation provides evidence for multiple aggregated states. *J. Mol. Biol.*, **346**, 603−616.

Calamai, M., Taddei, N., Stefani, M., Ramponi, G., Chiti, F. (2003). Relative influence of hydrophobicity and net charge in the aggregation of two homologous proteins. *Biochemistry* **42**, 15078−15083.

Calamai, M., Tartaglia, G. G., Vendruscolo, M., Chiti, F., Dobson, C.M. (2008). Mutational Analysis of the Aggregation-Prone and Disaggregation-Prone Regions of Acylphosphatase. *J. Mol. Biol.,* epub ahead of print.

Chiti, F., Calamai, M., Taddei, N., Stefani, M., Ramponi, G., Dobson, C. M. (2002). Studies of the aggregation of mutant proteins in vitro provide insights into the genetics of amyloid diseases. *Proc. Natl. Acad. Sci. USA*, **99**, 16419−16426.

Chiti, F., Dobson, C. M. (2006). Protein misfolding, functional amyloid and human disease. *Annu.Rev.Biochem.*, **75**, 333−66.

Chiti, F., Stefani, M., Taddei, N., Ramponi, G., Dobson, C. M. (2003). Rationalization of the effects of mutations on peptide and protein aggregation rates. *Nature,* **424**, 805−808.

Chou, P. Y. & Fasman, G. D. (1978). Prediction of the secondary structure of proteins from their amino acid sequence. *Adv. Enzymol. Relat. Areas Mol. Biol.,* **47**, 45−148.

Chu, K., Vojtchovsky, J., McMahon, B. H., Sweet, R. M., Berendzen, J., Schlichting, I. (2000). Structure of a ligand-binding intermediate in wild-type carbonmonoxy myoglobin. *Nature*, **403:** 921−923.

Drapeau, G. R. (1977). Cleavage at glutamic acid with staphylococcal protease. *Methods Enzymol.,* **47**, 189−191.

DyBay, K. F., Pawar, A. P., Chiti, F., Zurdo, J., Dobson, C. M. & Vendruscolo, M. (2004). Prediction of the absolute aggregation rates of amyloidogenic polipeptide chains. *J. Mol. Biol.* **341**, 1317−1326.

Fändrich, M., Flecther, M. A., Dobson, C. M. (2001). Amyloid fibrils from muscle myoglobin. *Nature*, **410**, 165−166.

Fändrich, M., Forge, V., Buder, K., Kittler, M., Dobson, C. M., Diekmann, S. (2003). Myoglobin forms amyloid fibrils by association of unfolded polypeptide segments. *Proc. Natl. Acad. Sci. USA,* **100**, 15463–15468.

Fruton, J. S. (1970) The specificity and mechanism of pepsin action. *Adv. Enzymol. Relat. Areas Mol. Biol.,* **33**, 401–443.

Garnier, J., Gibrat, J-F., Robson, B. (1996). GOR secondary structure prediction method version IV. *Meth. Enzymol*. **266**, 540–553.

Gazit, E. (2002). A possible role for π-stacking in the self-assembly of amyloid fibrils. *FASEB J.,* **16**, 77–83.

Gill, S. C. & von Hippel, P. H. (1989). Calculation of protein extinction coefficients from amino acid sequence data. *Anal. Biochem.,* **182**, 319–326.

Guijarro, J. I., Sunde, M, Jones, J. A., Campbell, I. D., Dobson, C. M. (1998). *Proc. Natl. Acad. Sci. USA*, **95**, 4224–4228.

Hoyer, W., Cherny, D., Subramaniam, V, Jovin, T. M. (2004) Impact of the acidic C-terminal region comprising amino acids 109-140 on α-synuclein aggregation in vitro. *Biochemistry* **43**, 16233–16242.

Jennings, P. A. and Wright, P. E. (1993). Formation of a molten globule intermediate early in the kinetic folding pathway of apomyoglobin. *Science,* **262**, 892–896.

Kallberg, Y., Gustafsson, M., Persson, B., Thyberg, J., Johansson, J. (2001). Prediction of amyloid fibril-forming proteins. *J. Biol. Chem.,* **276**, 12945–12950.

Kendrew, J. C., Bodo, G., Dintzis, H. M., Parrish, R. G., Wyckoff, H. & Phillips, D. C. (1958). A three-dimensional model of the myoglobin molecule obtained by x-ray analysis. *Nature* **181**, 662–666 .

Le Vine, H. (1993). Thioflavin T interaction with synthetic Alzheimer's disease beta-amyloid peptides: Detection of amyloid aggregation in solution. *Protein Sci.,* **2**, 404–410.

Loh, S. N., Kay, M. S., Baldwin, R. L. (1995). Structure and stability of a second molten globule intermediate in the apomyoglobin folding pathway. *Proc. Natl. Acad. Sci USA,* **92**, 5446–5450.

Malmo, C., Vilasi, S., Iannuzi, C., Tacchi, S., Cametti, C., Irace, G. and Sirangelo, I. (2006) Tetracycline inhibits W7FW14F apomyoglobin fibril extension and keeps the amyloid protein in a pre-fibrillar, highly cytotoxic state. *The FASEB J,* **20**, 346–347.

Meersman, F. and Dobson, C. M. (2006). Probing the pressure-temperature stability of amyloid fibrils provides new insights into their molecular properties. *Biochim. Biophys Acta*., **1764**, 452–460.

Nishimura, C., Dyson, H. J., Wright, P. E. (2002) The apomyoglobin folding pathway revisited: structural heterogeneity in the kinetic burst phase intermediate. *J. Mol. Biol.,* **322**, 483-489.

Otzen, D. E., Kristensen, O., Oliveberg, M. (2000). Designed protein tetramer zipped together with a hydrophobic Alzheimer homology: a structural clue to amyloid assembly. *Proc. Natl. Acad. Sci. USA*, **97**, 9907–9912.

Pawar, A. P., DuBay, K. F., Zurdo, J., Chiti, F., Vendruscolo, M. & Dobson, C. M. (2005). Prediction of "aggregation-prone" and "aggregation-susceptible" regions in proteins associated with neurodegenerative disease. *J. Mol. Biol.* **350**, 379–392.

Porat, Y., Mazor, Y., Efrat, S., Gazit, E. (2004). Inhibition of islet amyloid polypeptide fibril formation: A potential role for heteroaromatic interactions . *Biochemistry*, **43**, 14454–14462.

Schmittschmitt, J. P., Scholtz, J. M. (2003). The role of protein stability, solubility, and net charge in amyloid fibril formation. *Protein Sci*., **12**, 2374–2378.

Scopes R. K. (1974). Measurement of protein by spectraphotometry at 205 nm. *Anal. Biochem*., **59**, 277–282.

Sirangelo, I., Malmo, C., Casillo, M., Mezzogiorno, A., Papa, M., Irace, G. (2002). Tryptophanyl Substitutions in Apomyoglobin Determine Protein Aggregation and Amyloid-like Fibril Formation at Physiological pH. *J. Biol. Chem.,* **277**, 45887–45891.

Sirangelo, I., Malmo, C., Iannuzzi, C., Mezzogiorno, A., Bianco, M. R., Papa, M., Irace, G. (2004) Fibrillogenesis and Cytotoxic Activity of the Amyloid-forming Apomyoglobin Mutant W7FW14F. *J. Biol. Chem.,* **279**, 13183–13189.

Stefani, M., Dobson, C. M. (2003). Protein aggregation and aggregate toxicity: new insights into protein folding, misfolding diseases and biological evolution. *J. Mol. Med.*, **81**, 678–699.

Tartaglia, G. G., Pawar, A. P., Campioni, S., Dobson, C. M., Chiti, F. & Vedruscolo, M. (2008). Prediction of Aggregation-Prone Regions in Structured Proteins. *J. Mol. Biol.* **380**, 425–436.

Villegas, V., Zurdo, J., Filimonov, V. V., Avilés, F. X., Dobson, C. M., Serrano, L. (2000). Protein engineering as a strategy to avoid formation of amyloid fibrils. *Protein Sci.*, **9**,1700–1708.

Yoon, S. and Welsh, W. J. (2004) Detecting hidden sequence propensity for amyloid fibril formation. *Protein Sci.*, **13**, 2149–2160.

Young, J. D. and Carpenter, F. H. (1961). Isolation and characterization of products formed by the action of trypsin on insulin. *J. Biol. Chem.*, **236**, 743–748.

doi:10.1016/j.jmb.2007.01.072 *J. Mol. Biol.* (2007) **367**, 1237–1245

JMB

Available online at www.sciencedirect.com

ScienceDirect

ELSEVIER

COMMUNICATION

Amyloid Fibril Formation and Disaggregation of Fragment 1-29 of Apomyoglobin: Insights into the Effect of pH on Protein Fibrillogenesis

Paola Picotti[1], Giorgia De Franceschi[1], Erica Frare[1], Barbara Spolaore[1] Marcello Zambonin[1], Fabrizio Chiti[2], Patrizia Polverino de Laureto[1]* and Angelo Fontana[1]*

[1]*CRIBI Biotechnology Centre University of Padua Viale G. Colombo 3 35121 Padua, Italy*

[2]*Department of Biochemical Sciences, University of Florence Viale G. Morgagni 50 50134 Florence, Italy*

**Corresponding authors*

The N-terminal fragment 1–29 of horse heart apomyoglobin ($apoMb_{1–29}$) is highly prone to form amyloid-like fibrils at low pH. Fibrillogenesis at pH 2.0 occurs following a nucleation-dependent growth mechanism, as evidenced by the thioflavin T (ThT) assay. Transmission electron microscopy (TEM) confirms the presence of regular amyloid-like fibrils and far-UV circular dichroism (CD) spectra indicate the acquisition of a high content of β-sheet structure. ThT assay, TEM and CD highlight fast and complete disaggregation of the fibrils, if the pH of a suspension of mature fibrils is increased to 8.3. It is of interest that amyloid-like fibrils form again if the pH of the solution is brought back to 2.0. While $apoMb_{1–29}$ fibrils obtained at pH 2.0 are resistant to proteolysis by pepsin, the disaggregated fibrils are easily cleaved at pH 8.3 by trypsin and V8 protease, and some of the resulting fragments aggregate very quickly in the proteolysis mixture, forming amyloid-like fibrils. We show that the increase of amyloidogenicity of $apoMb_{1–29}$ following acidification or proteolysis at pH 8.3 can be attributed to the decrease of the peptide net charge following these alterations. The results observed here for $apoMb_{1–29}$ provide an experimental basis for explaining the effect of charge and pH on amyloid fibril formation by both unfolded and folded protein systems.

Keywords: protein aggregation; amyloid; protein fragments; electron microscopy; circular dichroism

Introduction

Polypeptide chains appear to have a general tendency to convert, under specific experimental conditions, from their soluble states into well-organized aggregates that have structural properties similar to those of the extracellular amyloid fibrils associated with a number of diseases, such as the amyloidoses and Alzheimer's disease, or of the intracellular inclusions that form in a number of neuropathic conditions, including Parkinson's disease or frontotemporal dementia.[1–10] These aggregates are characterized by a fibrillar morphology, as shown by transmission electron microscopy (TEM) or atomic force microscopy, an extended cross-β structure, as revealed by X-ray fibre diffraction data, and a high affinity for specific dyes such as Congo red and thioflavin T (ThT).[3,11–13] The generic potential of polypeptide chains to generate these fibrillar aggregates is relevant for a number of reasons. Firstly, fibril formation represents an essential feature of the behavior of polypeptide chains that needs to be fully understood for a thorough characterization of the dynamics and conformational changes of

Abbreviations used: apoMb, apomyoglobin; $apoMb_{1–29}$, N-terminal fragment 1–29 of horse heart apoMb; E/I, enzyme to inhibitor ratio; E/S, enzyme to substrate ratio; ESI-MS, electrospray ionization-mass spectrometry; GdnHCl, guanidine hydrochloride; HIC, hydrophobic interaction chromatography; RP, reverse-phase; $[\theta]_{MRW}$, mean residue ellipticity; TEM, transmission electron microscopy; TFA, trifluoroacetic acid; ThT, thioflavin T.

E-mail addresses of the corresponding authors: patrizia.polverinodelaureto@unipd.it; angelo.fontana@unipd.it

0022-2836/$ - see front matter

proteins.[6,8,9] Secondly, formation of amyloid fibrils, or intracellular inclusions with amyloid-like characteristics, is associated with more than 40 pathological conditions in humans, all having distinct and well-described clinical profiles.[10] Finally, such fibrillar species can serve biological functions in living organisms,[10] the most fascinating of them being the ability of amyloid-like fibrils to serve as transmissible genetic traits distinct from DNA genes.[14] Therefore, investigating the mechanism of amyloid fibril formation will hopefully shed light on a process that represents an essential feature of the chemistry of proteins, has a central role in human pathology and constitutes an important aspect of the biology of living organisms.

Numerous observations indicate that electrostatic interactions play a key role in the formation and stabilization of fibrillar aggregates. For example, ribonuclease Sa easily forms ThT-positive and β-sheet-containing aggregates in the presence of denaturing conditions of trifluoroethanol at a pH value corresponding to its isoelectric point (pI) and thus when the protein has a net charge of zero.[15] Similarly, mutations decreasing the positive net charge of human muscle acylphosphatase, partially unfolded in trifluoroethanol, resulted in an accelerated formation of β-sheet-containing aggregates able to bind ThT, whereas mutations increasing the net charge resulted in the opposite effect.[16] Further indications of the importance of charge in protein aggregation come from observations on α-synuclein. This "natively unfolded" protein[17–23] at neutral pH has a high negative net charge due to the presence of several acidic residues in the C-terminal region. Deletions of the C-terminal segment causes fibril formation to be accelerated, with the acceleration being proportional to the extent of the truncation.[21] Acceleration of fibril formation by full-length α-synuclein at neutral pH can be achieved by polyamines having a high positive compensatory charge, such as spermine and other polycations,[22,24] or small cations such as Na^+, Mg^{2+} or Ca^{2+}.[21,25,26] We note here that many mutations associated with familial forms of protein deposition diseases are pathogenic because they decrease the net charge of the protein forming the deposits.[10,16] Overall, these results indicate that amyloid aggregation is most favored under conditions in which the net charge of protein molecules is diminished and, consequently, the electrostatic repulsion between them is minimized. However, the inverse correlation between amyloidogenicity of natively or chemically unfolded proteins and net charge apparently contrasts with the increased tendency of some globular proteins to form amyloid-like fibrils following acidification (pH ~2.0), when the net charge of the protein is generally highly positive.[27–33]

In order to investigate further the importance of net charge on protein aggregation, we propose to study the aggregation and disaggregation processes of a fragment of horse heart apomyoglobin (apoMb) spanning residues 1–29 ($apoMb_{1–29}$) (see Figure 1(a)). This peptide appears to be a suitable experimental model as: (i) it is unstructured and does not form a folded conformation in any of the conditions investigated; (ii) it forms fibrillar aggregates that are morphologically, structurally and tinctorially in-

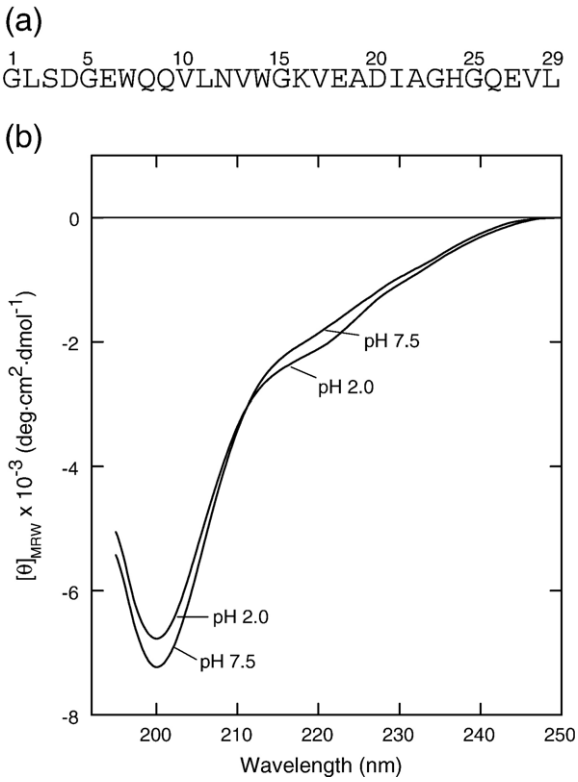

Figure 1. (a) Amino acid sequence of the peptide fragment spanning residues 1–29 of horse hearth apomyoglobin ($apoMb_{1–29}$).[56] (b) Far-UV CD spectra of $apoMb_{1–29}$ at pH 7.5 and 2.0. $ApoMb_{1-29}$ was obtained by limited proteolysis of apoMb (2 mg/ml) by pepsin at 25 °C, in 0.01 M HCl (pH 2.0), at an E/S ratio of 1:100 (w/w). The reaction was stopped after 90 s by adding pepstatin A (1 mg/ml) at an E/I ratio of 1:5 (w/w). The $apoMb_{1–29}$ fragment contained in the proteolysis mixture at pH 2.0 was purified by hydrophobic interaction chromatography (HIC) using a Resource™ Phe column (Amersham Bioscience, Uppsala, Sweden), equilibrated and eluted at a flow-rate of 1 ml/min initially with 0.01 M HCl (pH 2.0) and then with 10 mM Tris–HCl (pH 7.5). The effluent from the column was monitored by measuring the absorbance at 280 nm. Essentially homogeneous $apoMb_{1–29}$ fragment was eluted from the HIC column with Tris–HCl (pH 7.5) as a single chromatographic peak. The CD spectrum at pH 7.5 was obtained from a sample of the fragment just recovered from the HIC column and that at pH 2.0 was recorded immediately after pH adjustment. The same CD spectra were obtained at pH 7.5 and 8.3. Far-UV CD spectra were recorded at 25 °C with a Jasco J-710 spectropolarimeter (Tokyo, Japan) using quartz cells with a 1 mm path-length. Fragment concentration was evaluated from absorption measurements at 280 nm utilizing a double-beam Lambda-25 spectrophotometer (Perkin Elmer, Norwalk, CT, USA). Extinction coefficients at 280 nm were calculated as described.[57] CD measurements were performed at a peptide concentration of about 0.2 mg/ml. The results are reported in terms of mean residue ellipticity $[\theta]_{MRW}$.

distinguishable from those forming under pathological conditions; and (iii) it has a high ratio of acidic *versus* basic residues. The latter property is particular important, as this system has a high negative net charge at neutral pH and a low net charge at acidic pH. We show that formation of amyloid-like fibrils by apoMb$_{1–29}$ occurs readily at pH 2.0, whereas at pH values close to neutrality the peptide remains soluble and even its fibrils, pre-formed at low pH, disaggregate.

Effect of pH on the formation of amyloid fibrils by apoMb$_{1–29}$

ApoMb$_{1–29}$ was prepared by limited proteolysis of apoMb with pepsin at pH 2.0, following our studies aimed at unraveling molecular features of the partly folded states of apoMb[34] under acidic solvent conditions using the limited proteolysis approach.[35–37] The fragment was purified from the proteolysis mixture by hydrophobic interaction chromatography (HIC) (see the legend to Figure 1). The apoMb$_{1–29}$ fragment was eluted from the HIC-column with Tris–HCl buffer (pH 7.5) and used immediately for additional experiments. We have found that lyophilization causes significant aggregation of the fragment and was therefore avoided. A sample of the peptide in Tris–HCl buffer (pH 7.5) was shown by gel-filtration chromatography on a Superdex-75 column (not shown) to be largely monomeric.

The far-UV circular dichroism (CD) spectrum of apoMb$_{1–29}$ is typical of a fully unfolded polypeptide, since it is characterized by a pronounced minimum at ~200 nm,[38] at pH 7.5 or 2.0 (Figure 1(b)). The largely unfolded structure of horse apoMb$_{1–29}$ at both acidic and neutral pH contrasts with the β-sheet structure at pH 5.8 reported for the analogous 1–36 fragment of sperm whale apoMb.[39] Since this last fragment was prepared by recombinant methods, purified by chromatography and lyophilized, it could be well that the far-UV CD spectra of the sperm whale peptide were taken on an aggregated material resulting from the lyophilization step.[39] Alternatively, the different behavior of the two peptides may reside in the amino acid sequence differences or from the fact that the extra seven residues at the C terminus can stabilize β-sheet structure in sperm whale apoMb$_{1–36}$ that is otherwise unstable in horse apoMb$_{1–29}$.

To induce fibril formation, the apoMb$_{1–29}$ fragment has been incubated at 37 °C for five days at a concentration of 0.2 mg/ml and pH 2.0. The analysis of the aggregated peptide sample by TEM shows the presence of long, unbranched fibrils with a diameter of 9.0(±1.2) nm, characteristic of amyloid structures (Figure 2(a)). Some larger structures appear to be made by two twisted fibrils, with an overall diameter of 16.1(±0.8) nm. The sample produces a marked intensity gain of ThT fluorescence, supporting further the presence of ordered amyloid-like structures that selectively bind the dye (Figure 3(a), filled circles).[40] The far-UV CD spectrum of this peptide sample (Figure 3(b), sample a) displays the minimum at ~218 nm characteristic of β-sheet secondary structure, whereas the monomeric peptide appears to be largely unfolded (see Figure 1(b)).

In order to verify the stability of the amyloid-like aggregates to pH changes, the pH of the fibril sample was adjusted to 8.3 by adding a minimal volume of a 1 M Tris. The sample was analyzed immediately by CD, TEM and ThT-binding assay to evaluate the effect induced by the pH change on the structural and morphological properties of the fibrils. The TEM picture shows that the sample of the fibrils exposed to pH 8.3 is highly heterogeneous, being characterized by disordered aggregates (Figure 2(b_1)) and rare fibrillar structures with a diameter of 14.3(±1.2) nm (Figure 2(b_2)). Indeed, the ThT-binding assay shows a dramatic decrease of the ThT fluorescence intensity, which indicates a lower content of amyloid fibrils (Figure 3(a), open circles). The CD analysis shows the disappearance of the band at 218 nm and an increase in intensity of the signal at 200 nm, indicating that the β-sheet-containing aggregates convert into unstructured, possibly monomeric, peptide species (Figure 3(b), sample b).

The sample of apoMb$_{1–29}$ fibrils exposed to pH 8.3 was left for up to 24 h at room temperature. TEM analysis shows that the sample becomes highly heterogeneous, the predominant species being large amorphous aggregates characterized by a diameter of 25.0(±5.0) nm (not shown). The ThT fluorescence intensity is even lower than that of the sample just titrated at pH 8.3, indicating a further break-up of ordered fibrils (Figure 3(a), open circles). In agreement with the TEM and ThT assay results, the CD spectrum of the sample kept at pH 8.3 for 24 h continues to be characterized by a pronounced minimum at 200 nm (Figure 3(b), sample c). Hence, the variation of pH caused a large morphological alteration of the fibrils and a significant reversion of the fibrils into more immature species, including the unstructured monomer.

After incubation for 24 h at pH 8.3, the same peptide sample was acidified to pH 2.0 by addition of a minimal volume of 2 M HCl. The TEM images, acquired immediately after re-acidification, show the presence of pre-fibrillar aggregates with diameters ranging from 18.8 nm to 26.5 nm and rare typical fibrils with a diameter of 8.1(±1) nm (Figure 2(c_1) and (c_2)). The ThT fluorescence intensity of this sample is initially very low, but a time-dependent increase is observed upon incubation at pH 2.0 (Figure 3(a), filled squares). The increase of ThT fluorescence occurs more slowly and reaches a lower final value compared to that obtained directly without the disaggregation step at pH 8.3 (Figure 3(a), compare filled circles and squares). This is probably due to the fact that this sample is characterized by a lower concentration of peptide, resulting from the several dilution steps, and by the presence of amorphous aggregates that may interfere with the fibril formation process. The CD spectrum immediately after re-acidification is that of a largely random polypeptide (Figure 3(b), sample d).

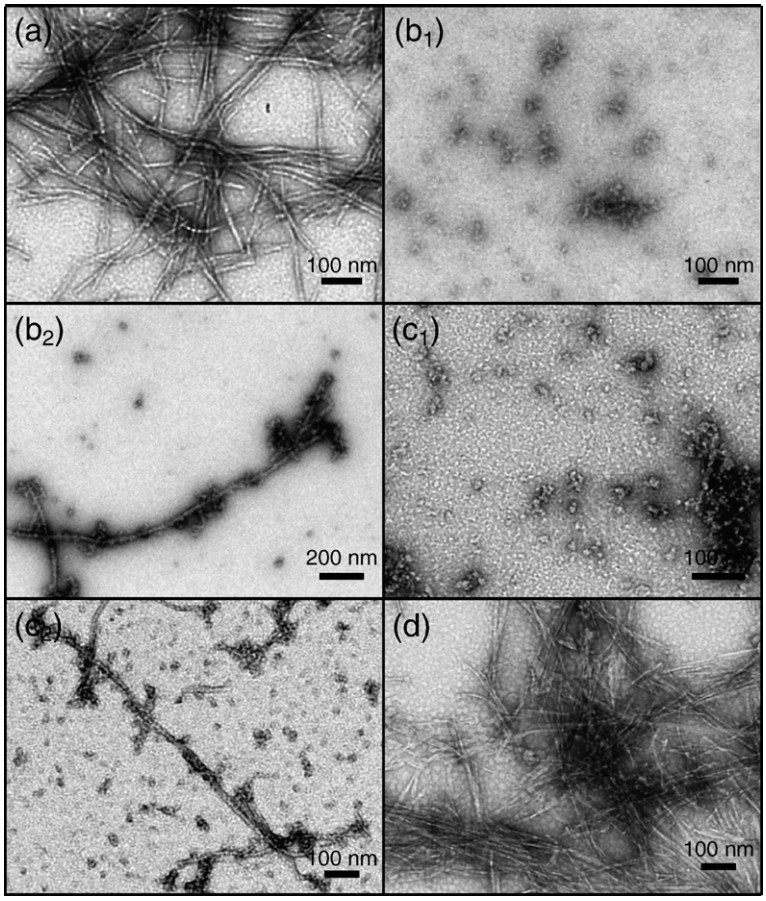

Figure 2. TEM pictures of apoMb$_{1–29}$ fibrils. (a) The solution containing a sample of apoMb$_{1–29}$ fibrils obtained at pH 2.0 after five days of incubation has been titrated to pH 8.3 (b_1 and b_2). Then the pH of the solution was lowered again to pH 2.0 and re-incubated for five days under these conditions (d). For TEM analysis, a drop of the peptide samples (0.2 mg/ml) was placed on a Butvar-coated copper grid (400-square mesh) (TAAB-Laboratories Equipment Ltd, Berks, UK) and dried. The samples were negatively stained with a drop of 1% (w/v) uranyl acetate solution and observed with a Tecnai G^2 12 Twin transmission electron microscope (FEI Company, Hillsboro, OR, USA), operating at an excitation voltage of 100 kV.

After leaving this sample at 37 °C for up to five days at pH 2.0, very organized and homogeneous amyloid fibrils with a diameter of 8.0(±1.2) nm formed again (Figure 2(d)), showing morphological features similar to those of the fibrils formed initially at pH 2.0 before the two consecutive changes of pH, in agreement with the significant increase of the ThT fluorescence intensity of this sample (Figure 3(a), filled squares). During incubation at pH 2.0, the CD spectrum undergoes an increase of the 218 nm band and a concomitant decrease of the intensity of the minimum at 200 nm (not shown). After five days, the CD spectrum is dominated by an intense negative band at 218 nm (Figure 3(b), sample e), but this band is less intense than that of the peptide sample obtained after the first step of acidification (sample a), likely indicating that upon re-acidification amorphous peptide aggregates are formed, besides fibrils. Overall, these findings indicate that the aggregates and/or monomers derived by the pH-induced dissolution of the fibrils are able to reassemble into amyloid fibrils, if the solvent conditions that mostly favor their formation are restored.

Proteolysis of apoMb$_{1–29}$

The fibrils formed after incubation of fragment apoMb$_{1–29}$ at pH 2.0 for five days have been isolated by ultracentrifugation and then analyzed by reverse phase (RP)-HPLC. The chromatographic profile of the peptide material in the pellet, after dissolution of the fibrils by 7.4 M GdnHCl, indicates that it is composed by intact full-length apoMb$_{1–29}$ and that no fragmentation has occurred during incubation of the fragment at low pH, as assessed by mass spectrometry analysis of the main peak of the RP-HPLC chromatogram (Figure 4(a), top). The apoMb$_{1–29}$ fibrils formed after incubation of the fragment at pH 2.0 for five days (see Figure 4(b), left) are resistant to proteolytic degradation by pepsin (data not shown).

Since incubation of the fibrils at pH 8.3 leads to their complete dissolution (see above), we performed proteolysis experiments on apoMb$_{1–29}$ fibrils that were purified by ultracentrifugation and then suspended in 10 mM Tris–HCl (pH 8.3), in the presence of both trypsin and V8 protease. Trypsin is expected to cleave the fragment at Lys16 and V8 protease is expected to cleave at Glu6, Glu18 and Glu27. The proteolysis mixture, after incubation overnight, showed an opalescent aspect, so it was ultracentrifuged in order to isolate the soluble and insoluble fractions. A number of small fragments have been found in the supernatant by RP-HPLC (Figure 4(a), bottom), and they have been identified by mass spectrometry analysis (Table 1). They correspond to several fragments spanning almost all regions of the peptide. Some of these peptides result from non-specific cleavages mostly at the level of hydrophobic residues, but these are produced in much smaller amounts. By contrast, the pellet after dissolution by 7.4 M GdnHCl appears to be mostly

constituted by fragments 7–16 and 7–18 and, to a lesser extent, by fragments 1–16 and 1–18 (Figure 4(a), middle). Therefore, peptides encompassing the central part of apoMb$_{1–29}$ produced by V8 protease and trypsin attack of the fragment are highly prone to aggregate, whereas peptides from the N and C-terminal regions of the fragment remain mostly soluble in the proteolysis mixture at pH 8.3. TEM analysis shows that the pellet obtained after proteolysis of apoMb$_{1–29}$ contains fibrillar structures with a mean diameter of 7.1(±0.5) nm (Figure 4(b), right).

The aggregation propensity of apoMb$_{1–29}$ on pH appears to be determined by electrostatic factors

The fast aggregation of the apoMb$_{1–29}$ peptide contrasts with the harsh conditions required to produce fibrils from the whole 153 residue chain of apoMb (pH 9.0, 65 °C, for up to 25 days).[41,42] Amyloid fibril formation by apoMb$_{1–29}$ was found to occur easily at acidic pH, while at pH 8.3 the peptide remains soluble, and even pre-formed fibrils convert back to non-amyloid amorphous aggregates and monomeric species. In its soluble form, before aggregation occurs, apoMb$_{1–29}$ is an unstructured peptide at both pH values (Figure 1(b)). This rules out a pH-induced conformational change as the cause of aggregation, as generally is the case for proteins that at neutral pH adopt a well defined folded structure that is disrupted upon acidification. The aggregation properties of apoMb$_{1–29}$ can be rationalized by considering the pH-dependent change of net charge of the unstructured peptide. Protonation of the six negative moieties (two Asp, three Glu and the C terminus) of the peptide at low pH strongly reduces the electrostatic repulsion between the various peptide molecules, thus facilitating their association and stabilizing the resulting fibrils. The electrostatic argument can explain why apoMb$_{1–29}$ can form fibrils at pH 8.3 when subjected to limited proteolysis with trypsin and V8 protease (see Figure 4). Under these conditions, apoMb$_{1–29}$ can be cleaved into various fragments, but only some of them can form fibrils. In particular, the predominant constituent fragments of the fibrils, i.e. fragments 7–16 and 7–18, have a net charge value of +1 and 0, respectively.

The increase of net charge of apoMb$_{1–29}$ caused by the change of pH back to neutral values promotes disaggregation. It was found that the net charge is an important determinant of both the rate of aggregation of a fully or partially unfolded protein,[16] and of the disaggregation rate of the resulting aggregates (M. Calamai, personal communication). These effects

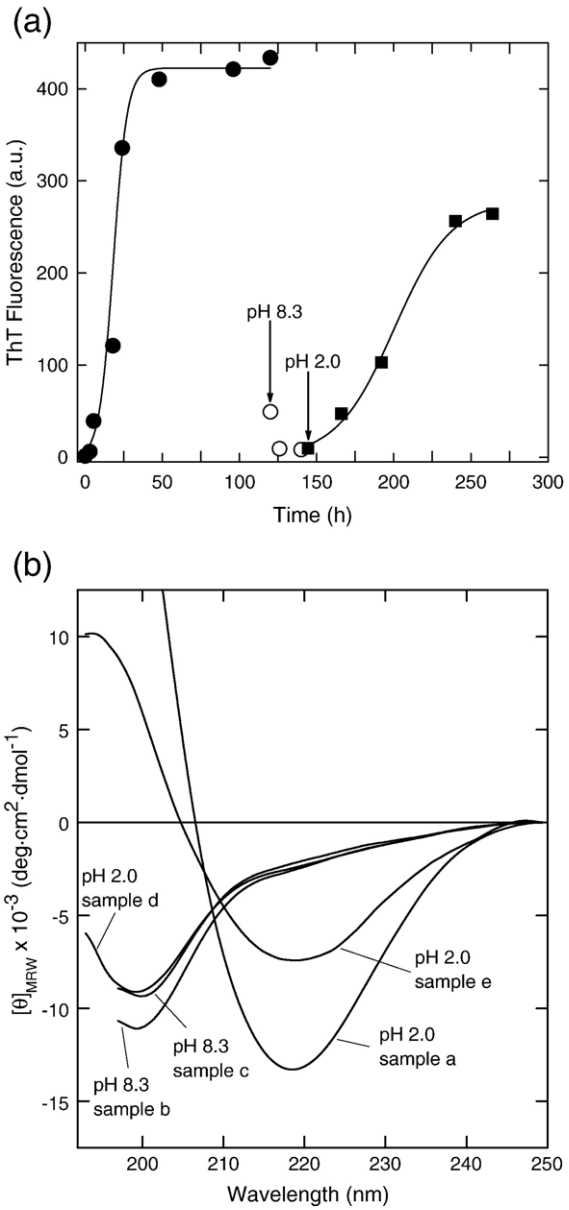

Figure 3. (a) Time-course analysis of the aggregation process of apoMb$_{1–29}$ by thioflavin T (ThT) fluorescence assay. Arrows indicate changes of pH. (b) Evolution of secondary structure of apoMb$_{1–29}$ monitored by far-UV CD spectroscopy. Spectra of apoMb$_{1–29}$ (0.2 mg/ml) incubated at pH 2.0 for five days (sample a), after titration at pH 8.3 (sample b), left at pH 8.3 for 24 h (sample c), left again at pH 2.0 (sample d) and left for five days at pH 2.0 (sample e). Fibrils were obtained incubating apoMb$_{1–29}$ (0.2 mg/ml) at pH 2.0 for five days at 37 °C. Before incubation, the peptide solution was filtered with a 0.22 μm pore size filter to eliminate large oligomers that could affect the aggregation process. To induce disaggregation, the pH of the solution (1.5 ml) containing fibrils from apoMb$_{1–29}$ was brought to 8.3 by adding a minimal amount (up to 5 μl) of 1 M Tris. The sample was then incubated for 24 h at room temperature. Finally, the sample (1 ml) was acidified again to pH 2.0 with 2 M HCl (up to 5 μl) and incubated for five days at 37 °C. The ThT binding assay[40] was performed by adding a freshly prepared 25 μM ThT solution in 25 mM sodium phosphate (pH 6.0) to 120 μl of protein samples containing aggregates, reaching a final volume of 500 μl. Fluorescence emission measurements were conducted at 25 °C on a Perkin-Elmer model LS-50B spectrofluorimeter (Norwalk, CT, USA), utilizing a 2 mm×10 mm pathlength cuvette. The excitation wavelength was 440 nm and ThT fluorescence emission was measured at 485 nm.

cause an overall thermodynamic stabilization and destabilization of the amyloid aggregates following a decrease or increase of net charge, respectively. This is in agreement with the observation reported here that amyloid fibrils of $apoMb_{1–29}$ can form and disaggregate in a reversible manner as a result of the changes of net charge resulting from modifications of pH.

Correlation of $apoMb_{1–29}$ fibrillogenesis with predictions

It is of interest to relate the results of this experimental study to those obtained by using the algorithms developed recently for predicting the rate of aggregation and for identifying the most amyloidogenic regions of polypeptide chains. Firstly, a previously described algorithm allows the aggregation rate constant (k) for an unstructured peptide or protein to be determined as a function of pH, ionic strength and protein concentration.[43] The experimental rate constant of aggregation of $apoMb_{1–29}$ under the conditions investigated here, determined as the rate constant of the exponential phase followed with ThT fluorescence (Figure 3(a), filled circles), is within experimental error that predicted for the sequence of $apoMb_{1–29}$ under the conditions studied (experimental $\log(k) = -4.22 \pm 0.12$ *versus* theoretical $\log(k) = -3.65 \pm 0.4$). Moreover, it was proposed that the regions of the sequence of an unstructured protein or peptide, as the case of $apoMb_{1–29}$, that promote the process of amyloid aggregation can be determined using an algorithm

Table 1. Molecular masses of fragments obtained by proteolysis of $apoMb_{1–29}$ by trypsin and V8-protease

	Molecular mass (Da)	
Fragment[a]	Found[b]	Calculated[c]
14–16	389.24	389.21
1–6	576.22	576.24
12–16	602.36	602.32
19–27	896.42	896.40
20–28	924.59	924.43
9–16	942.61	942.53
19–29	1108.59	1108.55
17–27	1124.53	1124.51
7–16	1256.69	1256.67
7–18	1484.80	1484.78
1–16	1814.96	1814.90
1–18	2043.09	2043.01
1–29	3134.75	3133.55

[a] Peptides obtained by proteolysis of $apoMb_{1–29}$ with trypsin and V8-protease. The peptides were purified by RP-HPLC (Figure 4(a)) and are listed in the order of increasing molecular mass.
[b] Experimental molecular masses determined by ESI-MS.
[c] Molecular masses calculated from the amino acid sequence of apoMb.[56]

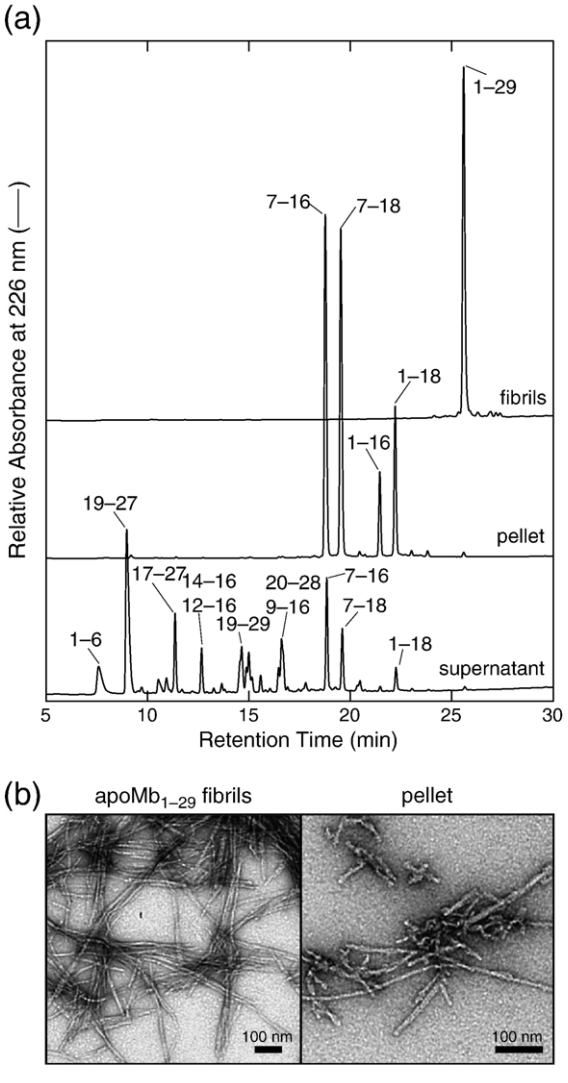

Figure 4. (a) Reverse-phase (RP)-HPLC analysis of the peptide material recovered from the $apoMb_{1–29}$ fibrils after dissolution in 7.4 M GdnHCl (top), from the pellet (middle) and supernatant (bottom) after overnight dissolution of the fibrils at pH 8.3 and concomitant tryptic and V8-protease digestion. The samples analyzed were obtained by ultracentrifugation in order to separate fibrils from the fragments released into the supernatant. (b) TEM pictures of $apoMb_{1–29}$ fibrils (left) and of the aggregated material formed after proteolysis with trypsin and V8 protease of $apoMb_{1–29}$ fibrils re-dissolved at pH 8.3 (right). Fibrils obtained incubating $apoMb_{1–29}$ at pH 2.0 for up to five days were subjected to proteolysis with trypsin and V8-protease in 10 mM Tris–HCl (8.3) at pH 25 °C. Both enzymes were added to the same solution to reach a protease to substrate ratio E/S of 1:50 (w/w). After 24 h, the proteolysis mixture was centrifuged (380,000g for 90 min at 4 °C) to separate soluble proteolytic fragments from aggregated material. The pellet and the supernatant, the first after dissolution in 7.4 M GdnHCl, were analyzed by RP-HPLC using an Eclipse XDB-C_8 column (4.6 mm × 150 mm) (Zorbax Columns, Agilent Technologies, Aston, PA, USA) eluted with a linear gradient of acetonitrile containing 0.1% (v/v) TFA from 5% to 60% (v/v) in 30 min at a flowrate of 0.8 ml/min. The effluent from the column was monitored by measuring the absorbance at 226 nm. The identity of all fragments was assessed by mass-spectrometry (Table 1). Electrospray ionization (ESI) mass spectrometry (MS) analysis of the peptides was carried out on a Micro Q-Tof mass spectrometer (Waters, Manchester, UK).

that evaluates the intrinsic propensity of the various amino acid residues to aggregate, on the grounds of physicochemical factors such as hydrophobicity, charge, propensity to form β-sheet and α-helical structure.[44] The aggregation propensity profile of apoMb$_{1–29}$ at neutral pH shows a single peak with a high intrinsic aggregation propensity, spanning approximately residues 8–16 (not shown), in very good agreement with the experimental results reported here. Finally, the use of a computational algorithm that can detect non-native (hidden) sequence propensity for amyloid fibril formation in proteins leads to the identification of few amyloidogenic regions along the 153 residue chain of apoMb, including the N-terminal region up to residue 21.[45]

Conclusions

Having an excess of acidic residues, the unstructured apoMb$_{1–29}$ peptide aggregates easily only at acidic pH values, when the negatively charged carboxylate groups are protonated and the strong negative net charge is decreased. This is in agreement with the behavior observed for other unstructured protein systems having a similarly high content of acidic residues. The natively unfolded and negatively charged α-synuclein aggregates preferentially at low pH values.[23] Polyglutamate aggregates only when it is neutralized by lowering the pH to a value of 4 or less.[46] On the other hand, several globular proteins with a more balanced number of positively and negatively charged residues have been found to form amyloid aggregates at low pH, i.e. under conditions where proteins are positively charged.[27–33] This can be explained by considering that folded proteins need to unfold, at least partially, to convert into amyloid aggregates.[1,8,9,48] The increase of positive net charge of a protein at low pH will decrease the intrinsic aggregation propensity, as discussed above, but it will also decrease the conformational stability of the protein, thus allowing the protein to adopt an ensemble of fully or partially unfolded conformations that are highly prone to aggregate.[47]

In a number of studies it has been demonstrated that net charge, hydrophobicity, the presence of abundant aromatic residues and β-sheet propensity can have important roles in the amyloidogenicity of polypeptides.[43,44,48] Here, it is shown that modulation of the net charge of fragment apoMb$_{1–29}$ and its sub-fragments by change of pH can be of utmost importance for fibril formation. This does not, of course, rule out the importance in amyloid aggregation of the other factors mentioned above. Indeed, the agreement between the region found experimentally to promote aggregation (residues 7–16 and 7–18) and that predicted to induce aggregation theoretically (approximately residues 8–16), is based on the grounds that all these factors, in addition to charge, promote fibril formation.[44] Changes of pH will affect the charge of ionizable groups of apoMb$_{1–29}$ and charge-related factors become predominant in determining the observed differences in aggregation behavior of the peptide at neutral or low pH.

The results of this study indicate that peptides can be used as an important research tool for investigating the molecular recognition and self-assembly mechanisms that underlie the protein fibrillogenesis phenomenon. Peptide models have provided fundamental insights into the mechanism of amyloid formation and, moreover, helped the discovery and rational design of inhibitors of protein aggregation.[49–54] The apoMb$_{1–29}$ peptide system offers several advantages as a peptide model, since it can be induced to form fibrils easily in a reversible way simply by modulating the pH of the solution. The easy and fast dissolution of the apoMb$_{1–29}$ fibrils by exposing them to a mildly alkaline aqueous solution contrasts with the well-known difficulty in solubilizing amyloid precipitates, which usually requires strong chaotropic agents or organic solvents such as 6 M GdnHCl or DMSO.[55] The results presented here will prompt additional studies by using analogs of apoMb$_{1–29}$ and its sub-fragments produced by chemical synthesis.

Acknowledgements

We thank Dr Manuela Grandesso for performing some of the experiments mentioned here. We acknowledge the financial support of the Italian Ministry of University and Research (PRIN-2003, PRIN-2004, PRIN-2006 and FIRB-2003 Project No. RBNEOPX83 on Protein Folding and Aggregation).

References

1. Kelly, J. W. (1998). The alternative conformations of amyloidogenic proteins and their multi-step assembly pathways. *Curr. Opin. Struct. Biol.* **8**, 101–106.
2. Rochet, J. C. & Lansbury, P. T., Jr (2000). Amyloid fibrillogenesis: themes and variations. *Curr. Opin. Struct. Biol.* **10**, 60–68.
3. Serpell, L. C. (2000). Alzheimer's amyloid fibrils: structure and assembly. *Biochim. Biophys. Acta*, **1502**, 16–30.
4. Horwich, A. (2002). Protein aggregation in disease: a role for folding intermediates forming specific multimeric interactions. *J. Clin. Invest.* **110**, 1221–1232.
5. Westermark, P. (2005). Aspects of human amyloid forms and their fibril polypeptides. *FEBS J.* **272**, 5942–5949.
6. Jahn, T. R. & Radford, S. E. (2005). The yin and yang of protein folding. *FEBS J.* **272**, 5962–5970.
7. Dobson, C. M. (1999). Protein misfolding, evolution and disease. *Trends Biochem. Sci.* **24**, 329–332.
8. Dobson, C. M. (2003). Protein folding and misfolding. *Nature*, **426**, 884–890.
9. Dobson, C. M. (2006). Protein aggregation and its consequences for human diseases. *Protein Pept. Letters*, **13**, 219–227.
10. Chiti, F. & Dobson, C. M. (2006). Protein misfolding,

functional amyloid and human disease. *Annu. Rev. Biochem.* **75**, 333–366.
11. Sunde, M. & Blake, C. C. (1997). The structure of amyloid fibrils by electron microscopy and X-ray diffraction. *Advan. Protein Chem.* **50**, 123–159.
12. Tycko, R. (2004). Progress towards a molecular-level structural understanding of amyloid fibrils. *Curr. Opin. Struct. Biol.* **14**, 96–103.
13. Makin, O. S. & Serpell, L. C. (2005). Structures for amyloid fibrils. *FEBS J.* **272**, 5950–5961.
14. Chien, P., Weissman, J. S. & DePace, A. H. (2004). Emerging principles of conformation-based prion inheritance. *Annu. Rev. Biochem.* **73**, 617–656.
15. Schmittschmitt, J. P. & Scholtz, J. M. (2003). The role of protein stability, solubility and net charge in amyloid fibril formation. *Protein Sci.* **12**, 2374–2378.
16. Chiti, F., Calamai, M., Taddei, N., Stefani, M., Ramponi, G. & Dobson, C. M. (2002). Studies of the aggregation of mutant proteins in vitro provide insights into the genetics of amyloid diseases. *Proc. Natl Acad. Sci. USA*, **99**, 16419–16426.
17. Wright, P. E. & Dyson, H. J. (1999). Intrinsically unstructured proteins: reassessing the protein structure-function paradigm. *J. Mol. Biol.* **293**, 321–331.
18. Dyson, H. J. & Wright, P. E. (2002). Coupling of folding and binding for unstructured proteins. *Curr. Opin. Struct. Biol.* **12**, 54–60.
19. Tompa, P. (2002). Intrinsically unstructured proteins. *Trends Biochem. Sci.* **27**, 527–533.
20. Fink, A. L. (2005). Natively unfolded proteins. *Curr. Opin. Struct. Biol.* **15**, 35–41.
21. Hoyer, W., Cherny, D., Subramaniam, V. & Jovin, T. M. (2004). Impact of the acidic C-terminal region comprising amino acids 109–140 on α-synuclein aggregation in vitro. *Biochemistry*, **43**, 16233–16242.
22. Fernandez, C. O., Hoyer, W., Zweckstetter, M., Jares-Erijman, E. A., Subramaniam, V., Griesinger, C. & Jovin, T. M. (2004). NMR of α-synuclein-polyamine complexes elucidates the mechanism and kinetics of induced aggregation. *EMBO J.* **23**, 2039–2046.
23. Uversky, V. N., Li, J. & Fink, A. L. (2001). Evidence for a partially folded intermediate in α-synuclein fibril formation. *J. Biol. Chem.* **276**, 10737–10744.
24. Göers, J., Uversky, V. N. & Fink, A. L. (2003). Polycation-induced oligomerization and accelerated fibrillation of human α-synuclein in vitro. *Protein Sci.* **12**, 702–707.
25. Uversky, V. N., Li, J. & Fink, A. L. (2001). Metal-triggered structural transformation, aggregation and fibrillation of human α-synuclein. *J. Biol. Chem.* **276**, 44284–44296.
26. Lowe, R., Poutney, D., Jensen, P. H., Gai, W. P. & Voelker, N. H. (2004). Calcium(II) selectivity induces α-synuclein annular oligomers via interaction with the C-terminal domain. *Protein Sci.* **13**, 3245–3252.
27. Guijarro, J. I., Sunde, M., Jones, J. A., Campbell, I. D. & Dobson, C. M. (1998). Amyloid fibril formation by an SH3 domain. *Proc. Natl Acad. Sci. USA*, **95**, 4224–4228.
28. Chiti, F., Bucciantini, M., Capanni, C., Taddei, N., Dobson, C. M. & Stefani, M. (2001). Solution conditions can promote formation of either amyloid protofilaments or mature fibrils from the HypF N-terminal domain. *Protein Sci.* **10**, 2541–2547.
29. Kad, N. M., Myers, S. L., Smith, D. P., Smith, D. A., Radford, S. E. & Thomson, N. H. (2003). Hierarchical assembly of beta2-microglobulin amyloid in vitro revealed by atomic force microscopy. *J. Mol. Biol.* **330**, 785–797.
30. Modler, A. J., Gast, K., Lutsch, G. & Damaschun, G. (2003). Assembly of amyloid protofibrils via critical oligomers: a novel pathway of amyloid formation. *J. Mol. Biol.* **325**, 135–148.
31. Frare, E., Polverino de Laureto, P., Zurdo, J., Dobson, C. M. & Fontana, A. (2004). A highly amyloidogenic region of hen lysozyme. *J. Mol. Biol.* **340**, 1153–1165.
32. Frare, E., Mossuto, M. F., Polverino de Laureto, P., Dumoulin, M., Dobson, C. M. & Fontana, A. (2006). Identification of the core structure of lysozyme amyloid fibrils by proteolysis. *J. Mol. Biol.* **361**, 551–561.
33. Polverino de Laureto, P., Taddei, N., Frare, E., Capanni, C., Costantini, S., Zurdo, J. *et al.* (2003). Protein aggregation and amyloid formation by an SH3 domain probed by limited proteolysis. *J. Mol. Biol.* **334**, 129–141.
34. Eliezer, D., Yao, J., Dyson, H. J. & Wright, P. E. (1998). Structural and dynamic characterization of partially folded states of apomyoglobin and implications for protein folding. *Nature Struct. Biol.* **5**, 148–155.
35. Fontana, A., Zambonin, M., Polverino de Laureto, P., De Filippis, V., Clementi, A. & Scaramella, E. (1997). Probing the conformational state of apomyoglobin by limited proteolysis. *J. Mol. Biol.* **266**, 223–230.
36. Fontana, A., Polverino de Laureto, P., De Filippis, V., Scaramella, E. & Zambonin, M. (1997). Probing the partly folded states of proteins by limited proteolysis. *Fold. Des.* **2**, R17–R26.
37. Fontana, A., Polverino de Laureto, P., Spolaore, B., Frare, E., Picotti, P. & Zambonin, M. (2004). Probing protein structure by limited proteolysis. *Acta. Biochim. Pol.* **51**, 299–321.
38. Woody, R. W. (1995). Circular dichroism. *Methods Enzymol.* **246**, 34–71.
39. Chow, C. C., Chow, C., Raghunathan, V., Huppert, T. J., Kimball, E. B. & Cavagnero, S. (2003). Chain length dependence of apomyoglobin folding: structural evolution from misfolded sheets to native helices. *Biochemistry*, **42**, 7090–7099.
40. Le Vine, H. (1993). Thioflavin T interaction with synthetic Alzheimer's diseases beta-amyloid peptides: detection of amyloid aggregation in solution. *Protein Sci.* **2**, 404–410.
41. Fändrich, M., Fletcher, M. A. & Dobson, C. M. (2001). Amyloid fibrils from muscle myoglobin. *Nature*, **410**, 165–166.
42. Fändrich, M., Forge, V., Buder, K., Kittler, M., Dobson, C. M. & Dickmann, S. (2003). Myoglobin forms amyloid fibrils by association of unfolded polypeptide segments. *Proc. Natl Acad. Sci. USA*, **100**, 15463–15468.
43. DuBay, K. F., Pawar, A. P., Chiti, F., Zurdo, J., Dobson, C. M. & Vendruscolo, M. (2004). Prediction of the absolute aggregation rates of amyloidogenic polypeptide chains. *J. Mol. Biol.* **341**, 1317–1326.
44. Pawar, A. P., DuBay, K. F., Zurdo, J., Chiti, F., Vendruscolo, M. & Dobson, C. M. (2005). Prediction of "aggregation prone" and "aggregation susceptible" regions in proteins associated with neurodegenerative diseases. *J. Mol. Biol.* **350**, 379–392.
45. Yoon, S. & Welsh, W. J. (2004). Detecting hidden sequence propensity for amyloid formation. *Protein Sci.* **13**, 2149–2160.
46. Fändrich, M. & Dobson, C. M. (2002). The behaviour of polyamino acids reveals an inverse side chain effect in amyloid structure formation. *EMBO J.* **21**, 5682–5690.
47. Uversky, V. N. & Fink, A. L. (2004). Conformational constraints for amyloid fibrillation: the importance of being unfolded. *Biochim. Biophys. Acta*, **1698**, 131–153.
48. Jones, S., Manning, J., Kad, N. M. & Radford, S. E.

(2003). Amyloid-forming peptides from β_2-microglobulin: insights into the mechanism of fibril formation in vitro. *J. Mol. Biol.* **325**, 249–257.
49. Zurdo, J. (2005). Polypeptide models to understand misfolding and amyloidogenesis and their relevance in a protein design and therapeutics. *Protein Peptide Letters*, **12**, 171–187.
50. Findeis, M. A. (2002). Peptide inhibitors of the beta-amyloid aggregation. *Curr. Top. Med. Chem.* **2**, 417–423.
51. Lopez de la Paz, M., Goldie, K., Zurdo, J., Lacroix, E., Dobson, C. M., Hoenger, A. & Serrano, L. (2002). *De novo* designed peptide-based amyloid fibrils. *Proc. Natl Acad. Sci. USA*, **99**, 16052–16057.
52. Pastor, M. T., Chopo, A. & Lopez de la Paz, M. (2005). Design of model systems for amyloid formation: lessons for prediction and inhibition. *Curr. Opin. Struct. Biol.* **15**, 57–63.
53. Makin, O. S., Atkins, E., Sikorski, P., Johansson, J. & Serpell, L. C. (2005). Molecular basis for amyloid fibril formation and stability. *Proc. Natl Acad. Sci. USA*, **102**, 315–320.
54. Cohen, T., Frydman-Marom, A., Rechter, M. & Gazit, E. (2006). Inhibition of amyloid fibril formation and cytotoxicity by hydroxyindole derivatives. *Biochemistry*, **45**, 4727–4735.
55. Meersman, F. & Dobson, C. M. (2006). Probing the pressure-temperature stability of amyloid fibrils provides new insights into their molecular properties. *Biochim. Biophys. Acta*, **1764**, 452–460.
56. Dautrevaux, M., Boulanger, Y., Han, K. & Biserte, G. (1969). Covalent structure of horse myoglobin. *Eur. J. Biochem.* **11**, 267–277.
57. Gill, S. C. & von Hippel, P. H. (1989). Calculation of protein extinction coefficients from amino acid sequence data. *Anal. Biochem.* **182**, 319–326.

Edited by J. Weissman

(Received 7 July 2006; received in revised form 23 January 2007; accepted 27 January 2007)
Available online 3 February 2007

Chapter 3

Parkinson's disease and α-synuclein

3.1 PARKINSON'S DISEASE: NEUROPATHOLOGICAL HALLMARKS

Parkinson's disease (PD) was first described by James Parkinson in 1817 in "An Essay of Shaking Palsy". PD is the second most-prevalent neurodegenerative disorder after Alzheimer's disease. It is an irreversible, progressive disease that impairs movement. The clinical phenotypes are resting tremors, bradykinesia, muscular rigidity and postural instability. Non-motoric symptoms, like automic, cognitive and psychiatric problems can be also present; however cognitive ability remains intact in most PD sufferers, at least in the early stages of the disease. Incidence increases markedly with age; hence young-onset Parkinson's disease, defined as occurrence before age 40, accounts for just 5% of newly diagnosed cases (Irvine et al., 2008). Moreover, upon reaching the 65-69 age range, 0.6% of the population are affected, increasing to 2.6 % of those aged 85-89 (de Rijk et al., 2000). The majority of cases of PD are idiopathic and sporadic, but in 5-10% of cases there is a genetic component, showing both recessive and dominant modes of inheritance.

PD is characterized by depigmentation of the *substantia nigra pars compacta*, caused by the selective and progressive loss of dopaminergic (DA) neurons, and by the presence of eosinophillic, intraneuronal proteinaceous, inclusions known as Lewy bodies (LBs) and dystrophic Lewy neurites in the surviving neurons (Fig. 3.1). Because patients suffering from other neurological disorders can display parkinsonian features, a definitive diagnosis of Parkinson's disease can be confirmed only by *post mortem* histopathological examination of the *substantia nigra* for loss of pigmented neurons and presence of LBs in remaining neurons. Identification of LBs has been facilitated by immunostaining for particular proteins; initially for ubiquitin and more recently for α-synuclein, now regarded as the major protein constituent (Shults, 2006). Such staining reveals filaments that, when purified and examined by immuno-electron microscopy, can be seen to contain α-syn (Spillantini et al., 1998). The recombinant protein forms similar filaments when it is allowed to aggregate *in vitro* (Crowther et al., 1998) (Fig. 3.1).

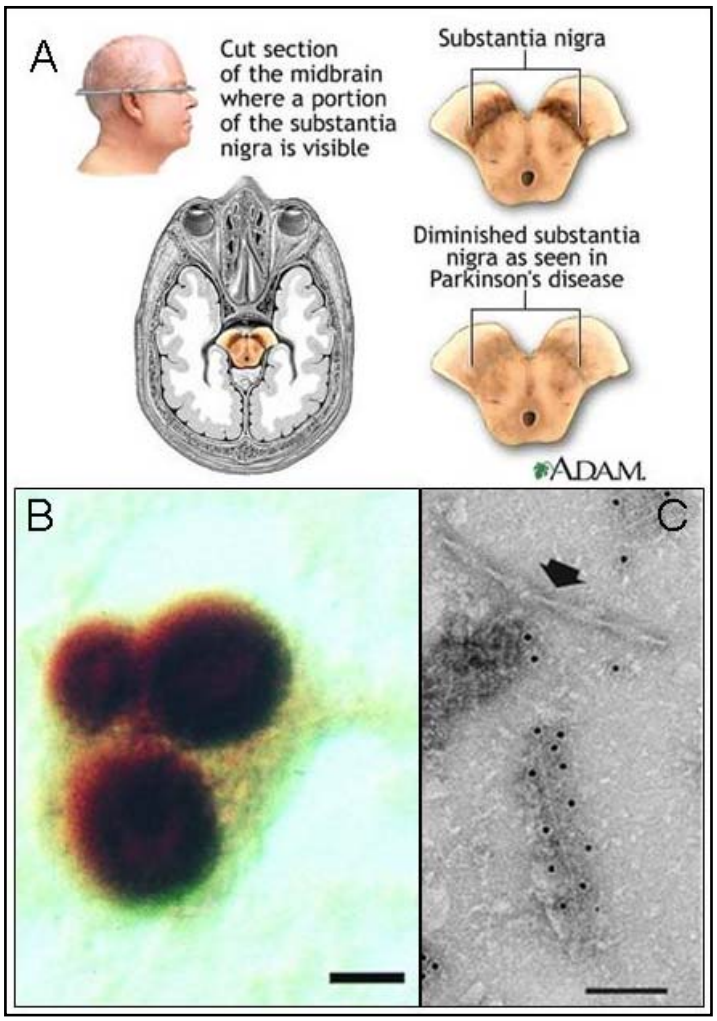

Fig. 3.1 Pathological hallmarks of PD. **(A)** Schematic representation of *substantia nigra*: it is evident the loss of pigmented neurons in PD patients. **(B)** Nerve cell with three LBs that are double-stained for α-syn and ubiquitin. The halo of each LB is strongly immunoreactive for ubiquitin, whereas both the core and the halo of each Lewy body are immunoreactive for α-syn. (Bar = 10 μm.). **(C)** Filaments from cingulate cortex of patients with dementia with LBs labelled with anti-α-synuclein antibody PER4. The gold particles conjugated to the second antibody appear as black dots; there is also an unlabeled paired helical filament (arrow). (Bar = 100 nm). (B and C reprinted from Spillantini et al., 1998)

DA neurons operate in a pathway that controls voluntary movement. This involves signals being relayed from the cerebral cortex through the basal ganglia back to the cortex and then on to muscles. Neurons from the *substantia nigra pars compacta* project axons that release dopamine in synapses on interneurons in the striatum. As the dopamine-containing neurons die, failure to complete this circuit results in inability to coordinate movement (Fig. 3.2). Neuromelanin, the black pigment that gives its name to the *substantia nigra*, is a byproduct from the metabolic pathway for dopamine synthesis. When the symptoms of PD first become apparent, more than 70% of the dopamine-containing neurons have already been lost, releasing their neuromelanin and hence turning the tissue less black. It is now apparent, however, that many regions of the brain are affected in Parkinson's disease, and indeed in the early stages it may affect only a lower region of the brain stem called the *medulla oblongata*, spreading gradually upward through the basal ganglia into the cortical areas (Irvine et al., 2008; Braak et al., 2003).

Symptoms of PD could be reversed temporarily by pharmacologic interventions to restore striatal dopaminergic neurotransmission (LeWitt, 2008; Hornykiewicz, 2002). This reversal can be accomplished by DA agonists, compounds that directly stimulate postsynaptic striatal dopamine receptors (Fig. 3.2). The administration of dopamine itself is ineffective because dopamine cannot cross the blood–brain barrier (Nutt et al., 1984). Levodopa (3,4-dihydroxy-L-phenylalanine), a naturally occurring amino acid, is an intermediate in the pathway of dopamine synthesis. After oral ingestion, levodopa is actively transported from the upper small intestine into the circulation by a mechanism specific for large, neutral L-amino acids. Because of ongoing metabolism and the distribution of levodopa throughout the body, only a small fraction of the drug reaches the brain after active transport across the blood–brain barrier. Once there, dopamine is rapidly formed from levodopa by aromatic L-amino acid decarboxylase (AAAD). Moreover, the coadministration of other drugs can improve the efficacy of levodopa. In conclusion, current medications only provide symptomatic relief and fail to halt the death of DA neurons. A major hurdle in development of neuroprotective therapies are due to limited understanding of disease processes leading to death of DA neurons (Thomas & Beal, 2007).

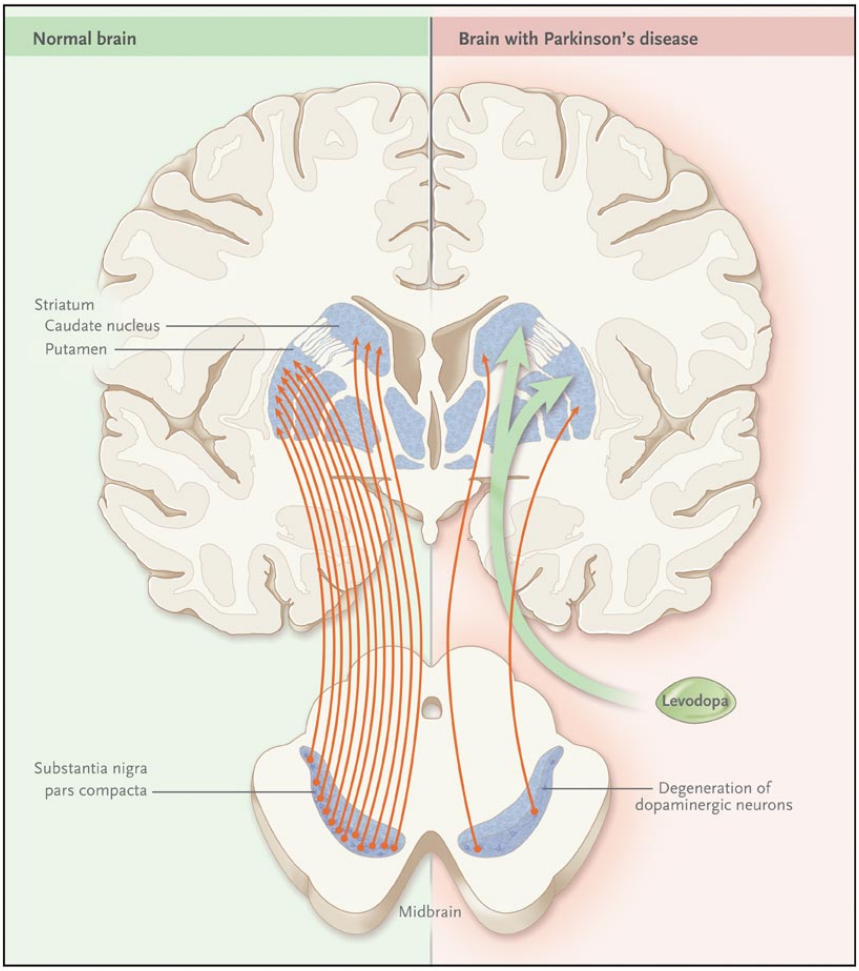

Fig. 3.2 A schematic comparison of coronal brain slices from a control subject (left) and a patient with PD (right) illustrates the major neurodegenerative loss of dopamine-synthesizing neurons in the *substantia nigra pars compacta*, projecting to striatal nuclei (caudate and putamen) in the cerebrum. Exogenous levodopa administered for treatment of PD is transported to the brain, where it enhances striatal dopaminergic neurotransmission. (reprinted from LeWitt, 2008).

3.2 PATHOGENESIS OF PARKINSON'S DISEASE

The causes of the DA neuronal demise in familial and sporadic forms of PD are elusive, but recent findings suggest that both environmental factors and genetic susceptibilities are associated with PD pathogenesis. The hypothesis that environmental factors play a role in the etiology of PD were done after the discovery of a group of intravenous drug users who unwittingly injected a synthetic analog of demerol that was contaminated with 1-methyl-4-phenyl-1,2,3,6-tetrahydropyridine (MPTP) causing an acute, permanent parkinsonian state that was levodopa responsive (Langston et al, 1985). Once inside the brain, MPTP enters astrocytes and is converted into its active metabolite, MPP^+ (1-methyl-4-phenylpyrdinium), which then can enter dopamine neurons and exert its toxicity. Although not typically found in the environment itself, the ability of MPTP to reproduce so many of the features of PD intensified the search for potential environmental toxicants that might contribute to the development of PD (Hatcher et al., 2008). Moreover, epidemiological studies had suggested a link between long-term exposure to agricultural pesticides, such as rotenone and paraquat. Rotenone, a plant derivative used as an insecticide, is known to be an inhibitor of NADH dehydrogenase. Chronic infusion of either rotenone or MPTP in rodents results in parkinsonism-like behavior and pathology, including the formation of inclusion bodies, and indeed these are among the best animal models for the human disease (Dauer et al., 2003).

The majority of PD cases are sporadic, but the discovery of genes linked to rare familial forms of PD have confirmed the role of genetics in development of PD, and provided important information in understanding molecular pathogenesis of the common sporadic disease (Thomas & Beal, 2007).

3.2.1 Pathogenic mutations in PD pathogenesis

Linkage data has identified eleven loci, named *PARK*; six of the genes with pathogenic mutations have now been identified (Table 3.1). These include two autosomal dominant genes, α-synuclein (*SNCA*) and leucine-rich repeat kinase 2 (LRRK2), and three autosomal recessive genes, parkin, DJ-1 and PTEN-induced putative kinase 1 (PINK1). The 6th gene, ubiquitin carboxyl-terminal esterase L1 (UCHL1, previously known as *PARK5*), has only been found in one small family, and its importance in familial PD is still uncertain. There are four remaining loci (*PARK3*, *PARK9*, *PARK10* and *PARK11*) for which linkage has been identified; however, the causative genes have not yet

been discovered (Wood-Kaczmar et al., 2006).

Table 3.1 Genetic mutations identifying for PD (Wood-Kaczmar et al., 2006).

Locus	Gene (protein)	MOI	Protein function	Clinical presentation
PARK1	α-synuclein (*SNCA*)	AD	Unknown synaptic function	*Duplications:* Idiopathic PD; some postural tremor; slow progression; *Triplications*: PD; PD with dementia; diffuse LBs disease; aggressive course; Mutations A53T, A30P, E46K: Idiopathic PD; parkinsonism and diffuse LBs
PARK2	Parkin	AR	E3 ubiquitin ligase	Parkinsonism; slow progression
PARK5	UCHL1	AD	Ubiquitin hydrolase and ligase	PD
PARK6	PINK1	AR	Mitochondrial Ser-Thr Kinase	Parkinsonism
PARK7	DJ-1	AR	Oxidative stress response ?	Parkinsonism
PARK8	LRRK2	AD	Unknown protein kinase	PD

Abbreviations: AD, autosomal dominant; AR, autosomal recessive; LBs, Lewy bodies; MOI, mode of inheritance.

α-Synuclein (α-syn)

Mutations in the *SNCA* gene were first identified in large kindred with autosomal dominant parkinsonism (Polymeropoulos et al., 1997). Three autosomal dominant mutations have now been identified that segregate with familial PD, A53T, A30P and E46K substitutions (Cookson et al., 2005). Subsequently, it was discovered that genomic duplications and triplications at the α-syn locus can also cause autosomal dominant, early onset PD (Singleton et al., 2003). The age of onset and severity of the disease phenotype seems to correlate with *SNCA* copy number, suggesting a gene-dosage effect. PD patients who carry duplications at the *SNCA* locus (which generate three copies of the gene) tend to have PD, which develops slowly from the 4th decade of life. Triplication events, which produce four copies of the *SNCA* gene, cause disease earlier (mid 20–mid 30) with a clinical presentation ranging in severity from idiopathic PD, PD with dementia or diffuse Lewy body disease (Farrer et al., 2004).

α-Syn is a small (140 amino acids) natively unfolded protein that is a member of family that includes β-synuclein, γ-synuclein and synoretin. It is enriched in the adult human brain where it is expressed ubiquitously but heterogeneously, with highest levels of protein reported in deeper layers of the cerebral neocortex, the hippocampus (CA2 and

CA3 regions) and the SN. The protein is expressed within glia and neurons where it is particularly abundant at presynaptic terminals (Iwai et al., 1995; Mori et al., 2002). The physiological function of α-syn is not well understood but it seems to have a role in synaptic plasticity and in regulation of dopamine neurotransmission. Other studies have evidenced that α-syn may function as a chaperone protein, based on its abundance in cytosol, its natively unfolded structure, and its prevention of protein aggregation. The physiological function of α-syn is also related with lipids and membrane since this protein seems to modulate presynaptic vesicle pool size and vesicle recycling. A deeper discussion about the function of α-syn will be reported in § 3.3.

The pathological role of α-syn in PD seems to be linked to its aggregation properties. Indeed, α-syn is the principal constituent of LBs and Lewy neuritis in sporadic and in familial PD. α-Syn is an amyloidogenic protein and aggregates *in vitro* in a concentration-dependent manner to form fibrils reminiscent of those observed in Lewy bodies (Conway et al., 2000; Serpell et al., 2000). Furthermore, elevated expression levels of α-syn in the brain, caused by rare genomic multiplications of the *SNCA* gene, increases the deposition of soluble α-syn into insoluble aggregates (Miller et al., 2004). Transgenic mice that overexpress wild-type or mutant α-syn have given conflicting results (Fleming et al., 2005). However, models in *Drosophilia melanogaster* demonstrated that high levels of α-syn cause abnormal protein aggregation and neurotoxicity in DA neurons. α-Syn expressed in *D. melanogaster* is phosphorylated at serine 129. When serine 129 is mutated to a non-phosphorylatable residue, there is in increased aggregate formation and reduced cell death in DA neurons (Chen et al., 2005). Human α-syn is also extensively phosphorylated at serine 129 in LBs but the importance of this post-translational modification has yet to be demonstrated in sporadic PD (Fujiwara et al., 2002).

In its aggregation pathway α-syn can form soluble oligomers and protofibrils that are toxic to some cell cultures, including the dopaminergic SH-SY5Y human neuroblastoma cell line (El-Agnaf et al., 2001, Volles et al, 2001; Volles & Lansbury, 2003). It is thought that the soluble, oligomeric forms of α-syn are the toxic species rather than the insoluble fibrils within the inclusion body. Both A53T and A30P mutants show an increased propensity to form these so called protofibrils, which can permeabilize vesicles in a way that is reminiscent of bacterial pore-forming toxins (Volles et al., 2001). Dopamine and related catecholamines have been shown to interact with α-syn and stabilize the protofibril stage of aggregation (Conway et al., 2001; Mazzulli et al., 2007)

providing a possible explanation for the increased susceptibility of DA neurons. Levels of soluble oligomers are also affected by fatty acids, being upregulated by polyunsaturated fatty acids (Sharon et al., 2003). α-Syn aggregation is also increased in the presence of metals and pesticides, which may be environmental risk factors (Uversky et al., 2002).

Furthermore, expression of mutant forms of α-syn in cells promotes mitochondrial defects and cell death and enhances susceptibility to oxidative stress. On the other hand, mice deficient in α-syn are resistant to toxicity induced by MPTP and other mitochondrial toxins (Klivenyi et al., 2006).

Parkin

The *PARK2* locus codes for the enzyme parkin, which is a ubiquitin E3-ligase (E3s). E3s act as substrate-recognition molecules during the synthesis and attachment of polyubiquitin chains to proteins that are targeted for degradation by ubiquitin proteasome system (UPS) (Shimura et al., 2000). Mutations in the parkin gene are the predominant cause of juvenile and early onset recessive parkinsonism (von Coelln et al., 2004). Parkin mutations are present in ~ 50% of all individuals with recessive, early onset (<45 years) parkinsonism, and in 77% of sporadic cases with disease onset before the age of 20. Some missense and nonsense mutations, deletions and rearrangements in the parkin gene have also been reported (West & Maidment, 2004). At least ten familial-associated parkin mutations have now been shown to disrupt differentially the solubility, localization, binding and ubiquitination properties of parkin *in vitro* (Sriram et al., 2005). Inactivation of parkin leads to reduction in UPS-mediated degradation of its substrates. Several candidate parkin substrates have been identified, including proteins that are implicated in PD such as synphilin-1 and a glycosylated form of α-syn. Recent studies have highlighted a protective role for parkin within mitochondria. Reduced levels of mitochondrial proteins involved in mitochondrial oxidative phosphorylation were reported in parkin knockout mice (Palacino et la., 2004). Parkin has been shown to localize to the mitochondrial matrix, where it enhances mitochondrial gene transcription and biogenesis in proliferating cells. In addition, a recent study demonstrates α-syn-induced mitochondrial dysfunction is further enhanced due to lack of parkin activity *in vivo* implicating crucial role of parkin in modulating mitochondrial functions in α-syn-induced PD (Stichel et al., 2007). Parkin functions as a multipurpose neuroprotective protein in a variety of toxic insults crucial for dopamine neuron survival. New research has identified neuroprotective mechanisms

mediated by parkin. It seems to mediate neuroprotection through activation of IkappaB kinase/nuclear factor-kappaB signaling, whereas parkin mutants failed to stimulate this pathway (Henn et al., 2007).

PTEN-induced kinase-1 (PINK1)

Mutations in the *PINK1* gene were identified to cause early-onset familial PD (Valente et al., 2004). PINK1 is a 581 amino acid protein that contains an N-terminal mitochondrial targeting sequences and a highly conserved protein kinase domain similar to serine/threonine kinases of the Ca2+ calmodulin family. It has a ubiquitous and punctate expression pattern suggesting mitochondrial localization (Gandhi et al., 2006).

Very little is known about the precise function of PINK1 although its mitochondrial localization, the presence of kinase domain with identification of majority of mutations in the kinase domain and regions close to it, suggest a role in mitochondrial dysfunction, protein stability and kinase pathways in pathogenesis of PD. Indeed, overexpression of PINK1 protects cells from mitochondrial depolarization and apoptosis induced by the proteasomal inhibitor MG132, and from mitochondrially-induced apoptosis triggered by staurosporine. Expression of pathogenic mutations of *PINK1* that are predicted to inactivate it (E240K, L489P and K219M) do not protect against basal or apoptosis-inducing agents, implying that kinase activity is required for this effect. Parkin could restore normal mitochondrial morphology, DNA and protein content, but did not rescue the sensitivity of PINK1 mutant flies to apoptosis induced by stressors. This suggests that PINK1 and parkin interact to protect mitochondrial integrity, with PINK1 upstream of parkin (Wood-Kaczmar et al., 2006; Thomas & Beal, 2007).

DJ-1

Rare mutations in DJ-1 also cause autosomal recessive early onset PD (Bonofati et al., 2004). DJ-1 mutations account for 1–2% of all early-onset PD, with a number of different pathogenic mutations, including exonic deletions, truncations and homozygous and heterozygous point mutations. DJ-1 is a highly conserved protein of 189 amino acids that belongs to the DJ-1/Thi/PfpI protein super family (Thomas & Beal, 2007).

It is enriched in the brain where it is largely cytoplasmic except for a pool of DJ-1, which localizes to mitochondria (Zhang et al., 2005). The protein contains many residues that are readily oxidized, and it is thought to protect neurons from oxidative stress by acting as a redox-dependent chaperone. DJ-1 is oxidatively damaged in the brains of

patients with idiopathic PD, thus suggesting a mechanism of protein aggregation in these diseases that is mediated by high levels of oxidative stress (Choi et al., 2006). DJ-1 knockout mice show motor impairments and nigrostriatal dopaminergic dysfunction associated with attenuation of D2-mediated responses, resulting in increased re-uptake of dopamine by the dopamine transporter. The model lacks SN degeneration, suggesting that loss of DJ-1 function might confer increased susceptibility to parkinsonism as a result of underlying SN dysfunction (Wood-Kaczmar et al., 2006).

Leucine-rich repeat kinase 2 (LRRK2)

Mutations in the LRRK2 cause autosomal dominant PD (Zimprich et al., 2004). At least nine pathogenic mutations have been identified so far, including two that map to the kinase domain (Khan et al., 2005). The most-common pathogenic *LRRK2* mutation in Caucasians is the G2019S substitution, which causes parkinsonism closely resembling idiopathic PD, and accounts for ~ 5% of familial PD and 1.5% of sporadic cases (Gilks et al., 2005). In certain populations, however, the frequency of G2019S mutation is strikingly high: in North African Arabs, the frequency of this mutation is 37% in familial PD and 41% in sporadic PD. In Ashkenazi Jews, the frequency of the G2019S reaches 29.7% in familial PD and 13.3% in sporadic PD. mutations in the *LRRK2* gene give rise to diverse, widespread neuropathological features. For example, the *LRRK2* R1441C substitution in a Caucasian family was associated with intriguing pleomorphic pathology, including α-synuclein inclusions and tauopathy in addition to the classic selective SN degeneration (Zimprich et al., 2004).

LRRK2 encodes a 280 kDa multidomain protein that belongs to the ROCO family, a novel group of RAS GTPase superfamily. The precise physiological role of LRRK2 protein is unknown but the presence of multifunctional domains suggests involvement in wide variety of functions. The precise tissue and intracellular localization remain unclear but the expression within the human SN has been confirmed using quantitative real-time-PCR. Characterization of LRRK2 protein *in vitro* has so far been limited to overexpression cell models where it is reported to be predominantly cytoplasmic (West et al., 2005). Interestingly, LRRK2 protein can be detected in Lewy neurites and Lewy bodies of sporadic PD (Zhu et al., 2006).

Purified LRRK2 protein demonstrates kinase activity *in vitro* and the I2020T and G2019S mutations enhanced kinase activity (West et al., 2005). Although some mutations might have a toxic gain-of-function effect through an increase in kinase activity *in vitro*,

this has not yet been shown in any *in vivo* model. However, recent findings show significant alterations in phosphorilation of key proteins involved in MAPK signaling in leukocytes from patients with G2019S mutations implicating abnormal protein phosphorilation.

3.2.2 Intersecting pathways in PD pathogenesis

From the recent studies that were summed up previously in this chapter, PD can be defined as a complex disorder with multiple etiological factors involved in disease pathogenesis (Wood-Kaczmar et al., 2006; Thomas & Beal, 2007). PD may depend on a complex set of circumstances that include genetic factors, environmental exposures and loss of cellular protective mechanisms. Although the precise mechanisms of preferential DA cell death and inclusion formation in PD remain unclear, key factors are strongly implicated in the pathogenesis of both familial and sporadic PD, including mitochondrial dysfunction, protein phosphorylation, oxidative stress, protein misfolding and impairment of ubiquitin proteasome system (UPS). In Fig. 3.3 are reported a schematic representation of several different pathways that are important in modulating pathogenic events. Briefly, environmental factors similar to pesticides and toxins directly induce both oxidative damage and mitochondrial dysfunctions. α-Syn undergoes aggregation either due to pathogenic mutations or catechol oxidation which in turn compromise UPS function, induce endoplasmic reticulum stress and cause mitochondrial dysfunction. Mitochondrial dysfunction and oxidative damage lead to deficits in ATP which may compromise UPS function promoting abnormal protein aggregation. β-Synuclein is known to prevent α-syn aggregation through activation of Akt signaling. Parkin, an ubiquitin E3 ligase, promotes proteasomal degradation, increases mitochondrial biogenesis by activating mitochondrial transcription factor A (TFAM) and block PINK1-induced mitochondrial dysfunction, while pathogenic mutations, oxidative and nitrosative damage, severely compromise its protective function. DJ-1 protects against oxidative stress, functions as a chaperone to block α-syn aggregation and protects against mitochondrial dysfunction. PINK1 seems to protect against mitochondrial dysfunction which is compromised due to pathogenic mutations, although the precise function of PINK1 in mitochondria still needs to be determined. LRRK2 seems to play a role in synaptic vesicle functions, neurite outgrowth. Pathogenic mutations in LRRK2 cause abnormal protein phosphorylation which induce mitochondria-dependent cell death. In addition, a pathogenic role of PI3kinase-Akt

(phosphatidylinositol 3-kinase/Akt) and Nrf2/ARE signaling is implicated in PD pathogenesis. Familial PD-linked genes namely parkin, DJ-1 and PINK1 activate PI3 kinase-Akt signaling, while activation of Nrf2/ARE pathway prevents against oxidative damage and mitochondrial dysfunction promoting cell survival.

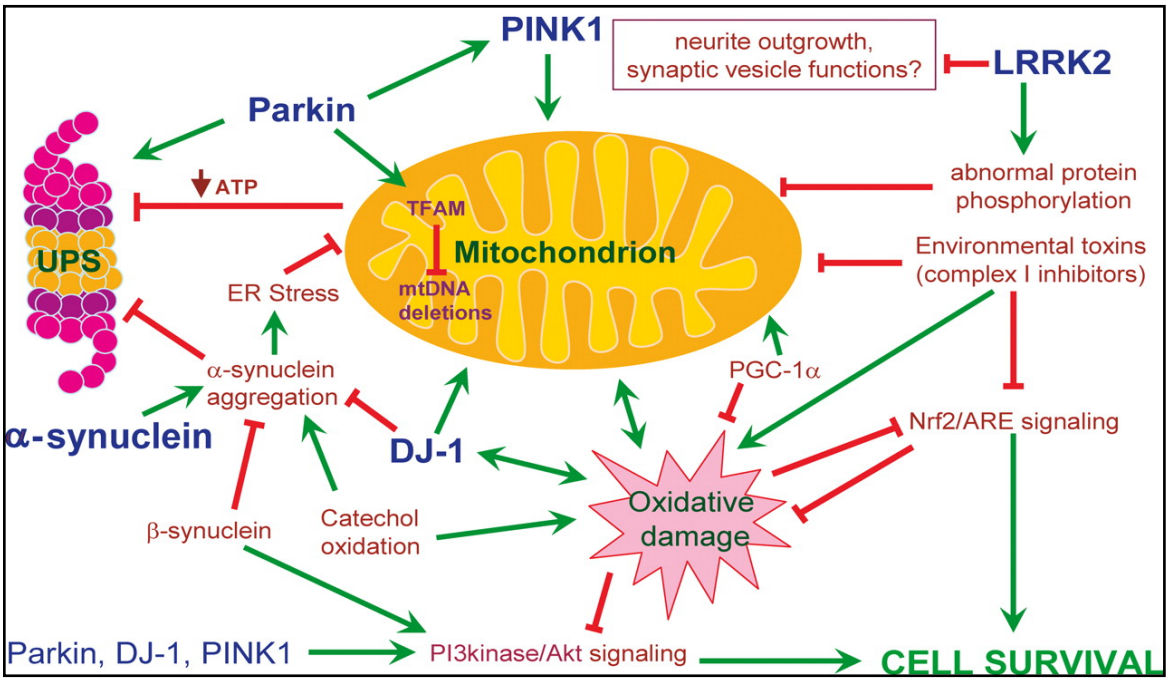

Fig. 3.3 Common intersecting pathways in PD pathogenesis (reprinted from Thomas & Beal, 2007). Green arrows indicate promoting or activating effects while red lines with blunt ends indicate inhibitory effects.

3.3 α-SYNUCLEIN

As previously mentioned (see §3.3.2), α-syn is a 140 amino acid protein that is highly expressed in the central nervous system, particularly at the presynaptic nerve terminals. It is the major component of LBs, the cytoplasmic proteinaceous aggregates pathognomonic for PD. These filamentous aggregates have a fibrillar structure with a cross-β-sheet core typical of amyloid (see § 1.2). Mutations or overexpression of the human α-syn gene have been linked to early-onset autosomal dominant PD. The mechanisms by which an abnormality in the structure or the expression of α-syn can cause PD have not been elucidated, nor is it known if the fibrillar deposits of α-syn play a toxic, protective, or no role in the pathogenesis of the disease (Ellis et al., 2005).

3.3.1 Structure and conformational properties of α-synuclein

α-Syn is a natively unfolded protein of still unknown function. Its sequence can be divided into three regions (Fig. 3.4). The N-terminal region, residues 1–60, includes the sites of three familial PD mutations and contains four 11-aminoacid, imperfect repeats with a highly conserved hexameric motif (KTKEGV). The N-terminal region is predicted to form amphipathic α-helices, typical of the lipid-binding domain of apolipoproteins (George et al., 1995; Clayton &George, 1998). The central region, residues 61–95, comprises the highly aggregation-prone NAC (non Amyloid-β Component) sequence (Ueda et al., 1993; Han et al., 1995). This region contains the remaining three imperfect repeats. The C-terminal region, residues 96–140, is highly enriched in acidic residues and prolines. Three highly conserved tyrosine residues are located in this region that is disordered in most conditions.

α-Syn is a typical intrinsically disordered (or natively unfolded) protein, which possesses little or no ordered structure under physiological conditions in vitro (Uversky et al., 2001). Intrinsically disordered proteins have recently been recognized as a new protein class, which are gaining considerable attention due to their capability to perform numerous biological functions despite the lack of unique structure (Wright and Dyson 1999; Uversky et al. 2000, 2005, 2007). These proteins exist as dynamic and highly flexible ensembles that undergo a number of distinct interconversions on different time scales. Recent studies have shown that monomeric α-syn has a more compact structure than expected for a completely unfolded polypeptide and this compactness has been linked to inhibition of fibrillation due to burial of the hydrophobic NAC domain

(Bertoncini et al., 2005; Dedmon et al., 2005; Bernardo et al., 2005). Small angle X-ray scattering analysis showed that the radius of gyration, *R*g, which is used to describe the dimensions of polypeptide chain, is ~ 40 Å of native α-syn, which is much larger than that predicted for a folded globular protein of 140 residues (15 Å), but significantly smaller than that for a fully unfolded random coil (52 Å). Recently, NMR studies have shown that α-syn adopts an ensemble of conformations that are stabilized by long-range interactions. In particular, a long-range intramolecular interaction between the C-terminal region (residues 120–140) and the central part of α-syn (residues 30–100) was noted (Bertoncini, et al., 2005).

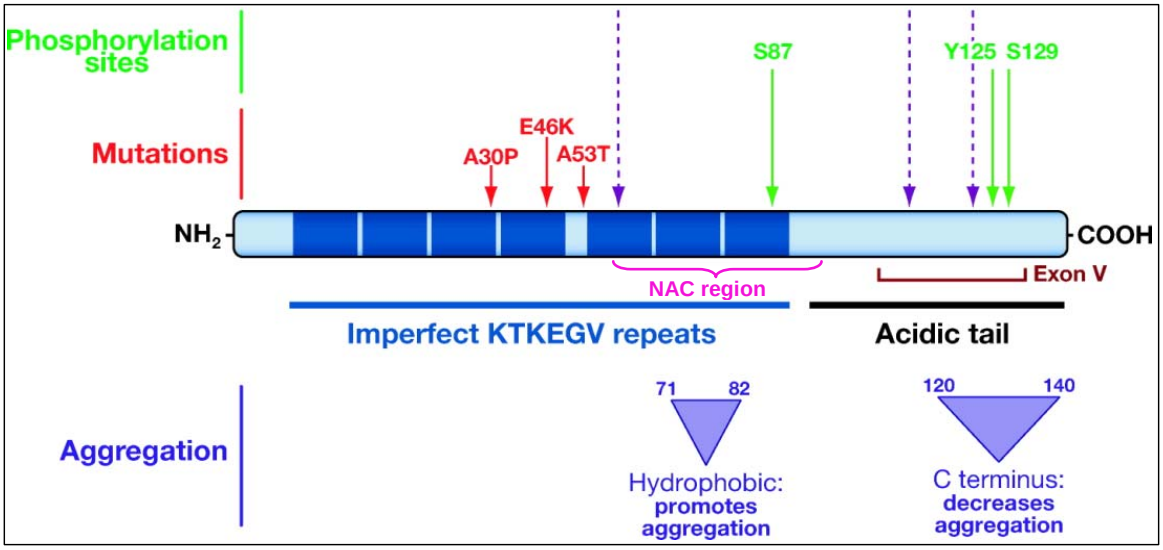

Fig. 3.4 Schematic of the primary structure of α-syn and indication of its most important characteristics.

The conformational behavior of α-syn under a variety of conditions was extensively analyzed (Uversky, 2003). The structure of α-syn is extremely sensitive to its environment and can be easily modulated by a change in conditions. Beside an extended state, α-syn can acquire a pre-molten globule state in several conditions such as low pH, high temperature, in the presence of various metal ions and as a result of spontaneous oligomerization both *in vitro* and *in vivo* (Uversky, et al., 2001; Uversky, 2007). Moreover, an α-helical membrane bound form (Davidson et al., 1998; Eliezer et al., 2001) and α-helical and β-structural species in organic solvent (Munishkina et al., 2003) were described. α-Syn is able to form morphologically distinct oligomers and aggregates such as dimers, oligomeric protofibrillar species and insoluble amorphous aggregates and

amyloid fibrils. Based on this conformational behavior, the concept of a protein-chameleon was proposed, which holds that the structure of α-syn is modulated by its environment to a dramatic degree. That is, the choice among all the above mentioned conformations is determined by the peculiarities of protein surroundings (Uversky, 2003; Uversky et al., 2007).

3.3.2 Physiological role of α-synuclein

Despite the evidence for a key function of α-syn in the onset of PD, its physiological function in the brain is still unclear. There are a lot of putative biological functions and possible interactions of α-syn. It was suggested to be involved in synaptic plasticity and in regulation of dopamine neurotransmission. Indeed, in the Zebra finch, α-syn is transiently expressed in a telencephalic area associated with song acquisition during the critical period for song learning (George et al., 1995). Moreover, α-syn knockout mice exhibit enhanced DA release at nigrostriatal terminals only in response to paired electrical stimuli, suggesting that α-syn is an activity-dependent, negative regulator of dopaminergic neurotransmission (Abeliovich et al., 2000). Other studies have demonstrated a putative function of α-syn as a chaperone protein, based on its abundance in the cytosol, its natively unfolded structure, and its prevention of protein aggregation induced by heat shock or chemical treatment (Souza et al., 2000). It can act as a molecular chaperone assisting in the folding and refolding of synaptic proteins called soluble NSF (N-ethylmaleimide sensitive factor) attachment receptors (Chandra et al., 2005).

The physiological function of α-syn is also correlated with lipids and membranes. In pre-synaptic termini, monomeric α-syn exists in an equilibrium between free and plasma membrane- or vesicle-bound states (McLean et al., 2000), with approximately 15% of α-syn being membrane-bound (Lee et al., 2002). This close association with vesicular structures has led to the hypothesis that α-syn may regulate vesicular release and/or turnover and other synaptic functions in the central nervous system (Ueda et al.,1993; Clayton & George, 1998, 1999; Davidson et al. 1998; Lavedan, 1998). Genome-wide screening in yeast showed that nearly one-third of genes that enhance the toxicity of α-syn are functionally related to lipid metabolism and vesicle trafficking (Willingham et al., 2003). Over-expression of α-syn in a neuronal cell line and homozygous deletions of α-syn in mice were both accompanied by noticeable changes in membrane fluidity and in

cellular fatty acid uptake and metabolism (Sharon et al., 2003; Castagnet et al., 2005; Golovko et al., 2005; see also §3.4.4). A recent analysis of a yeast PD model with dosage sensitivity for α-syn expression (Outeiro & Lindquist, 2003) revealed that the earliest defects following α-syn expression were an inhibition of the endoplasmic reticulum to Golgi vesicular trafficking and an impairment of the endoplasmic reticulum associated degradation (Cooper et al., 2006). Finally, a recent study revealed that α-syn regulates catecholamine release from the synaptic vesicles, and its over-expression inhibits a vesicle 'priming' step that occurs after secretory vesicle trafficking to 'docking' sites but before calcium-dependent vesicle membrane fusion (Larsen et al., 2006).

3.3.3 Aggregation properties of α-synuclein

The aggregation process of α-syn was extensively studied as α-syn amyloid fibrils are observed in LBs, the cardinal hallmark of PD pathology (see Fig. 3.1). The *in vitro* kinetics of α-syn fibril formation show an initial lag-phase followed by an exponential growth phase and a final plateau, usually attributed to a nucleation-dependent polymerization (§ chapter 1). Mature amyloid fibrils grown *in vitro* typically vary in length from about 500 nm to 3 mm and, based on AFM images, have an height of 9.8 ±1.2 nm (Khurana et al., 2003).

Uversky and coworkers showed that, early stages of fibril formation involve the partial folding of α-syn into the highly fibrillation-prone pre-molten globule-like conformation, which represents a key intermediate on the fibrillation pathway (Uversky et al. 2001, Fink, 2006). Hence, factors that shift the equilibrium in favor of this partially folded conformation facilitate fibril formation. Thus, an increase in protein concentration is predicted to increase the concentration of the intermediate, and accordingly the rate of fibrillation, as observed (Uversky et al., 2001). However, if one considers that the intrinsically unstructured monomer presents long-range interactions between the C-terminal region and the central amyloidogenic NAC region, a fully unfolded, aggregation-prone, conformation may be attained early in the aggregation pathway, exposing the hydrophobic NAC region and facilitating aggregation (Paleček et al., 2008). Structural perturbations, that can favor the aggregation prone conformation, include the presence of positively charged ions able to interact with the C terminus, a decrease in pH that reduce the net charge of the C-terminal region, and the deletion of the C terminus; all result in a more rapid aggregation reaction (Hoyer et al., 2004).

Analysis by TEM and AFM has revealed that different final product may arise from the aggregation of α-syn depending on the experimental conditions: fibrils, oligomers, and insoluble amorphous aggregates (Fink, 2006). Although the central role of α-syn fibrillation in the pathogenesis of PD is well established, recent evidence indicates, that the fibril itself may not be the primary pathogenic species. On the contrary, soluble oligomers and protofibrils seem to be the toxic species (Volles et al., 2002). Unfortunately, the direct detection of defined prefibrillar intermediates has proven extremely difficult. The oligomeric species of α-syn are present during the lag-phase of the aggregation process and they are relatively unstable, transient and present at very low steady-state concentrations (Goldberg et al., 2000). Several oligomeric protofibrillar species with various morphologies were detected (Conway et al. 1998, 2000; Ding et al. 2002; Lashuel et al. 2002). The earliest form of α-syn protofibrils appeared to be predominantly spherical with heights varying between 2.5 and 4.2 nm (Conway et al. 2000; Ding et al. 2002). These spherical beads can then convert into beaded chain and rings (Ding et al. 2002). The incubation of the spherical α-syn oligomers with brain derived membranes was shown to also produce pore-like ring-type protofibrils (Ding et al. 2002). These species formed in the late lag phase are characterized by extensive β-structure and sufficient structural regularity to bind ThT and CR (Chiti & Dobson, 2006). A key question is whether these oligomers are on direct pathway to fibrils or are off-pathway but in equilibrium with monomer that can add to fibrils or can add directly to growing fibrils. However, the fact that these spherical oligomers disappear at the same rate that fibrils appear suggests that fibrils could be assembled directly from them via longitudinal association of the oligomers, rather than by binding of monomer species to the growing end of fibrils (Apetri et al., 2006; Fink, 2006). Recently, following the isolation and characterization of protofibrils, oligomeric species, that appeared to precede fibrils and structured protofibrils formation, were identified by several techniques: photo-induced cross-linking of α-syn (Li et al., 2006); electrochemical techniques (Paleček et al., 2007); intrinsic tryptophan fluorescence of Y39W α-syn (Dusa et al., 2006) and FRET measurements of Y125W/Y133F/Y136F α-syn (Kaylor et al., 2005); fluorescence of pyrene-labeled α-syn (Thirunavukkuarasu et al., 2008). Structured protofibrillar species could form from the reorganization or assembly of small and relatively disorganized oligomers that are formed rapidly after the initiation of aggregation process. In Fig. 3.5 a schematic representation of the hypothetical aggregation pathways of α-syn is reported.

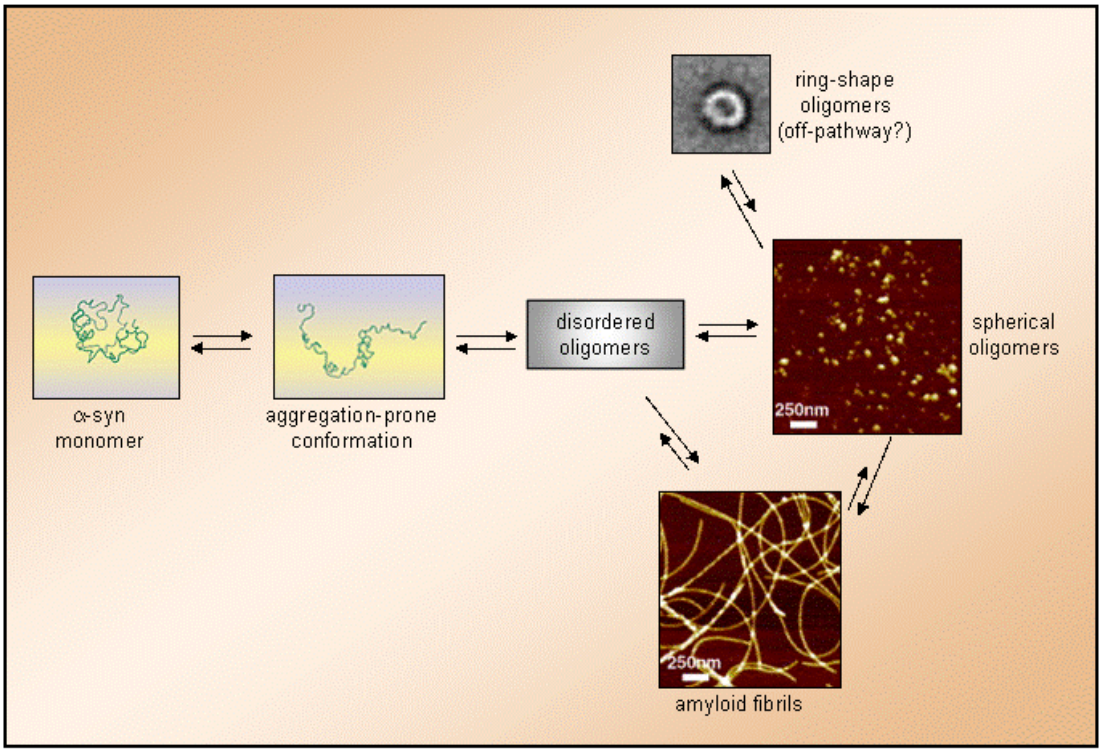

Fig.3.5 Schematic representation of the hypothetical aggregation pathways of α-syn. During α-syn fibrils formation several intermediate structures populate, including small oligomers, early-spherical protofibrils, membrane embedded pores or chain like aggregates. Therefore, α-syn fibrillization is not a simple two-state transition from monomer to fibrils, but rather a complex process that involves intermediates of various sizes and morphologies.

Furthermore, several modifications of α-syn lead to the formation of stable oligomers with very slow rates of dissociation. These modifications include oxidation of the four methionine residues to methionine sulfoxide (Hokenson et al., 2004), specific nitration of the tyrosine residues (Uversky et al., 2005), interaction with polyphenols such as bacalein (Zhu et al., 2004) and covalent modification by 4-hydroxynonenal (Qin et al., 2006). Typically these oligomers are formed more rapidly than fibrils, and as a consequence, no significant fibrillation occurs from these modified forms of α-syn. Biophysical characterization of these oligomers suggests that they have significant secondary and tertiary structure and are substantially more compact than monomeric α-syn. The stability of these oligomers indicates that the underlying structure of their subunits is different than that in the transient oligomers (Fink, 2006).

3.4 LIPIDS AND α-SYNUCLEIN

Since, as already mentioned (§ 3.3.2), α-syn is localized in the presynaptic nerve terminals and seems to modulate presynaptic pool size and neurotransmitter release, several studies were performed in order to analyze the interaction of α-syn with lipids and bilayer membranes. Recently, Beyer reviewed several aspects about the relation between α-syn and membranes and concluded that this interaction evinces a remarkable dichotomy, e.g. the binding of α-syn may be beneficial for the maintenance of the bilayer integrity or it may be deleterious for the membrane integrity; lipid interaction may promote or inhibit α-syn fibrillization, depending on the membrane composition, on the aggregative state of the protein and on the details of the experimental conditions (Beyer, 2007).

3.4.1 α-Synuclein and membrane properties

The lipid specificity of α-syn-membrane interaction was deeply investigated, but controversial results were obtained. For example high affinity for vesicles composed of phosphatidic acid was reported (Davidson et al. 1998, Perrin et al., 2000) which was not found in other studies (Jo et al., 2000; Ramakrishnan et al., 2003). However summing up, α-syn binds preferentially to small unilamellar vesicles containing acidic phospholipids such as phosphatidic acid, phosphatidylserine, and phosphatidylglycerol but not significantly to vesicles with a net neutral charge (Davidson et al., 1998; Jo et al., 2000; Perrin et al., 2000). Monounsaturated and polyunsaturated acyl groups in lipid vesicles increase the binding affinity of α-syn (Kubo et al., 2005). In conclusion, the interaction of α-syn with membranes is complex and dependent on the composition of the membranes, their curvature, as well as the ratio of membrane lipids to protein.

The observation that α-syn has a higher affinity for small vesicles than for vesicles of larger diameter, because of the higher surface-to-volume ratio of small vesicles, has suggested that it can effort a deep effect on bilayer properties. Indeed, the association of α-syn with negatively charged membranes of multilamellar vesicles has a profound effect on the integrity of these bilayers and causes the formation of non-bilayer or small vesicular structures (Madine et al., 2006). Moreover, the addition of monomeric α-syn to synaptic vesicles (Jo et al., 2004) or synthetic vesicles composed of brain sphingomyelin, DPPC, or POPC/POPG (Kamp & Beyer, 2006) increases the anisotropy of DHP, a fluorescent membrane probe sensitive to the ordering of fatty acid acyl chains. α-Syn not

only stabilizes the packing of the acyl chains but also increases the gel–liquid crystalline transition temperature (Kamp & Beyer, 2006). These observations suggest that the protein plays a role in modulating the organization of lipid membrane components and therefore, and they are in accord with the belief that the physiological function of α-syn may consist of stabilizing the synaptic vesicle reserve pool (Murphy et al., 2000).

3.4.2 Structure of membrane-bound α-synuclein

Far-UV CD and NMR data show that α-syn in the N-terminal region adopts an α-helical conformation on binding to membranes (Bisaglia et al., 2005; Eliezer et al., 2001; Bussell et al., 2003; Bussell et al., 2004; Ulmer et al., 2005; Chandra et al., 2003). An important paper demonstrated that α-syn assumes a bipartite structure upon binding to a SDS detergent micelles (Eliezer et al., 2001). The N-terminal 100 α-syn amino acids fold into an amphipathic helix that associates with the micelle–water interface whereas the acidic C-terminus of the protein remains unstructured. More insight into the micelle-induced α-syn structure became available from the carbon secondary shifts and from sequential NH-NH Nuclear Overhauser Enhancements (NOE), which showed that there are two helical regions in the N-terminal sequence, interrupted by a single helix break around residue 42 (Chandra et al., 2003; Bussell et al., 2003). A comparison with other proteins featuring the peculiar 11-mer repeat motives gave rise to the conclusion that the α-syn helical pitch is characterized by 3 turns over 11 residues (3/11 helix) rather than by 5 turns over 18 residues as in the standard version of an α-helix (Bussell et al., 2005). More recent NMR work revealed a distinct secondary structure of micelle-associated α-syn (Fig. 3.6 A): the two helices comprising residues 3–37 and 45–92, are oriented antiparallel, wrapped tightly around the SDS micelle and connected by an ordered antiparallel linker region, while the C-terminal protein tail remains highly mobile (Ulmer et al., 2005). Similar techniques were employed for a comparison of micelle binding of the A30P and A53T mutant α-syn proteins. It turned out that the former replacement perturbs the helical structure and the molecular dynamics of the protein whereas the A53T mutant is essentially indistinguishable from the wt protein. Cross-relaxation experiments also showed the partial insertion of the helices into the micellar interface (Ulmer et al., 2005). Similarly, paramagnetic relaxation enhancement of the α-syn backbone NH resonances in the presence of nitroxide labelled fatty acids indicated that the helical residues 61–95 are partially embedded in the SDS micelle (Bisaglia et al., 2005). In

structural biology, detergent micelles are commonly used as membrane-mimetic environments because their small size facilitates high-resolution structural analysis by NMR. However, it is often difficult to test whether the structure of proteins bound to micelles is the same as the respective membrane-bound form. Recently, it has been suggested that membrane-bound α-syn may have a similar structure to the micelle-bound form (Bortolus et al., 2008; Drescher et al., 2008). On the contrary, Jao and coworkers suggested an extended helical structure for α-syn bound to SUVs (Jao et al., 2004; Jao et al., 2008). The method of site-directed spin labeling was employed for an assessment of the structure of the protein bound at small unilamellar vesicles composed of phosphatidylcholine and phosphatidylserine (Jao et al., 2004). Spin labelling at 47 single sites, combined with an examination of the accessibility for oxygen or for a paramagnetic nickel complex, suggested an extended helical structure and enabled a detailed analysis of the α-syn topology with respect to the vesicle interface. This analysis confirmed the 3/11 helical arrangements and also suggested a bent shape of the helical part of the protein. Moreover, site-directed spin labeling and EPR-based approach (continuous-wave and pulse EPR) were used to determine the structure of α-syn bound to lipid membrane (Jao et al., 2008). α-Syn forms an extended, curved α-helical structure that is over 90 aa in length (Fig. 3.6 B) The monomeric helix has a superhelical twist similar to that of right-handed coiled-coils which, like α-syn, contain 11-aa repeats. The α-syn helix extends parallel to the curved membrane in a manner that allows conserved Lys and Glu residues to interact with the zwitterionic headgroups, while uncharged residues penetrate into the acyl chain region. In this work the authors argued also that the break between the α-syn helices in the presence of SDS is due to the small size and highly curvature of the micelle (Fig. 3.6 C) (Jao et al., 2008).

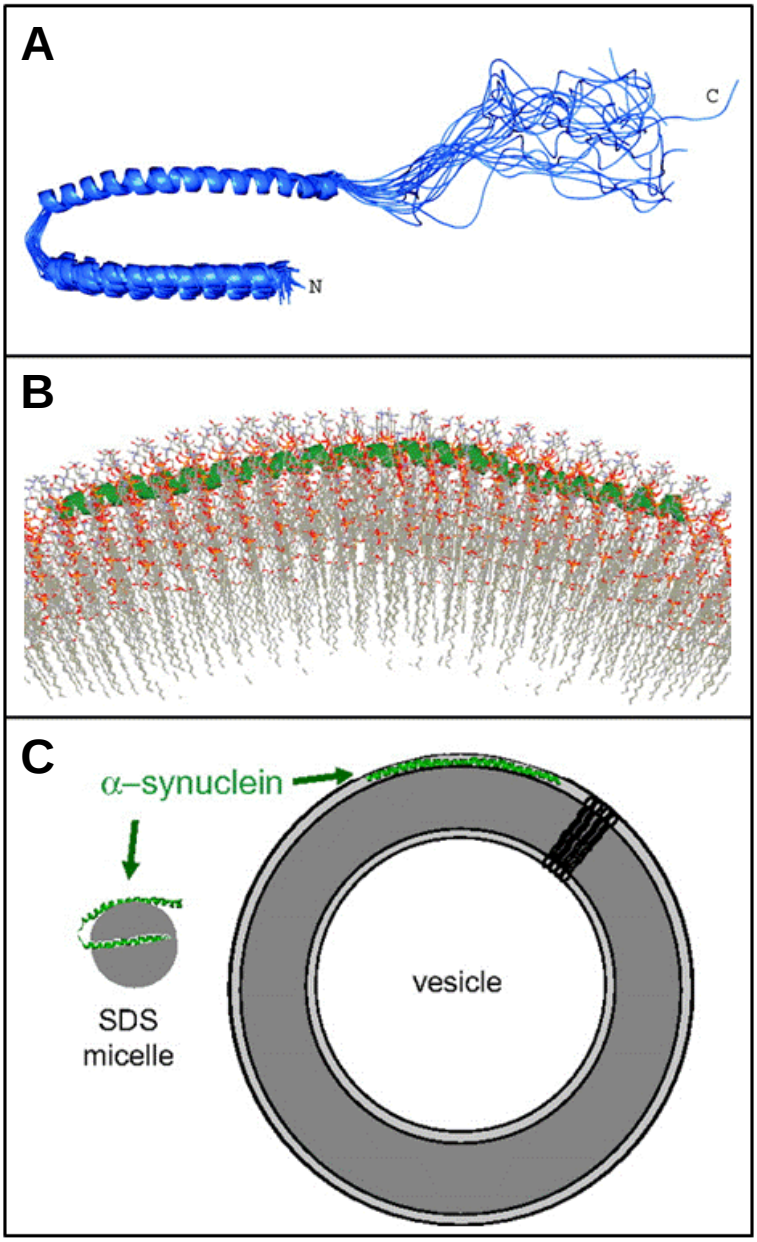

Fig. 3.6 (A) Structure of micelle-bound α-syn. Ensemble of twenty structures superimposed on helix-C. Helix-N (Val^{3}-Val^{37}) and helix-C (Lys^{45}-Thr^{92}) are connected by a short linker, followed by another short extended region (Gly^{93}-Lys^{97}) and a predominantly unstructured tail (Asp^{98}-Ala^{140}). **(B)** Representation of the interaction of α-syn with a curved lipid surface. A closer cross-sectional view of the α-syn interaction with the lipid surface. The protein (green) follows the curved surface of the vesicle, with the helical axis positioned just below the level of the phosphate groups of the lipids. **(C)** Comparison between the structures acquired by α-syn on micelles and SUVs (A reprinted from Ulmer et at., 2005; B and C reprinted from Jao et al., 2008).

3.4.3 α-Synuclein fibrillogenesis and membranes

Membranes and α-syn fibrillogenesis are correlated in two ways. Indeed, several observations suggest that the cytotoxicity of the oligomeric prefibrillar species of the protein is mediated by membrane damage and furthermore, α-syn aggregation process seems to be modulated by α-syn-lipid interaction.

α-Syn prefibrillar species have a tight membrane binding and the ability to permeabilize SUV composed of acidic phospholipids. An influx of Ca2+ ions into the vesicles, as detected by Fura-2 fluorescence, was attributed to the formation of pores consisting of α-syn oligomers in the vesicular bilayer (Volles et al., 2001; Volles & Lansbury, 2002; Volles & Lansbury, 2003). Small vesicles were more prone to permeabilization than larger ones, which conform with the binding preference of the α-syn monomer (Davidson et al., 1998). As already mentioned in § 3.3.3, the same authors later discovered annular and even tubular structures when the oligomeric aggregates of A30P and A53T α-syn were studied by electron microscopy and image reconstruction (Lashuel et al., 2002). These structures resembled the cytolytic β-barrel toxins of certain bacteria, suggesting that the annular shape directly accounts for a non-specific pore mechanism of the protofibril toxicity (Lashuel et al., 2002). Spherical protofibrils were also shown to bind much more tightly to brain-derived microsomal and mitochondrial membranes than monomers or fibrils. According to atomic force microscopy they eventually convert to the larger annular structures (Ding et al., 2002). Since α-syn oligomers (intracellular origin) have a cytotoxic effect when were added to human neuroblastoma cells and their action is on the outer cell membrane, it was suggested that the oligomer-mediated bilayer permeabilization may be rather unspecific (Kayed et al., 2003). Other authors, however, disagree with the channel interpretation. Rather, again on the basis of oligomer-induced membrane conductance, they concluded from the absence of single channel activity and ion selectivity that the oligomers were only peripherally associated with the membrane which allows ions to cross the perturbed lipid bilayer somehow on their own (Kayed et al., 2004).

The modulation of α-syn aggregation by lipid-protein interaction is an unresolved and debated question. If the binding to lipid vesicles and membranes is strong, the α-helix is stable and the formation of fibrils or prefibrillar oligomers, is slowed down or prevented (Zhu et al., 2003; Zhu & Fink, 2003). Under *in vitro* conditions of a high ratio of protein to lipid, where the protein is at high relative abundance with respect to the

interface, anionic membranes can promote the self-association of α-syn and accelerate fibrillation (Perrin et al., 2001, Cole et al., 2002; Lee et al., 2002; Necula et al., 2003). The mechanism of this aggregation is still unknown. However, in a review about the general problem of the role of lipid-protein interactions in amyloid-type protein fibril formation, it was reported there are several membrane-related factors promoting protein aggregation (Gorbenko & Kinnunen et al., 2006). Lipids seem to act as anti-chaperones facilitating protein transition into partially folded states more prone to aggregate. Another membrane-related phenomenon involves a protein accumulation at lipid-water interface that overcome the energy barrier for nucleation. The role of membranes in fibrillogenesis may involve also variations in the proportion of bilayer-buried and exposed regions of protein molecule; changes in the depth of bilayer penetration may be essential for a protein to act as a nucleus in fibril formation (Gorbenko & Kinnunen et al., 2006). Indeed, SDS-PAGE analysis revealed that wild type α-syn bound to synaptosomal membranes can seed the aggregation of cytosolic α-syn (Lee et al., 2002). These data suggestwere interpreted as indicating that a protein partially inserted into a lipid bilayer may act as an anchor for site-directed fibril assembly. Using environmentally sensitive probes it was demonstrated that wt α-syn exhibits predominant binding to the lipid headgroups, while the non-fibrillogenic mutant A53T inserts into the membrane interior to a greater extent so that the hydrophobic parts are buried within the bilayer. This masking of the hydrophobic, β-sheet promoting region was proposed to inhibit the self-assembly of the mutant protein into fibrils, while the superficial location of wt α-syn in membranes appears to favor seeding of fibril formation.

3.4.4 α-Synuclein and fatty acids

Recently, α-syn has been associated also with fatty acids (FAs). The protein seems to be implicated in fatty acid uptake and metabolism (Castagnet et al., 2005; Golovko et al., 2006, 2007, 2008). In astrocytes lacking α-syn, 16:0 (palmitic acid) and 20:4(ω6) (arachidonic acid) uptake is depressed, while 22:6(ω3) (docosahexaenoic acid-DHA) uptake is unaffected. In addition, the absence of α-syn disrupts the normal trafficking of these three fatty acids to specific lipid pools through an unknown mechanism (Castagnet et al., 2005). Similar to astrocytes, α-syn KO mice have reduced brain 16:0 uptake (45%) and 20:4(ω6) (12%) uptake in the absence of any change in brain 22:6(ω3) uptake (Golovko et al., 2005; Golovko et al., 2007). Thus, fatty acid uptake into the intact brain

is significantly depressed in the absence of α-syn. These authors measured also the incorporation rate and turnover of fatty acids in individual brain phospholipid pools. In α-syn-deficient mice, 16:0 metabolism is significantly altered with an increased rate of incorporation into phosphatidylcholine accompanied by reductions in incorporation rate into the other major phospholipids (Golovko et al., 2005). While in the absence of α-syn, there is only a minor reduction in the uptake of 20:4ω6 from the plasma, and there is a large and significant reduction in brain 20:4(ω6) metabolism. The incorporation rate for 20:4(ω6) into brain phospholipids is reduced over 50%, accounted for by a reduction in 20:4(ω6)-CoA (Golovko et al., 2006). Importantly, addition of physiologically relevant concentrations (3.15–6.3 nM) of wild type, but not mutant forms of α-syn, completely restores 20:4ω6-CoA formation in microsomes isolated from α-syn KO mice. Unlike wt α-syn, mutant forms of α-syn (A30P, E46K, and A53T) fail to modulate acyl-CoA synthetase (Acsl) activities, indicating that expression of these forms may function like the null. Although there is no net increase in 22:6(ω3) fatty acid uptake into the whole brain, the incorporation rate for 22:6(ω3) into brain phospholipids is increased over 50% in KO mice. Because 20:4(ω6) and 22:6(ω3) are the major polyunsaturated fatty acids in the brain, the increase in 22:6ω3 incorporation into brain phospholipids is considered to be compensatory for the reduction in rate of 20:4(ω6) incorporation into these lipid pools (Golovko et al., 2007). These results are consistent with the selective modulation by α-syn of specific ER-localized Acsl involved in 20:4(ω6)-CoA formation, but not in 22:6(ω3)-CoA formation. Moreover, when the intact mouse is subjected to a neurotraumatic event, such as ischemia, there is a net increase in the amount of prostanoids formed in α-syn-deficient mice (Golovko et al., 2008). This demonstrates the physiological relevance of the reduced recycling of 20:4(ω6) in these mice and so a profound and significant role for α-syn in brain inflammatory responses. Finally, it has been proposed that α-syn interacts with specific Acsl thereby modulating 20:4(ω6) metabolism and downstream events such as neuroinflammatory responses. α-Syn also directly affects lipid-mediated signal transduction through its interactions with phospholipases C and D. *In vitro* studies demonstrate that α-syn stimulates PLCβ activity by enhancing the G-protein coupled interaction with the enzyme (Narayana et al., 2005) and that it directly inhibits the activity of PLD2 (Payton et al., 2004; Ahn et al., 2002).

Moreover, Perrin and coworkers (Perrin et al., 2001) showed by electrophoretic

methods that α-syn forms multimers *in vitro* upon exposure to vesicles containing certain polyunsaturated fatty (PUFAs) acid acyl groups and that this process occurs at physiological concentrations. Since exposure of neuronal cell lines to PUFAs, in particular to DHA, increases the levels of α-syn oligomers, Sharon and coworkers (Sharon et al., 2003; Assayag et al., 2007) suggested that α-syn could interact with PUFAs *in vivo* to promote the formation of highly soluble oligomers that could precede the insoluble aggregates associated with neurodegeneration. Moreover, α-syn expression coupled with exposure to physiological levels of certain PUFAs enhanced clathrin-mediated endocytosis in neuronal and non-neuronal cultured cells and increased basal and evoked synaptic vesicle endocytosis in primary hippocampal cultures of wt and genetically depleted α-syn mouse brains. From these observations the authors argued that α-syn normally interacts with PUFAs to carry out its physiological functions, forming active forms of soluble oligomers. So, α-syn and PUFA mechanically alter membrane curvature as a result of enrichment of the plasma membrane with PUFAs, thereby facilitating endocytosis. Under certain potentially pathogenic conditions, this interaction may lead to neuronal membrane dysfunction and ultimately to α-syn aggregates and cell death (Ben Gedalya et al., 2008).

A detailed study of the molecular basis of the interaction between α-syn and PUFAs and an *in vitro* characterization of the resulting complex by several biophysical and biochemical methods are the topic of this PhD thesis.

3.5 REFERENCES

Abeliovich, A., Schmitz, Y., Fariñas, I., Choi-Lundberg, D., Ho, W. H., Castillo, P.E., Shinsky, N., Verdugo, J. M., Armanini, M., Ryan, A., Hynes, M., Phillips, H., Sulzer, D. & Rosenthal, A. (2000). Mice lacking alpha-synuclein display functional deficits in the nigrostriatal dopamine system. *Neuron*, **25**, 239–252.

Ahn, B. H., Rhim, H., Kim, S. Y., Sung, Y. M., Lee, M. Y., Choi, J. Y., Wolozin, B., Chang, J. S, Lee, Y. H., Kwon, T. K., Chung, K. C., Yoon, S. H., Hahn, S. J., Kim, M. S., Jo, Y. H., Min, D. S. (2002). alpha-Synuclein interacts with phospholipase D isozymes and inhibits pervanadate-induced phospholipase D activation in human embryonic kidney-293 cells. *J. Biol. Chem*., **277**, 12334–12342.

Apetri, M. M., Maiti, N. C., Zagorski, M. G., Carey, P. R., Anderson, V. E. (2006). Secondary structure of alpha-synuclein oligomers: characterization by raman and atomic force microscopy. *J. Mol. Biol*., **355**, 63–71.

Arima, K., Uéda, K., Sunohara, N., Hirai, S., Izumiyama, Y., Tonozuka-Uehara, H. & Kawai, M. (1998). Immunoelectron-microscopic demonstration of NACP/alpha-synuclein-epitopes on the filamentous component of Lewy bodies in Parkinson's disease and in dementia with Lewy bodies. *Brain Res*. **808**, 93–100.

Assayag, K., Yakunin, E., Loeb, V., Selkoe, D. J. & Sharon, R. (2007). Polyunsaturated fatty acids induce alpha-synuclein-related pathogenic changes in neuronal cells. *Am. J. Pathol.,* **171**, 2000–2011.

Ben Gedalya, T., Loeb, V., Israeli, E., Altschuler, Y., Selkoe, D. J., Sharon, R. (2008). alpha-Synuclein and PolyUnsaturated Fatty Acids Promote Clathrin Mediated Endocytosis and Synaptic Vesicle Recycling. *Traffic*, epub ahead of print.

Bertoncini, C. W., Jung, Y. S., Fernandez, C. O., Hoyer, W., Griesinger, C., Jovin, T. M., Zweckstetter, M. (2005). Release of long-range tertiary interactions potentiates aggregation of natively unstructured alpha-synuclein. *Proc. Natl. Acad. Sci. U S A.*, **102**, 1430–1435.

Beyer, K. (2007) Mechanistic aspects of Parkinson's disease: alpha-synuclein and the biomembrane. *Cell Biochem. Biophys*., **47**, 285–299.

Bisaglia, M., Tessari, I., Pinato, L., Bellanda, M., Girando, S., Fasano, M., Bergantino, E., Bubacco, L. & Mammi, S. (2005). A topological model of the interaction between alpha-synuclein and sodium dodecyl sulfate micelles. *Biochemistry,* **44**, 329–339.

Bonifati, V., Oostra, B. A., Heutink, P. (2004). Linking DJ-1 to neurodegeneration offers novel insights for understanding the pathogenesis of Parkinson's disease. *J. Mol. Med*., **82**, 163–174.

Bortolus, M., Tombolato, F., Tessari, I., Bisaglia, M., Mammi, S., Bubacco, L., Ferrarini, A., Maniero, A. L. (2008). Broken helix in vesicle and micelle-bound alpha-synuclein: insights from site-directed spin labeling-EPR experiments and MD simulations. *J. Am. Chem. Soc*., **130**, 6690–6691.

Braak, H., Del Tredici, K., Rüb, U., de Vos, R. A., Jansen Steur, E. N., Braak, E. (2003). Staging of brain pathology related to sporadic Parkinson's disease. *Neurobio.l Aging.*, **24**, 197–211.

Bussell, R. Jr., Eliezer, D. (2003). A structural and functional role for 11-mer repeats in alpha-synuclein and other exchangeable lipid binding proteins. *J. Mol. Biol*., **329**, 763–778.

Bussell, R. Jr., Eliezer, D. (2004). Effects of Parkinson's disease-linked mutations on the structure of lipid-associated alpha-synuclein. *Biochemistry*, **43**, 4810–4818.

Bussell, R. Jr., Ramlall, T. F., Eliezer, D. (2005). Helix periodicity, topology, and dynamics of membrane-associated alpha-synuclein. *Protein Sci.,* **14**, 862–872.

Cabin, D. E., Shimazu, K., Murphy, D., Cole, N. B., Gottschalk, W., McIlwain, K. L., Orrison, B., Chen, A., Ellis, C. E., Paylor, R., Lu, B. & Nussbaum, R.,L. (2002). Synaptic vesicle depletion correlates with attenuated synaptic responses to prolonged repetitive stimulation in mice lacking alpha-synuclein. *J. Neurosci.* **22**, 8797–8807.

Castagnet, P. I., Golovko, M. Y., Barceló-Coblijn, G. C., Nussbaum, R. L. & Murphy, E. J. (2005). Fatty acid incorporation is decreased in astrocytes cultured from alpha-synuclein gene-ablated mice. *J. Neurochem.* **94**, 839–849.

Chandra, S., Chen, X., Rizo, J., Jahn, R. & Südhof, T. C. (2003). A broken alpha -helix in folded alpha -Synuclein. *J. Biol. Chem*. **278**, 15313–15318.

Chen, L., Feany, M. B. (2005). Alpha-synuclein phosphorylation controls neurotoxicity and inclusion formation in a Drosophila model of Parkinson disease. *Nat. Neurosci.*, **8**, 657–663.

Chiti, F. and Dobson, C. M. (2006). Protein misfolding, functional amyloid, and human disease. *Annu. Rev. Biochem*., **75**, 333–366.

Choi, J., Sullards, M. C., Olzmann, J. A., Rees, H. D., Weintraub, S. T., Bostwick, D. E., Gearing, M., Levey, A. I., Chin, L. S., Li, L. (2006). Oxidative damage of DJ-1 is linked to sporadic Parkinson and Alzheimer diseases. *J. Biol. Chem*., **281**, 10816–10824.

Clayton, D. F. and George, J. M. (1998) The synucleins: a family of proteins involved in synaptic function, plasticity, neurodegeneration and disease. *Trends Neurosci*., **21**, 249–254.

Clayton, D. F. and George, J. M. (1999). Synucleins in synaptic plasticity and neurodegenerative disorders. *J. Neurosci. Res*., **58**, 120–129.

Cole, N. B., Murphy, D. D., Grider, T., Rueter, S., Brasaemle, D., Nussbaum, R. L. (2002). Lipid droplet binding and oligomerization properties of the Parkinson's disease protein alpha-synuclein. *J. Biol. Chem*., **277**, 6344–6352.

Conway, K. A., Harper, J. D., Lansbury, P. T. (1998). Accelerated in vitro fibril formation by a mutant alpha-synuclein linked to early-onset Parkinson disease. *Nat. Med.*, **4**, 1318–20.

Conway, K. A., Lee, S. J., Rochet, J. C., Ding, T. T., Williamson, R. E., Lansbury, P. T. Jr. (2000). Acceleration of oligomerization, not fibrillization, is a shared property of both alpha-synuclein mutations linked to early-onset Parkinson's disease: implications for pathogenesis and therapy. *Proc. Natl. Acad. Sci. U S A*., **97**, 571–576.

Conway, K. A., Harper, J. D., Lansbury, P. T. Jr. (2000). Fibrils formed in vitro from alpha-synuclein and two mutant forms linked to Parkinson's disease are typical amyloid. *Biochemistry*, **39**, 2552–2563.

Conway, K. A., Rochet, J. C., Bieganski, R. M., Lansbury, P. T. Jr. (2001). Kinetic stabilization of the alpha-synuclein protofibril by a dopamine-alpha-synuclein adduct. *Science*, **294**, 1346–1349.

Cookson, M. R. (2005). The biochemistry of Parkinson's disease. *Annu. Rev. Biochem.*, **74**, 29–52.

Cooper, A. A., Gitler, A. D., Cashikar, A., Haynes, C. M., Hill, K. J., Bhullar, B., Liu, K., Xu, K., Strathearn, K. E., Liu, F., Cao, S., Caldwell, K. A., Caldwell, G. A., Marsischky, G., Kolodner, R. D., Labaer, J., Rochet, J. C., Bonini, N. M., Lindquist, S. (2006). Alpha-synuclein blocks ER-Golgi traffic and Rab1 rescues neuron loss in Parkinson's models. *Science*, **313**, 324–328.

Croke, R. L., Sallum, C. O., Watson, E., Watt, E. D. & Alexandrescu, A. T. (2008). Hydrogen exchange of monomeric alpha-synuclein shows unfolded structure persists at physiological temperature and is independent of molecular crowding in Escherichia coli. *Protein Sci*. **17**, 1434–45.

Crowther, R. A., Jakes, R., Spillantini, M. G., Goedert, M. (1998). Synthetic filaments assembled from C-terminally truncated alpha-synuclein. *FEBS Lett*., **436**, 309–312.

Dalfó, E., Portero-Otín, M., Ayala, V., Martínez, A., Pamplona, R. & Ferrer, I. (2005). Evidence of oxidative stress in the neocortex in incidental Lewy body disease. *J. Neuropathol. Exp. Neurol.* **64**, 816–830.

Dauer, W., Przedborski, S. (2003). Parkinson's disease: mechanisms and models. *Neuron*., **39**, 889–909.

Davidson, W. S., Jonas, A., Clayton, D. F. & George, J. M. (1998). Stabilization of alpha-synuclein secondary structure upon binding to synthetic membranes. *J. Biol. Chem.* **273**, 9443–9449.

Dedmon, M. M., Lindorff-Larsen, K., Christodoulou, J., Vendruscolo, M., Dobson, C. M. (2005). Mapping long-range interactions in alpha-synuclein using spin-label NMR and ensemble molecular dynamics simulations. *J. Am. Chem. Soc*., **127**, 476–477.

de Rijk, M. C., Launer, L. J., Berger, K., Breteler, M. M., Dartigues, J. F., Baldereschi, M., Fratiglioni, L., Lobo, A., Martinez-Lage, J., Trenkwalder, C., Hofman, A. (2000). Prevalence of Parkinson's disease in Europe: A collaborative study of population-based cohorts. Neurologic Diseases in the Elderly Research Group. *Neurology*, **54**, S21–S23.

Ding, T. T., Lee, S. J., Rochet, J. C., Lansbury, P. T. Jr. (2002). Annular alpha-synuclein protofibrils are produced when spherical protofibrils are incubated in solution or bound to brain-derived membranes. *Biochemistry*, **41**, 10209–10217.

Drescher, M., Veldhuis, G., van Rooijen, B. D., Milikisyants, S., Subramaniam, V., Huber, M. (2008). Antiparallel arrangement of the helices of vesicle-bound alpha-synuclein. *J. Am. Chem. Soc*., **130**, 7796–7797.

Dunker, A. K., Brown, C. J. & Obradovic, Z. (2002). Identification and functions of usefully disordered proteins. *Adv. Protein Chem*. **62**, 25–49.

Dusa, A., Kaylor, J., Edridge, S., Bodner, N., Hong, D. P., Fink, A. L. (2006) Characterization of oligomers during alpha-synuclein aggregation using intrinsic tryptophan fluorescence. *Biochemistry*, **45**, 2752–2760.

Eliezer, D., Kutluay, E., Bussell, R. Jr & Browne, G. (2001). Conformational properties of alpha-synuclein in its free and lipid-associated states. *J. Mol. Biol*. **307**, 1061–1073.

Ellis, C. E., Murphy, E. J., Mitchell, D. C., Golovko, M. Y., Scaglia, F., Barceló-Coblijn, G. C. & Nussbaum, R. L. (2005). Mitochondrial lipid abnormality and electron transport chain impairment in mice lacking alpha-synuclein. *Mol. Cell. Biol*. **25**, 10190–10201.

El-Agnaf, O. M., Nagala, S., Patel, B. P., Austen, B.M. (2001). Non-fibrillar oligomeric species of the amyloid ABri peptide, implicated in familial British dementia, are more potent at inducing apoptotic cell death than protofibrils or mature fibrils. *J. Mol. Biol*., **310**, 157–68.

Farrer, M., Kachergus, J., Forno, L., Lincoln, S., Wang, D. S., Hulihan, M., Maraganore, D., Gwinn-Hardy, K., Wszolek, Z., Dickson, D., Langston, J. W. (2004). Comparison of kindreds with parkinsonism and alpha-synuclein genomic multiplications. *Ann. Neurol*., **55**, 174–179.

Fink, A. L. (2006). The aggregation and fibrillation of alpha-synuclein. *Acc. Chem. Res*., **39**, 628–634.

Fleming, S. M., Fernagut, P. O., Chesselet, M. F. (2005). Genetic mouse models of parkinsonism: strengths and limitations. *Neuro. Rx*., **2**, 495–503.

Fujiwara, H., Hasegawa, M., Dohmae, N., Kawashima, A., Masliah, E., Goldberg, M. S., Shen, J., Takio, K., Iwatsubo, T. (2002). alpha-Synuclein is phosphorylated in synucleinopathy lesions. *Nat. Cell. Biol*., **4**, 160–164.

Gandhi, S., Muqit, M. M., Stanyer, L., Healy, D. G., Abou-Sleiman, P. M., Hargreaves, I., Heales, S., Ganguly, M., Parsons, L., Lees, A. J., Latchman, D. S., Holton, J. L., Wood, N. W., Revesz, T. (2006). PINK1 protein in normal human brain and Parkinson's disease. *Brain*, 1**29**, 1720–1731.

George, J. M., Jin, H., Woods, W. S. & Clayton, D. F. (1995). Characterization of a novel protein regulated during the critical period for song learning in the zebra finch. *Neuron*, **15**, 361–372.

Gilks, W. P., Abou-Sleiman, P. M., Gandhi, S., Jain, S., Singleton, A., Lees, A. J., Shaw, K., Bhatia, K. P., Bonifati, V., Quinn, N. P., Lynch, J., Healy, D. G., Holton, J. L.,

Revesz, T., Wood, N. W. (2005). A common LRRK2 mutation in idiopathic Parkinson's disease. *Lancet*, **365**, 415–416.

Gitler, A. D. & Shorter, J. (2007). Prime time for alpha-synuclein. *J. Neurosci*. **27**, 2433–2434.

Goldberg, M. S., Lansbury, P. T. Jr. (2000). Is there a cause-and-effect relationship between alpha-synuclein fibrillization and Parkinson's disease? *Nat. Cell. Biol*., **2**, E115–119

Golovko, M. Y., Faergeman, N. J., Cole, N. B., Castagnet, P. I., Nussbaum, R. L., Murphy, E. J. (2005). Alpha-synuclein gene deletion decreases brain palmitate uptake and alters the palmitate metabolism in the absence of alpha-synuclein palmitate binding. *Biochemistry*, **44**, 8251–8259.

Golovko, M. Y., Rosenberger, T. A., Faergeman, N. J., Feddersen, S., Cole, N. B., Pribill, I., Berger, J., Nussbaum, R. L. & Murphy, E. J. (2006). Acyl-CoA synthetase activity links wild-type but not mutant alpha-synuclein to brain arachidonate metabolism. *Biochemistry,* **45**, 6956–6966.

Golovko, M. Y., Rosenberger, T. A., Feddersen, S., Faergeman, N. J., Murphy, E.J. (2007). Alpha-synuclein gene ablation increases docosahexaenoic acid incorporation and turnover in brain phospholipids. *J. Neurochem.* **101**, 201–211.

Golovko, M. Y., Barceló-Coblijn, G., Castagnet, P. I., Austin, S., Combs, C. K, Murphy, E. J. (2008). The role of alpha-synuclein in brain lipid metabolism: a downstream impact on brain inflammatory response. *Mol. Cell. Biochem.,* Dec 31.

Gorbenko, G. P., Kinnunen, P. K. (2006). The role of lipid-protein interactions in amyloid-type protein fibril formation. *Chem. Phys. Lipids*, **141**, 72–82.

Han, H., Weinreb, P. H., Lansbury, P. T. Jr. (1995). The core Alzheimer's peptide NAC forms amyloid fibrils which seed and are seeded by beta-amyloid: is NAC a common trigger or target in neurodegenerative disease? *Chem. Biol*., **2**, 163–169.

Hatcher, J. M., Pennell, K. D., Miller, G. W. (2008). Parkinson's disease and pesticides: a toxicological perspective. *Trends Pharmacol. Sci*., **29**, 322–329.

Henn, I. H., Bouman, L., Schlehe, J. S., Schlierf, A., Schramm, J. E., Wegener, E., Nakaso, K., Culmsee, C., Berninger, B., Krappmann, D., Tatzelt, J., Winklhofer, K. F. (2007). Parkin mediates neuroprotection through activation of IkappaB kinase/nuclear factor-kappaB signaling. *J. Neurosci*., **27**, 1868–1878.

Hokenson, M. J., Uversky, V. N., Goers, J., Yamin, G., Munishkina, L. A., Fink, A. L. (2004). Role of individual methionines in the fibrillation of methionine-oxidized alpha-synuclein. *Biochemistry*, **43**, 4621–4633.

Hornykiewicz O. (2002). L-DOPA: from a biologically inactive amino acid to a successful therapeutic agent. *Amino Acids.*, **23**, 65–70.

Hoyer, W., Cherny, D., Subramaniam, V., Jovin, T.M. (2004). Impact of the acidic C-terminal region comprising amino acids 109-140 on alpha-synuclein aggregation in vitro. *Biochemistry*, **43**, 16233–16242.

Irvine, G. B., El-Agnaf, O. M., Shankar, G. M., Walsh, D. M. (2008). Protein aggregation in the brain: the molecular basis for Alzheimer's and Parkinson's diseases. *Mol. Med*., **14**, 451–464.

Iwai, A., Masliah, E., Yoshimoto, M., Ge, N., Flanagan, L., de Silva, H. A., Kittel, A., Saitoh, T. (1995). The precursor protein of non-A beta component of Alzheimer's disease amyloid is a presynaptic protein of the central nervous system. *Neuron.,* **14**, 467–475.

Jao, C. C., Der-Sarkissian, A., Chen, J., Langen, R. (2004). Structure of membrane-bound alpha-synuclein studied by site-directed spin labeling. *Proc. Natl. Acad. Sci. U S A*, **101**, 8331–8336

Jao, C. C., Hegde, B. G., Chen, J., Haworth, I. S., Langen, R. (2008). Structure of membrane-bound alpha-synuclein from site-directed spin labeling and computational refinement. *Proc. Natl. Acad. Sci. U S A*, **105**, 19666–19671.

Jo, E., McLaurin, J., Yip, C. M., St George-Hyslop, P., Fraser, P. E. (2000). alpha-Synuclein membrane interactions and lipid specificity. *J. Biol. Chem*., **275**, 34328–34334.

Jo, E., Darabie, A. A., Han, K., Tandon, A., Fraser, P. E., McLaurin, J. (2004). alpha-Synuclein-synaptosomal membrane interactions: implications for fibrillogenesis. *Eur. J. Biochem*., **271**, 3180–3189.

Kamp, F. & Beyer, K. (2006) Binding of α-synuclein affects the lipid packing in bilayers of small vesicles. *J. Biol. Chem.* **281**, 9251–9259.

Kayed, R., Head, E., Thompson, J. L., McIntire, T. M., Milton, S. C., Cotman, C. W., Glabe, C. G. (2003). Common structure of soluble amyloid oligomers implies common mechanism of pathogenesis. *Science*, **300**, 486–489.

Kayed, R., Sokolov, Y., Edmonds, B., McIntire, T. M., Milton, S. C., Hall, J. E., Glabe, C. G. (2004). Permeabilization of lipid bilayers is a common conformation-dependent activity of soluble amyloid oligomers in protein misfolding diseases. *J. Biol. Chem*., **279**, 46363–46366.

Kaylor J, Bodner N, Edridge S, Yamin G, Hong DP, Fink AL. (2005). Characterization of oligomeric intermediates in alpha-synuclein fibrillation: FRET studies of Y125W/Y133F/Y136F alpha-synuclein. *J. Mol. Biol*., **353**, 357–372.

Khan, A., Ashcroft, A. E., Higenell, V., Korchazhkina, O. V., Exley, C. (2005). Metals accelerate the formation and direct the structure of amyloid fibrils of NAC. *J. Inorg. Biochem*., **99**, 1920–1927.

Khurana, R., Ionescu-Zanetti, C., Pope, M., Li, J., Nielson, L., Ramírez-Alvarado, M., Regan, L., Fink, A. L., Carter, S. A. (2003). A general model for amyloid fibril

assembly based on morphological studies using atomic force microscopy. *Biophys. J.*, **85**, 1135–44.

Klivenyi, P., Siwek, D., Gardian, G., Yang, L., Starkov, A., Cleren, C., Ferrante, R. J., Kowall, N. W., Abeliovich, A., Beal, M. F. (2006). Mice lacking alpha-synuclein are resistant to mitochondrial toxins. *Neurobiol. Dis.*, **21**, 541–548.

Krüger, R., Kuhn, W., Müller, T., Woitalla, D., Graeber, M., Kösel, S., Przuntek, H., Epplen, J. T., Schöls, L. & Riess, O. (1998). Ala30Pro mutation in the gene encoding alpha-synuclein in Parkinson's disease. *Nat. Genet.* **18**, 106–108.

Kubo, S., Nemani, V. M., Chalkley, R. J., Anthony, M. D., Hattori, N., Mizuno, Y., Edwards, R. H., Fortin, D. L. (2005). A combinatorial code for the interaction of alpha-synuclein with membranes. *J. Biol. Chem.*, **280**, 31664–31672.

Langston, J. W. (1985). MPTP neurotoxicity: an overview and characterization of phases of toxicity. *Life Sci.*, **36**, 201–206.

Larsen, K. E., Schmitz, Y., Troyer, M. D., Mosharov, E., Dietrich, P., Quazi, A. Z., Savalle, M., Nemani, V., Chaudhry, F. A., Edwards, R. H., Stefanis, L., Sulzer, D. (2006). Alpha-synuclein overexpression in PC12 and chromaffin cells impairs catecholamine release by interfering with a late step in exocytosis. *J. Neurosci.*, **26**, 11915–11922.

Lashuel, H. A., Hartley, D., Petre, B. M., Walz, T., Lansbury, P. T. Jr. (2002). Neurodegenerative disease: amyloid pores from pathogenic mutations. *Nature*, **418**, 291.

Lavedan, C., Leroy, E., Dehejia, A., Buchholtz, S., Dutra, A., Nussbaum, R. L., Polymeropoulos, M. H. (1998). Identification, localization and characterization of the human gamma-synuclein gene. *Hum. Genet.*, **103**, 106–112.

Lee, H. J, Choi, C., Lee, S. J. (2002). Membrane-bound alpha-synuclein has a high aggregation propensity and the ability to seed the aggregation of the cytosolic form. *J. Biol. Chem.*, **277**, 671–678.

Lewitt, P. A. (2008). Levodopa for the treatment of Parkinson's disease. *N. Engl. J. Med.*, **359**, 2468–2476.

Li, H. T., Lin, X. J., Xie, Y. Y., Hu, H. Y. (2006). The early events of alpha-synuclein oligomerization revealed by photo-induced cross-linking. *Protein Pept. Lett.*, **13**, 385–390.

Lücke, C., Gantz, D. L., Klimtchuk, E. & Hamilton J. A. (2006). Interactions between fatty acids and alpha-synuclein. *J. Lipid Res.* **47**, 1714–1724.

Madine, J., Doig, A. J., Middleton, D. A. (2006). A study of the regional effects of alpha-synuclein on the organization and stability of phospholipid bilayers. *Biochemistry*, **45**, 5783–5792.

Mazzulli, J. R., Armakola, M., Dumoulin, M., Parastatidis, I., Ischiropoulos, H. (2007). Cellular oligomerization of alpha-synuclein is determined by the interaction of oxidized catechols with a C-terminal sequence. *J. Biol. Chem*., **282**, 31621–31630.

McLean, P. J., Kawamata, H., Ribich, S. & Hyman, B. T. (2000). Membrane association and protein conformation of alpha-synuclein in intact neurons. Effect of Parkinson's disease-linked mutations. *J. Biol. Chem*. **275**, 8812–8816.

McNulty, B. C., Tripathy, A., Young, G. B., Charlton, L. M., Orans, J. & Pielak, G. J. (2006). Temperature-induced reversible conformational change in the first 100 residues of alpha-synuclein. *Protein Sci.* **15**, 602–608.

Miller, D. W., Hague, S. M., Clarimon, J., Baptista, M., Gwinn-Hardy, K., Cookson, M. R., Singleton, A. B. (2004). Alpha-synuclein in blood and brain from familial Parkinson disease with SNCA locus triplication. *Neurology*, **62**, 1835–1838.

Mori, F., Tanji, K., Yoshimoto, M., Takahashi, H., Wakabayashi, K. (2002). Demonstration of alpha-synuclein immunoreactivity in neuronal and glial cytoplasm in normal human brain tissue using proteinase K and formic acid pretreatment. *Exp. Neurol*., **176**, 98–104.

Munishkina, L. A., Phelan, C., Uversky, V. N., Fink, A. L. (2003). Conformational behavior and aggregation of alpha-synuclein in organic solvents: modeling the effects of membranes. *Biochemistry*, **42**, 2720–2730.

Murphy, D. D., Rueter, S. M., Trojanowski, J. Q., Lee, V. M. (2000). Synucleins are developmentally expressed, and alpha-synuclein regulates the size of the presynaptic vesicular pool in primary hippocampal neurons. *J. Neurosci*., **20**, 3214–3220.

Narayanan, V., Guo, Y. & Scarlata, S. (2005). Fluorescence studies suggest a role for alpha-synuclein in the phosphatidylinositol lipid signaling pathway. *Biochemistry,* **44**, 462–470.

Necula, M., Chirita, C. N. & Kuret, J. (2003). Rapid anionic micelle-mediated alpha-synuclein fibrillization in vitro. *J. Biol. Chem.* **278**, 46674–46680.

Nutt, J. G., Woodward, W. R., Hammerstad, J. P., Carter, J. H., Anderson, J. L. (1984). The "on-off" phenomenon in Parkinson's disease. Relation to levodopa absorption and transport. *N. Engl. J. Med*., **310**, 483–488.

Outeiro, T. F., Lindquist, S. (2003). Yeast cells provide insight into alpha-synuclein biology and pathobiology. *Science*, **302**, 1772–1775.

Palacino, J. J., Sagi, D., Goldberg, M. S., Krauss, S., Motz, C., Wacker, M., Klose, J., Shen, J. (2004). Mitochondrial dysfunction and oxidative damage in parkin-deficient mice. *J. Biol. Chem*., **279**, 18614–18622.

Paleček, E. and Ostatná, V. (2007). Electroactivity of Nonconjugated Proteins and Peptides. Towards Electroanalysis of All Proteins. *Electroanalysis*, **19**, 2383–2403.

Paleček, E., Ostatná, V., Masarík, M., Bertoncini, C. W., Jovin, T. M. (2008). Changes in interfacial properties of alpha-synuclein preceding its aggregation. *Analyst*, **133**, 76–84.

Parkinson, J. (2002). An essay on the shaking palsy. 1817. *J. Neuropsychiatry Clin. Neurosci.*, **14**, 223–236.

Payton, J. E., Perrin, R. J., Woods, W. S., George, J. M. (2004). Structural determinants of PLD2 inhibition by alpha-synuclein. *J. Mol. Biol*., **337**, 1001–1009.

Perrin, R. J., Woods, W. S., Clayton, D. F. & George J. M. (2000). Interaction of human alpha-Synuclein and Parkinson's disease variants with phospholipids. Structural analysis using site-directed mutagenesis. *J. Biol. Chem*. **275**, 34393–34398.

Perrin, R. J., Woods, W. S., Clayton, D. F. & George, J. M. (2001). Exposure to long chain polyunsaturated fatty acids triggers rapid multimerization of synucleins. *J. Biol. Chem*. **276**, 41958–41962.

Polymeropoulos, M. H., Lavedan, C., Leroy, E., Ide, S. E., Dehejia, A., Dutra, A., Pike, B., Root, H., Rubenstein, J., Boyer, R., Stenroos, E. S., Chandrasekharappa, S., Athanassiadou, A., Papapetropoulos, T., Johnson, W. G, Lazzarini, A. M., Duvoisin, R. C., Di Iorio, G., Golbe, L. I. & Nussbaum, R. L. (1997). Mutation in the alpha-synuclein gene identified in families with Parkinson's disease. *Science*, **276**, 2045–2047.

Qin, Z., Hu, D., Han, S., Reaney, S. H., Di Monte, D. A., Fink, A. L. (2007). Effect of 4-hydroxy-2-nonenal modification on alpha-synuclein aggregation. *J. Biol. Chem.*, **282**, 5862–5870.

Ramakrishnan, M., Jensen, P. H., Marsh, D. (2003). Alpha-synuclein association with phosphatidylglycerol probed by lipid spin labels. *Biochemistry*, **42**, 12919–12926.

Serpell, L. C., Sunde, M., Benson, M. D., Tennent, G. A., Pepys, M. B., Fraser, P. E. (2000). The protofilament substructure of amyloid fibrils. *J. Mol. Biol*., **300**, 1033–1039.

Sharon, R., Bar-Joseph, I., Frosch, M. P., Walsh, D. M., Hamilton, J. A. & Selkoe, D. J. (2003). The formation of highly soluble oligomers of alpha-synuclein is regulated by fatty acids and enhanced in Parkinson's disease. *Neuron*, **37**, 583–595.

Sharon, R., Bar-Joseph, I., Mirick, G. E., Serhan, C. N. & Selkoe, D. J. (2003). Altered fatty acid composition of dopaminergic neurons expressing alpha-synuclein and human brains with alpha-synucleinopathies. *J. Biol. Chem*. **278**, 49874–49881.

Sharon, R., Goldberg, M. S., Bar-Josef, I., Betensky, R. A., Shen, J. & Selkoe, D. J. (2001). Alpha-Synuclein occurs in lipid-rich high molecular weight complexes, binds fatty acids, and shows homology to the fatty acid-binding proteins. *Proc. Natl. Acad. Sci. U S A*, **98**, 9110–9115.

Shimura, H., Hattori, N., Kubo, S., Mizuno, Y., Asakawa, S., Minoshima, S., Shimizu, N., Iwai, K., Chiba, T., Tanaka, K., Suzuki, T. (2000). Familial Parkinson disease gene product, parkin, is a ubiquitin-protein ligase. *Nat. Genet*., **25**, 302–305.

Shults, C. W. (2006). Lewy bodies. *Proc. Natl. Acad. Sci. U S A*, **103**, 1661–1668.

Singleton, A. B., Farrer, M., Johnson, J., Singleton, A., Hague, S., Kachergus, J., Hulihan, M., Peuralinna, T., Dutra, A., Nussbaum, R., Lincoln, S., Crawley, A., Hanson, M., Maraganore, D., Adler, C., Cookson, M. R., Muenter, M., Baptista, M., Miller, D., Blancato, J., Hardy, J. & Gwinn-Hardy, K. (2003). alpha-Synuclein locus triplication causes Parkinson's disease. *Science*, **302**, 841.

Souza, J. M., Giasson, B. I., Lee, V. M. & Ischiropoulos, H. (2000). Chaperone-like activity of synucleins. *FEBS Lett.* **474**, 116–119.

Spillantini, M. G., Crowther, R. A., Jakes, R., Hasegawa, M. & Goedert, M. (1998). alpha-Synuclein in filamentous inclusions of Lewy bodies from Parkinson's disease and dementia with Lewy bodies. *Proc. Natl. Acad. Sci. U S A*, **95**, 6469–6473.

Sriram, S. R., Li, X., Ko, H. S., Chung, K. K., Wong, E., Lim, K. L., Dawson, V. L., Dawson, T. M. (2005). Familial-associated mutations differentially disrupt the solubility, localization, binding and ubiquitination properties of parkin. *Hum. Mol. Genet*., **14**, 2571–2586.

Stichel, C. C., Zhu, X. R., Bader, V., Linnartz, B., Schmidt, S., Lübbert, H. (2007). Mono- and double-mutant mouse models of Parkinson's disease display severe mitochondrial damage. *Hum. Mol. Genet*., **16**, 2377–2393.

Thirunavukkuarasu, S., Jares-Erijman, E. A., Jovin, T. M. (2008). Multiparametric fluorescence detection of early stages in the amyloid protein aggregation of pyrene-labeled alpha-synuclein. *J. Mol. Biol*., **378**, 1064–1073.

Thomas, B., Beal, M. F. (2007). Parkinson's disease. *Hum. Mol. Genet*., **16**, 183–194.

Uéda, K., Fukushima, H., Masliah, E., Xia, Y., Iwai, A., Yoshimoto, M., Otero, D. A., Kondo, J., Ihara, Y., Saitoh, T. (1993) Molecular cloning of cDNA encoding an unrecognized component of amyloid in Alzheimer disease. *Proc. Natl. Acad. Sci. U S A*, **90**, 11282–11286.

Ulmer, T. S., Bax, A., Cole, N. B. & Nussbaum, R. L. (2005). Structure and dynamics of micelle-bound human alpha-synuclein. *J. Biol. Chem*. **280**, 9595–9603.

Uversky, V. N., Gillespie, J. R., Fink, A. L. (2000). Why are "natively unfolded" proteins unstructured under physiologic conditions? *Proteins*, **41**, 415–427.

Uversky, V. N., Li, J., Fink, A. L. (2001). Metal-triggered structural transformations, aggregation, and fibrillation of human alpha-synuclein. A possible molecular NK between Parkinson's disease and heavy metal exposure. *J. Biol. Chem*., **276**, 44284–44296.

Uversky, V. N., Li, J., Fink, A. L. (2001). Evidence for a partially folded intermediate in alpha-synuclein fibril formation. *J. Biol. Chem*., **276**, 10737–10744.

Uversky, V. N. (2002). Natively unfolded proteins: A point where biology waits for physics. *Protein Sci.* **11**, 739–756.

Uversky, V. N. (2003). A protein-chameleon: conformational plasticity of alpha-synuclein, a disordered protein involved in neurodegenerative disorders. *J. Biomol. Struct. Dyn*., **21**, 211–234

Uversky, V. N., Yamin, G., Munishkina, L. A., Karymov, M. A., Millett, I. S., Doniach, S., Lyubchenko, Y. L., Fink, A. L. (2005). Effects of nitration on the structure and aggregation of alpha-synuclein. *Brain Res. Mol. Brain Res*., **134**, 84–102.

Uversky, V. N. (2007) Neuropathology, biochemistry, and biophysics of α-synuclein aggregation. *J. Neurochem*. **103,** 17–37.

Valente, E. M., Abou-Sleiman, P. M., Caputo, V., Muqit, M. M., Harvey, K., Gispert, S., Ali, Z., Del Turco, D., Bentivoglio, A. R., Healy, D. G., Albanese, A., Nussbaum, R., González-Maldonado, R., Deller, T., Salvi, S., Cortelli, P., Gilks, W. P., Latchman, D. S., Harvey, R. J., Dallapiccola, B., Auburger, G., Wood NW. (2004). Hereditary early-onset Parkinson's disease caused by mutations in PINK1. *Science*, **304**, 1158–1160.

Volles, M. J., Lee, S. J., Rochet, J. C., Shtilerman, M. D., Ding, T. T., Kessler, J. C., Lansbury, P. T Jr. (2001). Vesicle permeabilization by protofibrillar alpha-synuclein: implications for the pathogenesis and treatment of Parkinson's disease. *Biochemistry*, **40**, 7812–7819.

Volles, M. J., Lansbury, P. T. Jr. (2002). Vesicle permeabilization by protofibrillar alpha-synuclein is sensitive to Parkinson's disease-linked mutations and occurs by a pore-like mechanism. *Biochemistry*, **41**, 4595–4602.

Volles, M. J., Lansbury, P. T. Jr. (2003). Zeroing in on the pathogenic form of alpha-synuclein and its mechanism of neurotoxicity in Parkinson's disease. *Biochemistry*, **42**, 7871–7878.

Von Coelln, R., Thomas, B., Savitt, J. M., Lim, K. L., Sasaki, M., Hess, E. J., Dawson, V. L.,Dawson TM. (2004). Loss of locus coeruleus neurons and reduced startle in parkin null mice. *Proc Natl Acad Sci U S A*, **101**, 10744–10749.

West, A. B., Maidment, N. T. (2004). Genetics of parkin-linked disease. *Hum. Genet.*, **114**, 327–336.

West, A. B., Moore, D. J., Biskup, S., Bugayenko, A., Smith, W. W., Ross, C. A., Dawson, V. L., Dawson, T. M. (2005). Parkinson's disease-associated mutations in leucine-rich repeat kinase 2 augment kinase activity. *Proc. Natl. Acad. Sci. U S A*, **102**, 16842–16847.

Willingham, S., Outeiro, T. F., DeVit, M. J., Lindquist, S. L., Muchowski, P. J. (2003). Yeast genes that enhance the toxicity of a mutant huntingtin fragment or alpha-synuclein. *Science*, **302**, 1769–7172.

Wright, P. E., Dyson, H. J. (1999). Intrinsically unstructured proteins: re-assessing the protein structure-function paradigm. *J. Mol. Biol*., **293**, 321–331.

Wood-Kaczmar, A., Gandhi, S., Wood, N. W. (2006). Understanding the molecular causes of Parkinson's disease. *Trends Mol. Med*., **12**, 521–528.

Zarranz, J. J., Alegre, J., Gómez-Esteban, J. C., Lezcano, E., Ros, R., Ampuero, I., Vidal, L., Hoenicka, J., Rodriguez, O., Atarés, B., Llorens, V., Gomez Tortosa, E., del Ser, T., Muñoz, D. G. & de Yebenes, J. G. (2004). The new mutation, E46K, of alpha-synuclein causes Parkinson and Lewy body dementia. *Ann. Neurol.* **55**, 164–173.

Zhang, L., Shimoji, M., Thomas, B., Moore, D. J., Yu, S. W, Marupudi, N. I., Torp, R., Torgner, I. A., Ottersen, O. P., Dawson, T. M., Dawson, V.L. (2005). Mitochondrial localization of the Parkinson's disease related protein DJ-1: implications for pathogenesis. *Hum. Mol. Genet*., **14**, 2063–2073.

Zhu, M., Li, J., Fink, A. L. (2003). The association of alpha-synuclein with membranes affects bilayer structure, stability, and fibril formation. *J. Biol. Chem*., **278**, 40186–40197.

Zhu, M., Rajamani, S., Kaylor, J., Han, S., Zhou, F., Fink, A. L. (2004). The flavonoid baicalein inhibits fibrillation of alpha-synuclein and disaggregates existing fibrils. *J. Biol. Chem*.,**279**, 26846–26857.

Zhu, X., Babar, A., Siedlak, S. L., Yang, Q., Ito, G., Iwatsubo, T., Smith, M. A., Perry, G., Chen, S. G. (2006). LRRK2 in Parkinson's disease and dementia with Lewy bodies. *Mol Neurodegener*., Nov 30, 1–17.

Zimprich, A., Biskup, S., Leitner, P., Lichtner, P., Farrer, M., Lincoln, S., Kachergus, J., Hulihan, M., Uitti, R. J., Calne, D. B., Stoessl, A. J., Pfeiffer, R. F., Patenge, N., Carbajal, I. C., Vieregge, P., Asmus, F., Müller-Myhsok, B., Dickson, D. W., Meitinger, T., Strom, T. M., Wszolek, Z. K., Gasser, T. (2004). Mutations in LRRK2 cause autosomal-dominant parkinsonism with pleomorphic pathology. *Neuron*., **44**, 601–607.

Chapter 4

Insights into the molecular interaction between α-synuclein and fatty acids

4.1 INTRODUCTION

4.1.1 Nature of the interaction between α-synuclein and fatty acids

As already mentioned in the previews chapter, the role of α-syn is associated also to fatty acids. α-Syn seems to interact with fatty acid, in particular with unsatured and polyunsatured fatty acid (PUFA), but it is not yet elucidated if this interaction involves free fatty acid, as a fatty acid binding proteins (FABPs) (Sharon et al., 2001), or aggregate states of FAs (micelles, vesicles, oil droplets) (Necula et al., 2003; Broersen et al., 2006; Lücke et al., 2006; Assayag et al., 2007).

In cells, FAs are bound mainly to phospholipid membranes and to FABPs, when the latter are present (Hamilton & Kamp, 1999). Free cytosolic FA concentrations are generally low (in the nmol/L range). A principal force keeping them low is the formation of a thioester linkage between the FA carboxyl group and the thiol group of coenzyme A (yielding fatty acyl-CoA) within minutes after an FA enters a cell. The esterified FAs are then consumed for energy production by mitochondria and peroxisomes or else used for synthesis of lipids. FAs are assumed to cross cell membranes continuously, either actively by specific protein transporters or via flip-flop of the FA through the membrane (Hamilton, 1999).

A study reported that α-syn shares some regional sequence homologies with a FABP signature motif and that it can bind free radiolabeled 18:1 with low affinity, in a manner reminiscent of FABPs (Sharon et al., 2001). On the contrary, it was also demonstrated using titration microcalorimetry that α-syn binds both monomeric arachidonic acid (AA) and DHA with a K_d around 1-4 μM. This binding affinity is two orders of magnitude less than that for FABP, suggesting α-syn does not function in the same manner as FABP (Golovko et al., 2006, 2007; Richieri et al., 2000). Moreover, unlike classical FABPs, no specific FA-binding sites were detected for α-syn and no

conformational similarities to the characteristic FABP tertiary structure was observed using NMR spectroscopy (Lücke et al., 2006). By electron microscopy studies this latter work suggested also that one possible mode of binding could involve oleic acid (1 mM) bilayers at pH 7.8; these high-molecular-weight FA aggregates possess a net negative surface charge because they contain FA anions, and they were easily disrupted to form smaller particles in the presence of α-syn, indicating a direct protein-lipid interaction (Lücke et al., 2006). Necula and coworkers suggested that the alkyl moieties of fatty acids (in particular AA) support α-syn fibrillization by interacting to form micelles rather than by direct protein binding through these sites. Indeed, the presence of α-syn greatly depressed AA CMC compared with values determined in water or buffer alone and the AA is mostly micellar at concentrations that accelerated fibrillization (Necula et al., 2003). These results do not agree with the data obtained by Broersen and colleagues. In their studies they assert that α-syn rapidly responds to free DHA and AA by an increase in α-helical content, α-syn can counteract the natural tendency of DHA and AA to form micelles, and long exposure to free DHA, and to a lesser degree AA, gradually leads to the assembly of α-syn into fibrils (Broersen et al., 2006).

4.1.2 Docosahexaenoic acid: a polyunsaturated fatty acid

In this PhD project, the interaction of α-syn with docosahexaenoic acid (DHA) was investigated in detail.

Fatty acids consist of a polar carboxylic acid with a hydrophobic carbon chain. They are abbreviated according to the formula X:Y, where X states the number of carbons in the fatty acid chain and Y is the number of double bonds. ω3, ω6 or ω9 refers to the position of the first double bond counting from the methyl group (the end of the carbon chain). DHA, 22:6 (ω3), is an example of PUFA (polyunsaturated fatty acid) since it contains more than one double bond (Fig. 4.1 A, B). Monounsaturated fatty acids contain one double bond, such as oleic acid (OA 18:1), whereas saturated fatty acids have no double bonds, as palmitic acid (PA 16:0).

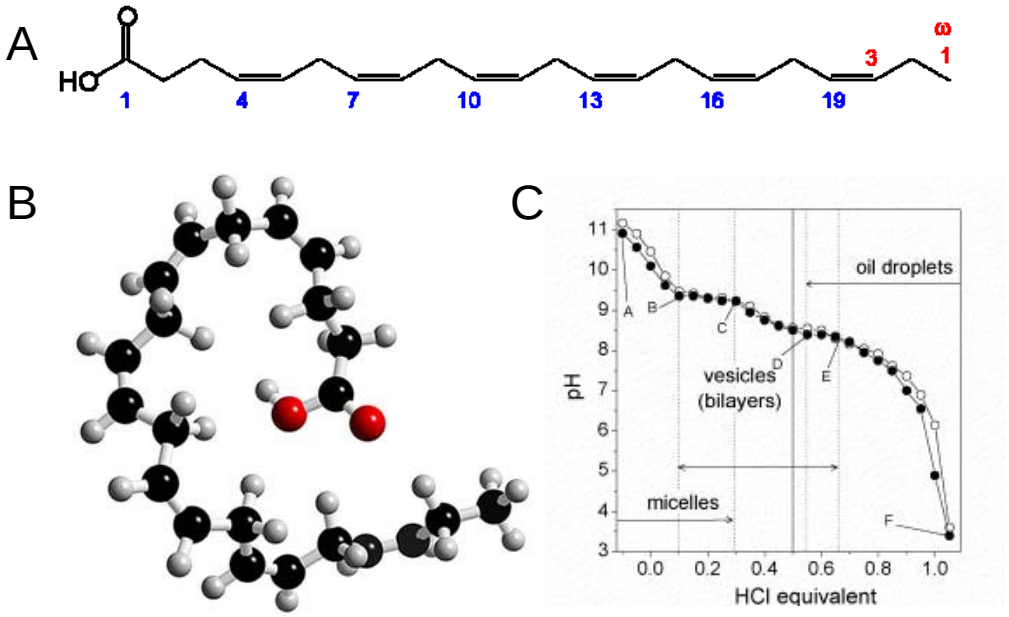

Fig. 4.1 Chemical structure **(A)** and 3D model structure **(B)** of docosahexaenoic acid. In **C** the equilibrium titration curve of 10 mM DHA, determined at 25°C is reported (reprinted from Namani et al., 2007).

From a chemical point of view, DHA is a simple amphiphilic molecule with a polar head group that can be in its protonated (−COOH) or deprotonated ($-COO^-$) state, depending on the experimental conditions. Aqueous mixtures of these two species of DHA show a complex aggregation behavior (Namani et al., 2007). Depending on the relative amounts of anionic and neutral DHA molecules, different phases form at thermodynamic equilibrium (Fig. 4.1 C). In the presence of a 10 mol% excess of NaOH,

10 mM DHA dissolves in water to yield a transparent micellar solution of deprotonated DHA molecules (*A* in Fig. 4.1 C). Upon addition of HCl, the pH drops until at 0.1 equiv. HCl, the solution starts to become turbid (*B* in Fig. 4.1 C). Addition of more than 0.55 equiv. HCl leads to the formation of oil droplets and finally to a phase separation if the samples are stored for several day. The region between *C* (0.30 equiv. HCl) and *D* (0.55 equiv. HCl) in Fig. 4.1 C, consists of two phases, self-closed bilayers (vesicles) and the bulk aqueous solution. This is the region in which the content of anionic DHA molecules is too low to form micelles and too high to form emulsion droplets (oil droplets). Between *C* and *D*, the molar ratio of the neutral form of DHA to anionic DHA varies between about 1:3 and 1:1. The vesicles are formed despite the unusual high degree of conformational flexibility of DHA (Garvish et al., 2003). However, DHA vesicles are chemically less stable due to the presence of five reactive bis-allylic methylene groups localized between the six double bonds in the DHA molecule (Namani et al., 2007).

DHA is a dietary essential (ω3) PUFA highly enriched in fish oils and concentrated up the food chain from photosynthetic and heterotrophic microalgae. In addition to these essential marine sources, DHA is also synthesized via an elongation and desaturation of the 20-carbon eicosapentanoic acid [EPA; 20:5(ω3)], or elongation of the 18-carbon (ω3) fatty acid, α-linolenic acid [ALA; 18:3(ω3)] enriched in flax, walnut, chia, and other photosynthesizing terrestrial plants (Lukiw & Bazan, 2008). In the brain, glia and endothelial cells of the microvasculature, but not neurons, have some capacity to synthesize DHA from ALA and other (ω3) precursor fatty acids, but whether or not this contributes significantly to total brain DHA is not clear. The high concentration of DHA in the capillary endothelium suggests that DHA is taken up from the diet via blood plasma DHA transporters including specific fatty-acid-binding lipoprotein carriers (Innis, 2007). DHA is an absolute requirement for the development of the human central nervous system (CNS), and the continuous maintenance of brain cell function, illustrating the strong mechanistic link between an adequate supply of essential PUFA in the diet and the sustenance of cognitive health. During postnatal development, rapid accretion of DHA in brain and retina takes place (Rapoport et al., 2007). DHA attains its highest concentration in CNS synapses and in retinal photoreceptors; in fact, up to 60% of all fatty acids esterified in neuronal plasma membrane phospholipids consist of DHA (Lukiw & Bazan, 2008; Adibhatla & Hatcher, 2008; Breckenridge, 1972).

DHA is important for several neuronal functions; indeed, it is crucial to maintain cellular activity by modulating membrane order, gene transcription, cell signaling and caspase activation (see the review of Marszalek and Lodish, 2005). Epidemiological studies have associated low ω3 PUFA consumption with high risk of developing Alzheimer's disease (AD). Moreover, a neuroprotective action of ω3 PUFAs has been observed in animal models of AD. Also a higher risk of developing PD are associated to high dietary intake of saturated fat and low intake of unsaturated FAs, but none have made a direct link between ω3 PUFA intake with the risk of developing PD (De Lau et al., 2005; Bousquet et al., 2008). A postmortem gas chromatographic analysis of brain FA profiles has revealed no significant differences in ω3 PUFA concentrations in brain cortex between PD patients and age-matched controls (Julien et al., 2006). On the contrary, a recent study provides the preclinical evidence that high ω3 PUFA consumption exerts a neuroprotective action against MPTP-induced toxicity (Bousquet et al., 2008). DHA levels have been shown also to be elevated in those brain areas containing α-syn inclusions in PD patients (Sharon et al., 2003), as well as in cerebral cortex in incidental LB disease, prior to α-syn inclusion (Dalfò et al., 2005).

4.1.3 Aim of the study

Since the nature of α-syn interaction with FAs is controversial and a systematic study is still lacking, the topic of my research is the investigation of the molecular details that regulate the α-syn-fatty acid interaction. The conformational features of the protein bound to FAs and the regions of α-syn involved in the interaction were analyzed by circular dichroism, proteolytic mapping, NMR measurements and by using truncated forms of the protein. Moreover, since the aggregation state of fatty acids (monomer, micelle, vesicle and oil droplet) has been shown to deeply affect both the molecular interaction with proteins and their resulting conformation, several measurements were carried out to clarify the state adopted by DHA in the presence of α-syn. Furthermore, another aspect of these studies concerns the analysis of fatty acid-mediated aggregation in order provide insights into the implication of lipids in amyloid formation *in vivo*.

4.2 MATERIALS AND METHODS

Materials

Proteinase K from *Tritirachium album* and porcine trypsin were purchased from the Sigma Chem. Co. (St. Louis, MO). All other chemicals were of analytical reagent grade and were obtained from Sigma or Fluka (Buchs, Switzerland).

Expression and purification of recombinant human α-synuclein and polypeptide syn1-99

Human α-synuclein cDNA was amplified by PCR with synthetic oligonucleotides (Sigma-Genosys) containing NcoI and XhoI restriction sites and designed to obtain the entire sequence of the protein (α-syn1-140) or the region coding for the first 99 amino acids (syn1-99). After digestion with restriction enzymes, the two PCR products were subcloned into the NcoI-XhoI-linearized pET28b expression plasmid (Novagen) and introduced into an *Escherichia coli* BL21(DE3) strain. Overexpression of proteins was achieved by growing cells in LB medium (1% Bacto tryptone, 0.5% yeast extract, 0.5% NaCl) at 37 °C to an OD_{600} of 0.6-0.8 followed by induction with 0.5 mM isopropyl β-thiogalactopyranoside for 4 h.

The purification of α-syn was conducted following this procedure. After boiling the cell homogenate for 15 min, the soluble fraction, containing the protein, was treated with 55% ammonium sulphate. The pellet was then resuspended, dialyzed and loaded into a Resource Q 6-ml column (Amersham Biosciences) and then eluted using a NaCl gradient (from 0 to 500 mM).

The purification of syn1-99 was obtained as follows. The cells were harvested by centrifugation and the pellet was resuspended in 30 ml 20 mM Hepes pH 7.0 per liter of LB medium. After adding 100 mM PMSF and protease inhibitors cocktails (Sigma), to have a final dilution of 1:100, the cells were lysated by sonication. After centrifugation, the soluble fraction was treated with 20% ammonium sulphate. The resulting supernatant was treated again with 50% ammonium sulphate. After the removal of soluble fraction, the pellet was resuspended in 5-10 ml 20 mM Hepes pH 7.0 and dialyzed overnight against water. The solution was centrifuged and filtered before loading it into a Resource S 1-ml column (Amersham Biosciences) and then eluted using a NaCl gradient (from 0 to 300 mM).

For both the polypeptides further purifications were obtained by RP-HPLC. α-Syn was purified in a Juppiter-C_{18} column (4.6 × 150 mm) (Phenomenex, CA, USA) eluted with a linear gradient of acetonitrile (0.085 % TFA) versus water (0.1 % TFA), from 5% to 38% in 5 min and from 38% to 43% at a flow rate of 0.6 ml/min. Syn1-99 was purified in a Juppiter-C_4 column (4.6 × 150 mm) (Phenomenex, CA, USA) eluted with a linear gradient of acetonitrile (0.085 % TFA) versus water (0.1 % TFA), from 5% to 65% at a flow rate of 0.8 ml/min. The identity and integrity of the eluted material were assessed by mass spectrometry. Finally, the polypeptides were lyophilized and stored at -20 °C.

Expression and purification of peptides syn1-52 and syn57-102

Histidine-tagged syn1-52 and syn57-102 was produced as described elsewhere (Bisaglia et al., 2005). Briefly, the peptides were expressed in *Escherichia coli* C41 cell line transfected with pET28b/syn1-52 and syn57-102 plasmids. The pET28b vector permits the fusion, at the N-terminal portion of the peptides, of a poly-histidine region (His-tag) followed by a thrombin cleavage site. The overexpression of the peptides was achieved by growing cells in LB medium (1% Bactotryptone, 0.5% yeast extract, 0.5% NaCl) at 37 °C to an OD_{600} of 0.6-0.8 followed by induction with 0.5 mM isopropyl β-thiogalactopyranoside for 5 h. The polypeptides were purified on a Cobalt-agarose resin (Clontech) using the manufacturer's recommended protocol. To eliminate the His-tag, the purified protein was digested with thrombin (Amersham Pharmacia), using the manufacturer's protocol. After cleavage, the His-tag was separated from the protein by HPLC purification using a Juppiter-C_4 column (4.6 × 150 mm) (Phenomenex, CA, USA) eluted with a linear gradient of acetonitrile (0.085 % TFA) versus water (0.1 % TFA), from 5% to 50% in 40 min at a flow rate of 0.6 ml/min. The identity and integrity of the eluted material were assessed by mass spectrometry. The polypeptides were lyophilized and stored at -20 °C.The final peptides contain extra G-S-H and G-S-H-M sequence at the N terminus of syn1-52 and syn57-102, respectively.

Chemical synthesis and purification of peptide syn108-140

The peptide corresponding to residues 108-140 of α-syn was synthesized by the solid-phase Fmoc method (Atherton & Sheppard, 1989) using an Applied Biosystems (Palo Alto, CA) peptide synthesizer (model 431A). Fmoc-protected amino acids were used with the following side chain protection: *tert*-butyl ether (tBu) for Tyr, *tert*-butyl

ester (OtBu) for Glu and Asp, and trityl (Trt) for Asn and Gln. Deprotection of the Fmoc group, at every cycle, was obtained by a 10 min treatment with 20% piperidine in *N*-methylpyrrolidone. Chain elongation was performed using a 10-fold excess (0.5 mmol) of Fmoc- protected amino acid, 2-(1*H*-benzotriazol-1-yl)-1,1,3,3-tetramethyluronium hexafluorophosphate, and 1-hydroxybenzotriazole (1:1:1) in the presence of a 20-fold excess of *N*,*N*-diisopropylethylamine. After completion of the last cycle, the resin was washed with *N*-methylpyrrolidone and a dichloromethane/methanol mixture (1:1, v/v) and then dried *in vacuum*. The synthetic peptide was cleaved from the resin and deprotected by treatment of the peptide-resin with a 95:5 (v/v) mixture of TFA and 1,2-ethanedithiol for 2 h at 4 °C. The resin was filtered, and cold diethyl ether was added to the solution to precipitate the crude peptide, which was recovered by centrifugation and purified by RP-HPLC using a Vydac C18 column eluted with a gradient of acetonitrile (0.085% TFA) versus water (0.1% TFA) (from 5 to 25% over 5 min and from 25 to 29% over 17 min).

Circular Dichroism

Protein concentrations were determined by absorption measurements at 280 nm using a double-beam Lambda-20 spectrophotometer from Perkin Elmer (Norwalk, CT). The extinction coefficients at 280 nm were 5960 M^{-1} (a-syn), 1490 M^{-1} (syn1-52, syn1-99), 4470 M^{-1} (syn108-140) as evaluated from its amino acid composition by the method of Gill and von Hippel (1989). The concentration of syn108-140 was calculated by monitoring sample absorbance at 205 nm (Scopes, 1974). Circular dichroism spectra were recorded on a Jasco J-710 (Tokyo, Japan) spectropolarimeter. Far-UV CD spectra were recorded using a 1-mm path-length quartz cell and a protein concentration of 5-15 μM. The mean residue ellipticity $[\theta]$ (deg·cm^2·dmol^{-1}) was calculated from the formula $[\theta] = (\theta_{obs}/10) \cdot (MRW/lc)$, where θ_{obs} is the observed ellipticity in deg, MRW is the mean residue molecular weight of the protein, l the optical pathlength in cm and c the protein concentration in g/mL. The spectra were recorded in PBS (8 mM Na_2HPO_4, 137 mM NaCl, 2 mM KH_2PO_4, 2.7 mM KCl), pH 7.4, in the absence or in the presence of DHA ranging from 5-500 μM.

NMR analysis

NMR experiments were performed on a Bruker Avance DMX600 spectrometer equipped with a gradient triple resonance probe. HSQC spectra were recorded on a 100

μM α-syn sample at 25 °C in 20 mM phosphate buffer (pH 7.4), in the absence or presence of 10 mM DHA. The experiments consisted of 256 increments of 512 time points each, acquired with 24 to 128 transients each. Spectra were processed to obtain matrices of 512 x 512 real points. Prior to Fourier transformation, 90° shifted sine and sine square functions were used in the f2 and f1 dimension, respectively.

Determination of DHA critical aggregate concentration based on turbidity measurements and pyrene fluorescence

Aliquots of DHA were stored at a concentration of 76 mM in 100% ethanol at −80°C. Air was evacuated with helium gas in order to prevent oxidation.

The aggregation of DHA, in the absence or in the presence of α-syn and the several peptides (2.5-5 μM), was analyzed by turbidity measurement at 400 nm of different samples containing increasing amounts of DHA (0-500 μM) in PBS, pH 7.4 (Namani & Walde, 2005). The analyses were carried out with a Perkin-Elmer model Lambda 25 UV-VIS spectrometer (Norwalk, CT, USA) using 10 mm path length quartz cuvette.

The critical concentration for aggregate formation of DHA was determined by the pyrene 1:3 ratio methods (Aguiar et al., 2003; Lòpez-Diaz et al., 2005; Zhai et al., 2005). Two series of pyrene fluorescence emission measurements (1 μM) were obtained increasing the fatty acid concentration from 0 to 500 μM in the absence or in the presence of the polypeptides (5 μM). The fluorescence emission spectra were recorded in PBS (pH 7.4) using an excitation wavelength of 335 nm and the intensity of the maxima corresponding to the first (I_1) and third (I_3) vibronic band, located near 373 and 384 nm respectively, was measured. A spectrofluorimeter FP6500 Jasco (Tokyo, Japan) was employed and a 2 x 10 mm path length quartz cuvette was used. The critical aggregate concentration was obtained from the inflection point of the pyrene 1:3 ratio plots, that can be described by a decreasing sigmoid of the Boltzmann type (Aguiar et al., 2003). The fluorescence emission of pyrene was recorded also up to 600 nm to monitor the increase of the signal near 470 nm (band I_{ex}), ascribed to the pyrene excimer emission (Turro et al., 1986) and the ratio I_{ex}/I_1 was plotted against the DHA concentration.

Transmission Electron Microscopy

In order to evaluate the morphology and the size of the species deriving from the self-assembly of DHA and from the aggregation process of α-syn, aliquots of the samples were examined by transmission electron microscopy (TEM). The samples relative to aggregation of α-syn were diluted 3 times with PBS. A drop of the samples solution was placed on a Butvar-coated copper grid (400-square mesh) (TAAB-Laboratories Equipment Ltd, Berks, UK), dried and negatively stained with a drop of uranyl acetate solution (1%, w/v). TEM pictures were taken on a Tecnai G^2 12 Twin instrument (FEI Company, Hillsboro, OR, USA), operating at an excitation voltage of 100 kV.

The size distribution of DHA samples in the presence of α-syn was obtained by the following procedure. 247 particles were manually extracted from micrographs using the semi-automatic procedure implemented in the BOXER program of EMAN software package (Ludtke et al., 1999). Only clearly defined spherical and isolated particles were selected and boxed in 48x48 pixels images. The particles were subsequently centered and aligned by cross-correlating the individual images to a rotationally averaged image. Once aligned, all images were rotationally averaged to obtain one dimensional radial profile. Center alignment and rotational averaging were done using SPIDER image processing system (Frank et al., 1996). The intensity profiles were fitted by a piecewise function which starts as a constant value (particle intensity) followed by half period cosine drop and again by a constant (background intensity). Particle half-length was taken as a pixel position at the midpoint of the cosine intensity drop. Mean particle diameter was obtained from a Gaussian fit to the histogram distribution while the diameter error was estimated from the Gaussian FWHM. Intensity profile fits and histogram analysis were performed with MATHEMATICA software package (Wolfram Research Inc., Champaign, USA).

Dynamic Light Scattering (DLS)

DLA measurements were carried out with a Zetasizer Nano-S instrument (Malvern Instrument, UK). This apparatus, which uses the backscattering detection (scattering angle θ=173°) and an avalanche photodiode detector (APD), is equipped with a Helium–Neon laser source (wavelength 633 nm; power 4.0 mW), and a thermostated sample chamber controlled by a thermoelectric Peltier. DLS measurements were performed at 25°C in PBS pH7.4 in duplicate. During every measurement 15 runs were collected.

Proteolysis of the protein-lipid complex

Proteolysis experiments of the complex formed by DHA and the several polypeptides were carried out at room temperature using proteinase K (Ebeling et al., 1974) at E/S ratio of 1:1000 (by weight) and trypsin at E/S ratio of 1:50 (by weight). The reactions were conducted in PBS, pH 7.4, in the absence or in the presence of different concentrations (10, 50, 250 μM) of DHA. The peptide concentrations were always 5 μM. The reactions were quenched at specified times by acidification with TFA in water (4%, v/v). The proteolysis mixtures were analyzed by RP-HPLC and SDS-PAGE according to Schägger and von Jagow (1987). For α-syn the HPLC analyses were conducted using a Vydac C_{18} column (4.6 mm × 250 mm; The Separations Group, Hesperia, CA), eluted with a gradient of acetonitrile/0.085% TFA *vs.* water/0.1% TFA from 5% to 25% in 5 min, from 25% to 28% in 13 min, from 28% to 39% in 3 min, from 39% to 45% in 21 min at a flow rate of 1 ml/min. The same column was used to analyze the proteolytic patter of ayn108-140 using a gradient of acetonitrile/0.085% TFA *vs.* water/0.1% TFA from 5% to 25% in 5 min, from 25% to 28.5% in 24 min, at a flow rate of 1 ml/min. For syn 1-99, syn1-52 and syn 57-102 the same gradient and the same columns utilized for the purification were used. Each column was provided by a HPLC security guard column SAX (Phenomenex, USA). The sites of cleavage along the polypeptide chains were identified by mass spectrometry analyses of the protein fragments purified by RP-HPLC. Mass determinations were obtained with an electrospray ionization (ESI) mass spectrometer with a Q-Tof analyzer (Micro) from Micromass (Manchester, UK). The measurements were conducted at a capillary voltage of 2.5-3 kV and a cone voltage of 30-35 V. The molecular masses of protein samples were estimated using the Mass-Lynx software 4.1 (Micromass).

α-Syn aggregation samples

In order to analyze the aggregation process of α-syn, samples have been incubated at 37 °C for up to 6 days at a protein concentration of 50 μM, in PBS, pH 7.4 in the presence of DHA (0.5 and 2.5 mM) in order to realize a fatty acid/protein molar ratio of 10 and 50, under shaking at 500 rpm with a thermo-mixer (Compact, Eppendorf, Hamburg, DE). The same experiment has been conducted without DHA. Aliquots of the

samples during incubation were examined by native-PAGE, Thioflavin T binding assay and TEM.

Native-PAGE

Native (non-denaturing) polyacrylamide gel electrophoresis was performed at a constant 100 V using a Mini–PROTEIN II Bio-Rad electrophoresis system using a Tris–HCl 12% (w/v) polyacrylamide gel. The bands were visualized by silver staining. Approximately 5 μg of protein were loaded into each well.

Thioflavin T binding assay (ThT)

The ThT binding assays were performed accordingly to LeVine (1993) using a freshly prepared 25 μM ThT solution in 25 mM sodium phosphate (pH 6.0) that had been passed through 0.45 μm filters. Aliquots (20 μl) of protein samples containing aggregates were taken at specified times and diluted into the ThT buffer (final volume 500 μl). Fluorescence emission measurements were conducted at 25 °C using an excitation wavelength of 440 nm and recording the ThT fluorescence emission spectra between 460 and 560 nm.

4.3 RESULTS

4.3.1 Characterization of the α-synuclein-DHA complex

Conformational analysis of α-syn in the presence of fatty acids

The secondary structure content of α-syn in the presence of different FAs (palmitic acid, PA, oleic acid, OA and docosahexaenoic acid, DHA) was evaluated by far-UV CD. The protein is unfolded in the absence of FAs and does not acquire any appreciable secondary structure in the presence of PA up to 500 μM (Fig. 4.2 A). The recorded spectra in the presence of OA and DHA between 250 and 197 nm are reported (Fig. 4.2 B and Fig.4.3 A, respectively) and the appearance of the two typical minima at 222 and 208 nm indicates the acquisition of α-helical secondary structure. The existence of an isodichroic point at 203 nm in the titration experiments (0-500 μM FAs), for both the FAs, suggests a simple two-state conformational transition between α-helix and random coil. To further analyze the structural transition of α-syn in the presence of DHA, in Fig. 4.3 B, the ellipticity of α-syn samples at 222 nm is shown as a function of the molar ratio between DHA and α-syn. A similar trend is obtained using both 5 (○) and 15 μM (●) α-syn and, increasing the amount of DHA, a corresponding increment of the ellipticity is observed. For DHA/protein molar ratios higher than ~60, the addition of fatty acid does not result in any further increase in helix content, that it is estimated to be ~70 % (Rohl et al., 1996). From the graph in Fig. 4.3 B, it can be estimated that ~35 DHA molecules are required per α-syn molecule for complete folding.

NMR structural characterization

To compare the conformational properties of free and DHA-bound α-syn, we recorded ^{1}H-^{15}N HSQC spectra of the protein alone and in the presence of saturating concentration of DHA (α-syn/DHA molar ratio of 1:100). The spectrum of α-syn (Fig. 4.3 A) exhibits a dense cluster of cross-peaks over a narrow range, in agreement with the fact that the protein is largely unfolded at pH 7.4. As already described (Chandra et al., 2003), at 25 °C the number of visible peaks (~ 70) is lower than expected (135). This behavior can be attributed to conformational exchange in the first 100 residues of α-syn (McNulty et al., 2006), or to fast chemical exchange between amide groups and the solvent (Croke et al., 2008). After the addition of DHA, many peaks disappear (Fig. 4.4

B). The positions of the remaining peaks are not changed, indicating that the corresponding residues do not bind lipids and continue to be unfolded and mobile in the presence of DHA. Interestingly, the spectrum obtained in the presence of DHA is quite similar to those previously recorded in the presence of acidic small unilamellar vesicles (Eliezer et al., 2001). The remaining peaks correspond to the C-terminal ~ 40 residues. The disappearance of the majority of peaks indicates that under the experimental conditions used here, the interaction of α-syn with DHA involves its first 100 residues and that DHA is assembled in aggregative species certainly bigger than micelles.

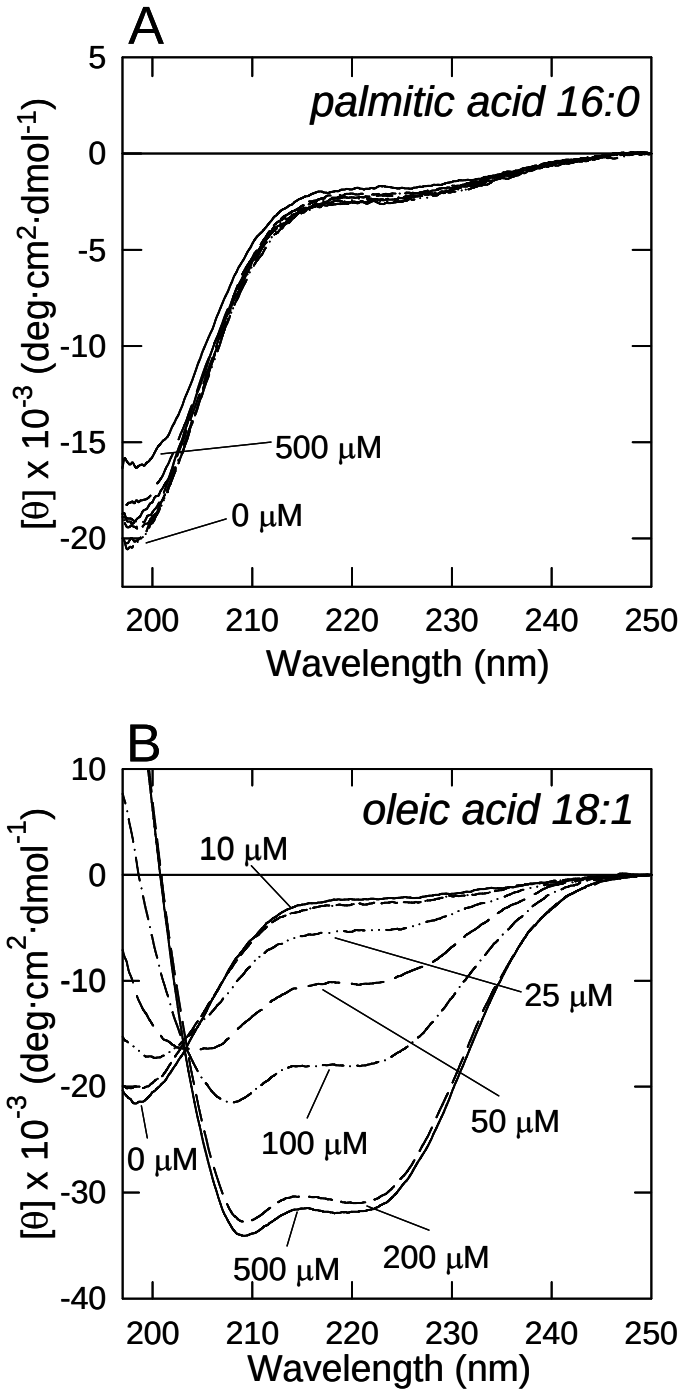

Fig. 4.2 Far UV CD of α-syn in the presence of increasing concentrations of palmitic acid **(A)** and oleic acid **(B)**. The spectra are recorded in PBS buffer pH 7.4 at a protein concentration of 5 μM, using a quartz cuvette with 1 mm of pathlength. The numbers close to the spectra indicate the amount (μM) of fatty acids.

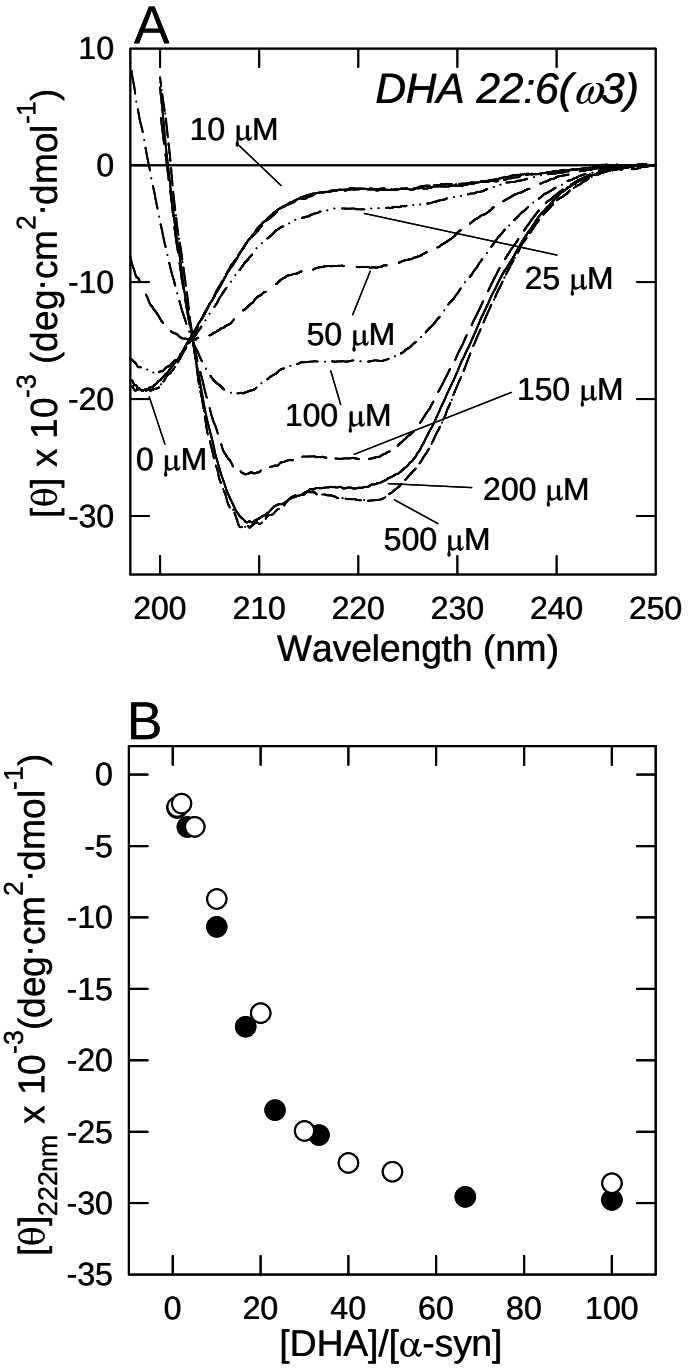

Fig. 4.3 (A) Far UV CD of α-syn in the presence of increasing concentrations of docosahexaenoic acid (DHA) The spectra are recorded in PBS buffer pH 7.5 at a protein concentration of 0.1 mg/ml, using a quartz cuvette with 1 mm of pathlength. The numbers close to the spectra indicate the amount (μM) of fatty acid. **(B)** Ellipticity at 222 nm as a function of the molar ratio between DHA and α-syn. Black circles refer to 5 μM α-syn, white circles to 15 μM.

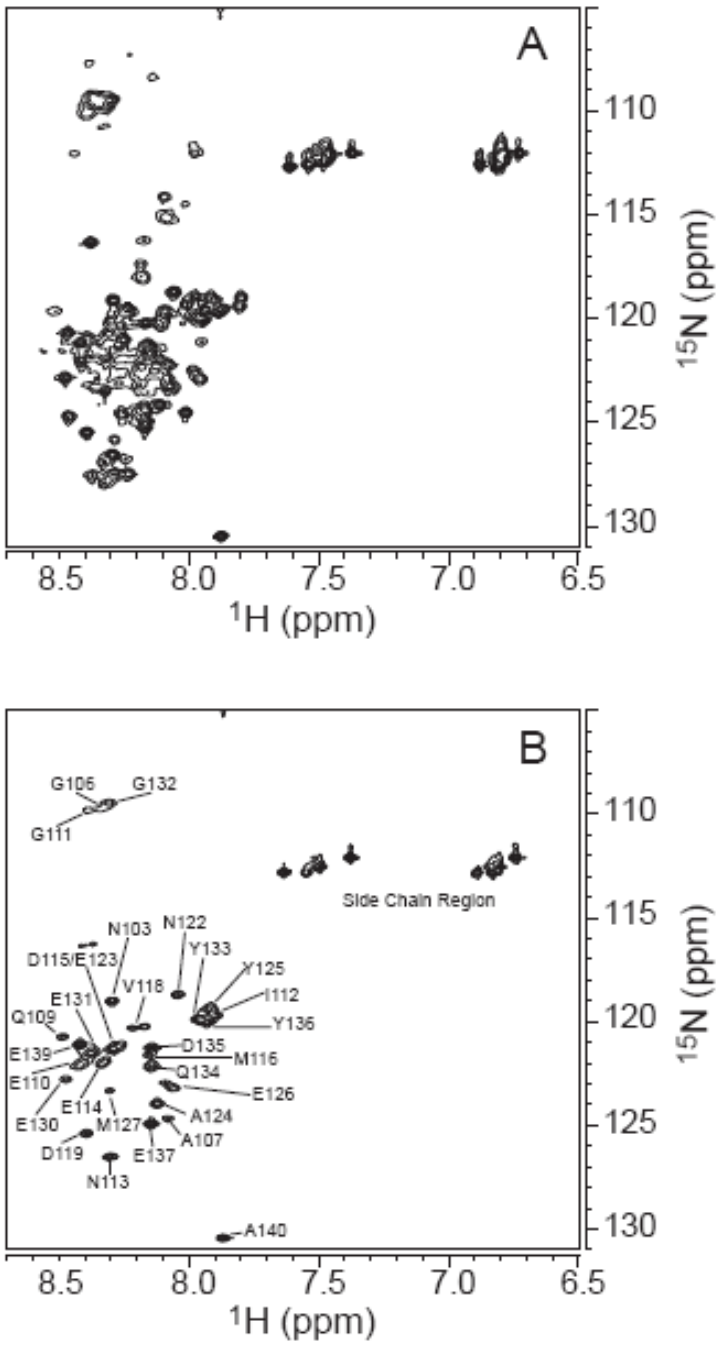

Fig. 4.4 ^{1}H-^{15}N correlation (HSQC) spectra of **(A)** α-syn in PBS, pH 7.4 and **(B)** α-syn in the presence of saturating concentrations of DHA. Fast amide proton exchange at 25 °C is responsible for the loss of several peaks in the spectrum of the free protein. The slower tumbling rate of the lipid aggregates obtained after the addition of DHA restricts the motion of the lipid-interacting residues, resulting in line broadening and in further loss of peaks.

Proteolytic mapping of the complex between α-syn and DHA

To directly define the region(s) of interaction of α-syn with DHA, a combination of proteolytic digestion and mass spectrometry was used. This strategy relies on the consideration that regions of the protein normally available to proteases exhibit limited accessibility when involved in interaction with lipids (Fontana et al., 2004; Polverino de Laureto et al., 2006). We used proteinase K (Ebeling et al., 1974), a particularly voracious protease, which displays broad substrate specificity, and trypsin, which specifically hydrolyzes peptide bonds containing basic residues at the C-terminus. Both proteases retain proteolytic activity in the presence of DHA (data not shown). Proteolysis experiments were conducted in the absence and in the presence of increasing concentrations of DHA (10, 50, 250 μM) and the proteolysis patterns were compared.

In Fig. 4.5 (top), the SDS-PAGE analysis of the digestion by proteinase K is reported. In the absence of DHA, the protein is easily degraded in small fragments (lanes 2, 3), as expected for an unfolded polypeptide chain. If the proteolysis is conducted in the presence of 10 μM DHA (DHA/protein molar ratio of 2), there is no significant change in the pattern and the electrophoretic band of full-length α-syn disappears from the mixture within a 30 minutes incubation with the protease (lanes 4, 5). Using a DHA/protein molar ratio of 10 (50 μM DHA), a partial protection from proteolysis of the protein is observed (lanes 6, 7), while in the presence of 250 μM DHA (molar ratio of 50), α-syn is cleaved only at few sites (lanes 8, 9). Specifically, in the proteolytic mixture corresponding to the 30 minutes of incubation of α-syn with the enzyme, two main bands are found at 7.5 and 9.0 kDa. The proteolysis mixtures were analyzed also by RP-HPLC (Fig. 4.5, bottom). In panels A and B, the chromatograms relative to the reaction conducted in the absence of DHA are shown. As already indicated by SDS-PAGE, α-syn is fragmented within 5 min by the protease and several peaks are detected in the chromatograms (panel A). The identities of protein fragments were obtained by mass spectrometry analysis of the fractions isolated by RP-HPLC (Table 4.1) and they span almost all the regions of the α-syn sequence. After a 1-hr incubation with the protease, the peaks relative to α-syn and all the bigger fragments disappear (panel B). In the presence of 250 μM DHA (panel C and D), α-syn is more resistant to proteinase K. Indeed, the intact protein is the main species after 5-min of incubation and only few peaks of low intensity are visible in the chromatogram (panel C). After a 1-hr reaction, only few fragments were produced (panel D). After a 5-min reaction, the main species found in the proteolytic mixture corresponds

to full length α-syn and very low amounts of fragments 1-89, 1-92, and the complementary fragments 90-140 and 93-140, indicating that the protein is initially cleaved at the peptide bonds Ala89-Ala90 and Thr92-Gly93. The predominant product after 1-hr of proteolysis is the peptide 1-72 (MM 7299.9 Da), while 1-89 (MM 8839.7 Da) does not accumulate and it is further cleaved forming fragment 1-72. This species remains in the proteolysis mixture also after prolonged (3-hr) incubation with the protease (data not shown). In both cases, fragment 90-140 seems to be quite resistant to proteolysis and fragments 93-140, 95-140 and 126-140 are produced in minor extent.

We also digested α-syn with trypsin in the absence (Fig. 4.6 A) and in the presence (Fig. 4.6 B, C) of DHA. The HPLC analyses of the proteolysis mixture are shown. After 1 hour, intact α-syn is still present in the mixture (Fig. 4.6 B), at variance with the reaction conducted in the absence of DHA (Fig. 4.6 A). From the chromatograms, a marked difference between the two reactions is evident, both in the yield and in the presence of fragment 1-80, when the fatty acid is present. After an overnight reaction in the presence of DHA (Fig. 4.6 C), the whole protein is present only in trace amounts and some species covering the N-terminal region of α-syn (1-102, 1-97, 1-96) form with the C-terminal complementary products (103-140, 98-140, 97-140). The most striking feature is that fragment 1-80 is still present and has not been further digested, indicating that it constitutes the most protected species.

To establish if the proteolytic products maintain the α-helical structure, we recorded far-UV CD spectra of the proteolysis mixture with proteinase K during incubation (up to 2 hours) (Fig. 4.7). The spectra indicate the stable presence of regular α-helices, albeit with a partial (20%) reduction of the helical content, indicating that the protease has digested for the most part the region(s) of α-syn devoid of regular secondary structure. In conclusion, in the presence of DHA, the protein appears to be highly susceptible to proteases hydrolysis in correspondence of the region 73-89, included in the NAC region (§3.3) and the most protected species maintains regular secondary structure.

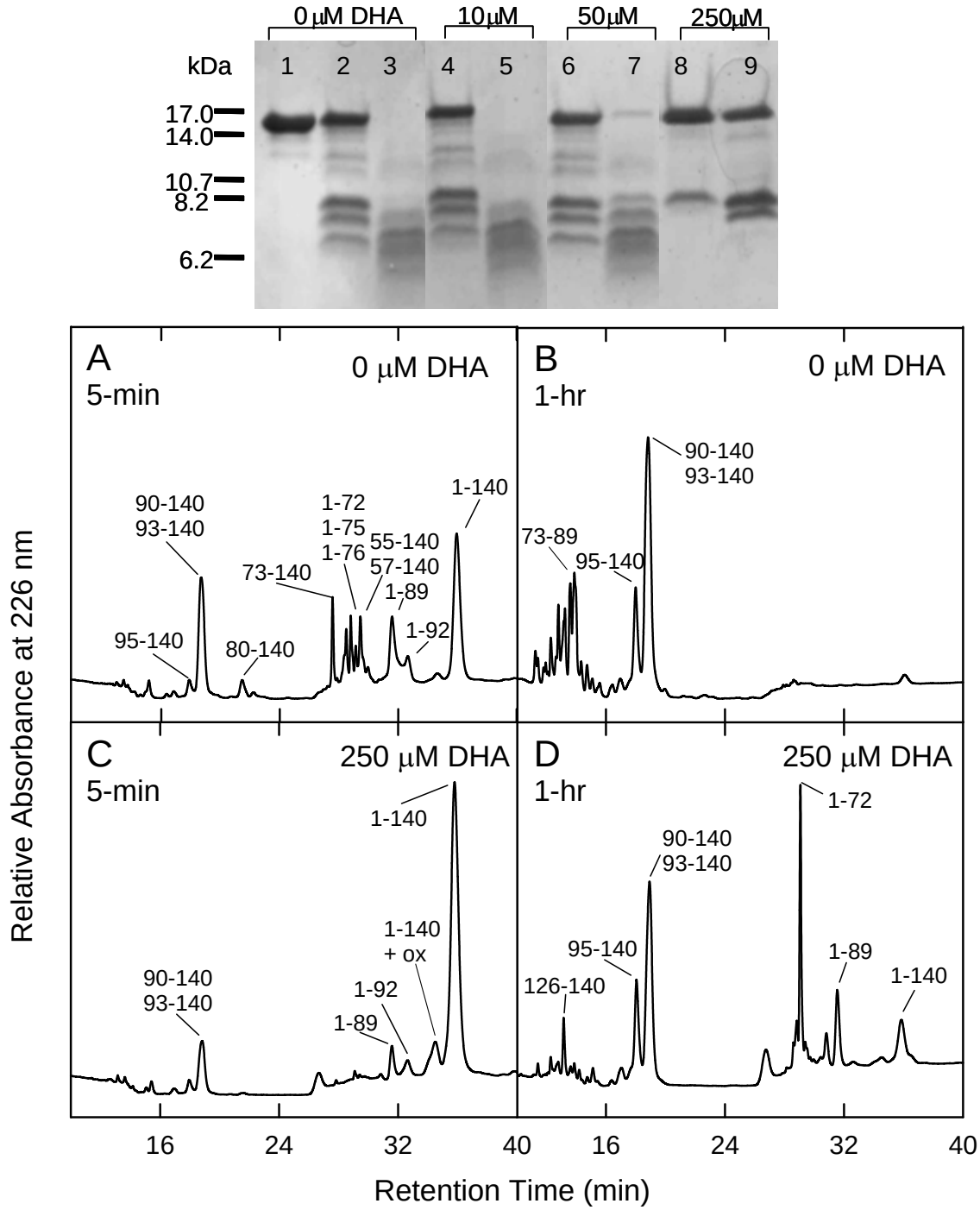

Fig. 4.5 Proteolysis of α-syn by proteinase K analyzed by SDS-PAGE (**top**) and RP-HPLC (**bottom**). The reactions were conducted at a protein concentration of 5 μM in PBS in the absence or in the presence of increasing concentrations of DHA (10, 50 and 250 μM) using an E/S ratio of 1:1000. Aliquots from the proteolysis mixture corresponding to 0 minutes (lane 1), 5 minutes (lanes 2, 4, 6, 8) and 30 minutes (lanes 3, 5, 7, 9) of incubation were analyzed. A partial BrCN digest of apomyoglobin was loaded onto the gel as a marker of molecular weights and the position of the relative bands is reported on the left. RP-HPLC chromatograms corresponding to the analysis of aliquots taken from the proteolysis mixture of α-syn and proteinase K after 5 and 60 minutes of incubation in the absence of DHA **(A, B)**, and in the presence of 250 μM DHA **(B, C)**. The identity of α-syn fragments was established by ESI-MS (Table 4.1).

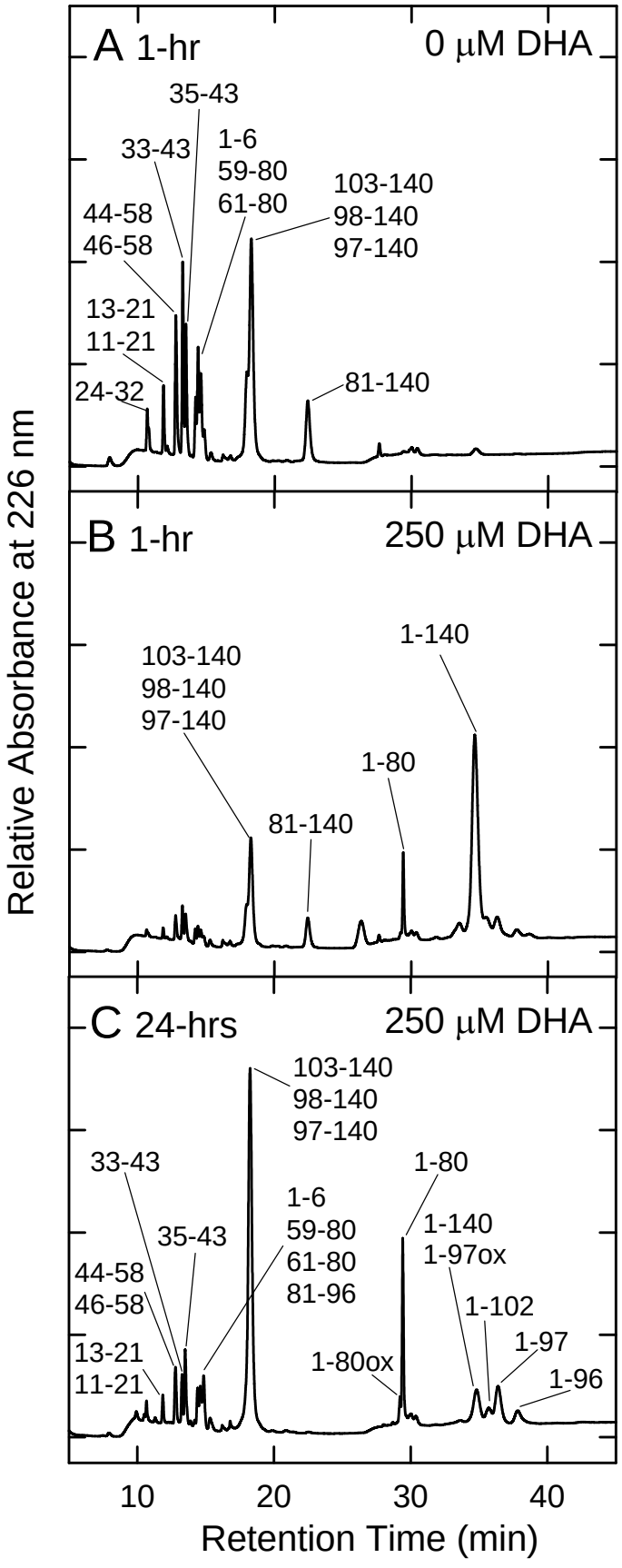

Fig. 4.6 Proteolysis of α-syn by trypsin analyzed by RP-HPLC. The reactions were conducted at a protein concentration of 5 μM in PBS buffer in the absence or in the presence of 250 μM DHA using an E/S ratio of 1:50. RP-HPLC chromatograms corresponding to the analysis of aliquots taken from the proteolysis mixture after 1 hr of incubation in the absence of DHA **(A)**, and after 1 hr and 24 hrs in the presence of 250 μM DHA **(B, C)** are shown.

Table 4.1 Molecular masses of fragments obtained by proteolysis of α-synuclein by proteinase K and trypsin

		Molecular mass (Da)	
Protease	Fragment[a]	Found[b]	Calculated[c]
Proteinase K	73–89	1558.3	1558.7
	126–140	1772.8	1773.8
	95–140	5186.2	5185.5
	93–140	5390.4	5389.7
	90–140	5633.3	5633.0
	80–140	6546.0	6547.0
	73–140	7173.2	7173.7
	1–72*	7304.2	7304.4
	1–75*	7561.8	7561.7
	1–76*	7632.7	7632.8
	57–140	8816.7	8815.5
	1–89*	8844.6	8845.1
	55–140	8986.7	8985.7
	1–92*	9087.7	9088.4
	1–140*	14460.9	14460.1
Trypsin	1–6	769.3	769.3
	24–32	829.4	829.4
	13–21	872.4	872.5
	35–43	950.5	950.5
	11–21	1071.6	1071.6
	33–43	1179.7	1179.6
	46–58	1295.0	1294.7
	81–96	1477.7	1477.7
	44–58	1523.8	1523.8
	61–80	1927.5	1927.0
	59–80	2156.5	2156.1
	103–140	4287.5	4288.4
	98–140	4829.7	4830.0
	97–140	4957.7	4958.2
	81–140	6419.0	6418.8
	1–80*	8058.6	8059.3
	1–96*	9519.5	9519.9
	1–97*	9648.0	9648.2
	1–102*	10189.2	10189.7

[a]Peptides obtained by proteolysis of α-synuclein by proteinase K and trypsin. The peptides were purified by RP-HPLC (see Figure 4.5 and 4.6) and listed in the order of increasing molecular weight.

[b]Experimental molecular masses determined by ESI-MS.

[c]Molecular masses calculated from the amino acid sequence of α-synuclein.

*In many cases, fragments containing methionine residues have been found also partially oxidized, so some mass values are incremented by 16 (1 ox) and/or 32 (2 ox) Da.

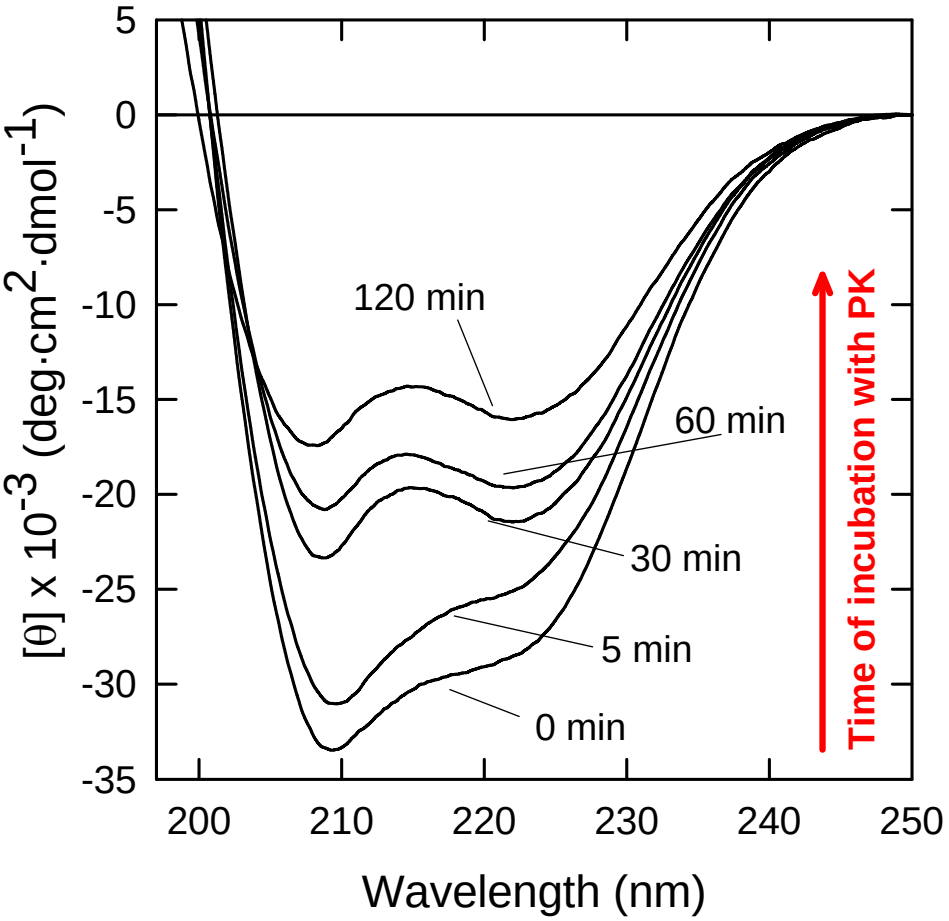

Fig. 4.7 Far-UV CD spectra of the proteolysis mixture with proteinase K. The reaction was conducted at a protein concentration of 5 μM in PBS in the presence of DHA (250 μM) with an E/S ratio of 1:1000. Spectra were recorded up to 2 hours at intervals during incubation.

4.3.2 α-Synuclein affects the aggregative properties of DHA

Critical aggregate concentration

Since a correlation between the physical state of DHA and its interaction with α-syn is still lacking, we have conducted systematic measurements to understand the effect of the protein on the fatty acid and the type of interaction that occurs between α-syn and DHA. The physical state and the self-aggregation process of DHA are strongly dependent on its concentration and ionic strength, but mostly on pH. Indeed, DHA can form micelles (pH range 9-11), vesicles (pH 8-9) and oil droplets (below pH 8) (Namani et al., 2007; Chen & Szostak, 2004). Turbidity methods have been used to measure the change of the scattered light caused by the formation of large aggregates, such as oil droplets and vesicles. These measurements allow the calculation of a critical concentration for aggregate formation (Namani & Walde, 2005). The optical density (OD) at 400 nm of solutions containing increasing concentrations (0-500 μM) of DHA in PBS at pH 7.4 was measured (Fig. 4.8 A, filled circles). Below a DHA concentration of 82 ±18 μM, there is no appreciable variation of turbidity at 400 nm. Increasing the concentration above this value, a sudden increase of OD is observed. This phenomenon indicates the formation of large fatty acid aggregates. The same measurements were conducted in the presence of α-syn (5 μM) and no significant increase of turbidity is observed up to ~500 μM DHA (Fig. 4.8 A, empty circles), suggesting that the protein is able to alter the DHA assembly. Moreover, addition of α-syn to a 500 μM DHA suspension, up to a final protein concentration of 5 μM, causes a sharp decrease of the OD at 400 nm (data not shown). If the turbidity is measured in the presence of 2.5 μM α-syn (Fig. 4.8 A, empty triangles), there is no variation of the optical density up to 240 ±25 μM DHA. Above this concentration, the turbidity starts to increase as a function of DHA concentration, showing that the amount of α-syn is not sufficient to prevent the formation of large lipid aggregates.

To better understand the effect of α-syn on the aggregation properties of DHA, we used pyrene as a fluorescent probe. We evaluated the ratio between the first and the third vibronic band (I_1 ~ 374 nm, I_3 ~ 383 nm) of the pyrene emission spectrum (Aguiar et al., 2003). The value of this ratio is correlated to the polarity of the environment and low values correspond to a non-polar surrounding (Kalyanasundaram & Thomas, 1977; Lòpez-Diaz et al., 2005). Increasing the amount of DHA, the I_1/I_3 ratio decreases. The experimental data points fit with a sigmoidal curve (Fig. 4.8 B, filled circles), indicating

the induction of a more hydrophobic micro-environment. The critical aggregation concentration (CAC) of the fatty acid, calculated at the inflection point of the plot (Aguiar et al., 2003) is 131 ±9 μM. In the presence of α-syn (5 μM), the I_1/I_3 ratio shows a steeper decrease with an inflection point at 47 ±13 μM (Fig. 4.8 B, empty circles). This indicates that the final aggregation state is reached at lower DHA concentrations, but does not imply that the non-polar environment produced by DHA alone and that induced by the presence of α-syn are the same. We have also analyzed the formation of the broad band centered at 470 nm and ascribed to the pyrene excimer emission. Pyrene can form an excited state dimer (excimer) only at concentrations higher than 1 μM or when it is dissolved in hydrophobic micro-domains (Sakai et al., 2006). The ratio (I_{ex}/I_1) between the maximum emission intensity of the excimer (I_{ex}) and the I_1 band of pyrene can be used to evaluate the efficiency of excimer formation. We plotted the I_{ex}/I_1 ratio as a function of DHA concentration (Fig. 4.8 B, inset) in the absence (filled circles) and in the presence (empty circles) of α-syn. Increasing the DHA amount, without the protein, the I_{ex}/I_1 ratio increases and a maximum value is reached at DHA concentration of 100 μM. Adding the protein, the I_{ex}/I_1 ratio follows a similar trend but the ratio reaches lower values (Fig. 4.8 B, inset, empty circles). This different behavior can derive from the fact that, in the absence of the protein, pyrene is dissolved in a larger hydrophobic volume, while α-syn forces DHA to form only aggregates with a small hydrophobic volume (Chen & Szostak, 2004).

Morphological analysis and sizing of DHA aggregates

A morphological analysis and a size determination were conducted by transmission electron microscopy (TEM) and dynamic light scattering (DLS).

TEM pictures of the DHA suspension in the presence of α-syn (Fig. 4.9 A, right) were taken and compared with the sample in the absence of the protein (Fig. 4.9 A, left). In the first case the image clearly indicates the presence of aggregates with an heterogeneous distribution of sizes, while in the second case, we observed smaller and regular species. The size distribution of DHA samples in the presence of α-syn was estimated from rotationally averaged images of individual particles. The resulting distribution shows a mean particle diameter of 13.3 ± 4.4 nm (Fig. 4.9 B).

We also try to determine the particle size of DHA aggregates by dynamic light scattering (DLS). As reported in Chen & Szostak, 2004, the DLS data were analyzed by

the method of cumulants and the hydrodynamic diameters of DHA particles were based on the Z-average values. The mean diameter of particles in a 250 μM DHA sample, prepared at pH 7.4 after 1-hr equilibration, is 414.2 nm with a polydispersivity index (PDI) of 0.297. When sample is prepared in the presence of 5 μM α-syn, the particle size is 68.7 nm with a PDI of 0.382. However, since TEM images suggest the presence of an heterogeneous population of aggregates and since the PDIs indicate a polydisperse system, DLS data were analyzed by a multimodal method. In Fig. 4.9 C the particle size distribution by volume is reported. The volume distribution is important for estimating the relative amounts of multiple size peaks samples. In a 250 μM DHA sample 95% of the distribution contribution derives from the particles that average around 517 nm, while in the presence of 5 μM α-syn 99.8% of the species have a smaller diameter of 34.19 nm; however, this last peak is very large (peak width of 31.48 nm) indicating that in the presence of α-syn the DHA aggregates undergo a resizing toward smaller species with a broad distribution.

The estimations by TEM and by DLS of the size DHA aggregates in the presence of the protein do not agree each other. An explanation should be both in the intrinsic complexity and instability of the system or in the preparation of the samples. Further studies are necessary to follow the equilibration of the smaller species by DLS analysis on time. Second, the negative staining and the sample drying for TEM specimens preparation should cause some alterations in DHA samples.

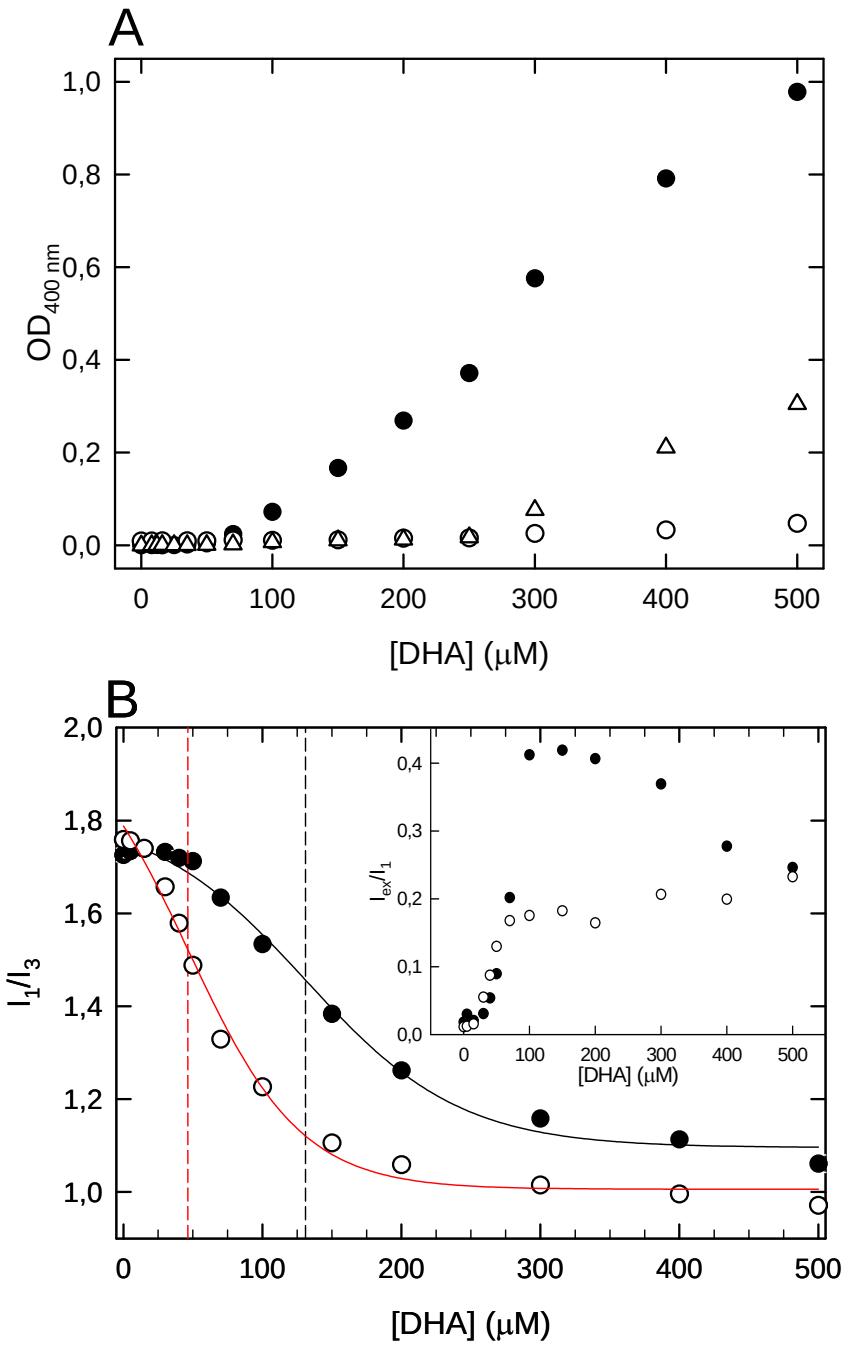

Fig. 4.8 Characterization of the physical state of DHA by turbidity method **(A)** and pyrene fluorescence **(B)**. **A**. Turbidimetric analysis was conducted at 400 nm with samples containing DHA up to 500 μM, in the absence (filled circles) and in the presence of α-syn (2.5 and 5 μM, empty triangles and empty circles, respectively). **B**. Ratio between the first and the third vibronic band (I_1/I_3) of the pyrene emission spectrum as a function of DHA concentration in the absence and in the presence of α-syn. **Inset:** I_{ex}/I_1 ratio as a function of DHA concentration in the absence and in the presence of α-syn (5 μM).

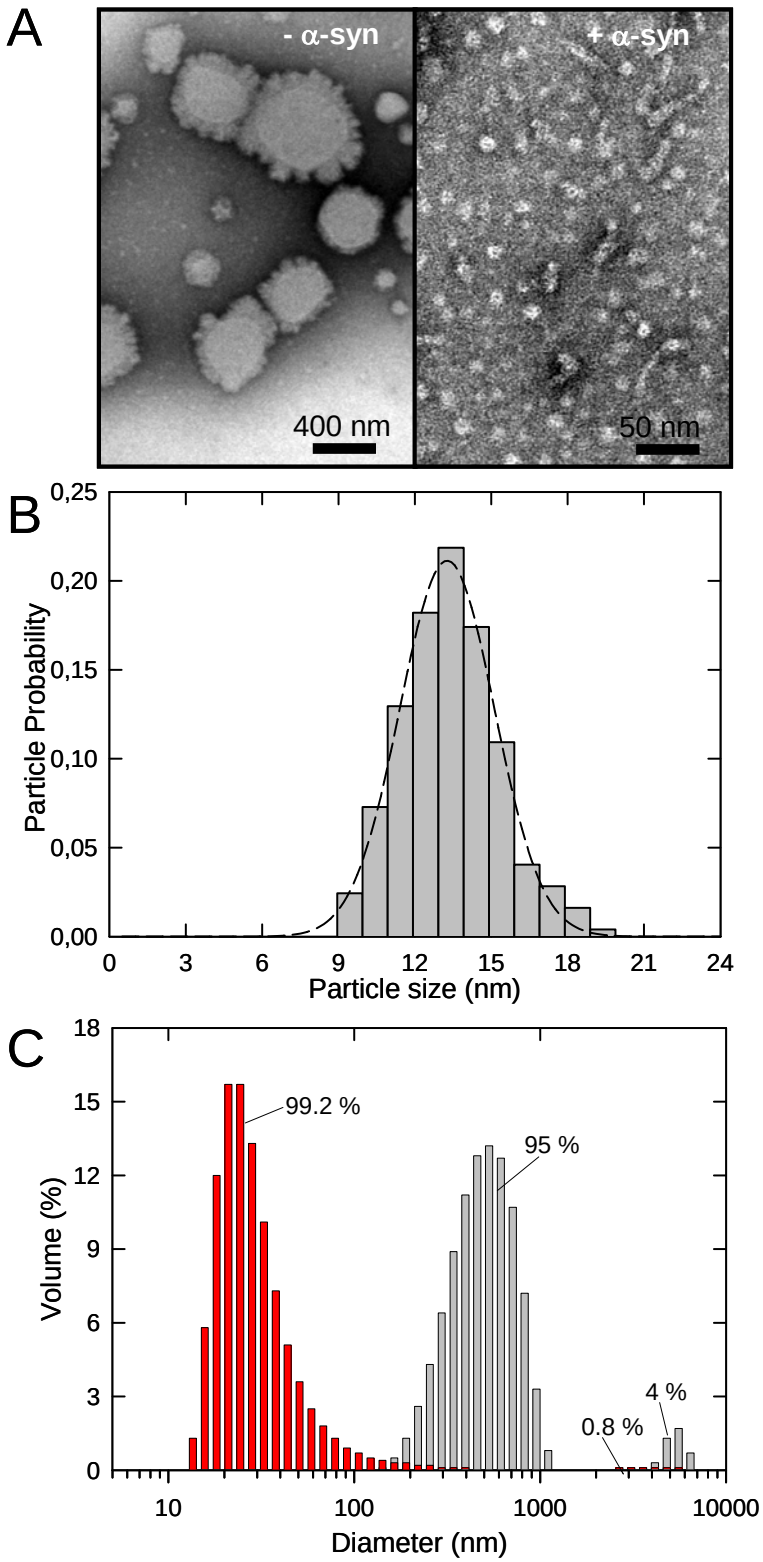

Fig. 4.9 (A) TEM images of samples of DHA (250 μM) in the presence (+ α-syn) and in the absence (-α-syn) of the protein. **(B)** Particle size distribution of DHA samples in the presence of α-syn estimated from rotationally averaged TEM images of individual particles. **(C)** DLS analysis of 250 μM DHA in the absence (grey bars) and in the presence of 5 μM α-syn (red bars). The percentages close to the bars indicate the distribution contribution of the measured particles.

4.3.3 Role of different regions of α-synuclein in the interaction with DHA

Conformational analysis

In order to investigate the involvement of different regions of α-syn in the interaction with DHA, truncated forms of the protein were prepared (Fig. 4.10 A). Syn1-99 lacks the acidic C-terminal region but retains all the seven imperfect repeats. Syn1-52 lacks also the NAC region (61-95) and includes four imperfect repeats. The central polypeptide syn57-102 includes the NAC region and the last three imperfect repeats. Finally, the peptide syn108-140 spans almost the whole acidic tail. At the N-terminal, the polypeptides syn1-52 and syn57-102 have an extra-sequence constituted by *GSH* and *GSHM* residues, respectively.

Far UV CD titration experiments of the several peptides in the presence of increasing concentration of DHA were performed. In Fig. 4.10 B, the ellipticity of the polypeptides and of α-syn samples at 222 nm (one of the two typical minima of α-helical secondary structure), is shown as a function of the molar ratio between DHA and the peptides. Increasing the amount of DHA, syn108-140 remains unfolded, while a corresponding increment of the ellipticity is observed for syn1-99, syn1-52 and syn57-102. The trends of the curves for syn1-99 and syn1-52 are quite similar to that of α-syn and the conformational transition involves the whole polypeptide chain; indeed syn1-99 has an helix content of ~87 % and syn1-52 of ~90 % (Rohl et al., 1996). Moreover, from the plots it can be estimated that ~ 40 and 38 DHA molecules are required per syn1-99 and syn1-52 molecule for complete folding. On the contrary, syn57-102 needs an higher amount of DHA to complete the transition and to reach the saturation of helix content that is estimated to be ~ 67 %.

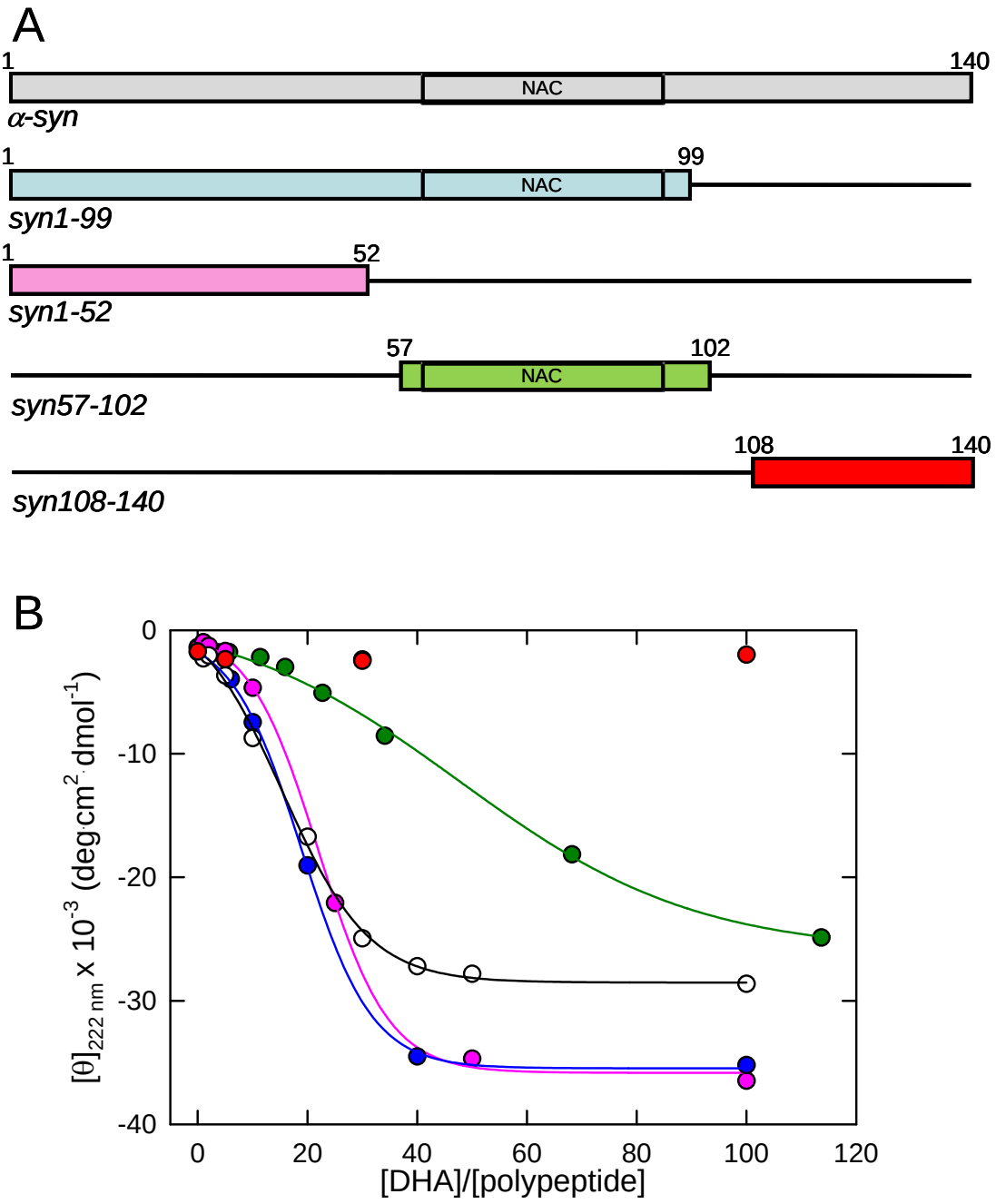

Fig. 4.10 (A) Schematic representation of truncated forms of α-syn. The α-syn species herewith studied correspond to the N-terminal fragments 1-99 (syn1-99, blue), 1-52 (syn1-52, pink), 57-102 (syn57-102, green) and the C-terminal fragment 108-140 (syn108-140, red). The N-terminal fragments are obtained by recombinant methods. At the N-terminal syn1-52 and syn57-102 have extra-sequence *GSH* and *GSHM* residues, respectively (see Materials & Methods). The C-terminal fragment has been obtained by chemical synthesis. **(B)** DHA-induced structural changes monitored by far-UV CD spectroscopy. CD signals at 222 nm are plotted against the molar ratio between DHA and polypeptides. The analysis was conducted in PBS pH 7.4, using a peptide concentration of 5 μM.

Proteolytic mapping

In order to verify the accessibility of the polypeptide chains of the different truncated form of α-syn once bound to DHA, we performed limited proteolysis experiments. We have used proteinase K as protease, since it displays enough substrate aspecificity and to have a comparison with the proteolysis conducted on α-syn. The HPLC analyses of the proteolytic mixture of syn1-99 and syn 1-52 with proteinase K (Fig.4.11 A and B, respectively), in the absence (top) and in the presence (bottom) of 250 μM DHA after 1 hour of incubation were reported. In the absence of DHA, both the peptides are cleaved quite rapidly and proteinase K cleavage produces a large number of peptides as indicated by the presence of numerous peaks in the chromatograms. The identification of the peptide materials was obtained by mass spectrometry analysis and the results are reported in Table 4.2. In the presence of the fatty acid, syn1-99 and syn1-52 show protease resistance and the peak relative to the intact peptide is the main species present in the chromatogram after 1 hour of incubation. For syn1-99 there is only a moderate proteolysis due to the free molecules in equilibrium; moreover, a peak relative to the oxidized form of syn1-99 are isolated. In the case of syn1-52 a partial cleavage occurs at the level of the peptide bond His50-Gly51 and fragment species 1-50 is produced. Also a small amount of 1-49 is detectable and the calculated mass indicates that partial oxidation of a Met residue is occurred (Table 4.2). We have also compared the proteolytic maps of syn57-102 and syn108-140 by proteinase K obtained in the absence and in the presence of 250 μM DHA. The HPLC analyses relative to the proteolysis mixtures of syn57-102 and syn108-40 are shown in Fig. 4.12 A and B, respectively, and the peptides masses are reported in Table 4.3. As already observed for the N-terminal fragments, in the absence of DHA syn 57-102 is cleaved by proteinase K generating many fragments that span all the sequence of the peptide chain. In the presence of DHA, only moderate fragmentation occurs, as assessed by the presence of small few peaks in the chromatograms and by the peak of intact syn57-102. Far UV CD assessed that at a molar ratio ([DHA]/[peptide]) of 50 not all the peptide molecules are bound to the lipid and part is still free, so it can be that proteolysis occurs on free molecules.(Fig. 4.10 B, green circles). At variance from the other syn species, syn108-140 results resistant to proteolytic attack in the absence as well as in the presence of the fatty acid. The unusual rigidity of the C-terminal tail of α-syn to proteases was already seen for the interaction between α-syn and SDS micelles (Polverino de Laureto et al., 2006). This fact cannot be

attributed to possible structural transitions of the C-terminal of the molecule, but rather to a protection deriving from the unusual sequence (14 negative charges and 5 Pro residues).

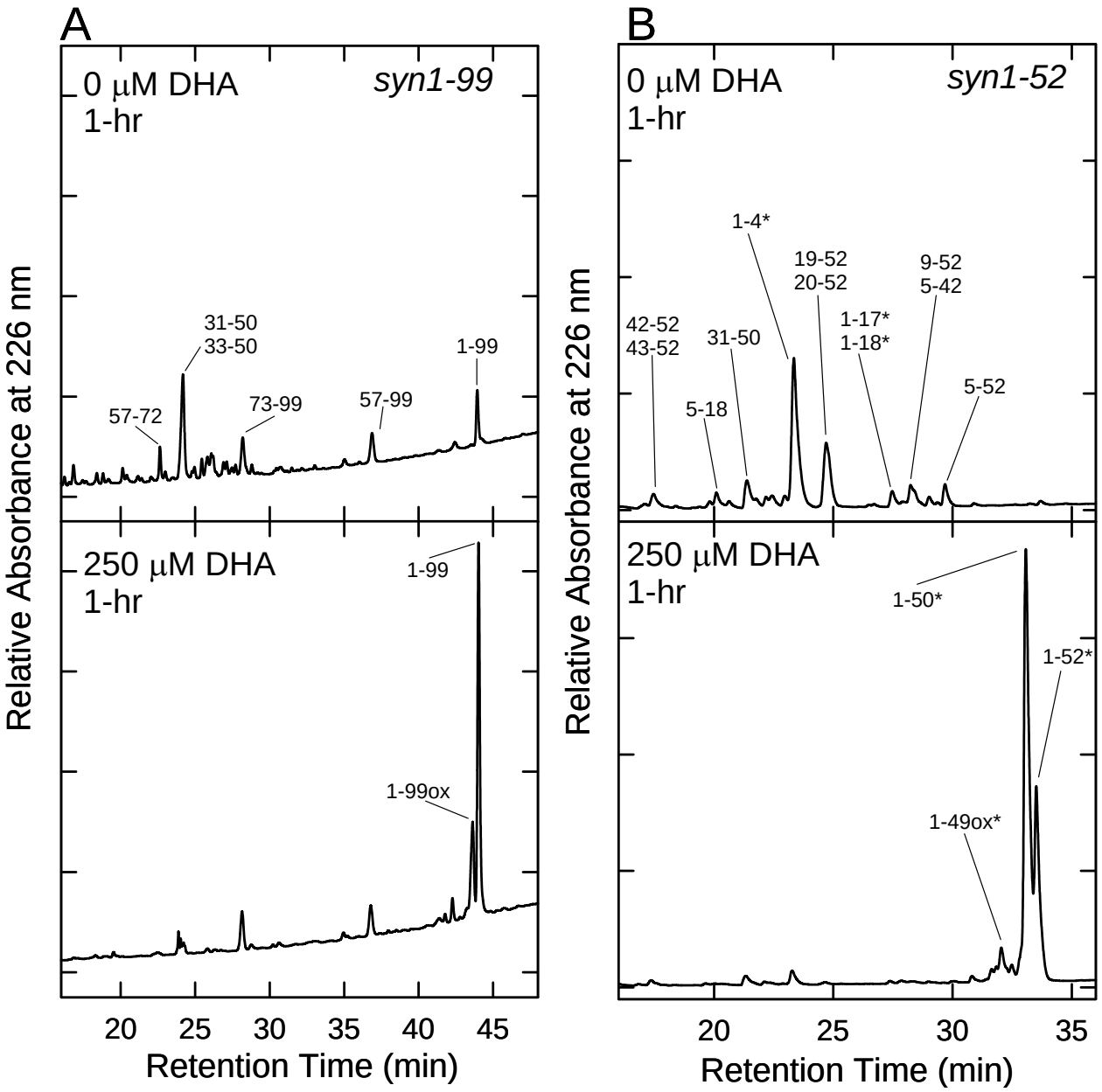

Fig. 4.11 Proteolysis of syn1-99 **(A)** and syn1-52 **(B)** by proteinase K analyzed by RP-HPLC. The reactions were conducted at a protein concentration of 5 μM in PBS buffer in the absence **(top)** or in the presence **(bottom)** of 250 μM DHA, using an E/S ratio of 1:1000. RP-HPLC chromatograms correspond to the analysis of aliquots taken from the proteolysis mixtures after 1-hr of incubation with the protease.

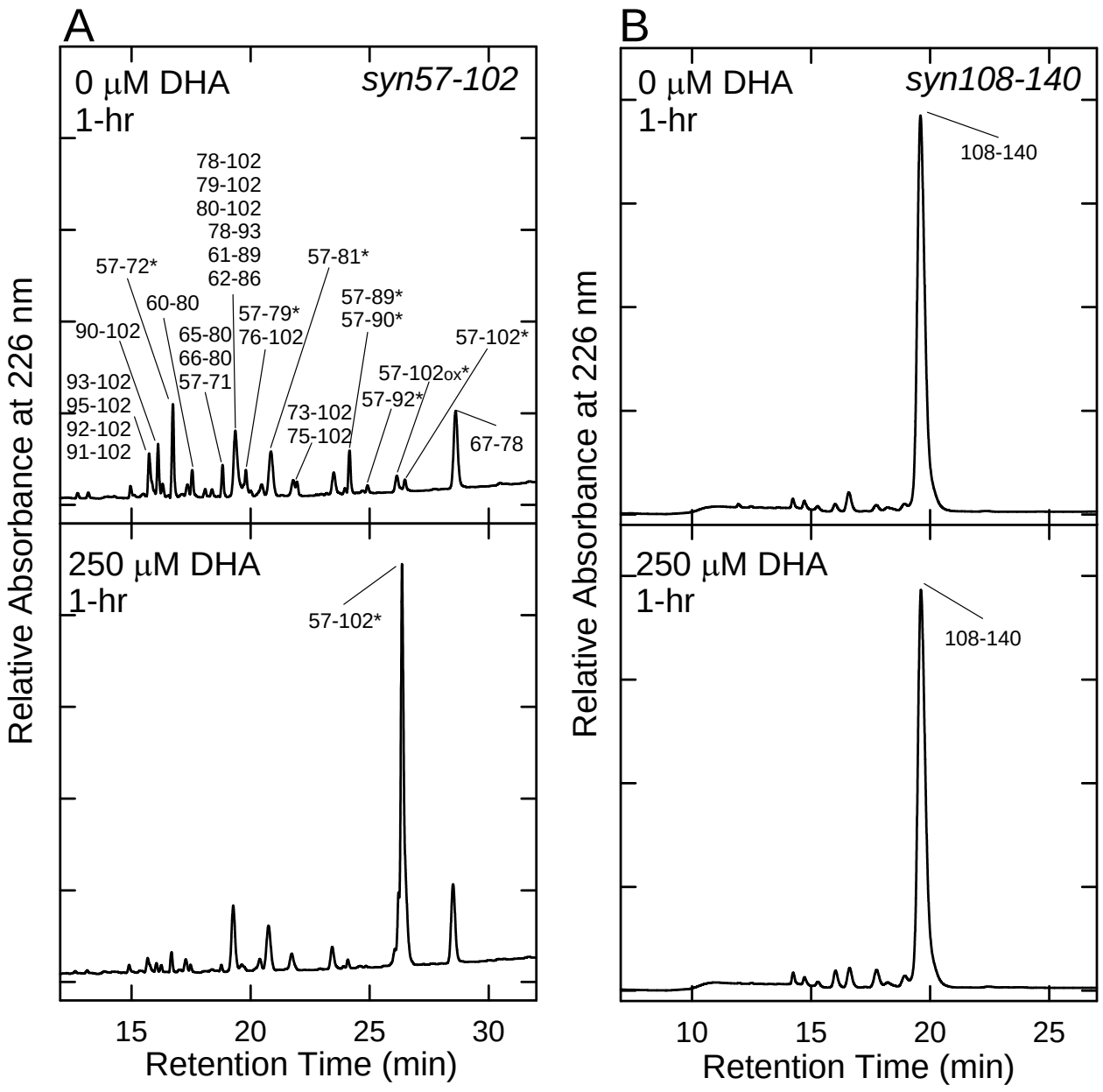

Fig. 4.12 Proteolysis of syn57-102 **(A)** and syn108-140 **(B)** by proteinase K analyzed by RP-HPLC. The reactions were conducted at a protein concentration of 5 μM in PBS buffer in the absence **(top)** or in the presence **(bottom)** of 250 μM DHA, using an E/S ratio of 1:1000. RP-HPLC chromatograms correspond to the analysis of aliquots taken from the proteolysis mixtures after 1-hr of incubation with the protease.

Table 4.2 Molecular masses of fragments obtained by proteolysis of syn1-99 and syn1-52 by proteinase K

		Molecular mass (Da)	
Polypeptide	Fragment[a]	Found[b]	Calculated[c]
syn1-99	57-72	1658.8	1659.8
	33-50	1930.3	1931.2
	31-50	2116.4	2116.4
	73-99	2604.2	2604.9
	57-99	4247.3	4246.7
	1-99	9892.6	9891.4
syn1-52	1-4*	792.4	791.8
	43-52	1053.7	1052.6
	42-52	1140.8	1139.6
	5-18	1388.0	1387.8
	1-17*	2090.4	2091.5
	31-50	2117.0	2116.5
	1-18*	2162.5	2162.5
	20-52	3385.8	3385.8
	19-52	3456.8	3456.9
	5-42	3792.6	3792.4
	9-52	4397.9	4398.0
	5-52	4827.6	4827.6
	1-49ox*	5323.9	5324.1
	1-50*	5445.6	5445.3
	1-52*	5601.4	5601.4

[a]Peptides obtained by proteolysis of syn1-99 and syn1-52 by proteinase K. The peptides were purified by RP-HPLC (see Figure 4.11) and listed in the order of increasing molecular weight.

[b]Experimental molecular masses determined by ESI-MS.

[c]Molecular masses calculated from the amino acid sequence of syn1-99 and syn1-52

*The peptides have an extra sequence (GSH) at the N-terminal.

Table 4.3 Molecular masses of fragments obtained by proteolysis of syn57-102 and syn108-140 by proteinase K

		Molecular mass (Da)	
Polypeptide	Fragment[a]	Found[b]	Calculated[c]
syn57-102	95-102	914.6	915.1
	67-78	1000.9	1001.1
	93-102	1118.7	1119.3
	92-102	1219.7	1220.4
	91-102	1290.8	1291.5
	66-80	1355.7	1356.5
	90-102	1361.8	1362.6
	78-93	1432.8	1431.5
	65-80	1468.9	1470.6
	57-71*	1971.2	1971.2
	60-80	2053.6	2056.3
	57-72*	2071.5	2072.3
	80-102	2276.0	2276.6
	62-86	2312.5	2313.6
	79-102	2404.4	2404.7
	78-102	2476.3	2475.8
	76-102	2645.8	2646.0
	57-79*	2699.3	2699.0
	61-89	2713.0	2714.0
	75-102	2747.1	2747.1
	73-102	2903.6	2903.3
	57-81*	2928.4	2928.3
	57-89*	3612.3	3613.0
	57-90*	3684.5	3684.1
	57-92*	3856.0	3856.3
	57-102*	4957.5	4957.6
	57-102ox*	4973.22	4973.6
syn108-140	108-140	3787.8	3787.9

[a]Peptides obtained by proteolysis of syn57-102 and syn108-140 by proteinase K. The peptides were purified by RP-HPLC (see Figure 4.12) and listed in the order of increasing molecular weight.

[b]Experimental molecular masses determined by ESI-MS.

[c]Molecular masses calculated from the amino acid sequence of syn57-102 and syn108-140

*The peptides have an extra sequence (GSHM) at the N-terminal.

Effects on DHA aggregates

The aggregation properties of DHA were also analyzed in the presence of the truncated forms of α-syn. Turbidity measurements show that the presence of the peptides (5 μM) with the exception of syn108-140, prevents the formation of large fatty acid aggregates (Fig 4.13), since there isn't an increase in OD at 400 nm. The turbidity of DHA samples was also measured in the presence of 2.5 μM syn57-102 (Fig. 4.13 C, green triangles): there is no variation of the OD up to 242 ±49 μM DHA. This value is very similar to that obtained with 2.5 μM α-syn. Above this concentration, the turbidity starts to increase as a function of DHA concentration, showing that the amount of syn57-102 is not sufficient to prevent the formation of large lipid aggregates. In the presence of syn108-140 (5 μM) there is no appreciable variation of turbidity at 400 nm up to 75 ±9 μM DHA. Increasing the concentration above this value, an increment of turbidity is observed, but the OD values are lower than those obtained for DHA samples alone (Fig. 4.13 D).

The CAC of DHA was also evaluated by pyrene fluorescence assay. In Fig. 4.14 the I_1/I_3 pyrene ratio was plotted as a function of DHA concentration in the presence of syn1-99 (A, blue circles), syn1-52 (B, pink circles), syn57-102 (C, green circles) and syn108-140 (D, red circles). In the plots I_1/I_3 pyrene ratio for DHA alone was reported as a control (black circles and line). For all the samples, increasing the DHA amount the I_1/I_3 ratio decreases. This fact suggests that a more hydrophobic micro-environment is induced. The experimental data points fit with a sigmoidal curve so the CACs of the fatty acid in the presence of the several peptides can be calculated at the inflection point of the plots (Aguiar et al., 2003). In the presence of 5 μM syn1-99 and syn1-52 , the I_1/I_3 ratio shows a steeper decrease with an inflection point at 71 ±7 μM and 69 ±22 μM DHA, respectively (Fig. 4.14 A, blue dash line and B, pink dash line). This indicates that syn1-99 and syn1-52 exert a similar effect in reducing FA concentration for aggregate formation, comparable to that of α-syn (47 ±13 μM). On the contrary, syn57-102 affects in minor extent the aggregative properties of DHA, since in the presence of this polypeptide CAC of DHA is 103 ±11 μM (Fig. 4.14 C, green dash line). The addition of syn108-140 does not interfere with pyrene fluorescence and it is possible to calculate a CAC for DHA of 140 ±8 μM (Fig. 4.14 D, red dash line).

A morphological analysis of DHA aggregate species were performed by TEM. In Fig.4.15 TEM images relative to FA samples in the presence of the different polypeptides

are reported. As controls, in panels A two representative pictures of DHA sample in PBS pH 7.4 are shown. They indicate the presence of DHA aggregates with an heterogeneous distribution of sizes. It is possible to see collapsed small spherical particles (red arrow) and large particles with different degree of contrast due to a different exclusion of the stain (green arrows). In panel B smaller spherical aggregates are formed in the presence of α-syn as already seen (§ 4.3.2). Also the presence of the other polypeptides with the exception of syn108-140 causes a resizing of DHA assemblies (panel C, D, E, F). In the presence of syn1-99 (panel C) and syn1-52 (panel D) DHA molecules form high contrast spherical aggregates with diameters of ~ 20 and ~ 24 nm, respectively. On the other hand, DHA assembles in smaller species also in the presence of syn57-102, but morphologically these aggregates can be described as collapsed spheres (panel E). The presence of syn108-140 does not modify DHA aggregates morphologies (panel F), TEM picture shows large spherical particles comparable to those observed for DHA samples (panel A). All these data obtained by different methods suggest that the N-terminal region of α-syn exerts a main role in modifying the aggregative properties of DHA.

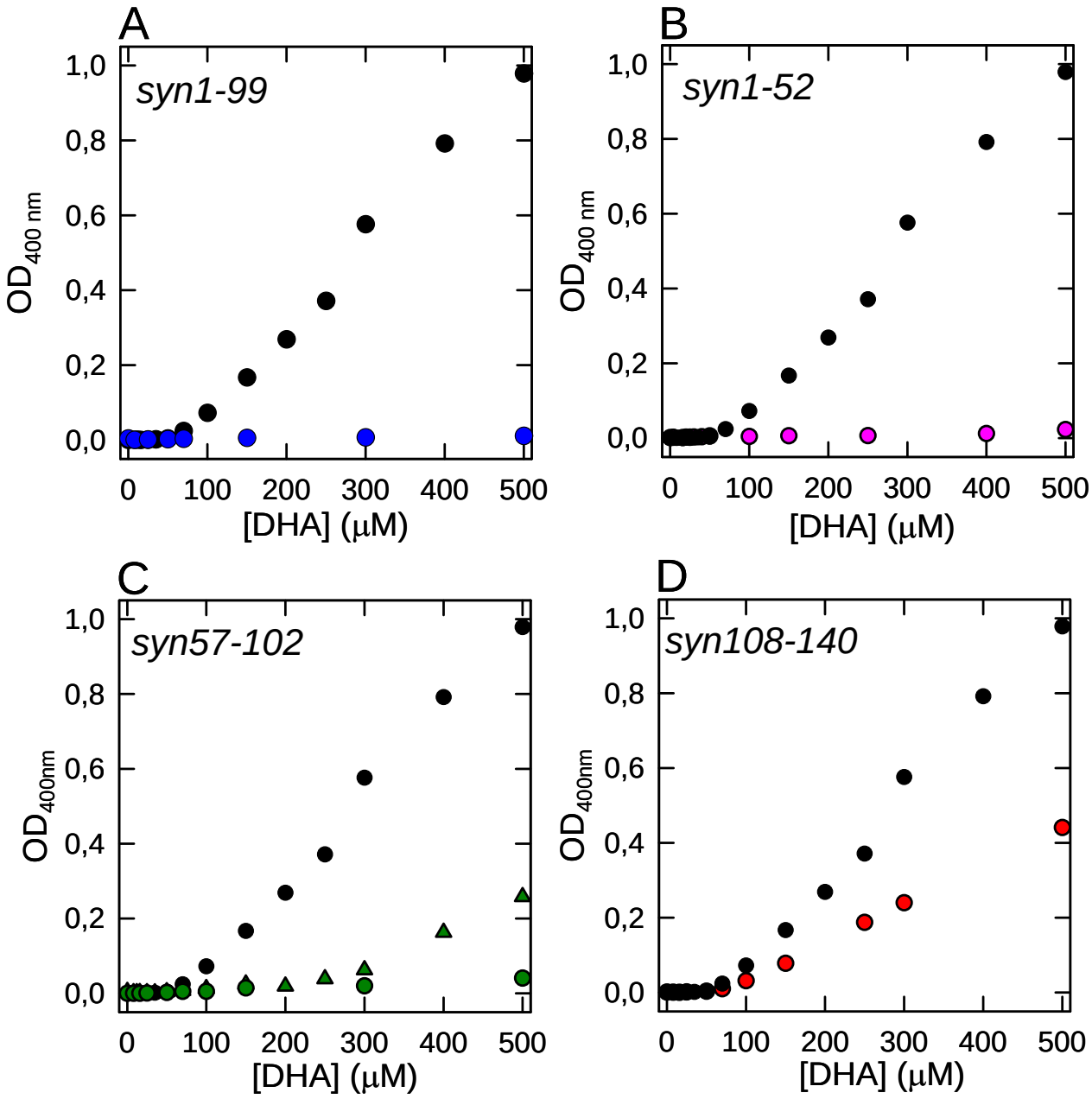

Fig. 4.13 Turbidity analysis at 400 nm of samples containing DHA up to 500 μM, in the absence (black circles) and in the presence of syn1-99 (**A**, 5 μM blue circles), syn1-52 (**B**, 5 μM, pink circles), syn57-102 (**C**, 2.5 μM, green triangles, 5 μM green circles) and syn108-140 (**D**, red circles).

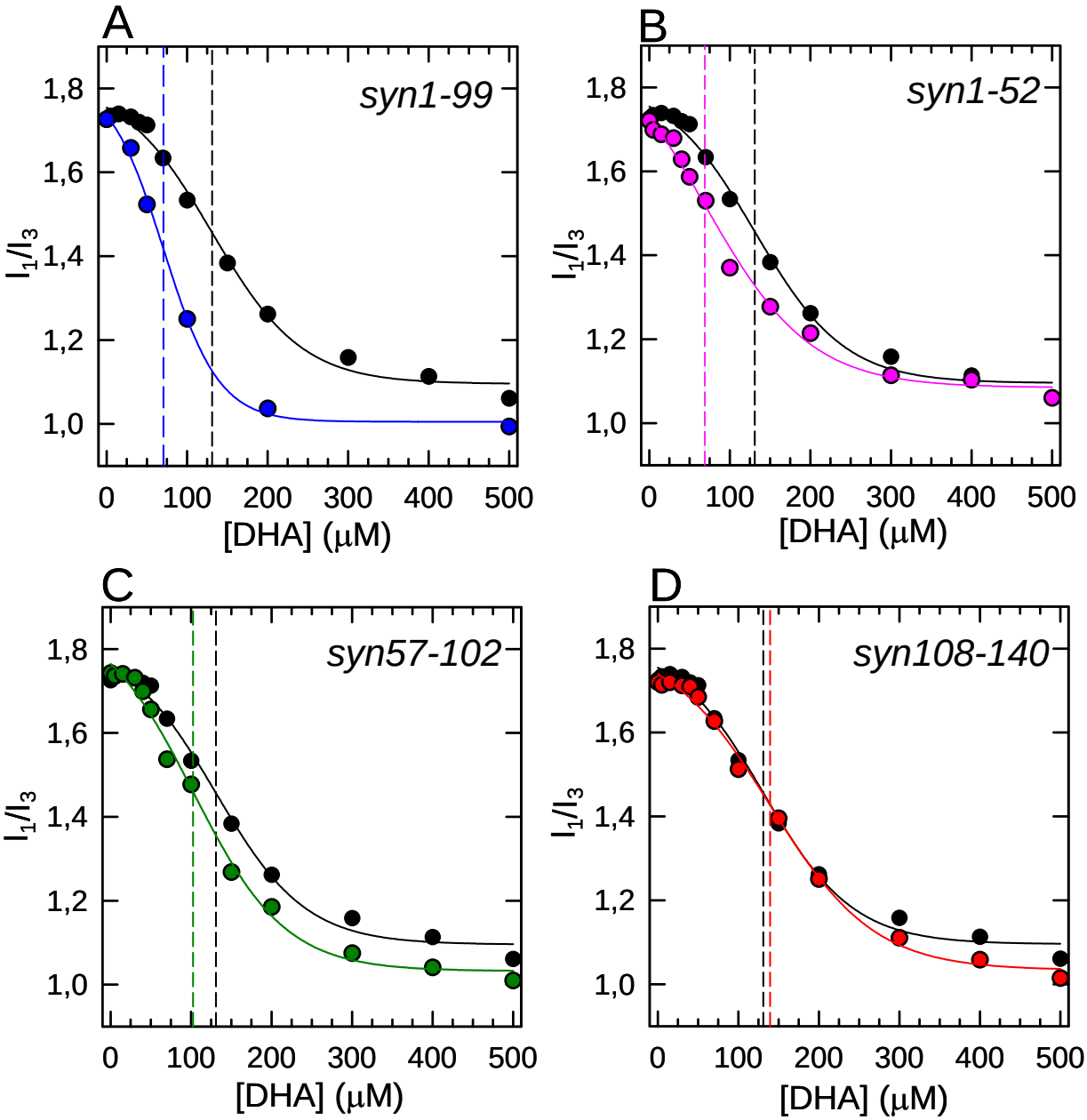

Fig. 4.14 Pyrene fluorescence assay. Ratio between the first and the third vibronic band (I_1/I_3) of the pyrene emission spectrum as a function of DHA concentration (0-500 μM) in the absence (black circles) and in the presence of α-syn fragments. The analyses were conducted using 5 μM peptide in PBS pH 7.4 and are reported as follows: **A**, syn1-99, **B,** syn1-52, **C,** syn57-102 and **D,** syn108-140.

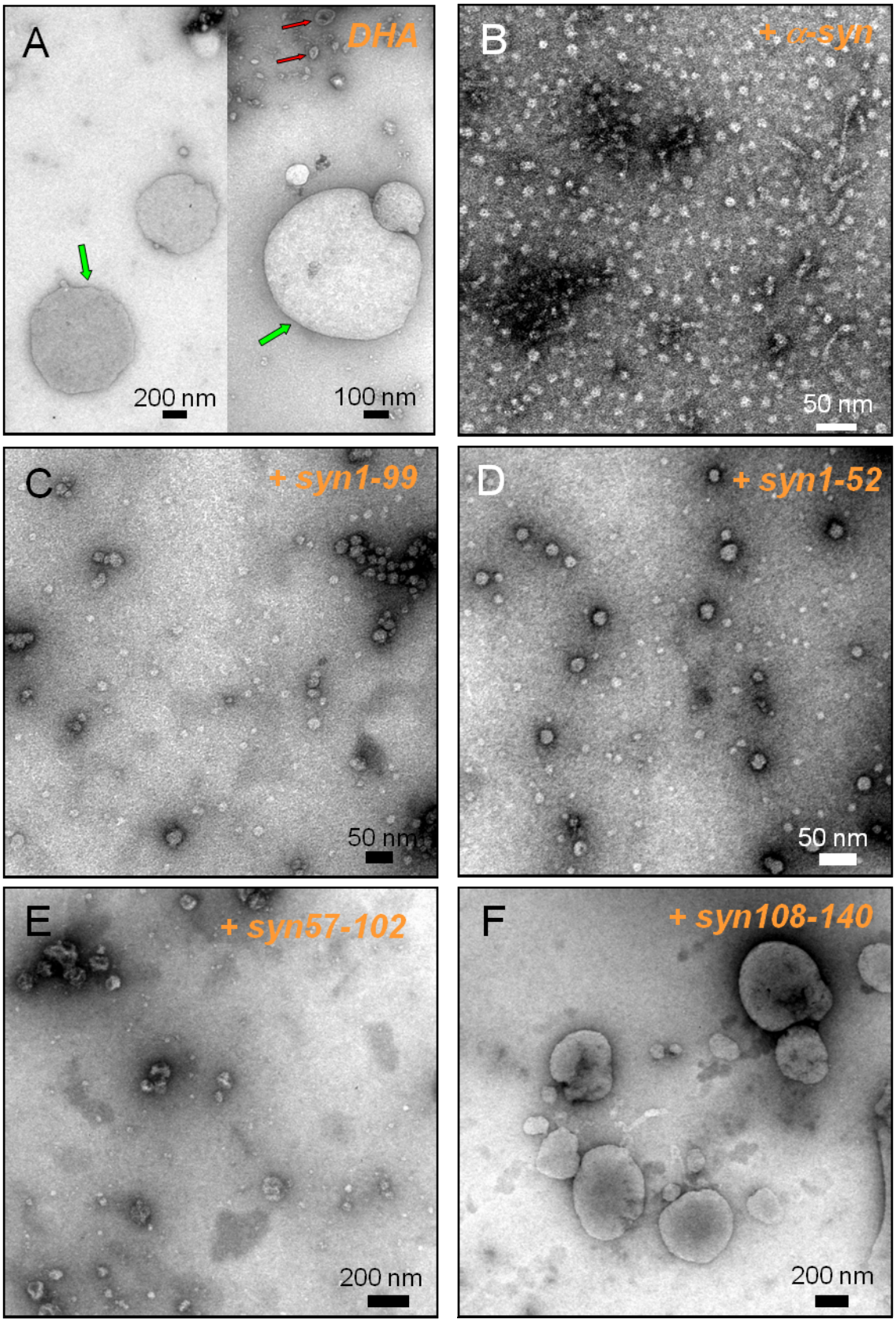

Fig. 4.15 TEM pictures of DHA samples in the absence **(A)** and in the presence of α-syn **(B)** or its truncated forms **(C-F)**.

4.3.4 Aggregation process of α-synuclein in the presence of DHA

Since several studies reported that α-syn in the presence of PUFAs can form both soluble oligomers that insoluble amyloid fibrils, the aggregation process of the protein was analyzed by several biochemical and biophysical methods.

Firstly, aggregation of α-syn samples (50 μM) containing different concentrations of DHA ([DHA]/[α-syn] molar ratios of 10 and 50) was monitored by native polyacrylamide gel electrophoresis (Fig. 4.16). This method is an excellent tool to reveal the presence of covalent and non-covalent oligomers and aggregates. In the absence of FA only one band relative to the α-syn monomer is detected up to 118 hrs (Fig. 4.16 A). On the contrary, in the presence of DHA in a molar ratio of 10, during incubation at 37°C 500 rpm, there are a decrease of the α-syn monomer and an increase of material into the wells. Also some smearing, which are indicative of a wide range of oligomeric species, can be observed on the top of the separating gel (Fig. 4.16 B). In the presence of DHA in a molar ratio of 50 the electrophoretic pattern is quite similar to those obtained with a lower concentration of DHA but more intense smearing is detected into the gel (Fig. 4.16 C). Since DHA promotes α-syn aggregation, a parameter such as the effect of lipid concentration on protein aggregation was evaluated. Indeed, the molar ratio determines the amount and type of the aggregate species of DHA in solution and the population of free unbound protein molecules.

A conformation analysis of α-syn at different stages of aggregation was carried out by using CD measurements. During incubation (37°C and shaking at 500 rpm) α-syn acquires a β-sheet conformation in the presence of DHA in a molar ratio of 10 (Fig. 4. 17 A). The initial spectrum of the protein reveals that 65 % of α-syn molecules are unfolded while the remaining population has an α-helix structure. During the aggregation process α-syn undergoes a conformational rearrangement. After 74 hrs of incubation, the spectrum is dominated by the band at 218 nm, evidencing a high content in β-structure. It is important to underline that, during the aggregation process triggered by saturating concentration of DHA (molar ratio of 50), we did not observe any conformational transition from α-helix to β-sheet during 142 hrs of incubation but only a partial reduction of the intensity of the CD signals (data not shown). Moreover, in the absence of DHA no conformational transition takes place and α-syn remains unfolded in solution up to 142 hrs.

In order to investigate the presence of amyloid-like fibrils in the samples, ThT binding assay was performed. Only the aggregates formed in the presence of non-saturating condition of DHA exhibit a common behaviour of amyloid like fibrils. Samples containing the lipid in a molar ratio of 10 show an increase of ThT fluorescence at 485 nm. The lag phase seems to be very short since growth phase reaches a plateau after only 25 hrs of incubation (Fig. 4.17 B). These data was confirmed by TEM. After 142 hrs of incubation in the absence of DHA and in the presence of saturating FA concentration (Fig. 4.18 A, C), there are not fibrillar aggregates. On the contrary, DHA, in a molar ratio [DHA]/[α-syn] of 10 (Fig 4.18 B), promotes fibrils formation. After 142 hrs of incubation, α-syn forms aggregates with amyloid-fibrillar morphology, long, unbranched with a diameter of 12-14 nm. In the presence of DHA, in a molar ratio [DHA]/[α-syn] of 50, worm-like fibrils (left) and spherical oligomers (right) (diameter ~ 11 nm) are detectable.

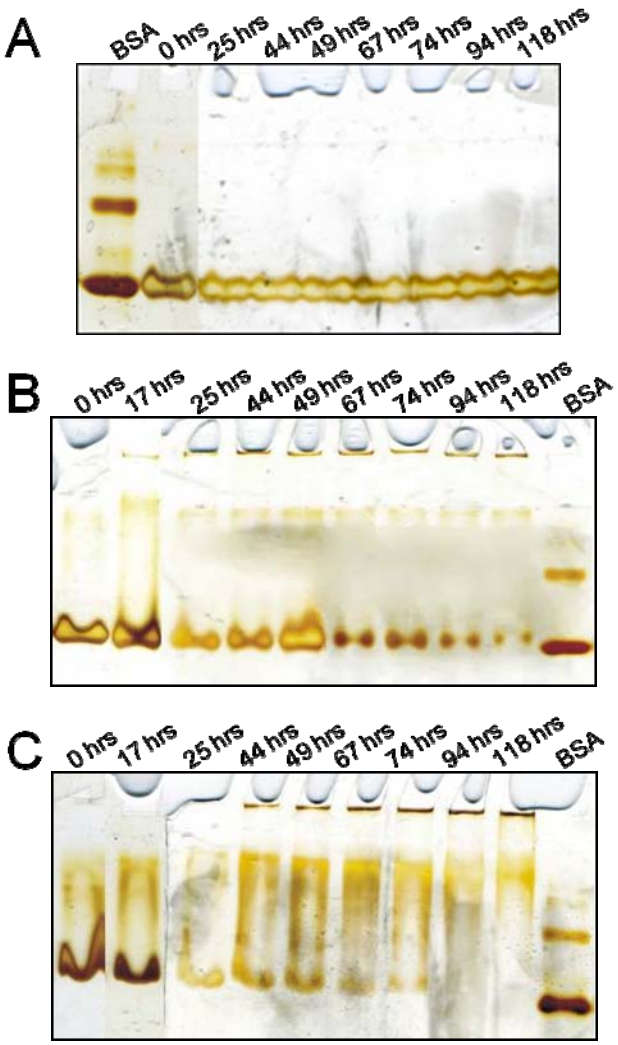

Fig. 4.16 α-Syn aggregation in the absence **(A)** and in the presence of DHA in a molar ratio [DHA]/[α-syn] of 10 **(B)** or 50 **(C)** monitored by native-PAGE.

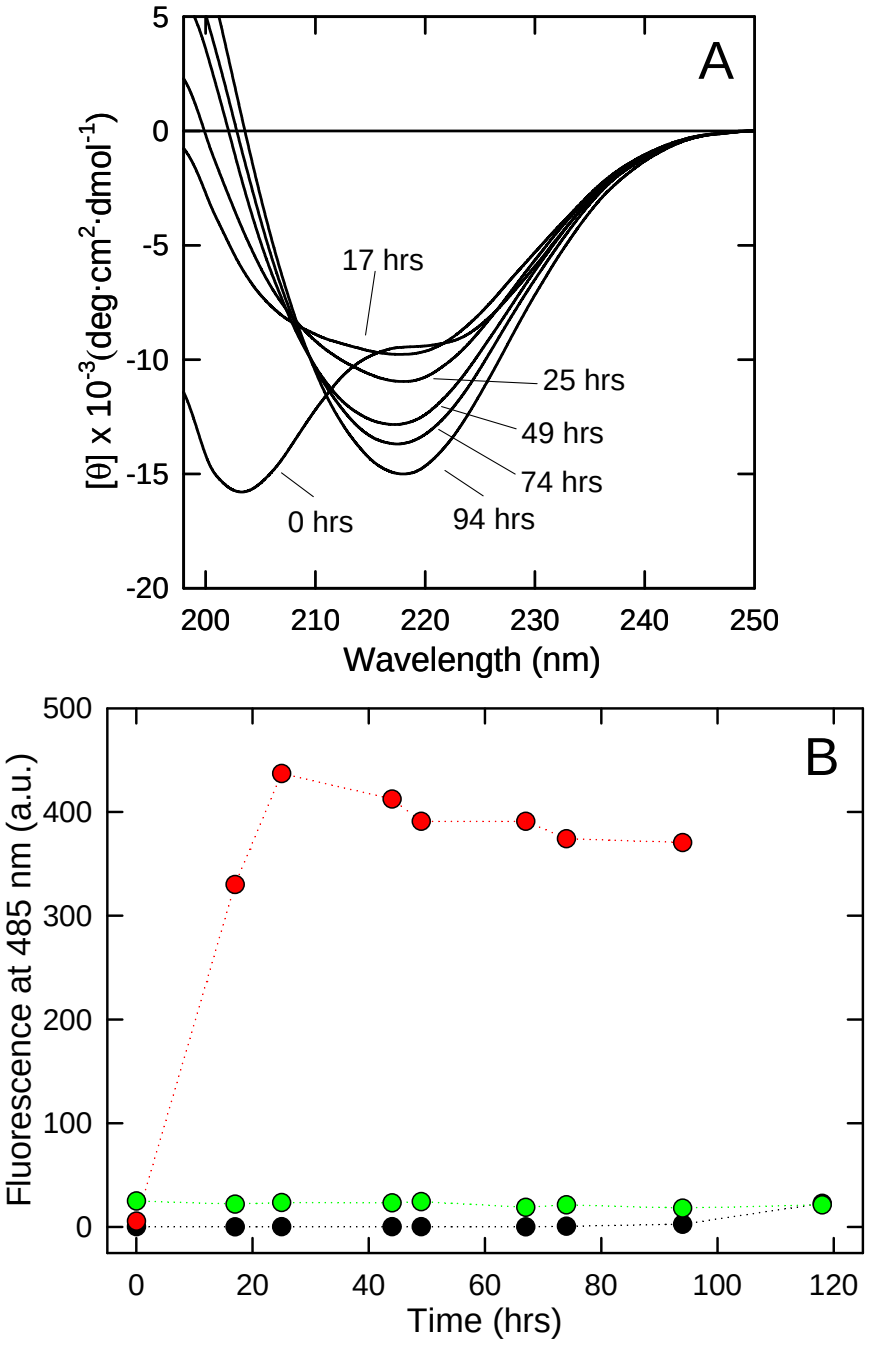

Fig. 4.17 (A) Evolution of the secondary structure of α-syn monitored by far-UV CD during aggregation in the presence of DHA in a molar ratio of 10. **(B)** Time-course analysis of the aggregation process of α-syn (PBS buffer, 37°C, shaking at 500 rpm) in absence (black circles) and in the presence of DHA in a molar ratio of 10 (red circles) or 50 (green circles) monitored by ThT fluorescence.

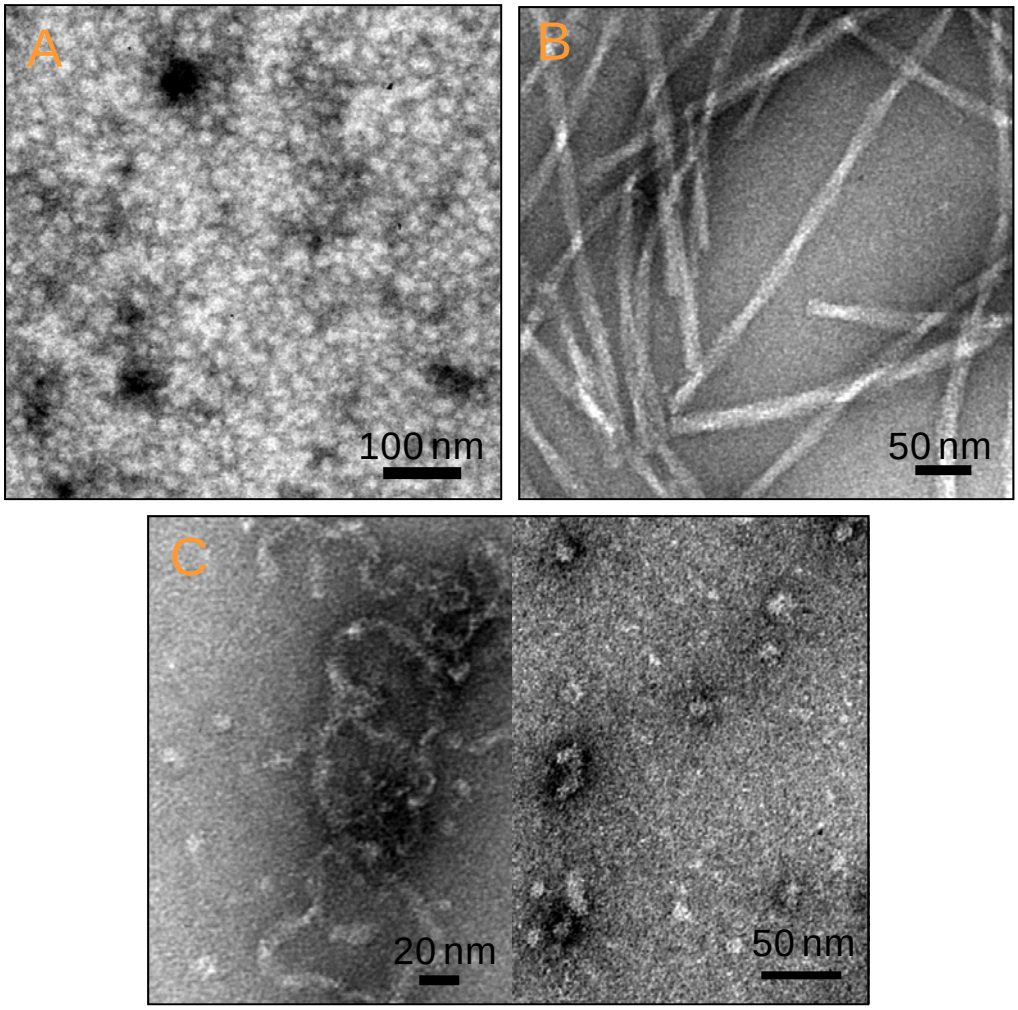

Fig. 4.18 The effect of DHA on aggregation process of α-syn was analyzed by TEM. TEM pictures relative to α-syn aggregation samples after 142 hrs of incubation in the absence **(A)** and in the presence of DHA (**B**, molar ratio of 10; **C**, molar ratio of 50) were reported.

4.4 DISCUSSION AND CONCLUSIONS

Many reports suggest that PUFAs are strictly connected to neurological disorders, including depression, Alzheimer's disease and Parkinson's disease (Marszalek & Lodish, 2005, and references therein). Specifically, alterations in PUFAs levels have been found related to aggregation of α-syn (Necula et al., 2003; Broersen et al., 2006; Perrin et al., 2001; Sharon et al., 2003; Assayag et al., 2007). It has been proposed that α-syn could interact with free FAs (Sharon et al., 2001; Broersen et al., 2006), or, alternatively, with FAs in a micellar or bilayer state (Necula et al. 2003; Lücke et al., 2006). A recent study also suggests that α-syn normally interacts with PUFAs to carry out its physiological functions, forming active forms of soluble oligomers (Ben Gedalya et al., 2008).

There is ample evidence that natively unfolded proteins, such as α-syn, are not a simple random coil, but rather form transient ordered structures that could be stabilized by the interactions with natural ligands or cofactors, which are able to affect their net charge or hydrophobicity (Uversky et al., 2007). In this study, we demonstrated that α-syn acquires an α-helical conformation in the presence of DHA, and that the imperfect repeats of α-syn sequence play an important role in the α-helix transition and thereby in the interaction with DHA. α-Syn strongly affects the self-association of the fatty acids and its N-terminal region has a crucial role even in the modulation of this process. The first 70 residues of the polypeptide chain of α-syn seem to be strongly involved in the interaction with DHA, while the NAC region results accessible to proteases. Moreover, we demonstrated that the interaction with DHA has important implication for α-syn aggregation.

Upon binding to DHA, α-syn adopts an α-helix secondary structure in a simple two state transition and the helix content is estimated to be ~70 %. The interaction between α-syn and micellar systems, especially those obtained using the detergent SDS, has been intensively studied by many groups and topological models have been drawn on the basis of NMR studies (Bisaglia et al., 2005; Ulmer et al., 2005; Bussel et al., 2004) and limited proteolysis experiments (Polverino de Laureto et al., 2006). In our case, the interaction involves an aggregated form of DHA since it does not allow a detailed NMR characterization of the N-terminal region of α-syn. On the other hand, the C-terminal acidic region (residues 100-140) remains unfolded and freely tumbling in solution (Fig. 4.15 B). Moreover, the HSQC spectra of α-syn in the presence of DHA are quite similar

to those recorded in the presence of acidic small unilamellar vesicles (Eliezer et al., 2001).

Proteolysis experiments coupled with mass spectrometry have proven useful to define the region of α-syn more directly interacting with DHA. A typical feature of a natively unfolded protein, such as α-syn, is to be largely sensitive to proteases because of its low compactness and lack of secondary and tertiary structure (Uversky, 2002). As a matter of fact, there are no regions with such persistent structure as to hinder protease's attack. Upon binding to DHA, α-syn appears to be quite resistant to proteolysis, as expected from the fact that the polypeptide has adopted an α-helix conformation which strictly involves the first 70 amino acid residues. The proteinase K-resistant product, which contributes to the CD spectra during proteolysis, is still characterized by the presence of α-helical secondary structure (Fig. 4.7). A considerable accessibility of α-syn polypeptide chain to proteinase K and trypsin is confined only at the level of region 70-90 (Fig. 4.19), providing evidence that this segment is the most flexible and sufficiently protruded to be protease-sensitive (Hubbard et al., 1994; Fontana et al., 1997). Of course, we do not know to which specific residue this region can be extended, because there are many potential cleavage sites along the sequence and to be effective a protease requires a stretch of residues (Fontana et al., 1997; Schechter, 1965). However, it is quite cogent that using two proteases with different specificity, proteolysis occurs at the level of the same region.

In the presence of non-saturating concentrations of DHA (molar ratio DHA/protein <50), the rate of proteolysis by proteinase K of α-syn is slower than that in the absence of DHA and with no accumulation of protected fragments. Above a molar ratio of 50, all α-syn molecules seem to be bound to the fatty acid as assessed by CD data and the fragment encompassing the N-terminal region 1-72 is the main product in this case. This clearly suggests that in the first case, there is the simultaneous presence of two different populations of conformers of α-syn, one free in solution and one bound to the lipid, probably in rapid interchange between each other. Although largely unfolded, as assessed by NMR, the C-terminal region hampers extensive proteolytic events in the case of proteinase K. This fact cannot be attributed to possible structural transitions of this part of the molecule, but rather to a protection deriving from the unusual sequence (14 negative charges and 5 Pro residues) (Polverino de Laureto et al., 2006).

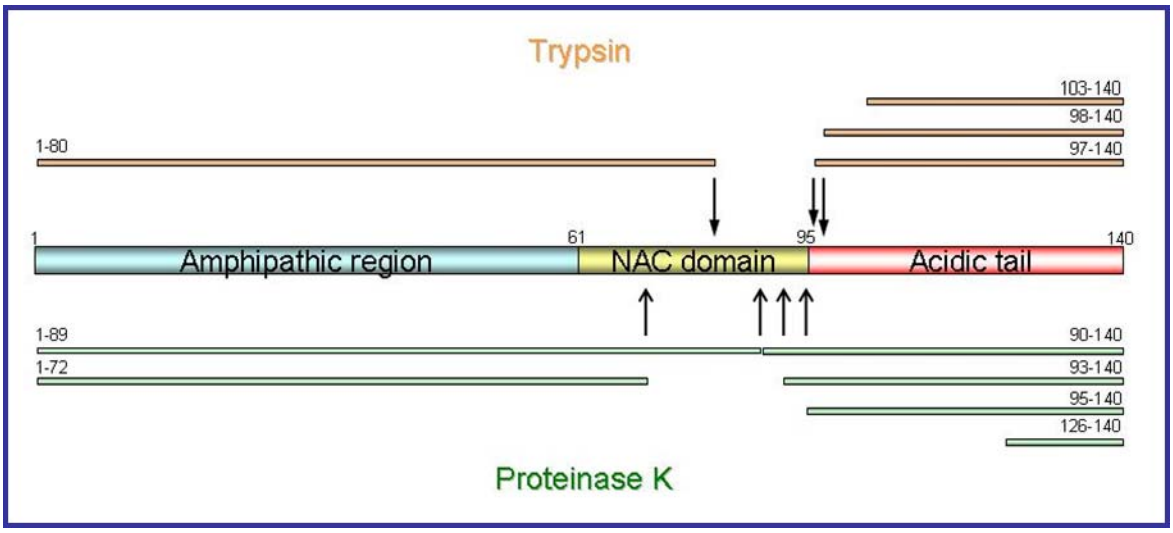

Fig. 4.19 Schematic representation of the main cleavage sites by trypsin **(top)** and proteinase K **(bottom)** in the polypeptide chain of α-syn in the presence of saturating concentration of DHA.

The conformational analyses of the truncated species of α-syn suggest that there is an important action of the 7 imperfect repeats in the random-helix transition of the protein induced by DHA. The 11-residue repeats of apolipoproteins are known to assume the conformation of amphipathic α-helix, which is essential for the binding to lipids. As predicted by the structural similarity to apolipoproteins, the N-terminal region of α-syn is shown to form an amphipathic α-helix that can interact with acidic phospholipids (Davidson et al., 1998; § 3.4.2). Here we demonstrate that this N-terminal amphipathic α-helix of α-syn is also required for its binding to DHA. Syn1-99, syn1-52 and syn57-102 have a similar isoelectric point, (9.4, 9.4 and 9.31) and they contain 7, 4 and 3 imperfect repeats of the entire molecule, respectively. However, syn1-99 and syn1-52 exhibit a similar conformational behavior in the presence of DHA. They completely undergo helical structural transition and their maximum folding is achieved at a lipid/peptide molar ratio (~ 40 and ~ 38, respectively) comparable to that required for α-syn (~35). At variance, syn57-102 reaches the maximum folding at a higher DHA/peptide molar ratio (> 100) and shows lower helix content (67%). Since this last peptide lacks the first 4 structural repeats, these results may suggest that these segments in the N-terminal region of α-syn, are important to trigger the conformational transition of α-syn in the presence of DHA. We don't have experimental evidences that competitive phenomena such as aggregation are taking place, but this could give another possible explanation of the inability of syn57-102 to completely convert its conformation in α-helical structure.

Furthermore syn108-140 remains unfolded in the presence of any kind or amount of lipid (Eliezer et al., 2001; Ulmer et al., 2005). However, proteolysis data shows that also the C-terminal region has a role in the α-syn lipid-bound conformation, since the truncated forms exhibit a different susceptibility to protease attack in comparison to the intact molecule. The fragment species herewith investigated are resistant to proteolysis in the presence of saturating concentrations of DHA. This gives an indication that, at variance from α-syn, all the peptide sequence is probably involved into the interaction and no particular regions are exposed. For example, the proteolysis of syn1-99 and syn57-102 in the presence of DHA do not produce any resistant peptides, like fragment 1-72 (Fig.4.5 D) that accumulates during the reaction with α-syn. These results suggest that the C-terminal tail could modulate the portion of α-syn buried into the lipid compartment. Phenomenon such as the electrostatic repulsion between the acidic residues of region 108-140 and the deprotonated head groups of the FA molecules could be involved in this process.

To define a unifying picture of the α-syn/DHA interaction, we characterized the species formed by DHA and the transition occurring in the presence of α-syn by several techniques. DHA can undergo self-aggregation phenomena strongly dependent on its concentration, ionic strength and temperature. In particular, it has been shown that pH defines precisely the species formed by DHA (Walde, 2006; Namani et al., 2007). The presence of partly ionized DHA molecules is required to stabilize bilayers and a net negative charge at the bilayer surface is generated. At room temperature and under neutral conditions (pH 7.4), an increase in DHA concentration leads to the oil droplets formation (Namani et al., 2007). When they are allowed to form spontaneously (Chen & Szostak, 2004), fatty acids aggregates are generally highly poly-dispersed and form an ensemble of morphologically distinct species in dynamic equilibrium. Under the conditions used in our experiments, DHA aggregates span a wide range of diameters from 50 to more than 600 nm and exhibit features compatible with the formation of lipid droplets, with a critical aggregate concentration in the 80-130 μM range (Fig. 4.8). Because the pH conditions are at close to the edge for the formation of vesicles, also a small amount of bi-layered structures can reasonably be formed. Indeed TEM pictures relative to DHA samples (Fig. 4.15 A) show the presence of several aggregates with different degree of contrast due to a different exclusion of the stain and also the presence of collapsed small spherical particles, resembling vesicles. The addition of the protein causes a deep

variation of both their size and properties. TEM observation and DLS show that the new product of DHA self-assembly has a more regular shape and a smaller diameter (Fig. 4.9). Moreover, pyrene fluorescence assay indicates that the final aggregation state is reached at lower DHA concentrations and that these species have a reduced hydrophobic volume (Fig. 4.8). Therefore, α-syn seems to exert a double effect, inhibiting the formation of giant aggregates and depressing the concentration for aggregate formation. Of interest is that this phenomenon is correlated to the availability of the protein; since, when all the protein molecules are bound to the fatty acid, the excess DHA is not prevented to form aggregates with various sizes. The ability of proteins to interfere with lipid packing in vesicles (Kamp & Beyer, 2006; Madine et al., 2006; Madine et al., 2008) as well as to distort micelles has been already observed (Ulmer et al., 2005). Lipid aggregates are very deformable because of the flexibility of the hydrocarbon chains. The shape and the dimension of the aggregate can adjust to maximize the interaction with the protein. In DHA, the presence of six double bonds confers high conformational flexibility to its self-assembly products (Gawrish et al., 2003). Moreover, depression of the critical micelle concentration for anionic detergents was regularly observed in the presence of cationic electrolytes including protein such as tau (Chirita et al., 2003) and results from the electrostatic interactions between positively charged amino acid side chains and negatively charged FAs or detergent. α-Syn is negatively charge at pH 7.4, but Necula and coworkers suggested that for amphoteric polyelectrolytes such as proteins, depression of anionic surfactant CMC is mediated by clustered charge rather than net charge (Necula et al., 2003). This conclusion is verified by our results deriving from analysis with truncated species of α-syn. Syn108-140, corresponding to the acidic C-terminus, does not alter the physical properties of DHA, while the syn1-99 and syn1-52 (the basic N-terminus, with a net charge of +4.0 and +3.2 respectively) exert a effect similar to α-syn in the reduction of FA concentration for aggregate formation. Syn57-102 (net charge of +2.1) has an ambiguous and weaker effect on DHA self-assembly properties, indeed it prevents the turbidity of DHA samples but it depresses the DHA CAC in minor extent. Probably both the short sequence and the low positive net charge contribute to this peptide behavior.

In our experimental conditions, initially DHA forms oil droplets and the presence of α-syn could cause only a resizing into nano droplets or could alter the aggregative properties of the FAs toward the formation of vesicles. Indeed, it is reasonable to assume

that the positively charged amino acid side chains of α-syn shield the negatively charged fatty acid polar head groups, determining also a decrease of their pKa. At pH 7.4, this causes a larger fraction of dissociated (ionized) fatty acid molecules to be present, possibly inducing the formation of vesicles (bilayer structure) in the presence of α-syn. Moreover, the protein-DHA interface may experience a locally modified dielectric constant, which further affects the ionization equilibrium. However, we don't have the clear cut evidence that the DHA species formed in the presence of the protein are vesicles: cryo-electron microscopy and the use of soluble dye molecule could give important information to verify the presence of lipid bilayers and of the interior aqueous space.

A general consideration concerns the ability of DHA and probably of other long chain PUFAs to induce oligomerization and fibrillation of α-syn (Perrin et al., 2001; Sharon et al., 2003; Broarsen et al., 2006) and also other amyloidogenic proteins (Wilson & Binder, 1997; Ma & Westermark, 2002). We conducted all the experiments about the study of α-syn DHA interaction under conditions designed to avoid fast protein aggregation, performing the measurements immediately after sample preparation and using very low protein concentrations. We observed SDS-resistant α-syn oligomers, corresponding to dimer, trimer and tetramer only after 48 hours (data not shown). Since fatty acids-induced protein oligomers are shown to be associated with decreased cell viability (Assaying et al., 2007) it is of utmost importance to define the exact mechanism responsible for PUFA-dependent multimerization and the specific role played by the aggregative state of the fatty acid in modulating this process. From our studies we can suggest a mechanism for α-syn fibril formation in the presence of DHA.

The partial exposure of the NAC region evidenced by proteolysis mapping has a deep effect on the aggregation propensity of α-syn. Indeed, the NAC region is the most hydrophobic and amyloidogenic segment of the α-syn polypeptide chain (Giasson et al., 2001; Miake et al., 2002). This segment that is not strictly involved into the interaction with DHA aggregates could work as an anchorage for nucleating fibrils growth. To develop regular fibrils, free protein molecules are required. In condition of a DHA/protein molar ratio of 10, anionic aggregate species of DHA are already present and 65% of protein is unbound. So protein fibrillogenesis is favored because the energy barrier of nucleation is overcome and the protein molecules bound to DHA aggregates may function as anchors for site directed fibril assembly. In the presence of saturating concentration of

DHA (DHA/protein molar ratio ≥ 50), fibrils formation is slowed down and only oligomeric species are formed. It is quite interesting that also SDS is able to induce α-syn fibril formation in a multiple structural forms (Ahmad et al., 2006, Ferreon and Deniz, 2007). Both of models are consistent with the existence of an ensemble of populations of α-syn and those with accessible hydrophobic surface and partial α-helical contents favor significantly protein aggregation. In our case, α-syn aggregation process is modulated by two contemporary factors. First, the interaction with DHA stabilizes a more amyloidogenic conformation of α-syn containing some α-helical secondary structure elements and that exposes part of the NAC region. Second, a particular ratio between DHA and the protein is important to allow the presence of free protein molecules that will be engaged in fibril growth.

In conclusion, our work may clarify the debated question on the type of interaction between α-syn and DHA, giving clear evidence for the formation of DHA aggregates in the presence of the protein which are different from those formed by DHA alone. Fatty acid aggregates can work as carriers for proteins, suggesting a more important role of lipids in neurodegeneration. Furthermore, though α-syn acquires concomitantly an α-helical conformation, proteolysis experiments showed that a region of the polypeptide chain remains accessible to proteases. This means that this region is not characterized by persistent structure, and it is conceivable that it could be involved in other interactions.

4.5 REFERENCES

Adibhatla, R. M. & Hatcher, J. F. (2008). Altered Lipid Metabolism in Brain Injury and Disorders. *Subcell. Biochem.***48**.

Aguiar, J., Carpena, P., Molina-Bolivar, J. A. & Ruiz C. C. (2003). On the determination of the critical micelle concentration by pyrene 1:3 ratio method. *J. Colloid Interface Sci.* **258**, 116–122.

Ahmad, M. F., Ramakrishna, T., Raman, B., Rao, Ch. M. (2006). Fibrillogenic and non-fibrillogenic ensembles of SDS-bound human alpha-synuclein. *J. Mol. Biol*., **364**, 1061–1072.

Assayag, K., Yakunin, E., Loeb, V., Selkoe, D. J. & Sharon, R. (2007). Polyunsaturated fatty acids induce alpha-synuclein-related pathogenic changes in neuronal cells. *Am. J. Pathol.* **171**, 2000–2011.

Atherton, E., and Sheppard, R. C. (1989) *Solid Phase Peptide Synthesis*, IRL Press, Oxford, U.K

Ben Gedalya, T., Loeb, V., Israeli, E., Altschuler, Y., Selkoe, D. J., Sharon, R. (2009). Alpha-synuclein and polyunsaturated fatty acids promote clathrin-mediated endocytosis and synaptic vesicle recycling. *Traffic*, **10**, 218–234.

Bisaglia, M., Trolio, A., Tessari, I., Bubacco, L., Mammi, S., Bergantino, E. (2005). Cloning, expression, purification, and spectroscopic analysis of the fragment 57-102 of human alpha-synuclein.. *Protein Expr Purif*., **39**, 90–96.

Bisaglia, M., Tessari, I., Pinato, L., Bellanda, M., Girando, S., Fasano, M., Bergantino, E., Bubacco, L. & Mammi, S. (2005). A topological model of the interaction between alpha-synuclein and sodium dodecyl sulfate micelles. *Biochemistry,* **44**, 329–339.

Bousquet, M., Saint-Pierre, M., Julien, C., Salem, N. Jr., Cicchetti, F., Calon, F. (2008). Beneficial effects of dietary omega-3 polyunsaturated fatty acid on toxin-induced neuronal degeneration in an animal model of Parkinson's disease. *FASEB J*., **22**, 1213–1225.

Breckenridge, W. C., Gombos, G & Morgan, I. G. (1972). The lipid composition of adult rat brain synaptosomal plasma membranes. *Biochim. Biophys. Acta*, **266**, 695–707.

Broersen, K., van den Brink, D., Fraser, G., Goedert, M. & Davletov, B. (2006). Alpha-synuclein adopts an alpha-helical conformation in the presence of polyunsaturated fatty acids to hinder micelle formation. *Biochemistry,* **45**, 15610–15616.

Bussell, R. Jr. & Eliezer, D. (2004). Effects of Parkinson's disease-linked mutations on the structure of lipid-associated alpha-synuclein. *Biochemistry,* **43**, 4810–4818.

Chandra, S., Chen, X., Rizo, J., Jahn, R. & Südhof, T. C. (2003). A broken alpha -helix in folded alpha -Synuclein. *J. Biol. Chem*. **278**, 15313–15318.

Chen, I. A. & Szostak, J. W. (2004). A kinetic study of the growth of fatty acid vesicles. *Biophys. J.* **87**, 988–998.

Chirita, C. N., Necula, M., Kuret, J. (2003). Anionic micelles and vesicles induce tau fibrillization in vitro. *J. Biol. Chem*., **278**, 25644–25650.

Croke, R. L., Sallum, C. O., Watson, E., Watt, E. D. & Alexandrescu, A. T. (2008). Hydrogen exchange of monomeric alpha-synuclein shows unfolded structure persists at physiological temperature and is independent of molecular crowding in Escherichia coli. *Protein Sci*. **17**, 1434–45.

Dalfó, E., Portero-Otín, M., Ayala, V., Martínez, A., Pamplona, R. & Ferrer, I. (2005). Evidence of oxidative stress in the neocortex in incidental Lewy body disease. *J. Neuropathol. Exp. Neurol,*. **64**, 816–830.

Davidson, W. S., Jonas, A., Clayton, D. F. & George, J. M. (1998). Stabilization of alpha-synuclein secondary structure upon binding to synthetic membranes. *J. Biol. Chem.,* **273**, 9443–9449.

de Lau, L. M., Bornebroek, M., Witteman, J. C., Hofman, A., Koudstaal, P. J., Breteler, M. M. (2005). Dietary fatty acids and the risk of Parkinson disease: the Rotterdam study. *Neurology*, **64**, 2040–2045.

Ebeling, W., Hennrich, N., Klockow, M., Meta, H., Orth, D., and Lang, H. (1974). Proteinase K from *Tritirachium album Limber*. *Eur. J. Biochem.* **47**, 91–97.

Eliezer, D., Kutluay, E., Bussell, R. Jr & Browne, G. (2001). Conformational properties of alpha-synuclein in its free and lipid-associated states. *J. Mol. Biol*. **307**, 1061–1073.

Ferreon AC, Deniz AA. (2007). Alpha-synuclein multistate folding thermodynamics: implications for protein misfolding and aggregation. *Biochemistry*, **46**, 4499–4509.

Fontana, A., Zambonin, M., Polverino de Laureto, P., De Filippis, V., Clementi, A. & Scaramella, E. (1997). Probing the conformational state of apomyoglobin by limited proteolysis. *J. Mol. Biol*. **266**, 223–230.

Fontana, A., Polverino de Laureto, P., Spolaore ,B., Frare, E., Ricotti, P. & Zambonin, M. (2004). Probing protein structure by limited proteolysis. *Acta Biochim Pol.* **51**, 299–321.

Frank, J., Radermacher, M., Penczek, P., Zhu, J., Li, Y., Ladjadj, M., Leith, A. J. (1996). SPIDER and WEB: processing and visualization of images in 3D electron microscopy and related fields. *Struct. Biol.* **116**, 190–199.

Gawrisch, K., Eldho, N. V. & Holte, L. L. (2003). The structure of DHA in phospholipid membranes. *Lipids*, **4**, 445–452

Giasson, B. I., Murray, I. V., Trojanowski, J. Q., Lee, V. M. (2001). A hydrophobic stretch of 12 amino acid residues in the middle of alpha-synuclein is essential for filament assembly. *J. Biol. Chem*., 2**76**, 2380–2386.

Gill, S. G & von Hippel, P. H. (1989) Calculation of protein extinction coefficients from amino acid sequence data. *Anal. Biochem.* **182**, 319–326.

Golovko, M. Y., Rosenberger, T. A., Faergeman, N. J., Feddersen, S., Cole, N. B., Pribill, I., Berger, J., Nussbaum, R. L. & Murphy, E. J. (2006). Acyl-CoA synthetase activity links wild-type but not mutant alpha-synuclein to brain arachidonate metabolism. *Biochemistry,* **45**, 6956–6966.

Golovko, M. Y., Rosenberger, T. A., Feddersen, S., Faergeman, N. J., Murphy, E.J. (2007). Alpha-synuclein gene ablation increases docosahexaenoic acid incorporation and turnover in brain phospholipids. *J. Neurochem.* **101**, 201–211.

Hamilton, J. A. (1999). Transport of fatty acids across membranes by the diffusion mechanism. *Prostaglandins Leukot. Essent. Fatty Acids*, **60**, 291–297.

Hamilton, J. A.; Kamp, F. (1999). How are free fatty acids transported in membranes? Is it by proteins or by free diffusion through the lipids? *Diabetes*, **48**, 2255–2269.

Huang, C., Ren, G., Zhou, H. & Wang, C. C. (2005). A new method for purification of recombinant human alpha-synuclein in Escherichia coli. *Protein Expr. Purif.* **42**, 173–177.

Hubbard, S. J., Eisenmenger, F.& Thornton, J. M. (1994). Modeling studies of the change in conformation required for cleavage of limited proteolytic sites. *Protein Sci.* **3**, 757–768.

Innis S. M. (2007). Dietary (n-3) fatty acids and brain development. *J. Nutr.,***137**, 855–859.

Julien, C., Berthiaume, L., Hadj-Tahar, A., Rajput, A. H., Bédard, P. J., Di Paolo, T., Julien, P., Calon, F. (2006). Postmortem brain fatty acid profile of levodopa-treated Parkinson disease patients and parkinsonian monkeys. *Neurochem. Int*., **48**, 404–414.

Kalyanasundaram, K. & Thomas J. K. (1977). Environmental Effects on Vibronic Band Intensities in Pyrene Monomer Fluorescence and Their Application in Studies of Micellar Systems. *J. Am. Chem. Soc.* **99**, 2039−2044.

Kamp, F. & Beyer, K. (2006) Binding of α-synuclein affects the lipid packing in bilayers of small vesicles. *J. Biol. Chem.* **281***,* 9251–9259.

Le Vine, H. (1993). Thioflavin T interaction with synthetic Alzheimer's disease beta-amyloid peptides: Detection of amyloid aggregation in solution. *Protein Sci.,* **2**, 404–410.

Lòpez-Diaz, D., Garcia-Mateos, I. & Velazqueez, M. M. (2005). Synergism in mixtures of zwitterionic and ionic surfactants. *Coll. Surf. A Physicochem. Eng. Aspects*, **270**, 153−162.

Ludtke, S. J., Baldwin, P. R. & Chiu, W. (1999). EMAN: semiautomated software for high-resolution single-particle reconstructions. *J. Struct. Biol.* **128**, 82–97.

Lücke, C., Gantz, D. L., Klimtchuk, E. & Hamilton J. A. (2006). Interactions between fatty acids and alpha-synuclein. *J. Lipid Res.* **47**, 1714–1724.

Lukiw, W. J., Bazan, N. G.. (2008). Docosahexaenoic acid and the aging brain. *J. Nutr*., **138**, 2510–2514.

Ma, Z. & Westermark, G. T. (2002). Effects of free fatty acid on polymerization of islet amyloid polypeptide (IAPP) in vitro and on amyloid fibril formation in cultivated isolated islets of transgenic mice overexpressing human IAPP. *Mol. Med.* **8**, 863–868.

Madine, J., Doig, A. J., Middleton, D. A. (2006). A study of the regional effects of alpha-synuclein on the organization and stability of phospholipid bilayers. Biochemistry, 45, 5783–92.

Madine, J., Hughes, E., Doig, A. J., Middleton, D. A. (2008). The effects of alpha-synuclein on phospholipid vesicle integrity: a study using 31P NMR and electron microscopy. *Mol. Membr. Biol*., **25**, 518–527.

Marszalek, J. R. & Lodish, H. F. (2005). Docosahexaenoic acid, fatty acid-interacting proteins, and neuronal function: breastmilk and fish are good for you. *Annu. Rev. Cell. Dev. Biol*. **21**, 633–57.

McNulty, B. C., Tripathy, A., Young, G. B., Charlton, L. M., Orans, J. & Pielak, G. J. (2006). Temperature-induced reversible conformational change in the first 100 residues of alpha-synuclein. *Protein Sci.* **15**, 602–608.

Miake, H., Mizusawa, H., Iwatsubo, T., Hasegawa, M. (2002). Biochemical characterization of the core structure of alpha-synuclein filaments. *J. Biol. Chem*., **277**, 19213–19219.

Namani, T. & Walde, P. (2005). From decanoate micelles to decanoic acid/dodecylbenzenesulfonate vesicles. *Langmuir*, **21**, 6210–6219.

Namani, T., Ishikawa, T., Morigaki, K. & Walde, P. (2007). Vesicles from docosahexaenoic acid. *Coll. Surf. B Biointer*. **54**, 118–123.

Necula, M., Chirita, C. N. & Kuret, J. (2003). Rapid anionic micelle-mediated alpha-synuclein fibrillization in vitro. *J. Biol. Chem.* **278**, 46674–46680.

Perrin, R. J., Woods, W. S., Clayton, D. F. & George, J. M. (2001). Exposure to long chain polyunsaturated fatty acids triggers rapid multimerization of synucleins. *J. Biol. Chem*. **276**, 41958–41962.

Polverino de Laureto, P., Tosatto, L., Frare, E., Marin, O., Uversky, V. N. & Fontana, A. (2006). Conformational properties of the SDS-bound state of alpha-synuclein probed by limited proteolysis: unexpected rigidity of the acidic C-terminal tail. *Biochemistry,* **45**, 11523–11531.

Rapoport, S. I., Rao, J. S., Igarashi, M. (2007). Brain metabolism of nutritionally essential polyunsaturated fatty acids depends on both the diet and the liver. *Prostaglandins Leukot. Essent. Fatty Acids,* **77**, 251–261

Richieri, G.. V., Ogata, R. T., Zimmerman, A. W. (2000). Fatty acid binding proteins from different tissues show distinct patterns of fatty acid interactions. *Biochemistry,* **39**, 7197–7204.

Rohl, C. A., Chakrabartty, A. & Baldwin, R. L. (1996). Helix propagation and N-cap propensities of the amino acids measured in alanine-based peptides in 40 volume percent trifluoroethanol. *Protein Sci*. **5**, 2623–37.

Sakai, T., Kaneko, Y., Tsujii, K. (2006). Premicellar aggregation of fatty acid N-methylethanolamides in aqueous solutions. *Langmuir*, **22**, 2039–2044.

Schägger, H., & von Jagow, G. (1987) Tricine-sodium dodecyl sulfate-polyacrylamide gel electrophoresis for the separation of proteins in the range from 1 to 100 kDa. *Anal. Biochem*. **166**, 368–379.

Schechter, I. & Berger, A. (1967). On the size of the active site in proteases. I. Papain. *Biochem. and Bioph. Res. Comm.* **27**, 157.

Scopes R. K. (1974). Measurement of protein by spectraphotometry at 205 nm. *Anal. Biochem*., **59**, 277–282.

Sharon, R., Goldberg, M. S., Bar-Josef, I., Betensky, R. A., Shen, J. & Selkoe, D. J. (2001). Alpha-Synuclein occurs in lipid-rich high molecular weight complexes, binds fatty acids, and shows homology to the fatty acid-binding proteins. *Proc. Natl. Acad. Sci. U S A*, **98**, 9110–9115.

Sharon, R., Bar-Joseph, I., Frosch, M. P., Walsh, D. M., Hamilton, J. A. & Selkoe, D. J. (2003). The formation of highly soluble oligomers of alpha-synuclein is regulated by fatty acids and enhanced in Parkinson's disease. *Neuron*, **37**, 583–595.

Sharon, R., Bar-Joseph, I., Mirick, G. E., Serhan, C. N. & Selkoe, D. J. (2003). Altered fatty acid composition of dopaminergic neurons expressing alpha-synuclein and human brains with alpha-synucleinopathies. *J. Biol. Chem*., **278**, 49874–49881.

Turro, N. J. & Kuo P. L. (1986). Pyrene Excimer Formation in Micelles of Nonionc Detergents and of Water-Soluble Polymers. *Langmuir*, **2**, 438–442.

Uéda, K., Fukushima, H., Masliah, E., Xia, Y., Iwai, A., Yoshimoto, M., Otero, D. A., Kondo, J., Ihara, Y. & Saitoh, T. (1993). Molecular cloning of cDNA encoding an unrecognized component of amyloid in Alzheimer disease. *Proc. Natl. Acad. Sci. U S A*, **90**, 11282–11286.

Ulmer, T. S., Bax, A., Cole, N. B. & Nussbaum, R. L. (2005). Structure and dynamics of micelle-bound human alpha-synuclein. *J. Biol. Chem*. **280**, 9595–9603.

Uversky, V. N. (2002). Natively unfolded proteins: A point where biology waits for physics. *Protein Sci.* **11**, 739–756.

Uversky, V. N. (2007) Neuropathology, biochemistry, and biophysics of α-synuclein aggregation. *J. Neurochem*. **103,** 17–37.

Walde, P. (2006). Surfactant assemblies and their various possible roles for the origin(s) of life. *Orig. Life Evol. Biosph*. **36**, 109–150.

Wilson, D. M. & Binder, L. I. (1997). Free fatty acids stimulate the polymerization of tau and amyloid beta peptides. In vitro evidence for a common effector of pathogenesis in Alzheimer's disease. *Am. J. Pathol.* **150**, 2181–2195.

Zhai, L., Zhang, J., Shi, Q., Chen, W. & Zhao, M. (2005). Transition from micelle to vesicle in aqueous mixtures of anionic/zwitterionic surfactants studied by fluorescence, conductivity, and turbidity methods. *J. Colloid. Interface Sci.* **284**, 698−703.

APPENDIX

Main analytical techniques used

I. Circular Dichroism

Circular dichroism (CD) is the election spectroscopic technique used to determine the presence and the type of secondary structure in peptides and proteins, to evaluate their tertiary structure and to monitor structural transitions during unfolding and folding processes (Woody, 1995; Kelly et al., 2005). CD refers to the differential adsorption of the left and right circularly polarized components of plane-polarised radiation. This effect will occur when a chromofore is chiral (optically active) either (a) intrinsically by reason of its structure, or (b) by being covalently linked to a chiral centre, or (c) by being placed in an asymmetric environment. In practice the plane polarized radiation is split into its two circularly polarized components by passage through a modulator subjected to an alternating (50 kHz) electric field. The modulator usually consists of a piezoelectric quartz crystal and a thin plate of isotropic material (e.g. quartz) tightly coupled to the crystal. The alternating electric field induced structural changes in the quartz crystal which make the plate transmit circularly polarized light at the extremes of the field. If, after the passage through the sample, the left and right circularly polarized components are not absorbed (or are absorbed to the same extent), combination of the components would regenerate radiation polarized in the original plane. However, if one of the components is absorbed by the sample to a greater extent than the other, the resultant radiation (combined components) would now be elliptically polarized, i.e. the resultant would trace out an ellipse. In practice, the CD instrument (spectropolarimeter) does not recombine the components, but detects the two components separately; it will then display the dichroism at a given wavelength of radiation expressed as either difference in absorbance of the two components ($\Delta A = A_L - A_R$) or as the ellipticity in degrees (θ) ($\theta = \tan^{-1}$ (b/a), where b and a are the minor and major axes of the resultant ellipse. There is a simple numerical relationship between ΔA and q (in degrees), i.e. $\theta = 33 (A_L - A_R)$.

A CD spectrum is obtained when the dichroism, i.e. the variation of θ expressed in mdeg, is measured as a function of wavelength. Once that the spectrum has been acquired, the measurements must be normalized in order to make them independent from the protein concentration and the cuvette pathlength. This step is reached expressing the ellipticity as mean residue ellipticity, $[\theta]_{MRW}$, calculated dividing the ellipticity for the

molar concentration (using as molecular weight the mean molecular weight for residue) and for the pathlength:

$$[\theta] = \theta \cdot MRW / 10 \cdot c \cdot d$$

Where θ is expressed in mdeg, the protein concentration c in mg/ml, the pathlength d in cm and MRW is the mean residue molecular weight, obtained dividing the protein molecular weight for the number of its amino acid residues. The value [θ] is expressed in $deg \cdot cm^2 \cdot dmol^{-1}$.

Every chiral chromophore or belonging to a chiral molecule presents a characteristic activity of circular dichroism, i.e. it is active at certain wavelength values. As far as proteins are concerned, interesting information can be obtained evaluating the region between 250 and 180 nm (far-UV CD). In this region the chromophore responsible for the dichroic signal is the amidic bond that presents a different ellipticity pattern depending on the conformation of the adjacent bond angles , i.e. depending on the kind of secondary structure in which it is embedded (alpha-helix, beta-sheet or random coil). Each kind of secondary structure possesses a typical spectrum, characterized by specific signals. Alpha-helix is characterized by two intense negative bands at 222 and 208 nm and one positive band at 192 nm. Beta-sheet structure presents a weak negative band at 218 nm and a positive band at 198 nm, while random coil structure shows a weak positive band at 218 nm and an intense negative one at ~ 198 nm (Fig. I.1).

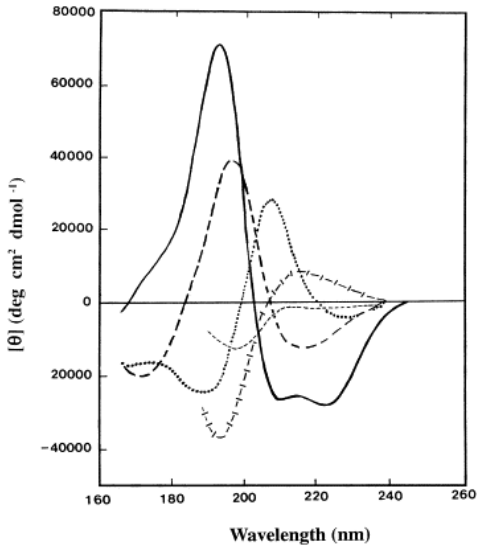

Fig. I.1. Far UV CD spectra associated with various types of secondary structure. Solid line, α-helix; long dashed line, anti-parallel β-sheet; dotted line, type I β-turn; cross dashed line, extended 31-helix or poly (Pro) II helix; short dashed line, irregular structure. (reprinted from Kelly et al., 2005)

II. Fluorescence

Fluorescence emission is observed when an excited electron returns from the first excited state back to the ground state. As some energy is always lost by non-radiative processes, such as vibrational transitions, the energy of the emitted light is always less than that of the absorbed light. Hence the fluorescence emission is shifted to longer wavelengths compared with the absorption of the respective chromophore. Fluorescence spectroscopy is one of the most powerful methods to study protein folding, dynamics, assembly, and interactions, as well as membrane structure. It has been successfully applied to investigate the complex mechanisms of protein aggregation including amyloid fibril formation and the interaction of amyloidogenic proteins with membranes, as well as their dynamic structures. Almost all proteins have natural fluorophores, tyrosine and tryptophan residues, which allow study of changes in protein conformation. Also site-specific labeling with external fluorophores is easily achievable by mutagenesis and chemical modifications. Fluorescence spectroscopy requires a small amount of material (pM–nM range) and has a high signal-to-noise ratio.

Thioflavin T assay

ThT is a fluorescent dye used as a non-covalent extrinsic fluorescent probe in studies of amyloid fibril formation (LeVine, 1993). It has a two-ring structure: the conjugated benzothiazol and aminobenzol rings are arranged in an almost planar orientation (ϕ 30°) in the minimum energy conformation (Fig. II.1) (Munishkina & Fink, 2007). During excitation, the rings rotate in order to obtain the most stable exited state conformation (ϕ 90°) which has low fluorescence efficiency. ThT may bind between the betasheets of the fibril; however, no experimental data exist to support this assumption. ThT has two excitation (~335 nm and 430 nm) and two corresponding emission peaks (425–455 nm and 483 nm). Excitation at ~350 nm results in emission at ~438 nm, whereas excitation at 440 nm leads to emission at ~483 nm. The binding to amyloid fibrils induces a blue shift of the ThT λmax from 483 nm to ~478 nm and probably stabilizes the planar form of the molecule and leads to a 10–500-fold increase in ThT fluorescence intensity.

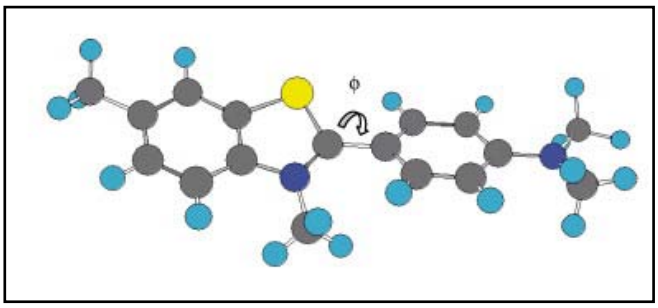

Fig. II.1. Ball-and-stick model of ThT: the rotational angle is around 30 °. Carbons are dark gray, hydrogens are cyan, nitrogens are blue, and sulfur is yellow. (Reprinted from Munishkina & Fink, 2007).

Pyrene Fluorescence

Pyrene is a polycyclic aromatic hydrocarbon (Fig. II.2, A) consisting of 4 fused benzene rings, resulting in a large, flat aromatic system. Pyrene is a valuable molecular probe for fluorescence spectroscopy, having a high quantum yield and lifetime (0.65 and 410 nanosecond, respectively, in ethanol at 293K). Its fluorescence emission spectrum is very sensitive to the solvent's polarity, so pyrene has been used as a probe to determine solvent environments. This is due to its excited state having a different, non-planar structure than the ground state. Certain emission bands are unaffected, but others vary in intensity due to the strength of interaction with a solvent. Indeed, the pyrene fluorescence fine structure presents five peaks (Fig. II.2, B). It is well established that the ratio between the intensities of the first (~ 373 nm) and the third (~ 384 nm) vibration bands of the pyrene environment (Kalyanasundaram & Thomas, 1977; Agiuar et al., 2003). Low values of the I_1/I_3 ratio correspond to a non polar environment. The change of I_1/I_3 value as a function of surfactant concentration is commonly used to determine the critical micelle concentration of surfactant solution, the critical aggregate concentration for polymer-surfactant complexes and also to have information on molecular dissolution of oil droplets dispersed in water. Pyrene can also adopt a dimeric structure, with molecules arranged in sandwiched pairs in order to form lattice units. This results in a high degree of symmetry, belonging to the C2h symmetry group. In solution, dimers exhibit high wavelength fluorescence (red-shift) and also excimer (excited state dimer of pyrene) formation (Fig. II.2, B). Pyrene excimer formation is a well-known concentration-dependent phenomenon in organic solutions. However, because of the low solubility of pyrene in water, pyrene excimer formation is not observed in pure water solutions. The ratio between the maximum emission intensity of the excimer and the I_1 band of pyrene represents the probability of excimer formation for pyrene molecules, in relation to the

local concentration in the environment (Turro et al., 1986). Thus, this ratio gives a good insight into the hydrophobic microdomains formed by surfactants in solution. Pyrene excimer formation is also used to study lateral diffusion of lipids and proteins (pyrene-labeled) in the lipid bilayer (Munishkina & Fink, 2007; Somerharju, 2002).

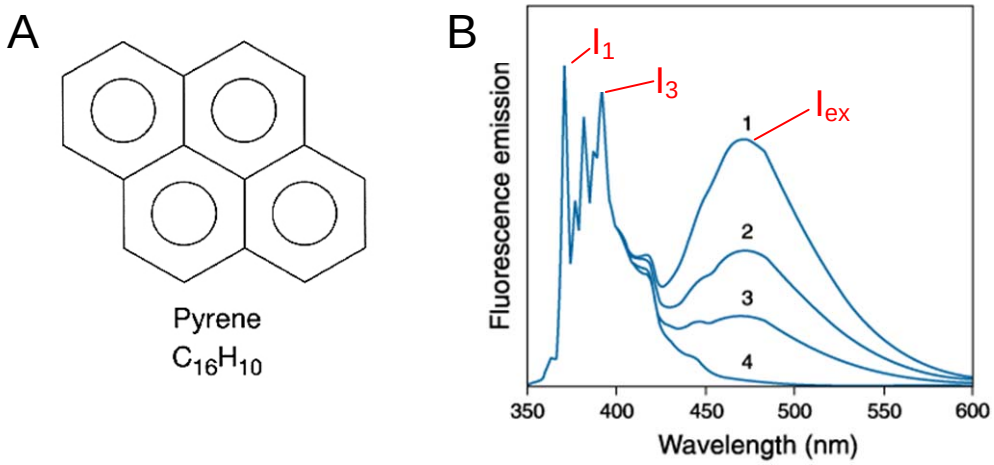

Fig. II.2. (A) Molecular structure of pyrene. (B) Typical fluorescence emission spectra of pyrene.

III. Proteolysis

Proteolysis of a protein substrate can occur only if the polypeptide chain can bind and adapt to specific stereochemistry of the proteases active site (Fontana et al., 2004). However, since the active site of proteases have not been designed by nature to fit the specific sequence and fixed stereochemistry of a stretch of at least 8-10 amino acid residues of a particular globular protein, an induced-fit mechanism of adaptation of the protein substrate to the active site of the protease is required for binding and formation of the transition state of the hydrolytic reaction. Therefore, the native rigid structure of a globular protein cannot act as a substrate for a protease, as documented by the fact that folded proteins under physiological conditions are rather resistant to proteolysis. This is no longer the case when the fully unfolded state (U) of a globular protein exists at equilibrium with the native state (N). However, the N↔U equilibrium is much shifted towards the native state under physiological conditions, according to the Boltzmann relationship DG= -RTln [U]/[N], where DG is 5-15 kcal/mol. Therefore, only a tiny fraction (10-6-10-9) of protein molecules is in the U state that is suitable for proteolysis. Consequently, native globular proteins are rather resistant to proteolytic degradation, as a

result of the fact that the N↔U equilibrium actually dictates and regulates the rate of proteolysis.

Nevertheless, even native globular proteins can be attacked by a protease and, in a number of cases, it has been shown that the peptide bond fission occurs only at one (or a few) peptide bond(s). This behavior results from the fact that a globular protein is not a static entity as can be inferred by a picture of its crystallographic determined 3D-structure, but instead is a dynamic system capable of fluctuations around its average native state at the level of both side chains and polypeptide backbone. Indeed, crystallographers analyze this protein mobility in terms of B-factor for both side chains and Cα-backbone. The main chain B-factor is a measure of average displacements of a polypeptide chain from its native structure, so that it can experience displacements leading to some local unfolding, it can be envisaged that these higher energy, locally unfolded states are those required for a native protein to be attacked by a proteolytic enzyme. Evidence for this mechanism of local unfolding requires for limited proteolysis has been provided by demonstrating a close correspondence between sites of limited proteolysis and sites of higher backbone displacements in the 316-residue polypeptide chain of thermolysin. It is plausible to suggest that limited proteolysis derives also from the fact that a specific chain segment of the folded protein substrate is sufficiently exposed to bind at the active site of the protease. However, the notion of exposure/protrusion/accessibility is a required property, but clearly not at all sufficient to explain the selective hydrolysis of just one peptide bond, since it is evident that even in a small globular protein there are many exposed sites (the all protein surface) which could be targets of proteolysis. Instead, enhanced chain flexibility (segmental mobility) appears to be the key feature of the site(s) of limited proteolysis.

The results obtained with thermolysin are in line with those derived from limited proteolysis experiments conducted on a variety of other proteins of known (3D) structure. In many cases, limited proteolysis was observed to occur at sites of the polypeptide chain displaying high segmental mobility or poorly resolved in the electron density map, implying significant static/dynamic disorder. Therefore, it was concluded that limited proteolysis of a globular protein occurs at flexible loops and, in particular, that chain segments in a regular secondary structure (such as helices) are not sites of limited proteolysis. Indeed Hubbard et al. (1998) conducted modeling studies of the conformational changes required for proteolytic cleavages and concluded that the sites of

limited proteolysis require a large conformational change (local unfolding) of a chain segment of up to 12 residues.

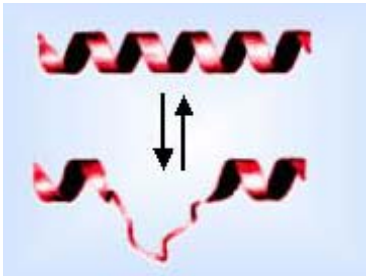

Fig. III.1 A segment of local unfolding is a suitable site of proteolysis

A possible explanation of the fact that helices and, in general, elements of regular secondary structure are not easily hydrolyzed by proteolytic enzymes can be given also on the basis of energetic considerations. If proteolysis is occurring at the centre of the helical segment, likely the helix is fully destroyed by end-effects and consequently all hydrogen bonds, which cooperatively stabilize it, are broken. On the other hand, a peptide bond fission at a disordered flexible site likely does not change much the energetic of that site, since the peptide hydrolysis can easily be compensated by some hydrogen bonds with water. Therefore, it can be proposed that proteolysis of rigid elements of secondary structure is thermodynamically very disadvantageous.

The limited proteolysis approach fro probing protein conformation implies that the proteolytic event should be dictated by the stereochemistry and flexibility of the protein substrate and not by the specificity of the attacking protease (Fontana et al., 1999; Hubbard, 1998). To this aim, the most suitable proteases are those displaying broad substrate specificity, such as subtilysin, thermolysin, proteinase K and pepsin (Bond, 1990). These endopeptidases display a moderate preference for hydrophobic or neutral amino acid residues, but often cleavages occur at other residues as well. The recommended approach is to perform trial experiments of proteolysis of the protein of interest in order to find out the most useful protease, the optimal protein substrate:protease (E:S) ratio and the effect of temperature and time of incubation (Fontana et al., 1999). Possible ways to control proteolysis is by using a low concentration of protease, short reaction times and low temperature. It is not easy to predict in advance the most useful experimental conditions for conducting a limited proteolysis experiment, since these depend upon the structure, dynamics, stability/rigidity

properties of the protein substrate and from the actual aim of the experiment, i.e., identification of the sites of protein flexibility, isolation of the rigid core of the protein or preparation of a nicked protein. In typical experiments of limited proteolysis, it has been found that an E:S ratio of 1:100 (by weight) is recommended, but occasionally both 1:20 or 1:5000 can be used. This results from the fact that there is a great variation in the rate of the selective peptide fission in a globular protein, requiring seconds or days for the limited proteolysis event. Moreover, if isolation of the nicked protein resulting from the initial proteolysis is desired, both the time and temperature of reaction should be properly controlled, since the nicked species may be present only transiently in the protein mixture. Indeed, a nicked protein is usually much more flexible and unstable than the native one and easily unfolds to a protein substrate that is finally degraded to small peptides

IV. Mass Spectrometry

Thanks to recent technological progresses, mass spectrometry has become one of the most powerful tool in protein analysis (Aebersold & Mann, 2003). A further incentive to the development of such techniques has come also from the huge amount of data deriving from the sequencing of entire genomes. Indeed, mass spectrometry (MS), allowing the identification of thousands of proteins starting from complex mixtures, has given significant insights into biological and medical matters. MS can be exploited in many fields, ranging from chemistry and biology to pharmaceutical analysis. It can be used to measure the accurate molecular weight of peptides or proteins, both chemically synthesized or produced by recombinant methods. Other applications are the evaluation of the purity of a protein sample, the identification of post-translational modifications, the monitoring of chemical/enzymatic reactions, the sequencing of proteins or oligonucleotides. Lately, MS has been used also to study the folding and unfolding processes of proteins, or the formation of sovramolecular complexes and the determination of macromolecular structures.

Analysis of peptides and proteins using MS has been allowed by the development of ionization techniques not inducing protein fragmentation. The instrument used in the work presented in this Thesis is an ESI-Q-TOF (*Electrospray-Quadrupole-Time of Flight*) from Micromass (Manchester, UK), an instrument (see the schematic below) having an electrospray sorgent and an analyzer system composed of two quadrupoles and

a time of flight, in series. Between the two analyzers there is a collision chamber, used, when needed, for ions fragmentation.

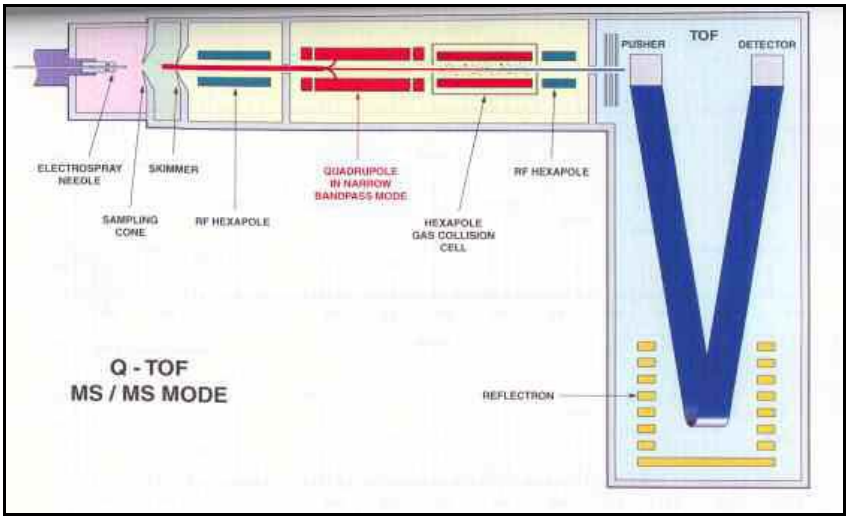

In a generic MS experiment, a peptide/protein sample, dissolved in a solvent mixture containing H_2O/Acetonitrile/formic acid, is injected in the electrospray (ESI) ion source through a very small, charged and usually metal capillary. In electrospray ionization, a liquid is pushed though the capillary, with the analyte, dissolved in a large amount of solvent, which is usually much more volatile than the analyte. Volatile acids, bases or buffers are often added to this solution too. The analyte exists as an ion in solution either in its anion or cation form. Because like charges repel, the liquid pushes itself out of the capillary and forms an aerosol, a mist of small droplets about 10 μm across. An uncharged carrier gas such as nitrogen is sometimes used to help to nebulize the liquid and to help evaporate the neutral solvent in the droplets. As the solvent evaporates, the analyte molecules are forced closer together, repel each other and break up the droplets. This process is called Coulombic fission because it is driven by repulsive Coulombic forces between charged molecules. When the analyte is an ion free of solvent, it moves to the mass analyzer.

In the following phase the ion produced is analyzed, in the instrument, by a Q-Tof Micro (Micromass, Manchester), that connects an ESI source with two combined analyzers quadrupole Tof (*time of flight*). Mass analyzers separate ions according to their mass-to-charge ratio, following the dynamic properties of charged particles in electric and magnetic fields in vacuum. The quadrupole mass analyzer uses oscillating electrical fields to selectively stabilize or destabilize ions passing through a radio frequency (RF) quadrupole field, acting as a mass selective filter. The time-of-flight (Tof) analyzer uses an electric field to accelerate the ions through the same potential, and then measures the

time they take to reach the detector. If the particles all have the same charge, then their kinetic energies will be identical, and their speed will depend only on their masses. Lighter ions will reach the detector first.

The data produced are represented in a mass chromatogram of total ion current (TIC), measured in the ion source. The instrument acquires a mass spectrum of the injected peptide/protein, based on an intensity vs. *m/z* (mass-to-charge ratio) plot. Afterwards, the instrument can determine the sequence of the peptides though a Tandem mass spectrometry analysis.

V. Transmission Electron Microscopy

Negative staining has been a useful specimen preparation technique for biological and medical electron microscopists for almost 50 years, following its introduction as an established procedure by Robert (Bob) Horne (Brenner et al., 1959).

Preparation of carbon supports

A solution of 0.5% w/v butvar was prepared in a 9% v/v glycerol–91% v/v chloroform emulsion. This emulsion is stable at room temperature and needs only to be vigorously shaken before use. Clean glass microscope slides were inserted into the glycerol–chloroform emulsion to approx. two thirds of their length and withdrawn vertically. Excess emulsion was removed by touching the end onto a tissue paper and one side of the slide/mica was wiped to remove the surface film. The slide was then positioned horizontally and the fluid film on the upper glass surface allowed to dry. The small glycerol–water droplets penetrate the drying film of butvar, thereby creating small holes. After wiping the edges of the slide with a tissue, the perforated butvar film was floated onto a clean water surface. An evenly opaque appearance indicates the presence of a suitable array of small holes. EM 400 mesh copper grids (shiny side up) were then placed on the floating film, and a piece of white paper over-layered without moving the grids. The paper slowly became completely wet and was then removed with forceps, along with the attached grids and perforated butvar film, and dried in a dust-free environment. The sheets of paper+grids and perforated butvar film were then carbon-coated. Before use, the butvar was dissolved by spraying the grids with chloroform and grids were briefly glow-discharge treated (20 s) immediately before use. The hole size ranges from *ca*.1 to 10 μm.

Preparation of negatively stained specimens on holey carbon supports

To prepare the specimens using carbon support films we used the single-droplet Parafilm procedure. Specimens were individually negatively stained with 1 % w/v uranyl acetate. Briefly, 25 µl sample droplets and 20 µl droplets of negative stain were placed in rows on a clean Parafilm surface. The sample was applied to the holey carbon support film by touching a grid to the droplet surface and most of the fluid removed by touching to the edge of a filter paper wedge. Then, depending upon the salt concentration of the sample solution, the negative stain solution was applied and removed as a single or multiple droplets (e.g. ×2 or ×3), with the intention of sequentially washing away the buffer and other salts or solutes that may interfere with the production of an amorphous stain-sugar film. At the final stage, maximal removal of negative stain was necessary, so the filter paper was held in contact with the grid edge for ca. 10–20 s, thereby leaving only a thin film of aqueous negative stain+sample. If this final precaution is not adhered to, the stain film will often tend to be too thick. Specimen grids, still held by fine forceps, were then positioned horizontally and the sample+stain allowed to air-dry at room temperature (22°C).

VI. Dynamic Light Scattering

DLS is based on the scattering fluctuation on a small volume in the time-scale of the molecular diffusion (typically microseconds), due to Brownian motion of the particles (due to random collision of molecules). The light scattered by particles is shifted according to Doppler Effect on their random motion. As the molecules diffuse randomly in the illuminated volume of the sample, they tend to locally cluster and separate from each other randomly. As the frequency shift, through Doppler Effect, is negligible for low-velocity molecules, the diffusion coefficient of the particle is obtained from the decay rate ($\tilde{A}$) of the intensity autocorrelation function using the relation $\tilde{A} = Dq2$ (ref). Finally, using the Stokes–Einstein equation, the value of the hydrodynamic radius (R_H) can be determined from D (ref).

$$D = \frac{\kappa T}{6\pi \eta R_H}$$

where ç is the dispersant viscosity, ê the Boltzmann constant and T the absolute temperature. Depending on the equipments and the quality of the sample preparation, the range of detection of the R_H varies from 0.6 nm to 6 µm.

The intensity-weighted diffusion coefficient (D) is calculated using several methods, such as Cumulants (Koppel, 1972; Frisken, 2001) or NNLS (non-negative least squares) or CONTIN (Provencher, 1982). They are algorithms used in DLS experiments to extract size information from the measured correlogram. Cumulants uses a monoexponential correlogram fit to get information about an average D. This analysis assumes a single particle family and represents the distribution as a simple Gaussian, with the Z-Average being the mean value and the PdI (polydispersity index) being the relative variance of the hypothetical Gaussian. Note, that for a Gaussian particle size distribution of width (ó) and Z average (X) it may be shown that the %Polydispersity from a Cumulant fit is ó/X and the PdI is ó2/X2. NNLS and CONTIN algorithms on the other hand, use a multiexponential correlogram fit to assess D distribution in a solution and attempt to extract more information. They model the correlogram as an intensity contribution for each of a number of size bands. These intensities are represented in the displayed size distribution as peaks, each with a characteristic width. In conclusion, while the Cumulant algorithm and the Z average are useful for describing general solution characteristics, for multimodal solutions consisting of multiple particle size groups, the Z average can be misleading. For multimodal solutions, it is more appropriate to fit the

correlation curve to a multiple exponential form, using common algorithms such as CONTIN or NNLS.

The area under each peak in the DLS measured intensity particle size distribution is proportional to the relative scattering intensity of each particle family. The scattering intensity is proportional to the square of the molecular weight (or R^6), and as such, the intensity distribution will tend to be skewed towards larger particle sizes. A transformation of the intensity to a volume or mass distribution can be accomplished using Mie theory, wherein the optical properties of the analyte are used to normalize the effects of the R^6 dependence of the scattering intensity.

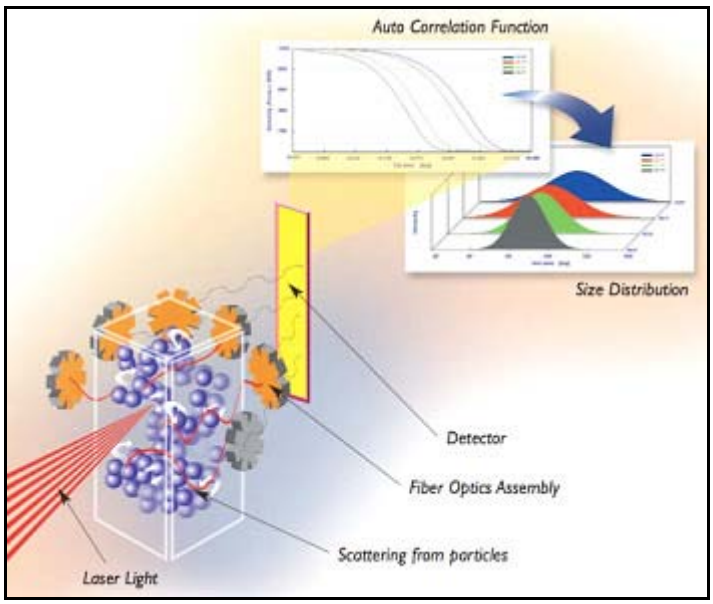

Fig. VI.1. Schematic representation of a DLS measurement.

VII. References

Aebersold, R. and Mann, M. (2003). Mass spectrometry-based proteomics. *Nature,* **422**, 198–207.

Aguiar, J., Carpena, P., Molina-Bolivar, J. A. & Ruiz C. C. (2003). On the determination of the critical micelle concentration by pyrene 1:3 ratio method. *J. Colloid Interface Sci.,* **258**, 116–122.

Brenner, S., Horne, R. W. (1959). A negative staining method for high resolution electron microscopy of viruses. *Biochim. Biophys. Acta*, **34**, 103–110.

Creighton, T. E. (1997). Protein Structure: A Practical Approach (Practical Approach Series).

Fontana, A., Polverino de Laureto, P., De Filippis, V., Scaramella, E., Zambonin, M. (1999). Limited proteolysis in the study of protein conformation. In Proteolytic Enzymes: Tools and Targets. Sterchi EE, Stocker W, eds, 257–284. Springer Verlag, Heidelberg.

Fontana, A., Polverino de Laureto, P., Spolaore, B., Frare, E., Picotti, P., Zambonin, M. (2004). Probing protein structure by limited proteolysis. *Acta Biochim. Pol.*, **51**, 299–321.

Frisken, B. J. (2001). Revisiting the method of cumulants for the analysis of dynamic light-scattering data. *Appl. Opt.*, **40**, 4087–4091.

Hubbard, S. J. (1998). The structural aspects of limited proteolysis of native proteins. *Biochim. Biophys. Acta*, **1382**, 191–206.

Kalyanasundaram, K. and Thomas J. K. (1977). Environmental Effects on Vibronic Band Intensities in Pyrene Monomer Fluorescence and Their Application in Studies of Micellar Systems. *J. Am. Chem. Soc.,* **99**, 2039−2044.

Kelly, S. M., Jess, T. J., Price, N. C. (2005). How to study proteins by circular dichroism. *Biochim. Biophys. Acta*, **1751**, 119–139.

Koppel, D. E. (1972). Analysis of macromolecular polidispersity in intensity correlation spectroscopy: the method of cumulants. *J. Chem. Phys.*, **57**, 4814–4820.

LeVine, H. (1993). Thioflavine T interaction with synthetic Alzheimer's disease beta-amyloid peptides: detection of amyloid aggregation in solution. *Protein Sci*., **2**, 404–410.

Munishkina, L. A. and Fink, A.L. (2007). Fluorescence as a method to reveal structures and membrane-interactions of amyloidogenic proteins. *Biochim. Biophys. Acta*, **1768**, 1862–1885.

Provencher, S. W. (1982). Contin – a general-purpose constrained regularization program for inverting noisy linear algebraic and integral equations. *Comput. Phys. Commun.,* **27**, 229–242.

Somerharju, P. (2002). Pyrene-labeled lipids as tools in membrane biophysics and cell biology. *Chem. Phys. Lipids*, **116**, 57–74.

Turro, N. J. and Kuo P. L. (1986). Pyrene Excimer Formation in Micelles of Nonionc Detergents and of Water-Soluble Polymers. *Langmuir*, **2**, 438–442.

Woody, R. W. (1995). Circular dichroism. *Methods Enzymol.,* **246**, 34–71.